UNIVERSITÄT DUISBURG ESSEN

Offen im Denken

Final report for the research project:

Investigation of Membrane Fouling in the Treatment of Oily Wastewater (W-UFO)

W-UFO contained three subprojects:

W-UFO I: Influence of droplet size distribution (04.2018 – 07.2018)

W-UFO II: Influence of Surfactants and Co-Surfactants (09.2020 – 10.2021)

W-UFO III^{+}: Influence of dissolved oil and process optimization (01.2022 – 03.2024)

Team:

University of Duisburg-Essen
Faculty of Engineering
Department of Mechanical Engineering and Process Engineering
Chair of Mechanical Process Engineering / Water Technology

Lotharstr. 1
47057 Duisburg
www.uni-due.de/wassertechnik/

Prof. Dr.-Ing. Stefan Panglisch (Project PI)
Telefon: 0203 379 -3477
stefan.panglisch@uni-due.de

Dr. Ibrahim ElSherbiny
ibrahim.elsherbiny@uni-due.de

M.Sc. Hasan Idrees (PhD Student)
hasan.idrees@uni-due.de

The project was funded by

Willy-Hager-Stiftung
c/o Technische Universität Kaiserslautern
Paul-Ehrlich-Straße 14
67663 Kaiserslautern

Contact:
Prof. Dr.-Ing. Heidrun Steinmetz

Table of Contents

Table of Contents **III**

1 Introduction 6

1.1 Problem definition 6

1.2 Objectives 9

1.3 Approach 11

1.3.1 Establishment of a standard protocol for the production of synthetic OWWE 11

1.3.2 Understanding the main fouling mechanisms of dead-end operated PES UF membranes 12

1.3.3 Improvement of the PES UF dead-end process by testing different strategies 12

1.3.4 Assessment of the developed strategies 13

1.4 Hypotheses 13

1.4.1 Establishment of a standard protocol for the production of synthetic OWWE 13

1.4.2 Understanding the main fouling mechanisms of dead-end operated PES UF membranes 14

1.4.3 Improvement of the PES UF dead-end process by testing different strategies 14

1.4.4 Assessment of the developed strategies: 15

1.5 W-UFO Project plan and project progress 16

1.5.1 W-UFO Project plan 16

1.5.2 Project progress overview 18

1.5.3 Publications 23

2 Literature review 25

2.1 Protocols for the production of synthetic oily wastewater effluents 25

2.2 Strategies for mitigating membrane fouling by emulsified oil 26

2.2.1 Surfactant-enhanced dead-end UF 27

2.2.2 Hybrid UF process: PAC-UF, coagulation-UF, and PAC-coagulation-UF 29

2.3 Management of produced water 30

2.3.1 Discharge methods and their limitations 31

2.3.2 Reuse applications and their limitations 35

2.4 Environmental and economic assessment 36

2.4.1 Carbon footprint as index for environmental impact assessment 37

2.4.2 Carbon footprint of SDS 39

2.4.3 Carbon footprint of electrical energy production 39

3 Material and methods 40

3.1 Chemicals 40

3.2 Membranes 41

3.2.1 Flat sheet membranes 41

3.2.2 Capillary membrane modules 42
3.3 Preparation of emulsified oils 43
3.3.1 Homogenizers 43
3.3.2 Preparation of HPH-based emulsified oil (E_1) 43
3.3.3 Preparation of US-based emulsified oil (E_2) 44
3.4 Characterization of the emulsified oils 44
3.4.1 Determination of WSO fraction 45
3.4.2 Quantification of the SDS concentration 46
3.4.3 Quality analysis of SDS samples 46
3.5 Adsorption experiments 47
3.6 Coagulation/flocculation jar-test experiments 47
3.7 Bench- and lab-scale filtration experiments 48
3.7.1 Filtration systems 48
3.7.2 Filtration Experiments 51
3.8 Hybrid UF tests with the dosage of PAC and/or coagulants 53
3.8.1 Hybrid UF tests using flat sheet membranes 53
3.8.2 Hybrid UF tests using capillary membrane modules 54
3.9 Semi-technical length and long-term hybrid filtration experiments 54
3.10 Statistical calculations and experimental design 55
3.10.1 Evaluation of membrane separation performance 55
3.10.2 Evaluation of membrane fouling 55
3.10.3 Statistical experimental design 58
3.11 Environmental and economic assessment 59
3.11.1 Energy consumption of dead-end and crossflow operation of membranes 60
4 Results and Discussions 63
4.1 Establishment of a standard protocol for the production of synthetic OWWE 63
4.1.1 Analysis of real PW sample 63
4.1.2 Preparation of HPH-based emulsified oil (E_1) 64
4.1.3 Preparation of US-based, emulsified oil (E_2) 67
4.1.4 Assessment of the preparation methods 70
4.2 Understanding the main fouling mechanisms of dead-end operated PES UF membranes 74
4.2.1 Influence of oil droplet size distribution on fouling behavior of flat sheet membranes with different pore size distribution 74
4.2.2 Contribution of water-soluble oil fraction in the membrane fouling 82
4.2.3 Role of surfactant type on the fouling behavior of flat sheet membranes 98

4.3 Improvement of the PES UF dead-end process by testing different strategies 108
4.3.1 Surfactant-enhanced dead-end ultrafiltration for tertiary treatment of produced water 108
4.3.2 Hybrid UF processes with PAC dosing and/or coagulants 152
4.4 Assessment of the developed strategies: 166
4.4.1 Economic assessment (cost) 167
4.4.2 Environmental assessment 172
4.4.3 Experiments relevant to practice 174
5 Conclusion 180
5.1 Establishment of a standard protocol for the production of synthetic OWWE. 180
5.2 Understanding the main fouling mechanisms of dead-end operated PES UF membranes 180
5.3 Improvement of the PES UF dead-end process by testing different strategies 181
5.3.1 Surfactant-enhanced dead-end UF 181
5.3.2 Hybrid UF process: PAC-UF, coagulation-UF, and PAC-coagulation-UF 182
5.4 Assessment of the developed strategies 183
6 Outlook 183
7 References 185
8 Appendices 197
8.1 Appendix A: Lists of abbreviations, figures, tables and equations **Fehler! Textmarke nicht definiert.**
8.1.1 List of Abbreviations 197
8.1.2 List of Figures 199
8.1.3 List of Tables 210

1 Introduction

1.1 Problem definition

Produced water (PW) is a complex oily wastewater associated with oil and gas industry [1, 2]. PW comprises mainly an oil-water mixture, dissolved organic and inorganic substances, suspended solids (e.g., corrosion products, waxes, asphaltenes) in addition to process chemicals (e.g., surfactants) [3-6]. The total organics present in the wastewater stream comprise dissolved and dispersed organics. Dissolved organics include aliphatic hydrocarbons, organic acids, phenols, organic sulfur compounds as well as polycyclic aromatic hydrocarbons (PAHs, e.g., naphthalene and phenanthrene) [7-9]. Dissolved oil fraction and organics are the primary substances considered as water-soluble oil fraction (WSO), which also include some polar dispersed organics [10]. WSO substances mainly consist of organic acids such as formic acid and propionic acid, PAHs like benzene, toluene, ethylbenzene, and xylene (BTEX), lower molecular weight aliphatic hydrocarbons, and phenols [11, 12]. PAHs and BTEX are of major concern due to their toxicity [13]. The ratio of dissolved to dispersed organics depends on factors such as oil composition, pH, salinity, Total Dissolved Solids (TDS), temperature, oil/water ratio, and the type of oilfield chemicals used [14, 15]. Generally, the solubility of hydrocarbons decreases with increasing molecular weight, and aromatic hydrocarbons have higher solubility than aliphatic hydrocarbons [16]. Oil content in PW is often classified with respect to the average oil droplets sizes into floated/free oil (> 150 µm), dispersed oil (20 - 150 µm), emulsified oil (< 20 µm) and dissolved oil (usually, < 0.5 wt. %) [17, 18]. However, it is complicated to define the exact composition of PW as it differs according to the geographical location, type of hydrocarbons and age of the well [19, 20]. The exact composition of PW can thus differ remarkably according to the geographical location [4].

Global PW production is estimated at a range of 30 – 69 Mm^3 / day; such estimates are expected to increase dramatically due to growing energy demands and wells aging [1, 8, 9]. Subsequently, PW is one of the largest waste streams that requires adequate management and treatment before discharge to environment or reuse as process water. Challenges of PW treatment are related to oil content (2 – 2,000 mg/L), high chemical demand, high salinity and total dissolved solids (up to 400,000 mg/L), total suspended solids (up to 1,000 mg/L) and residuals (e.g., brines) [6, 8, 21-23].

PW treatment processes differ based on the treatment goals as well as the location [1, 8]. Nevertheless, discharging treated PW effluents into the ocean must comply with global regulations ranging from 10 mg/L to 50 mg/L [9, 24]; in the EU, the limit is set at 30 mg/L. Typically, PW treatment starts with simple gravity separation to remove suspended solids and aggregates; this is followed by a primary treatment (e.g., hydrocyclone) and a secondary treatment (e.g., gas flotation) [1, 8, 23]. Conventional methods are generally able to remove free and dispersed oil fractions, whereas they cannot separate “stabilized” emulsified oil [8, 17, 18, 25]. A tertiary (or polishing) treatment is often required, based on the treatment goals, to meet either stringent oil and grease discharge regulations, or reuse requirements and/or reduce toxicity [8, 23, 26].

Different oil concentrations and characteristics were reported for the inlet at the polishing step; for instance, oil concentration range of 10 – 100 mg/L, chemical oxygen demand (COD) ranges up to 125 mg/L, turbidity range up to < 50 NTU [26-29]. Also, different oil droplet size distributions for real PW samples were reported in literature [30-35]. Stewart and Arnold (2011) [31] stated in their book that the typical size of the dispersed oil droplets in produced water is between 0.5 and 200 µm [31]. Ahmad et al. [32] conducted an analysis on the size distribution of actual PW sample from a well in Digboi, Assam, India and reported a droplet size distribution between 0.25 – 1.11 µm with an average of 0.49 µm [32]. Badrnezhad and Beni [33] provided a measurement for wastewater samples that was taken from a desalting plant in Ahwaz, Iran. They reported that the samples showed a droplet size between 0.5 and 1.5 µm with a modal value of the differential volume distribution about 0.83 µm [33]. Reyhani and Mashhadi Meighani [34] also measured the size distribution of wastewater samples from a desalination plant in Iran. They reported droplet sizes between 0.05 – 0.72 µm before primary treatment with skimmers and 0.2 – 0.8 µm after skimmers [34]. Beh et al [35] reported an average particle size for a PW sample of 0.21 µm [35]. However, the last two studies did not specify the type of size distribution considered here, i.e., number, volume, etc.

Great efforts from researchers around the globe are focused on the development of effective techniques for the tertiary treatment of PW, to finally reuse or safely discard this polluted water [23, 26, 36]. Pressure-driven membrane separation is a reliable and cost-effective technology for separation of small and most stabilized oil droplets (< 10 µm), i.e.,

emulsified oil [6, 17, 25, 37], by virtue of high oil retention, compact design, and relatively low energy cost [3, 9, 17, 22, 24]. Nevertheless, membrane fouling, inevitable intensive chemical cleaning, and frequent membrane replacement are among challenges limiting treatment process efficiency and imposing further requirements concerning safe handling and disposal of chemical cleaners [23, 25]. Membrane fouling by emulsified oil has been extensively studied [23, 38]. Different perspectives / phenomena were adopted based on the physical and chemical characteristics of both oil/water emulsion (or synthetic model feed water) and the membrane; however, oil droplets can generally foul porous membranes in certain ways. Oil droplets, with sizes close to or relatively smaller than membrane pore diameter, may deform, enter, and block the pores [23, 38, 39]. While bigger oil droplets are retained (via size exclusion mechanism) and form a dense cake layer on the membrane surface; in certain conditions, accumulating oil droplets in membrane vicinity may coalesce and form gel-polarized oil layer [23, 38, 40, 41].

Several studies focused on the application of ceramic membranes in PW treatment because of their good chemical and thermal resistances [6, 20]. Nevertheless, polymeric membranes, with hydrophilic (or oleophobic) character, are attracting increasing attention for emulsified oil filtration because of their cost-effectiveness, flexibility and versatility, compared to ceramic membranes. Polymeric microfiltration (MF) / ultrafiltration (UF) membranes are frequently employed either as standalone process or post-treatment process [23, 25]. A recent review article reported that 70 % of the publications on PW treatment using MF/UF membranes were conducted in crossflow mode, besides 8 % of the respective literature were performed at constant flux condition [23]. For instance, Salahi et al. (2015) reported on the performance of capillary UF membranes made of polyether sulfone (PES) for the treatment of API oil–water separator[1] effluent with a Total Organic Carbon (TOC) content of 81 mg/L in crossflow operation [28, 42]. Nevertheless, an effective dead-end operation with an optimized membrane performance can be more advantageous compared to crossflow operation because of less energy consumption and operating costs [23, 43, 44].

[1] The name is derived from the American Petroleum Institute (API) since such separators are designed according to their standards.

1.2 Objectives

The W-UFO research project aimed at the establishment of an efficient pressure-driven membrane-based treatment method for the purification of PW. This is targeted as a polishing step in the treatment process of oily wastewater effluents (i.e., produced water after primary and secondary treatment stages, hereafter abbreviated as OWWE), where oil concentration is reported to be in the range of 20 - 100 mg/L, and the average oil droplet size is commonly < 1 µm. Our vision was that an efficient dead-end filtration method may replace the widely employed crossflow membrane operation. This can be motivated by reduced operation costs, due to the less energy consumption by dead-end process compared to crossflow operation, and higher clean water productivity.

Conducting a comprehensive study on all available types and materials of UF membranes is impractical due to the extensive time and resources required. Therefore, this study focuses on a single membrane material. Among various polymeric membranes, PES, polyvinylidene fluoride (PVDF), polyacrylonitrile (PAN), and polysulfone (PSF) have been frequently reported in the literature for their efficacy in separating oil-in-water emulsions, particularly for produced water treatment [25, 45, 46]. The selection of membrane material was also influenced by cost and environmental impact considerations. PES is particularly favored in real-world applications; for instance, it accounted for approximately 49% of the MF/UF membranes used for desalination pretreatment in 2009, a figure that increased to about 63% by 2017 [47, 48]. The market dominance of PES MF/UF membranes is attributed to several advantages, including low cost, high permeability, narrow pore size distribution, compaction resistance, oxidant tolerance, and good chlorine resistance. However, PES does have some drawbacks, such as a relatively dense structure and rough surface [49]. Although PVDF and PAN membranes have higher oxidant tolerance compared to PES, they are associated with higher costs and broader pore size distributions [49]. PVDF is the second most common material for MF/UF membranes [47, 48] but the production of PVDF membranes releases fluorinated organics into the environment, and regulatory bodies, e.g. EU, are considering banning its production [50]. Based on these considerations, PES was selected for this study.

To achieve the ultimate project objective, a series of sub-objectives were identified and organized in a practical-relevant sequence:

1. Establishment of a standard protocol for the production of synthetic OWWE.

It was essential to develop and establish a reliable protocol for the production of synthetic emulsified oils that are based on crude oil and can mimic the characteristics of real produced water at the tertiary treatment step. This was important to get a sustainable source for model feed water, with controlled and reproducible characteristics, to be used in bench-scale and lab-scale filtration experiments.

2. Understanding the main fouling mechanisms of dead-end operated PES UF membranes.

To enhance the performance of UF membranes, it was imperative first to thoroughly understand UF membrane behavior during the filtration of various emulsified oils. This includes identifying the key influencing parameters such as oil droplet size or the composition of the feed (e.g., oil concentration, types and concentrations of surfactants, co-surfactants, and salt concentration), and analyzing the associated fouling mechanisms.

3. Improvement of the PES UF dead-end process by testing different strategies.

This study aimed to enhance the performance of PES UF membranes for the tertiary treatment of produced water. The focus was on optimizing the dead-end filtration process to potentially lower the overall energy requirements compared to crossflow operation, minimize reversible and irreversible membrane fouling, and improve fouling removal efficiency through hydraulic backwash (BW). These improvements are expected to decrease the frequency of chemical cleaning, extend membrane lifespan, and reduce the number of membrane modules needed.

4. Assessment of the developed strategies.

Critically assessing developed methods is essential to ensure their robustness, environmental friendliness, economic viability, and scalability. Robustness refers to the ability of a method to maintain reliable performance under varying conditions of its component or in the surrounding environment, which is crucial for consistent outcomes in real-world applications [51]. Environmentally friendly methods that results in as little

impact on the environment as possible during their life cycle are more favored and sustainable. Economic viability ensures that the methods are cost-effective, making them sustainable for long-term use.

Scalability poses significant challenges when moving from laboratory-scale to industrial-scale operations [52]. One of the primary challenges may be maintaining permeate quality, as larger scales may result in poorer retention of oils and surfactants. This issue can significantly impact the effectiveness of the treatment process. Additionally, there is a need to compare dead-end filtration with crossflow filtration. Dead-end may poses more challenges, as it is more prone for fouling and need more controlled system in comparing to crossflow regime, e.g. switching between filtration and BW each 30-60 min or running chemical cleaning when permeability drops below certain limit.

Thus, a thorough evaluation of these factors is crucial for developing effective, scalable methods that are robust, environmentally friendly, and economically viable for industrial applications.

1.3 Approach

A structured research methodology allowed comprehensive and efficient exploration of factors influencing the performance of PES UF membranes on both fundamental and semi-technical scales and suggesting of reliable practical solutions to control oil fouling and enhance the membrane performance.

1.3.1 Establishment of a standard protocol for the production of synthetic OWWE

To achieve this objective, the following approach was planned.

1. Development of a standard preparation procedure for emulsified oils mimicking the characteristics of real produced water at the tertiary treatment step. With regard to this, two preparation methods from literature, one based on high-pressure homogenizer (HPH) and one based on ultrasonication (US) (see section 2.1), were investigated.
2. Upscaling the standard preparation procedure to obtain model emulsified oils with controlled characteristics and high reproducibility at considerable volumes for the lab-scale filtration experiments.

1.3.2 Understanding the main fouling mechanisms of dead-end operated PES UF membranes

To achieve this objective, the following approach was planned.

1. Performing intensive bench-scale and lab-scale filtration experiments using PES UF membranes and employing different membrane configurations (flat-sheet membranes, multibore capillary membranes, single-fiber capillary membranes) and operating conditions (constant flux, constant pressure, dead-end, crossflow).
2. Analysis of the underling fouling mechanisms (see section 2.2), as well as studying the interplay between the oil droplet size distribution and the membrane pore size distribution.
3. Systematic investigation of the effects of different feed components (e.g., oil concentration, surfactant types and concentration, co-surfactants, salt concentration) on the fouling behavior of PES UF membranes.
4. Investigating the contribution of water-soluble oil fraction in the membrane fouling. This may play an important role, since the water-soluble oil fraction may penetrate the membrane and cause sever pore blockage.

1.3.3 Improvement of the PES UF dead-end process by testing different strategies

In this subobjective, two main tasks with several sub-tasks were planned (see section 2.2.1 and 2.2.2):

1. Surfactant-enhanced UF process: dosing surfactant to feed prior to the filtration step to promote oil fouling reversibility and enhance membrane backwash efficiency.
    a. Investigating the role of the surfactant types (i.e., anionic, cationic and non-ionic) on the fouling behavior of flat sheet membranes
    b. Investigating the efficiency of surfactant-enhanced dead-end UF. This includes testing the effect of dosing surfactant at different concentrations below the CMC and study their effect on the fouling rate, backwash efficiency and elimination performance.

2. Investigating the applicability of hybrid UF process, like combination with Powdered Activated Carbon (PAC) or coagulation: PAC-UF, coagulation-UF, and PAC-coagulation-UF.

    a. Bench-scale adsorption experiments using commercial PAC products to investigate the adsorption isotherm and kinetics.

    b. Lab-scale coagulation experiments (jar tests) using different commercial iron- and aluminum-based inorganic coagulants

    c. Mini-plant filtration tests on the efficiency of hybrid UF process: PAC-UF, coagulation-UF, and PAC-coagulation-UF

1.3.4 Assessment of the developed strategies

To validate and examine the applicability of the developed treatment protocols following aspects were examined (see section 2.3 and 2.4):

1. Examining scalability of the results on longer membrane modules with increased active surface area and conduct long-term mini-plant experiments (see section 3.7.1.3).
2. Assessing the compliance of the quality of the produced UF-permeates with the discharge or reuse regulations.
3. Assessment of the economic feasibility and environmental sustainability of the strategies developed, comparing the proposed dead-end operation with crossflow operation as a reference, as this is the current standard for the use of membranes in tertiary PW treatment.

1.4 Hypotheses

In the design of the research scheme for this project, the experiments list was created to examine the following research hypotheses.

1.4.1 Establishment of a standard protocol for the production of synthetic OWWE

a. Reference HPH-based and US-based methods for preparation of emulsified oil can be successfully reproduced, in terms of the chemical composition and the droplet size distribution.

b. Both methods can be upgraded and adapted to produce sufficient synthetic model water volumes necessary for mini-plant-scale experiments.

c. The produced oil emulsions exhibit characteristics similar to PW prior to tertiary treatment step.

d. Oil emulsions prepared by different methods but having the same chemical composition should show / cause analogous fouling behavior during membrane filtration.

1.4.2 Understanding the main fouling mechanisms of dead-end operated PES UF membranes

a. The performance of UF and MF membranes is significantly influenced by the relationship between oil droplet size distribution and membrane pore size.

b. Membranes with pores similar to oil droplet size will experience standard pore blocking; smaller pores will cause surface fouling (for more details about the blocking mechanisms see [53]).

c. Dissolved crude oil components, i.e., WSO, may penetrate into the membrane pores and cause severe fouling.

1.4.3 Improvement of the PES UF dead-end process by testing different strategies

1.4.3.1 Surfactant-enhanced dead-end UF

a. Surfactants, co-surfactants, and salts increase fouling of UF caused by emulsified oils.

b. Different surfactant types (cationic, anionic, non-ionic) will result in varied fouling behaviors.

c. Dead-end filtration of sub-micron sized surfactant-free emulsified oil through UF membranes can cause severe organic fouling.

d. Dosing anionic surfactant, sodium dodecyl sulfate (SDS) at concentrations below the critical micelle concentration (CMC), can be sufficient to modify oil droplets characteristics in the emulsified oil by introducing stable negative charges.

e. SDS will adsorb on/into PES membrane causing a decline in membrane permeability. Such permeability decline can be restored via typical hydraulic backwashing.

f. Modifying the characteristics of oil droplets and PES membrane using anionic surfactant (SDS) can minimize hydrophobic-hydrophobic interaction, thereby reducing hydraulic irreversible fouling, and increasing backwashing efficiency.

g. Optimizing the operation conditions like the filtration flux, filtration duration, BW flux and BW duration can significantly enhance the membrane performance.

1.4.3.2 Hybrid UF process: PAC-UF, coagulation-UF, and PAC-coagulation-UF

a. Major portion of the oil components will adsorb on the PAC resulting in a multi-component adsorption isotherm.

b. Most of the adsorbable components will adsorb on the outer surface or in the macropores. This will result in fast kinetics.

c. Dosing coagulants to emulsified oils will increase the oil coalescence and eliminate major portion of the oil droplets. Coagulants with different types are expected to have different elimination rates.

d. Dosing PAC will reduce the fouling propensity of the membrane and enhance the hydraulic backwash efficiency.

e. Dosing PAC and/or coagulation will enhance the membrane separation performance by reducing the residual concentration of oil in the UF permeate.

1.4.4 Assessment of the developed strategies:

a. The developed strategies are robust and consistent within different the experimental setup and similar results will be acquired when implementing membranes from different manufacturer or chemicals from different supplier.

b. Similar environmental impact for crossflow and enhanced dead-end operation in terms of carbon footprint (CFP). For dead-end the main difference to crossflow is caused by SDS-dosage. For crossflow difference to dead-end is mainly due to high energy consumption.

c. The developed strategies would be more economically feasible than the crossflow operation mode due to high energy costs in the crossflow operation.

d. Similar performance for the PES-UF membranes to be acquired when testing these on membrane modules with the technical length, at bigger surface area or on longer term.

1.5 W-UFO Project plan and project progress

1.5.1 W-UFO Project plan

The research plan was divided into three distinct subprojects, named as W-UFO I, II and III^{+}. Each of the first two subprojects spanned approximately one year, while W-UFO III^{+} took place over two years. That allowed dynamic adaptation of the workplan for every subproject based on the outputs and knowledge gained by the previous one. **Table 1** presents a comprehensive overview of all tasks undertaken, organized according to the work package (WP) associated with each subproject.

Table 1: The tasks of the W-UFO project, the associated with the W-UFO I, II and III^{+} sub-projects and the respective work package

Task	Task Description	Sub-Project - Work Package
1	**Establishment of a standard protocol for the production of synthetic OWWE**	
1.1	Reproduce and upgrade two common methods to fit the research purpose.	I-WP2 / II-WP1 / III+-WP3.a
2	**Understanding the main fouling mechanisms of dead-end operated PES UF membranes**	
2.1	Examining the membrane filtration performance in bench- and lab-scale	I-WP3 / II-WP2 / III^{+}-WP3.b+c
2.2	Analysis of the underling fouling mechanisms	I-WP3 / II-WP2 / III^{+}-WP3.b+c
2.3	Investigating the interplay of droplet size distribution and the pore size distribution	I-WP3 / I-WP4
2.4	Investigating the contribution of water-soluble oil fraction in the membrane fouling	III^{+}-WP1
3	**Improvement of the PES UF dead-end process by testing different strategies**	
3.1a	Investigating the role of surfactant type on the fouling behavior of flat sheet membranes	II-WP2.1 / II-WP3
3.1b	Investigating the surfactant-enhanced dead-end UF	II-WP2.2 / II-WP3 / III^{+}-WP2.b+c
3.2a-c	Hybrid UF process: PAC-UF, coagulation-UF, and PAC-coagulation-UF	III^{+}-WP2.a
4	**Assessment of developed strategies:**	
4.1	Examining scalability of the results on longer membrane modules.	III^{+}-WP5
4.2	Assessing the compliance with the discharge or reuse regulations	III^{+}-WP4.a
4.3	Economic and Sustainability assessment	III^{+}-WP4.b+c

1.5.2 Project progress overview

Overall, the majority of the work was completed as outlined in the initial plan. However, some adaptations were necessary. Changes to the plan or budget were properly requested and subsequently approved by the Willy-Hager Foundation in advance, and all deviations were comprehensively reported.

1.5.2.1 W-UFO I

All work packages were executed as planned in the original proposal. During the project execution and based on experiments outputs, two parameters were however altered from the original plan:

- Emulsions with oil droplets in size range of 50 – 2,000 nm, instead of 5 to 200 nm (as planned) were prepared. First reason was to simulate a real produced water sample got from an oil company and which we analyzed for the droplet size distribution. Second reason was to match the droplet size in this way that droplets are mostly smaller or in the range of the pore size of MF and at the same time mostly larger than the pores of UF.
- Polymeric membranes were also employed, besides ceramic membranes (as planned) for filtration experiments at constant flux and those at constant pressure conditions. Using cost-efficient polymeric membranes was more feasible for using new membrane for each experiment, which was a necessity since ceramic membranes suffered from irreversible fouling that could not be restored completely by any tested cleaning agent. In addition, polymeric membranes had an advantage of ease internal morphological testing using scanning electron microscope.

Because of unexpected pump failure and other technical issues, a new lab-scale filtration unit was needed, we proposed to use the budget which was supposed to be used for purchasing a temperature controller (Ministat 240w mit Regler „Pilot ONE“) that was proposed in the project. A fully automated plant was designed and ordered after getting the approval from the project administration. Further technical issues were faced especially with the high-pressure homogenizer which went out of order several times, these all led

to a certain delay in the project progress. As a result, an extension of the project lifetime of four month was needed to achieve the project target.

1.5.2.2 W-UFO II

In W-UFO II, also all work packages were started at the respective times, according to the work plan. Nevertheless, due to the COVID-19 conditions in the fall of 2020 and early 2021, university access and lab capacity were significantly limited, resulting in a delay in the progress. Therefore, W-UFO II was extended for 2 months.

1.5.2.3 W-UFO III+

Table 2 provides a detailed comparison between the planned work and the work actually conducted within the project. The progress can be summarized as follows:

- At the beginning of the project additional unplanned work was carried out. Which included analyzing the mechanisms of actions underling the improved fouling reversibly and enhanced backwash efficiency by SDS-enhanced UF process. Additional efforts were also invested in carrying out further experiments, analysis and modeling of the results acquired within the W-UFO II subproject. These efforts were necessary for the preparation of a manuscript for a peer-reviewed article that was successfully published in Separation and purification technology journal.
- WP1: The work commenced as scheduled. Each experiment were planned to be carried three times at three oil concentrations of 10, 25 and 50 mg/L. However, after completing those with 25 and 50 mg/L, which equal two-thirds of the amount experiments, it was discovered that the dissolved oil fraction did not result in significant fouling. Consequently, fouling mechanisms could not be modeled. And those experiments with oil concentration of 10 mg/L were deemed unnecessary since no effect of the dissolved oil fraction could be demonstrated. As a result, the number of experiments conducted in WP1 was lower than initially proposed. The time for these experiments was implemented at other work packages.
- In WP2, task (a) was conducted as planned. The acquired results were very interesting and promising, so that the work was extended at some points. More experiments were carried out in subtask i, to investigate whether the activation state of

the powdered activated carbon will affect the performance of the PAC. In subtask iii, doubled number of planned experiments was carried out, because it was very interesting to compare the acquired results with membranes with bigger pore size, i.e., MF membranes. Also, more experiments were carried out in subtask iv. Here experiments were not only conducted with one PAC, but rather with three different PAC types and some experiments with different PAC-dosage.

- During the execution of Tasks (b) and (c) from WP2, it was observed that the filtration behavior of the SDS-modified emulsified oils differed from that observed in the W-UFO II project. This discrepancy was first attributed to potential variations in the quality of SDS procured from different suppliers or changes in membrane characteristics. After an extensive investigation, it was determined that the SDS-enhanced UF method is sensitive to minor alterations in the system setup. Consequently, over 100 experiments were conducted for these tasks, exceeding the originally planned 70 experiments. Task (c) was initially designed to follow a statistical design of experiments (DOE); however, this unforeseen significant fluctuations in the materials and the related variations in performance parameters necessitated an adjustment and expansion of the experimental plan. We decided to suspend the development of mathematical relationships through statistical experimental design and instead conduct more individual experiments with direct parameter comparisons to reliably capture trends.
- In WP3, tasks (a) and (b) were conducted as planned. However, the four experiments planned for task (c) could not be completed as they depended on the outcomes of the experiments from WP2(c).
- In WP4, the cost and environmental assessments, as well as the study on discharge regulations, were carried out as planned.
- In WP5, the long-term experiments with modules at the technical length were partially completed as scheduled. However, the experiments involving SDS-enhanced UF were not fully conducted.

Overall, a total of over 300 experiments were conducted, in comparison to the 269 experiments planned in the project proposal.

Table 2: A detailed list for planned and conducted experiments in all WPs during W-UFO III+

WP	Task	Sub-Task	Pg*	Proposed experiments	Qty of Exp. Plan	Qty of Exp. Done
1	a		18	Separation of model feed water at 3 oil concentrations (10, 25, 50 mg/L) using three filters (0.1, 0.2 and 0.45 µm) × 2 trials - analysis of permeates (TOC, oil droplet size distribution, WSO) and comparison with unfiltered model feed water.	18 + 63	12 + ~40
	b		18	One-cycle filtration experiments using 2 types of feeds (i.e., one filtered, and one unfiltered) × 3 oil concentrations (10, 25, 50 mg/L) × 2 trials	12	8
	c+ d		19	Modeling of fouling mechanisms and correlating between fouling mechanism and feed components for the outcome results from experiments of task (b)	12	-
2	a	i	19	Bench-scale adsorption experiments: adsorption isotherm experiments using 3 types of PAC at 50 mg/L and oil concentration of 25 mg/L, 2 trials. Adsorption kinetics experiments using three PAC concentrations and oil concentrations of 25 mg/L, 2 trials	24	28
		ii	19	Lab-scale coagulation tests: 2 types of coagulants (one Fe-based and one Al-based) × 3 - 5 different dosages × 1 oil concentrations (25 mg/L) × 2 trials	20	20
		iii	20	One filtration-cycle experiments using 5 permeates (i.e., three from PAC process and two from coagulation process) × 1 oil concentrations (25 mg/L) × 2 trials	10	20
		iv	20	Lab-scale hybrid experiments using 3 combinations (PAC-UF, coagulant-UF, PAC-coagulant-UF) (one PAC type and one coagulant type) × 1 oil concentration (25 mg/L) × 2 trials	6	16
	b+c	-	20	Mini plant tests: • Dead-end: 3 SDS dosing scenarios (i.e., one-time, continuous, periodic dosing) × 1 oil concentrations (25 mg/L) × 2 trials • Crossflow: 2 CFV (0.75, 2.5 m/s) × 1 oil concentrations (25 mg/L) × 2 trials • Optimizing operation conditions: Flux, Duration, BW Flux, BW Duration and pure water duration after BW	~70	105
3	a		23	Reproduction of synthetic oily feed from literature at two oil concentrations (10, 25 mg/L), characterizations (oil droplet size distribution, TOC, WSF), 2 trials	12	~12
	b		24	Lab-scale dead-end and crossflow filtration experiments without SDS dosing: 3 filtration conditions (i.e., dead-end, crossflow@ CFV 0.75 and 2.5 m/s) × 2 oil concentrations (10, 25 mg/L) ×2 trials.	12	12
	c		24	Lab-scale dead-end filtration experiments with SDS dosing @optimized conditions × 2 oil concentrations (10, 25 mg/L) ×2 trials.	4	0
5	a		24	Long term dead-end and crossflow (using one CFV) filtration experiments, one oil concentration 25 mg/L, constant operation period (7 days), 2 trials	4	2

WP	Task	Sub-Task	Pg*	Proposed experiments	Qty of Exp. Plan	Done
	b		24	Long term combined PAC / coagulation with SDS-enhanced UF filtration experiments in dead-end operation, one oil concentration 25 mg/L, constant operation period (7 days), 2 trials	2	1
				Subtotal	269	273
	Additional Experiments			With membrane from different supplier	-	8
				With SDS from different supplier	-	8
				SDS quantification method	-	12
				Total Sum	269	301

* Page number in the W-UFO III^{+} Proposal

1.5.3 Publications

The main scientific outputs of the W-UFO project were presented in two peer-reviewed papers, three conference papers, ten national and international scientific conferences as oral presentations and six as poster as following:

Following Peer-reviewed papers were published:

1. Idrees, H., Al-Ethawi, A., ElSherbiny, I. M. A. and Panglisch, S. 2023. Surfactant-enhanced dead-end ultrafiltration for tertiary treatment of produced water. Separation and purification technology, 311, 123225.
2. Idrees, H., Alhanini, H., Panglisch, S. & Elsherbiny, I. M. A. 2024. Assessment and Upgrading of Preparation Protocols for Emulsified Crude Oils Mimicking Real Produced Water Characteristics Chemie Ingenieur Technik, 96, 513-521.

Following Conference papers were published

1. Idrees, H., ElSherbiny, I. M. A., & Panglisch, S. (2023). Promoting organic fouling reversibility via introduction of sodium dodecyl sulfate prior to ultrafiltration of produced water, in IWA Particle Separation 2023, Johannesburg – South Africa.
2. Idrees, H., ElSherbiny, I. M. A., & Panglisch, S. (2023). Promoting fouling reversibility via introduction of sodium dodecyl sulfate prior to ultrafiltration of produced water in polishing step. In Filtech 2023, Cologne - Germany.
3. Idrees, H., Zohri, M. A., ElSherbiny, I., & Panglisch, S. (2019). Influence of oil droplet size distribution on the fouling mechanisms of UF/MF membranes during filtration of oil nano-emulsions. In Filtech 2019, Cologne - Germany.

The work was presented at following conferences as oral presentation:

1. IWA Particle Separation Conference, December 2023, Johannesburg, South Africa
2. DAAD Knowledge Exchange Workshop, October 2023, Alexandria, Egypt
3. Filtech, February 2023, cologne, Germany
4. Achema Congress, August 2022, Frankfurt, Germany
5. DGMT-Tagung 2021, Membranen zum Schutz von Klima und Ressourcen, March 2021, Online
6. ICOM, 12th International Congress on Membranes and Membrane Processes, December 2020, Online
7. DECHEMA Jahrestreffen der ProcessNet-Fachgruppen Hochdruckverfahrenstechnik und Membrantechnik, February 2020, Freising, Germany
8. MemDes, 4th International Conference on Desalination using Membrane Technology, December 2019, Perth, Australia.
9. IWA Particle Separation Specialist Conference, November 2019, Massachusetts, USA
10. Filtech, October 2019, Cologne, Germany

The work was presented at following conferences as poster presentation:

1. Jahrestreffen der DECHEMA/VDI-Fachgruppe Membrantechnik, February 2024, Frankfurt, Germany
2. MemDes, 6th International Conference on Desalination using Membrane Technology, November 2023, Sitges, Spain
3. Aachener Membran Kolloquium, 2022, Aachen, Germany
4. IWA Membrane Technology conference, 2019, Toulouse, France
5. Aachener Membran Kolloquium, 2018, Aachen, Germany
6. Euromembrane, 2018, Valencia, Spain

Three additional manuscripts will be submitted following the completion of the project.

- „Einsatz von Membrantechnologie zur effizienten Aufbereitung ölhaltiger Abwässer“ to be submitted by August to “Wasser und Abfall” journal
- “Influence of oil droplet size distribution on the fouling mechanisms of UF/MF membranes during filtration of oil emulsions. Was originally planned for Desalination journal, the journal may eventually be changed. Deadline is not fixed.
- “Enhanced dead-end ultrafiltration via combination with PACs and coagulant for tertiary treatment of produced water” Journal to be defined later.

2 Literature review

2.1 Protocols for the production of synthetic oily wastewater effluents

Several emulsification techniques are employed in literature [54-56]. For instance, Tadros et al. (2016) reviewed several emulsification methods and assessed them based on the size of the produced droplets [54]. They measured the Sauter mean diameter (d_{32}), which physically describes a poly-dispersed collective, e.g., oil emulsion, with a diameter of an equivalent mono-dispersed ensemble of spherical particles that has the same ratio of volume to surface area as the poly-dispersed system. Tadros concluded that emulsification using high-pressure homogenizer, HPH, and ultrasonication, US, produced an emulsion with smaller droplets, compared to other methods, e.g. stator-rotor mixers and colloid mill [54].

Additionally, the research group of Prof. Czermak compared three emulsification methods, stator-rotor mixer, HPH and membrane emulsification [55]. HPH-based method was concluded to be the most suitable method for further investigations tertiary PW treatment using ceramic membranes. Using HPH-based method, they could replicate real PW samples [57-59]. For instance, in a study by Ebrahimi et al. (2018), an investigation was carried out involving the analysis of actual PW samples as well as the preparation of synthetic oil emulsions simulating the real samples [57]. Emulsified oils were generated by premixing crude oil and pure water utilizing a stator-rotor mixer. Subsequently, the emulsified oils were subjected to HPH at 450 bar. The resultant emulsified oils exhibited a droplet size distribution from 0.1 to about 20 µm, with a peak of a modal value observed at approximately 1.8 µm [57].

Notably, Ebrahimi et al. (2018) reported that the produced synthetic emulsified oil was stable, in terms of droplet size distribution, for a duration of up to ten days [57]. One advantage of this method is its exceptional adaptability for different crude oil, surfactants, and salts ratios. The emulsified oil was prepared firstly without any additives (e.g., surfactants or salts). Consequently, the oil concentration in the emulsified oils could be adjusted by means of dilution. This allowed the preparation of oil emulsions with oil concentrations down to the ranges of 30 - 200 ppm as dispersed oil and 50 - 87 ppm as total carbon (TC). Additionally, the researchers were able to simply introduce certain concentrations of surfactants and/or salts as required for their experiments. Nevertheless, despite the inherent

versatility of this method concerning the composition, certain improvement on the method were needed; for instance, the adaption of the method to produce emulsified oils exhibiting different droplet size distribution profiles.

Other researchers employed US as a primary energy source to produce emulsified oil to replicate PW characteristics [60-62]. Dardor et al. (2021) conducted a separate investigation, where they could successfully yield an emulsified oil that simulated the characteristics of real PW samples collected from oil and gas exploitation processes in Qatar. This emulsified oil was reported to exhibit a remarkable stability over a duration of 80 days. It had an oil droplet size distribution from 1 µm to 63 µm, with reported values of 4.6 µm, 2.31 µm and 6.4 µm for mean, $D_{50,v}$ and $D_{90,V}$ of the volume distribution, respectively [60].

Another research group analyzed real PW samples and introduced a method for producing synthetic PW [32, 61]. Their method included mixing oil and water, then sonicating for 5-10 h, mostly 6 h were applied. This method was more time-consuming than the method introduced by Dardor et al. (2021) [60], therefore it is only suitable for low-volume bench-scale experiments. Besides, their results showed that increasing the oil concentration during production of emulsified oil led to higher average droplet size values, i.e., higher number of big droplets were generated [61].

2.2 Strategies for mitigating membrane fouling by emulsified oil

Different strategies for mitigating membrane fouling by emulsified oil, in dead-end operations, were investigated in literature [23, 25, 36]. Generally, these efforts can be classified into three main categories; (i) development of fouling-resistant membranes, (ii) surface modification of commercial membranes to enhance anti-fouling properties, and (iii) optimization of filtration process parameters, on lab-scale or pilot-scale, employing commercial membranes. Numerous publications were reported on laboratory-developed fouling-resistant membranes, as in review articles [23, 25, 36]. For instance, Abdel-Aty et al. (2020) tested isotropic MF membranes made of PES for oil-water separation using synthetic oil emulsions with oil concentrations up to 5,000 mg/L, achieving oil rejection of over 98% [63]. Lai et al. (2017) reported an improved antifouling performance for PES-based mixed-matrix membranes when filtering synthetic oil emulsions with oil concentrations up to 2,000 mg/L [64]. Additionally, Ahmad et al. (2020) reported on the development of polyvinyl chloride-based and PSF-based mixed matrix fouling-resistant membranes for the

filtration of synthetic and real produced water with oil concentrations in range of 100 – 400 mg/L [25], where influences of various preparation parameters on the membrane performance were extensively studied [25, 32, 65]. Moreover, surface modification of commercial ready-to-use MF/UF membranes using various antifouling coatings was reported [23, 25, 36]. Idrees et. al. (2021) compared standard and surface-modified PES UF membranes (by in-situ polyzwitterionic hydrogel coating) for the treatment of complex crude oil emulsions with oil concentrations below 10 mg/L and different concentrations of salt and surfactant [56]. Nevertheless, such attempts (i.e., laboratory-developed fouling resistant-membranes and surface-modification of ready-to-use membranes) may be considered rather far from full-scale (real) application because of challenges of upscaling such complex membrane structures, production costs, besides further process optimization (i.e., membrane operation) is still required. Instead, optimization of filtration process parameters can offer more reliable and cost-effective control on membrane fouling and promote the overall process efficiency [6, 8, 25], e.g., optimization of periodic hydraulic and chemical cleaning [5], dosing of coagulants or flocculants prior to membrane filtration [66]. Teodosiu et al. (1999) investigated the influences of dead-end filtration conditions on the performance of PES-UF membranes for the treatment of secondary refinery effluent with TOC concentration below 10 mg/L; the membrane lost almost 50 % of its permeability after 1 h of filtration [67]. Subsequently, more effective approaches for mitigating the fouling of commercial ready-to-use UF membranes in dead-end filtration of emulsified oils at conditions close to real application are critically needed.

2.2.1 Surfactant-enhanced dead-end UF

Recent studies revealed that surfactants can be also employed to reduce membrane fouling; they are adsorbed on emulsified oil and/or membrane surface / matrix, altering the characteristics of oil droplets (e.g., zeta-potential, oil droplet size) and the membrane (e.g., surface affinity, effective pore diameter) [23, 41, 68, 69]. Surfactants are amphiphilic compounds comprising a polar head and a non-polar tail; such dual functionality determines their ability for self-assembly behavior, adsorption at liquid-liquid (e.g., water/oil) or liquid-solid interfaces (e.g., membranes), and lowering surface tension [38, 70]. Adsorption of ionic (charged) surfactants on oil droplets below CMC can minimize coalescence by the Gibbs-Marangoni effect, and hence, promote stability of oil/water emulsions [6, 38].

Therefore, surfactants, either naturally existing or dosed, are intensively employed during oil extraction, recovery, and transport processes [6, 23, 68].

Sufficient understanding of membrane fouling by surfactant-stabilized emulsified oil is considered rather limited because of the complexity of the system. Interactions at three interfaces (i.e., surfactant-oil, oil-membrane, and surfactant-membrane) must be considered [23, 40, 68]. Lu et al. (2015) reported that surfactant adsorption onto membrane surface can influence the emulsified oil stability in the membrane vicinity and mitigate oil droplets coalescence [18]. However, these effects are substantially influenced by the surfactant type (i.e., anionic, cationic, zwitterionic and non-ionic) [18, 38, 40, 41, 68]. For instance, Matos et al. (2016) found that anionic and non-ionic surfactant-stabilized emulsified oils caused fouling to ceramic membranes via concentration polarization mechanism followed by cake layer formation at fluxes higher than the critical flux, whereas adsorption was the main fouling mechanism for cationic surfactant-stabilized emulsified oil [41]. More insights into the impacts of surfactants in emulsified oil with micro-sized oil droplets (~ 20 µm) on the fouling propensity of PVDF MF membranes were also reported [40, 71]. Extent of membrane fouling was better related to the repulsive forces between surfactant-stabilized oil droplets and the membrane rather than the attractive ones. Oppositely charged surfactant-stabilized oil droplets were more adsorbed to the membrane resulting in a flux enhancement, whereas non-ionic surfactant-stabilized oil droplets with least repulsive energy caused the most severe membrane fouling [40]. Surfactant monomers adsorption onto membranes is often explained by either electrostatic interaction or hydrophobic association between surfactant molecules and the membrane sites [38, 70]

Different surfactant : oil concentration ratios were employed in literature; some studies employed 1:1 concentration ratio [40, 71], while others expressed surfactant concentration as function of CMC (up to 10x CMC) [41, 72]. The applicability of dosing SDS at concentrations below CMC into emulsified oil prior to membrane filtration to modify the characteristics of both oil droplets and membrane surface and promote the performance of polymeric capillary membranes in multiple-cycle dead-end filtration has not been studied so far.

2.2.2 Hybrid UF process: PAC-UF, coagulation-UF, and PAC-coagulation-UF

Hybrid UF processes with coagulation was intensively reported for enhancing the membrane performance and reducing the membrane fouling compared to the operation of standalone UF membranes [73]. Zhong et al. (2003) studied the application of coagulation-MF process with zirconia ceramic membrane for the treatment of oily wastewater from refinery processes [74]. Rasouli et al (2017) tested an in-line coagulation prior to ceramic MF membranes [75]. They reported that aluminum sulfate was the most effective coagulant; it enhanced the membrane and improved the oil retention from 96.2% to 99%. Almojjly et al. (2018) compared the performance of coagulation (using ferrous sulfate and aluminum sulfate), sand filters and the combination of coagulation and sand filters as pretreatment process for membrane filtration of oil/water emulsions from vegetable oil effluents. For emulsions with oil concentrations >50 mg/L, hybrid coagulation-sand filters showed the best performance. Sand filters alone were sufficient as a pretreatment for oil concentrations < 50 mg/L [76].

Ozbey-Unal et al (2018) investigated the performance of coagulation using different types and concentrations of poly aluminum chloride (PACL) at different pH values in conjunction with different UF, nanofiltration (NF) and reverse osmosis (RO) membranes for the treatment of olive oil process water effluents [77]. The best performance was found for the coagulant dose of 4 mg/L at pH of 3.

PAC was also implemented. Abbasi et al. (2011) studied a PAC-MF process to treat oily wastewaters using synthesized mullite and mullite-alumina ceramic membranes [78]. The PAC-dosage ranged between 100 – 1,200 mg/L. They found that the optimum dosage was different for each type of membrane. PAC dosing increased the membrane flux up to 61% and improved TOC retention from 93.8% to 97.4% for mullite membranes and from 89.6% to 92.4% for mullite-alumina membranes [78]. Rasouli et al. (2017) observed increased oil retention in four types of ceramic membranes compared to standalone MF. While PAC increased concentrations of 100 – 800 mg/L improved flux, it remained lower than that of standalone MF membranes in three of the four types. The reduction in permeate flux was stated to be due to fine PAC particles and oil droplets blocking membrane pores. However, increasing PAC concentration to 800 mg/L enhances the fluy by reducing membrane fouling through crushing the membrane surface [79]. Such enhancement was

also reported by Kose-Mutlu et al. (2017) when testing the dosage of PAC at the feed of MF membranes made of PVDF for the treatment of field produced water [80].

Zhang et al. (2005) tested the effect of separate and combined PAC-dosage and coagulation in conjunction with UF membranes for the treatment of oil refinery wastewater [81]. PAC-dosage at concentration of 20 mg/L prior UF membranes was reported to enhance the flux, reduce the fouling rate and enhance the backwash efficiency of the accumulated fouling via a hydraulic backwash for 30 s. Less membrane fouling was also noticed when HCA-coagulant (poly dimethyl diallyl propyl ammonium chloride) was dosed prior to the UF. They showed that simultaneously adding PAC and coagulation to the system could significantly improve the performance of the UF membrane. The optimal doses were 15 mg/L for PAC and 0.8 mL/L for HCA, achieving TOC removal rates of over 99% [81].

2.3 Management of produced water

When planning an offshore project, regulatory bodies conduct an environmental impact assessment to identify, predict, and evaluate potential impacts on the environment and surrounding marine ecosystems [82]. As shown in Figure 1, the environmental impact factor, developed originally in Norway, considers various factors of PW discharge that can affect the environment [83].

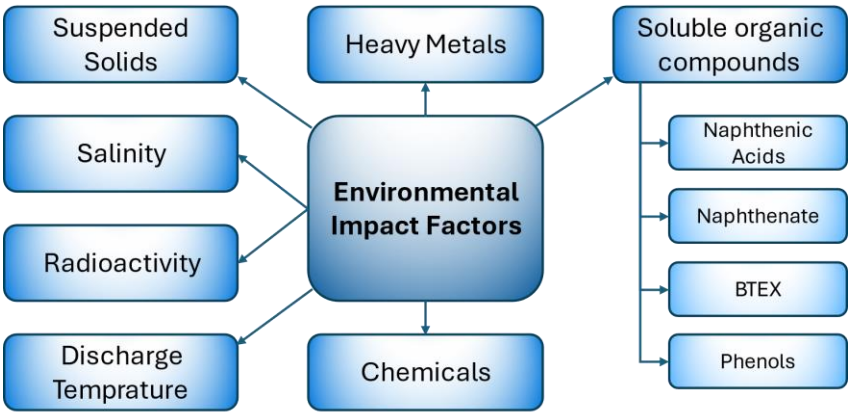

Figure 1: Environmental impact factors of produced water discharge

The management of the produced water effluents differs depending on the composition of the produced water, the need for reinjecting it within the oil extraction process and local regulations and their enforcement [84]. In most of the advanced countries, two essential monitoring techniques are generally used, the first overlooks the discharge quality and the

second assesses the environmental impacts and effects on marine life due to the discharge [85]. However, in many developing and emerging economies, regulations aimed at preventing water contamination are often insufficient or not enforced effectively, if they exist at all [84].

2.3.1 Discharge methods and their limitations

Produced water treatment varies between onshore and offshore facilities due to space, weight restrictions, and differing treatment priorities. For the operation of PW sites often Total Oil and Grease (TOG), TOC, and TDS [83, 86, 87] are parameters used for the definition of oil discharge limits. Onshore facilities focus on reducing salt content, while offshore facilities prioritize meeting oil and grease discharge limits [88]. In case of offshore wells, it is discharged into the ocean bodies after certain treatment, which must follow environmental discharge regulations set by the respective governing bodies [89, 90]. Table 3 shows some discharge limits for the TOG concentration at different regions across the globe. A high TOG concentration in water bodies can have a significant negative impact on the surrounding ecosystem, as the oil can coat plants and animals, causing suffocation due to oxygen depletion [91].

Table 3: TOG Limits for offshore operations in different regions [83, 85, 89, 90, 92]

Region	Legal base	Daily maximum	Monthly maximum average	Measurement method
North Sea	OSPAR Convention	-	30 mg/L	GC-FID, FWMC
Baltic Sea	HELCOM Convention	15 mg/L	-	
Mediterranean Sea	Barcelona Convention	100 mg/L	40 mg/L	
Red Sea	Kuwait Convention	100 mg/L	40 mg/L	
China	GB 4914-85	70 mg/L	50 mg/L	
Indonesia	KLH No 19-2010	25 mg/L (onshore) 50 mg/L (offshore)	-	
Thailand	NEQA 1992; Gov. Reg. 20/90	100 mg/L	40 mg/L	
Vietnam	Decision no. 333/QB 1990	-	40 mg/L	

Region	Legal base	Daily maximum	Monthly maximum average	Measurement method
Unites States (Alaska)	EPA /93	42 mg/L	29 mg/L	EPA 1664 Method Gravimetric
Canada (North Atlantic)	Act RSC 1987	44 mg/L	30 mg/L	SM 5520 C Infrared SM 5520 F Gravimetric GC-FID
Abu Dhabi (United Arab Emirates)	ADS 23/2017	TOG = 10 mg/L TOC 75mg/L	10 mg/L	
Libya	-	100 mg/L	60 mg/L	
Nigeria	-	72 mg/L	20 mg/L	
Brazil	CONAMA 393/2007	42 mg/L	29 mg/L	Gravimetric
Australia	-	50 mg/L	30 mg/L	

2.3.1.1 Germany and OSPAR conviction

Countries including Germany, Belgium, Netherlands, France, Spain, Portugal, Finland, Sweden, Ireland, Switzerland, Denmark, Norway, Iceland, Luxembourg, and the United Kingdom follow the limitations defined by the convention for the protection of the marine environment of the north-east Atlantic (OSPAR) for offshore facilities [83]. During its inaugural gathering in 1998, the OSPAR Commission (also known as the Oslo-Paris Commission) merged and updated the 1972 Oslo Convention regulating waste disposal in marine environments and the 1974 Paris Convention targeting pollution from onshore sources into the water bodies [93]. Two main principles are followed by OSPAR, the precautionary principle and the polluter-pays-principle, and it strives for elimination of discharges, emissions and losses of PW pollutants in the long run, aiming to continuously minimize hazardous discharge into the environment such that the concentrations in the water bodies drop to background levels for naturally occurring substances, and insignificant for synthetic man-made substances [83, 85, 93].

In 2001, the initial limit for offshore oil discharges was set at a TOG value of 40 mg/L, and all production platforms within the OSPAR jurisdiction were advised to meet a monthly average TOG discharge threshold of 30 mg/L for the dispersed oil discharge by the end of 2006 [89, 93]. However, it is worth mentioning that the average discharge concentration

ranged between 12.4 to 14.1 mg/L in the time between 2009 to 2019, which is significantly below the defined limit.

OSPAR North-East Atlantic Environment Strategy (NEAES) 2010-2020 was launched in 2010 to update the previously defined goals and strategies, and amendments included objectives against climate change, ocean acidification, and against eutrophication, defined as the unwanted effects caused by anthropogenic enrichment of nutrients in water [94]. In October 2021, NEAES 2030 was implemented as a further update [95]. According to NEAES 2030, OSPAR Offshore Industry Committee and Hazardous Substances and Eutrophication Committee overlook the spills, discharges and emissions of the oil and gas industry, and identifies contaminants or hazardous substances which may affect the marine environment, including plastics, nanomaterials and produced water [95]. Furthermore, dumping or abandonment of oil and gas infrastructure that is no longer in use is prohibited by OSPAR, and any decommissioned structures must be taken onshore for disposal [82].

2.3.1.2 USA

In USA, around 47% of onshore PW is disposed of via deep injection wells [88, 96], 46% is reused in later oil or gas extraction processes, only about 3% is discharged into the environment and less than 1% is treated for beneficial reuse and 3% is lost to evaporation. Conversely, over 80% of offshore produced water is discharged into the ocean, necessitating compliance with TOG limits determined by the United States Environmental Protection Agency (EPA) [88].

PW is governed by a complex framework of federal state, and local regulations, addressing various aspects of PW management, construction, and operations. EPA oversees these regulations, but each state has its own regulatory agencies and requirements tailored to state-specific practices and laws [96]. The PW management is governed by two federal regulatory programs and two laws: The National Pollutant Discharge Elimination System program through the Clean Water Act and the Underground Injection Control program through the Safe Drinking Water Act. The implementation of both regulations is associated to the EPA [90, 96]. The surface discharge is mainly regulated by the first regulation, the deep well injection is regulated by the second one [90, 96]. In environmental and climate studies either the 98th or the 100th longitude meridian western Greenwich is used as dividing line between the arid western states and the humid eastern states [97].

The EPA is using the 98th meridian as a dividing line to separate the discharge permitting, so that, states western to the 98th meridian have different limitations compared to states on or eastern the 98th meridian [96].

Onshore oil and gas extraction activities are legally not allowed to discharge PW into neighboring water bodies unless these facilities lie western of the 98th meridian, or if they produce 10 barrels of crude oil per day or lower [1, 90, 96]. In coastal areas, the same rule applies with the only exception of Cook Inlet in Alaska where PW is discharged according to the TOG limits [90]. On the other hand, underground injection has been grouped into different classes depending on the purpose and quality of reinjection, and all new wells must be inspected by the authorities before they are constructed and reinjection begins, with special focus on the injection pressure as well as the internal and external integrity of the wells [90]. Furthermore, any wells which have not been used for extraction for two years must be abandoned [90]. For offshore facilities, effluent limit guidelines have been established for extraction operations based on TOG limits, set at 29 mg/L as the monthly average limit and 42 mg/L as the daily average [83, 85, 88]. The EPA 1664 analysis method is normally performed, where TOG is measured by gravimetry using n-hexane as the extraction solvent [89].

2.3.1.3 Africa

Nigeria is the sixth largest oil producer in the world, and the largest in Africa. The Niger Delta region, located in southern Nigeria with the Atlantic Ocean to its south, has witnessed significant environmental degradation between 1983 and 2015, due to oil spills and improperly discharged PW [98, 99]. As modifications are seldomly made, the regulations and monitored parameters are neither strictly applied, nor diverse enough to guarantee that discharges are non-hazardous [100, 101]. In comparison to the sixteen PAHs monitored under the US standard analysis, only ten PAHs are regulated by the applicable environmental guidelines and standards for the petroleum industry in Nigeria guidelines from 2018, indicating the toxicity guidelines are inadequate [100].

In the Niger Delta, the main regulating body for PW discharges is the Department of Petroleum Resources, and the discharge guidelines were issued in the environmental guidelines and standards for the petroleum industry in Nigeria, limiting onshore TOG discharge at 10 mg/L, coastal and offshore discharge at 20 mg/L [98, 100, 102].

2.3.2 Reuse applications and their limitations

With the limiting discharge standards, there is elevated research and incorporation of PW recycling processes. If the quality and basic composition of the PW are altered to meet required standards, this wastewater can turn into a resource [90]. To achieve these standards, PW must be treated, starting with traditional removal of insoluble oil, boron, iron and microorganisms, followed by further treatment based on the specific needs of the reuse activity [1]. Some commonly applied PW reuse and recycling techniques include PW reinjection, consumption by farm animals, irrigation, and as industrial process and cooling water [89, 103]. Reuse of PW not only contributes towards PW disposal but can also enable improved oil recovery [90].

Reuse techniques can be divided into internal reuse within the oil and gas industry, and external reuse. PW reinjection is the least expensive and most applied internal reuse technique, and more than 90% of the worlds PW is reinjected [89]. Reinjecting water into oil and gas reservoirs can uphold the hydraulic pressure and enhance recovery [86, 89]. Regulations govern reinjection as well, and the overall requirements for water injection include TSS (Total Suspended Solids) levels below 10 mg/L and TOG concentrations less than 42 mg/L, and injection pumps and production wells must be protected against sand and other small particles [89]. Another method of PW internal reuse in regions where low PW volumes are generated is for hydraulic fracturing. This is a technique used for unconventional oil and gas extraction from deep underground reservoirs, where high pressure mixture of sand and water, and sometimes chemical additives are pumped into wells to create cracks and fissures in the underground rock formations, thus enabling branched movement of water in the subsurface [104, 105]. A study conducted in the USA [105] suggests that internal reuse of PW should be maximized in the oil and gas industry, as hydraulic fracturing requires large amounts of water and PW generated in certain areas such as the Permian Basin (Texas, USA) could easily satisfy this requirement.

Excessive water which is not used is injected in the deep wells after a certain treatment. The treatment measures include removal of suspended solids, oil and grease, followed by addition chemicals such as antiscalants, biocides and corrosion inhibitors, for protection of the well and pumping equipment [1]. However, deep well injection volumes must be precautionarily adjusted, as in some cases such as the Anadarko Basin in Oklahoma,

concerns have been raised about induced seismic activity (earthquakes) due to high reinjection rates [1, 106].

Further treatment of the PW to drinking water regulation levels also enables domestic use and reinjection into aquifers, however the treatment and monitoring costs would be much higher than current drinking water production techniques, and coupled with the disposal concerns for extremely saline brine it becomes an uneconomic option [103, 105].

Water demand for irrigation exceeds the PW generation in some regions [105]. After specific pre-treatment, PW can also contribute towards agricultural irrigation in arid areas, and as a water source for livestock and wildlife. In each case, the PW must be treated for salinity and toxicity distinctly, to ensure safe discharge and beneficial use without endangerment to plant and animal life as well as the environment [89, 90, 103]. If PW is not treated correctly before irrigational use, photosynthesis of crops can be severely affected [107]. In the Gulf of Mexico, treated PW with a maximum TOG of 35 mg/L can be used for livestock, wildlife and agricultural use [98].

Work done by Chen et al. (2021) shows that Cl^-, Na^+ and TDS of PW must be lowered before application in irrigational fields as these factors affect the water adsorption capability of plants and the soil permeability. Furthermore, Biological Oxygen Demand (BOD), COD, Total Nitrogen and iron levels must be diminished [108].

If the locations of the oil extraction wells are close to industrial areas, the generated PW could be transported for low costs to the industries and power plants for usage in cooling towers or for thermoelectric cooling, if sufficiently large volumes are available [89, 105]. Potentially, the PW can be used for fire-fighting, against wildfires and in sprinkler systems, for dust control while paving gravel roads, and for vehicle and equipment washing, but again only after specific treatment to meet discharge standards as the water would end up in the sewer system as surface runoff [90, 103].

2.4 Environmental and economic assessment

To assess the feasibility of the developed strategies, they were compared to the crossflow operation as a reference, since it is the current standard for membrane application in tertiary PW treatment [27, 109, 110]. The primary differences between crossflow filtration and the developed enhanced dead-end UF strategies are the substances dosed, such as

SDS, coagulant, or PAC, the electrical energy consumed in the process and the frequency of membrane replacement. Membrane replacement is a significant factor due to differing fouling rates and cleaning intensities between methods. However, evaluating this factor requires long-term experiments spanning several weeks and multiple cleaning cycles. This requires data that is not available in this report. Consequently, the influence of membrane lifetime was not considered in this study. Instead, the focus was on examining the differences in dosed substances and electrical energy consumption. These differences formed the basis for assessing the environmental and economic feasibility of the enhanced dead-end methods.

2.4.1 Carbon footprint as index for environmental impact assessment

In recent years, Carbon Footprint, CFP, has been widely adopted as a measure of environmental sustainability. Initially part of the “ecological footprint” concept, CFP referred to the productive land and sea area required to sustain the human population, expressed in hectares. Specifically, CFP was defined as the land area needed to absorb the CO_2 produced by human activity, linking environmental impact to land area requirements [111, 112].

Due to the significance of global warming in international environmental policy, CFP has evolved separately from the ecological footprint. It now measures carbon emissions resulting from specific activities or accumulated over a product life cycle. Nowadays it is suggested that CFP relates to the mass or weight of carbon emissions generated by an individual, organization, or product, rather than an area of land [111, 112]. CFP has gained popularity among governments, industries, and NGOs, drawing attention from businesses, consumers, and policymakers. However, its recent adoption by the academic community has led to confusion and a lack of consensus on its definition and measurement [111, 113].

Scientific literature reviews, such as those by Wright et al. (2011), propose that CFP measures total CO_2 and CH_4 emissions for a specific population, system, or activity, considering all relevant sources and excluding other greenhouse gases (GHGs) [111]. Another definition views CFP as an environmental sustainability indicator, representing total GHG emissions produced by an activity or accumulated during a product life cycle in CO_2

equivalents [114]. The calculation rules for CFP are standardized by ISO 14067, last updated in 2013 and 2018 [112, 113].

To assess GHG-emissions in terms of CO_2 equivalence, Global Warming Potential (GWP) is frequently used. It provides a straightforward method for incorporating various GHGs that contribute to climate change into a CFP over a 100-year timeframe. According to the IPCC (2013), the is "an index measuring the radiative forcing following an emission of a unit mass of a given substance, accumulated over a chosen time horizon, relative to that of the reference substance, carbon dioxide" [115].

The efficiency of an economic or sectoral activity in terms of GHG emissions is measured by the Carbon Intensity (CI). CI calculates the amount of equivalent CO_2 emitted per unit of economic activity. For electricity, CI is expressed as gCO_{2eq}/kWh, representing the GHG emissions equivalent to CO_2 produced per unit of electricity generated or consumed. Between 1990 and 2019, the CI in most European countries decreased due to the increased use of renewable energy sources such as wind, solar, biomass, and biogas [116-118].

Other indices have been used in the literature to describe the environmental impact of products or activities. For instance, GHG emissions represent the total mass of greenhouse gases emitted by a person, organization, or product. CFP calculations, which consider all relevant GHG, are also referred to as the "climate footprint" or "GHG footprint". Another metric, the global temperature change potential, serves as an alternative to GWP, although it is not widely used by policymakers [111]. However, the CFP is not a fixed value, it strongly depends on the production method, location and the method of calculating the CFP and the considered parameters. Table 4 lists the CFP values of certain products can differ depending on the production method and place as well as on the CFP calculation method.

Table 4: CFP values of certain products

Product	CFP in Kg CO_2e/kg	Reference
sodium hydroxide (NaOH)	1.12	[119]
Sodium carbonate (Na2CO3)	1.32	[120]
Calcium chloride (CaCl2)	1.53	[119]

Calcium carbonate (CaCO3)	0.03 - 0.04	[119]
Sodium hypochlorite (NaOCl, 13 % w/w)	0.068 – 0.43	[121]
ferric chloride (FeCl3, 42 % w/w)	0.06–1.02	[121]
Soap bar produced in Brazil	1.65	[122]

2.4.2 Carbon footprint of SDS

Surfactants like SDS are classified as emerging contaminants. These substances are commonly found in the environment due to improper disposal, leading to pollution and ecological imbalances. The absence of strict regulations on surfactant management and disposal is a significant concern [123]. Although SDS is biodegradable and considered safe for the environment, it remains largely unregulated and rarely monitored. Regulatory bodies have differing opinions on SDS regulation, with some highlighting environmental risks and others indicating minimal [123, 124].

There is limited information available on the environmental impact of SDS. A recent study by Nogueira et al. (2019) conducted a 'cradle-to-gate' life cycle assessment of a similar surfactant. In this study the environmental performance of one ton of Sodium Lauryl Ether Sulfate containing 3 mol of ethylene oxide (SLES 3EO) was evaluated [125]. The study measured the impact in terms CFP according to ISO guidelines, revealing a baseline scenario with a CFP of 1,870 kg CO_2e per ton of SLES.

2.4.3 Carbon footprint of electrical energy production

The CFP or CI respectively of the produced energy differ from one country to another, depending on the source and technology mainly used for the production of the electricity [126]. In general, the CFP or CI respectively of electricity is reduced overtime due to implementation of more advanced and renewable energy resources. For example, according to the European environmental agency [127], the CI of electricity generation in EU in general is decreasing over years as illustrated in Figure 2. In 1990, CI for the generated electricity was noted at 652, 490, 602 and 205 g CO_2e/kWh in 1990 for Germany, EU, Netherlands and France, respectively. These values decreased till 2020, then they slightly increased by 2022 marking values of 366, 251, 321 and 68 g CO_2e/kWh, respectively.

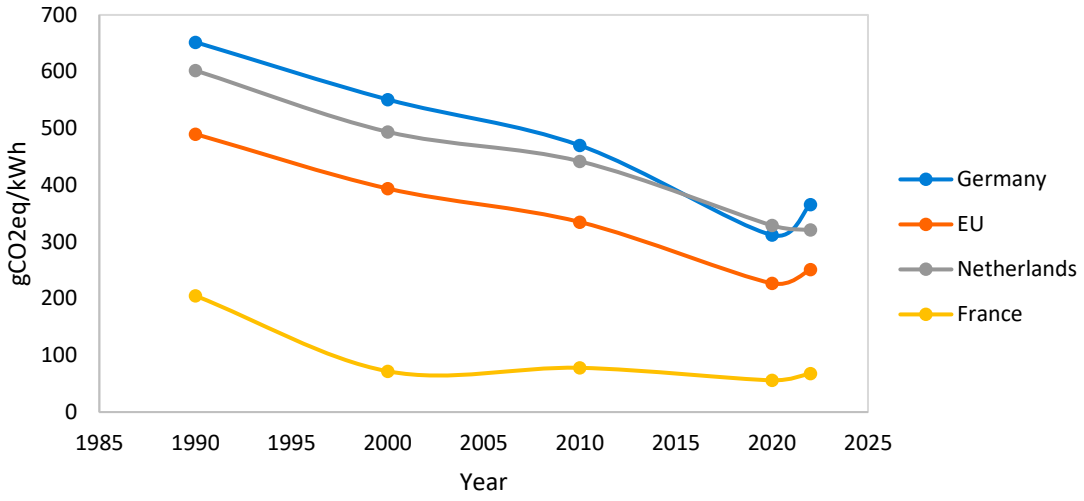

Figure 2: Carbon intensity in gCO_{2eq}/kWh of electricity generation over years for different European countries

For instance, the CI of electricity in Sweden, Egypt, and Saudi Arabia were reported as 45, 475 and 558 g CO_2e/kWh, respectively.

3 Material and methods

3.1 Chemicals

For the preparation of emulsified oils, a light standard crude oil (AR-2048, 2.01 wt.% Sulfur), from Alpha Resources LLC, USA, was used. Pure water (DI) was provided by a reverse osmosis water system (Model: Osmose 190, Denerle, Germany) with a permeate quality (conductivity: ~ 35 µS/cm, dissolved organic carbon content: < 0.2 ppm).

In this study, two SDS products from different suppliers were utilized. The first product, designated as SDS_{VWR}, was sourced from VWR International, Belgium. The second product, referred to as SDS_{TS}, was obtained from Thermo Scientific, India. Multiple batches of SDS_{VWR} were procured, with the majority ordered in 2021 and labeled as $SDS_{VWR,21}$. The remaining batches, ordered in 2023, were designated as $SDS_{VWR,23}$. Unless otherwise specified, all experiments in this study were conducted using $SDS_{VWR,21}$.

Other types of surfactant were also implemented: non-ionic Polysorbate 20 (Tween® 20), the cationic cetyltrimethylammonium bromide (CTAB) and the non-ionic co-surfactant 2-pentanol.

For the simulation of seawater salts, two options were implemented in this study. A ready-to-use artificial seawater salt (ASW) was used, type: AB Reef Salt, from Aqua Medic, Germany. Also, a synthetic salts mixture of NaCl, $CaCl_2 \cdot 2H_2O$, $MgCl_2 \cdot 6H_2O$, KCl, Na_2SO_4, NH_4Cl, and $NaHCO_3$, was employed. Salts were purchased from Carl Roth, VWR, Carl Roth, Riedel-de Haen, J.T. Baker, Merck, and Carl Roth, respectively.

For the analysis of PAHs concentration, cyclohexane was purchased from Alfa Aesar Thermo Fisher GmbH, Germany. For the analysis of the SDS concentration, dimethylformamide from VWR and Stains-all dye from Thermo Scientific were utilized. A buffer solution was made of monopotassium phosphate and disodium phosphate, both purchased from Merk. For membrane cleaning, NaOH and NaOCl were obtained from VWR International. Sodium Metabisulphite ($Na_2S_2O_5$) from Carl Roth GmbH & Co. KG was used for storing the membranes.

For the lab-scale performance experiments, the primary coagulants Nüscofloc Fe and Nüscofloc ALF were provided by Dr. Nüsken Chemie GmbH, Germany. PAC adsorbents were made by milling three commercially available granular activated carbon products, ABG-H, HMA-B and ORG-K, made from the different raw materials wood, anthracite, and coconut shells, respectively.

3.2 Membranes

3.2.1 Flat sheet membranes

A set of MF and UF polyether sulfone flat sheet membranes with different average pore diameters were employed, see Table 5. Membranes were purchased from the three suppliers Mann+Hummel, Pall membranes and inge-Dupont GmbH, Germany. Fresh and clean flat sheet membrane sample was used for every experiment. All membrane samples had an active surface area of 13.85 cm^2.

Table 5: Specifications for flat sheet membranes employed in this project

Acronym	Commercial name	Average pore diameter or MWCO	Produced by
UP150	Nadir® UP150	150 kDa	Mann+Hummel
UB50	Trisep® UB50,	50 kDa	Mann+Hummel
IG	-	0.02 µm	inge / BASF
S800	Supor® 800	0.80 µm	Pall
S450	Supor® 450	0.45 µm	Pall
S200	Supor® 200	0.20 µm	Pall
S100	Supor® 100	0.10 µm	Pall

3.2.2 Capillary membrane modules

Two types of capillary membranes were implemented, Multibore membrane modules from inge-Dupont GmbH, Germany and X-Flow from Pentair, Germany. Both membranes exhibit a nominal pore diameter of 20 nm. These membranes were implemented at different module configurations, as indicated in Table 6. The main difference between the modules was the total surface area. Short modules had a length of 30 cm and a diameter of about 2,5 cm (1 Inch). Long modules had a length of about 150 cm and diameter of about 1 inch as well.

Table 6: Specifications for capillary membrane modules employed in this project

Acronym	Actice Surface area cm²	Module type	Nr. of capillaries	Membrane type
SM	515	Short (Rx)	70 (10 Fibers)	Multibore
SM_2	103	Short (Rx)	14 (2 Fibers)	Multibore
SM_1	51.5	Short (Rx)	7 (1 Fiber)	Multibore
LM	0.22	Long	8	Multibore
LM_2	0.055	Long	2	Multibore
SX	800	Short (Rx)	12	X-Flow

As receiving, membrane modules were post-treated to remove manufacturing and preserving chemicals using NaOCl at concentration of 200 mg/L of free chlorine at pH 12 for one day followed by a chemical cleaning. Thereafter, cleaned modules were stored in 0.05% $Na_2S_2O_5$ ready for use.

3.3 Preparation of emulsified oils

3.3.1 Homogenizers

Three different types of homogenizers were implemented in this study:

3.3.1.1 Stator-rotor mixer

For premixing crude oil in water, a high-speed stator-rotor mixer (type: Ultra-Turrax® T25, IKA-Werke GmbH & Co. KG, Germany) was employed to produce fine homogenized oil-water mixture, prior to the HPH, Ultra-Turrax® T25 is designed for dispersing and emulsifying liquid media in batch operation with a maximal energy output of 350 watts.

3.3.1.2 High pressure homogenizer (HPH)

The HPH is an inline dispersing machine used for continuous production of superfine emulsions, even nano-emulsions. The HPH is manufactured by IKA®-Werke GmbH & Co. KG, Germany. During homogenizing, high pressure is generated by the reduced cross-section in the homogenizing valve, thereafter strong turbulent streams are generated by releasing of the high pressure in a very narrow adjustable gab of the valve. Subsequently, these strong turbulent streams can result in an intensive homogenization of oil-water mixtures.

3.3.1.3 Ultrasonication (US)

Two types of US homogenizers were implemented, bath ultrasonication (type: Branson 5200, Branson Ultrasonics, USA) with a sonication power of 70 watts, and horn ultrasonication (Type: UIP250, Hielscher Ultrasonics GmbH, Germany) operating with a nominal power of 250 watts.

3.3.2 Preparation of HPH-based emulsified oil (E_1)

Crude oil was added to DI water, at different volumetric ratio of 1:250, 1:500 or 1:1,000, without any other reagents, then Ultra-Turrax® was applied to the oil/water mixture to produce a premix emulsion. Afterwards, the premix was passed twice through HPH at an emulsification pressure ranging from 450 – 1,900 bar for several emulsification passes ranging from 1 – 8 passes and for different O/W ratios to produce stable oil-in-water emulsion with different droplet size distribution profiles, specifically $E_{1,S}$, $E_{1,M}$, $E_{1,B}$ that stand for

small, middle and big-sized distribution, respectively. Surfactant-free emulsified oils with different oil contents in the range of 1 - 50 mg/L (as TOC) were prepared. For the preparation of complex oil-in-water emulsions (i.e., with surfactants) SDS was added to the final product of the HPH at different concentrations (0, 0.12, 0.48 and 1.2 g/L) and the emulsified oil was stirred at 500 rpm for 10 min.

The filtration experiments in this study implemented $E_{1,M}$ unless other specifications were mentioned.

3.3.3 Preparation of US-based emulsified oil (E_2)

The methodology reported by Dardor et al. (2021) was used for the production of US-based emulsified oil. [60]. First, the brine solution, designed to simulate the salt composition found in actual PW samples, was prepared. The brine solution consisted of NaCl, $CaCl_2 \cdot 2H_2O$, $MgCl_2 \cdot 6H_2O$, KCl, Na_2SO_4, NH_4Cl, and $NaHCO_3$ at concentrations of 2.39, 1.1, 0.52, 0.10, 0.07, 0.03 and 0.14 g/L, respectively. Subsequently, SDS was introduced into the brine solution at a concentration of 60 mg/L, followed by the addition of crude oil at a volumetric ratio of 0.36 ml/L. Premixing was achieved through magnetic stirring at 1,000 rpm for 30 min. The resulting premix was then subjected to bath ultrasonication for 30 min at a sonication power of 70 watts. The sonicated product was then transferred to a separating funnel to simulate primary skimming or phase separation to remove free oil layer as is common in practice. Finally, this sonicated and decanted product was labeled as $E_{2,P}$.

To generate the necessary emulsified oil volumes for the mini-plant-scale filtration experiments within a reasonable time, the described method was upgraded by employing more powerful horn ultrasonic treatment operating at a power rating of 250 watts for a duration of 2 min. Such products were labeled as $E_{2,U}$.

3.4 Characterization of the emulsified oils

The emulsified oils were characterized in terms of oil droplet size distribution using a laser diffraction particle size analyzer (Model: LS 13320, Beckman Coulter, USA). It measures the particle size distribution of dispersed materials in the liquid state in the of range of 0.017 to 2,000 µm. The emulsified oils were also characterized with respect to TOC (Shmidazu, Japan), zeta-potential (NanoSizer, Malvern, UK), pH (PH 197i, WTW),

turbidity (Nephla turbidity meter, Dr. Lange GmbH & Co. KG) and conductivity (Cond 197i, WTW). Furthermore, the emulsified oils were characterized in terms of WSO fraction (cf. section 3.4.1) and in case SDS was dosed of SDS concentration (3.4.2).

3.4.1 Determination of WSO fraction

The WSO fraction in the prepared emulsified oils was separated to examine its influence on membrane fouling (cf. section 4.2.2). Three methods were tested. The first method was based on the quantification of PAHs following the DIN 38407–39:2011–09 using gas chromatography with a mass spectrometric detector (GC–MS, model 5973, Hewlett-Packard, USA). This analysis was made at GBA Gesellschaft für Bioanalytik mbH, Germany. The two other methods were tested using GC-MS (see section 3.4.1.1) and Fluorophotometer with emission-excitation matrix (FEEM; see section 3.4.1.2) in our labs at UDE.

3.4.1.1 Determination of WSO using GC-MS method

Samples were analyzed with a GC-MS (Model: Clarus 690 / Clarus SQ8 C from PerkinElmer inc., Germany). Stir bar sorptive extraction using Gerstel-Twisters® with 0.5 mm PDMS coating and 10 mm length was employed for the enrichment of oil compounds. Samples were stirred for 2 h at 300 rpm, afterwards the stir bars were dried with lab tissue and transferred into glass tubes. The glass tubes, with the stir bars inside, were heated to 250°C for 8 min in a TurboMatrix 650 thermal desorption unit (PerkinElmer Inc., Germany). The desorbed compounds were collected on a cryotrap at -30°C. The cryotrap was flash-heated to 280°C, and the compounds were transferred onto an Elite 5MS GC-column (PerkinElmer Inc., Germany) through a pre-heated transfer line at a temperature of 280°C. The split ratio was adjusted in a way that ~7.5% of the total sample amount was loaded onto the GC column.

3.4.1.2 Determination of WSO using FEEM method

To establish a fast and reliable method for the quantitative determination of PAHs in the model emulsified oils, which can also be applied in our labs, a standard method of ASTM D5412-93 was examined. PAHs were extracted from emulsified oil samples using cyclohexane, then organic extract was analyzed using Fluorophotometer with emission-excitation matrix (FEEM, Type: RF-6000, Shimadzu, Japan).

3.4.2 Quantification of the SDS concentration

The SDS concentration in the emulsified oil (and permeates in case of filtration experiments) was quantitively analyzed using four methods. The first method was based on the measurement of TOC content (using TOC-L device, Shmidazu, Japan). The second method was based on the use of ion chromatography as reported in literature by [128-130]. To examine this method, an ion chromatography purchased from Metrohm Ltd, Switzerland was implemented. The third method was based on the use of electrical conductivity as reported in [131, 132]. Prior to measurement, a calibration curve for SDS was made for the concentration range of 0 – 4.8 g/L. A conductivity-meter (Type: Cond-197i, WTW Instruments, Germany) was employed. The fourth method was the Stains-all dye method according to Rusconi et al. 2001 [133] and further improved by Rupprecht et al. 2015 [134]. Stains-all dye stock solution was prepared by mixing 67.4 mg of Stains-all dye with 33.7 ml of Dimethylformamide. Thereafter, 1 ml of the stock solution was diluted into 19 mL of DI to prepare the so-called “Working solution”. A Sorensen phosphate buffer solution (made of monopotassium phosphate and disodium phosphate) was used to keep the pH constant at 7.2. The final assay was prepared by mixing 640 µL of DI, 100 µL of the phosphate buffer, 10 µl of the sample and 250 µl of the working solution. The sample was measured with UV-Vis spectrophotometer (Lambda 20, PerkinElmer, Germany) at wavelength of 220 – 600 nm. A calibration curve was made between SDS concentration at the range 0 – 0.1 g/L and UV absorption coefficient at wavelength 453 nm (UV_{453}).

3.4.3 Quality analysis of SDS samples

The quality of both SDS_{TS} and $SDS_{VWR,23}$ was analyzed. An elemental analysis was conducted to determine the carbon, hydrogen, nitrogen, and sulfur content. This analysis was performed by the Microanalytical Laboratory at the Faculty of Chemistry, Institute of Inorganic Chemistry, University of Duisburg-Essen. Three samples of each type of SDS were analyzed. Fourier transform infrared (FT-IR) was also analyzed using an FT-IR spectrometer from PerkinElmer, Germany. The CMC value was also experimentally measured, alongside two reference SDS samples with purities of 95% and >99%. These measurements were conducted at the labs of MSB Breitwieser MessSysteme, Augsburg, Germany.

3.5 Adsorption experiments

To investigate the adsorption behavior, a series of adsorption experiments were performed using three milled commercially available granular activated carbon (GAC) products named as ABG-H, HMA-B and ORG-K, made from the different raw materials wood, anthracite, and coconut shells, respectively. For the adsorption experiments all GAC products were milled into respective PAC with a comparable particle size ($D_{50,v}$ = 5 ~ 8 µm).

Kinetic tests were carried out, in which PAC was dosed at concentration of 50 mg/L to 2 L of surfactant-free emulsified oil with oil concentration of 25 mg/L. Thereafter, the bottle with the mixture was placed on a shaker, and samples were taken after 1, 2, 3, 4, 5, 6, 7, 8, 9, 10, 30 and 60 min as well as after 1.5, 2, 4, 24 and 48 h. Samples were filtered through a glass fiber filter and analyzed for UV absorption coefficient at a wavelength of 254 nm (UV_{254}) and dissolved organic content (DOC).

Adsorption isotherm experiments were carried out to produce the adsorption isotherms and the required PAC-dosage to achieve the highest possible oil removal. The PAC concentration was varied in the range of 1, 2, 5, 10, 20, 30, 40, 50, 60, 70, 80, 90, 100, 150, 200, 250, 300, 350, and 400 mg/L. The different individual concentrations of PAC were dosed to ten bottles containing surfactant-free emulsified oil with oil concentration of 25 mg/L. Depending on the founding in the kinetic experiments, cf. section 4.3.2.1, the equilibrium time was set to 24 h. Thereafter, the PAC-oil suspension was filtered through 0.45 µm filter, then UV_{254} and DOC residual concentrations were measured and compared against the blank sample (i.e., filtered PAC-free emulsified oil).

3.6 Coagulation/flocculation jar-test experiments

To determine the optimum coagulation/flocculation parameters for the oil removal, a series of typical jar-test experiments were carried out according to W218 DVGW [135] protocol using iron- and aluminum-based coagulants at concentrations of 0 - 12 mg/L and 0 – 6 mg/L, respectively. The model feed of 1.8 L surfactant-free oil emulsion with oil concentration of 25 mg/L were placed in 2 L beakers that were equipped with stators. After dosing the coagulants, samples were mixed with centrally placed rotor mixer. The coagulation/flocculation experiment contained four phases, rapid mixing, microfloc formation, macrofloc building (flocculation) and sedimentation, each phase took place for 10 s, 1 min,

5 min and 20 min, respectively, and using a mixing speed of 200, 50, 20 and 0 rpm, respectively, which resulted in G-Values of about 413, 54, 14 and 0 1/s, respectively. During the experiments, pH was adjusted to a constant value of ~7.0. Finally, samples of the supernatant (4 cm below the water surface) were taken and filtered using syringe filters made of PES with pore size of 0.45 µm and analyzed for DOC, UV_{254}, turbidity, pH, and conductivity.

3.7 Bench- and lab-scale filtration experiments

3.7.1 Filtration systems

3.7.1.1 Manually operated bench-scale dead-end filtration unit

The manually operated bench-scale filtration unit (see Figure 3) was operated at constant pressure. The flow rate was determined by weighing the collected permeate volume at certain time intervals.

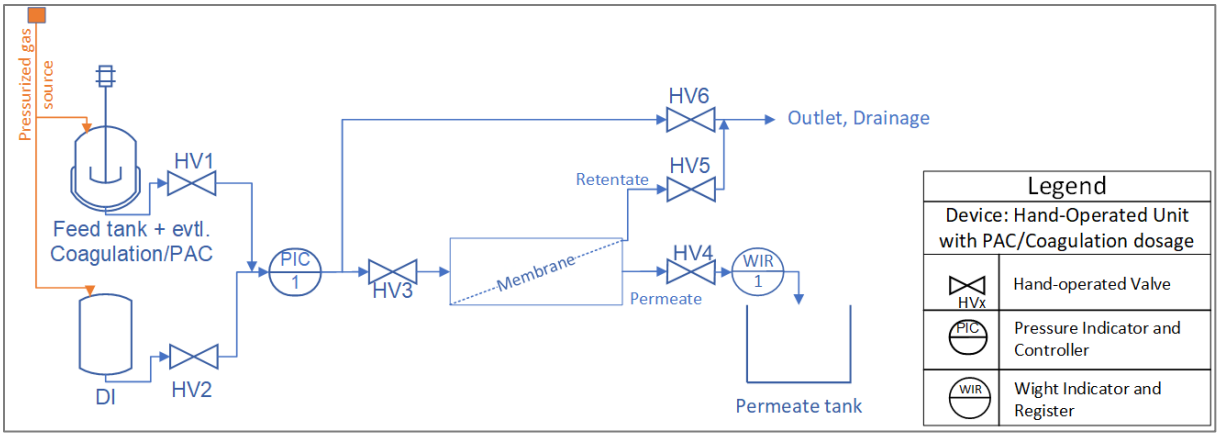

Figure 3: Schematic representation of the bench-scale dead-end filtration unit for flat-sheet membranes operated manually at constant pressure

The constant pressure was maintained via a pressure vessel that was connected to a constant air pressure source. All valves and pressure gauges were controlled manually.

3.7.1.2 Automated bench-scale dead-end filtration unit (Playground)

Figure 4 represents a scheme for the fully automated bench-scale filtration unit named playground, that was manufactured by Damecon-convergence, Netherlands. Playground is an automated system that can be operated at constant pressure of up to 6 bar and

constant flux conditions up to a flow rate of 2 L/h. This unit was applied for testing both flat sheet membranes and SM_1 and SM_2 capillary membrane modules.

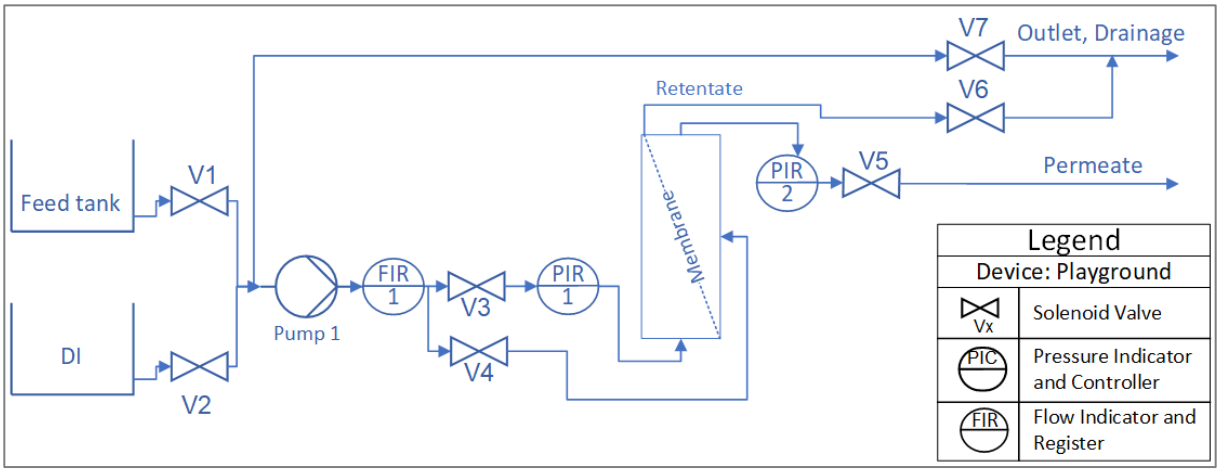

Figure 4: Schematic representation of the "Playground" bench-scale dead-end filtration unit operated at constant flow

For synergistic combination of UF with the dosage of PAC and/or coagulants, the Playground was modified to fit the purpose of the experiments, as illustrated in Figure 5. It was equipped with two additional pressurized vessels, each with a mechanical stirrer. The other two pressure vessels were montaged to serve as emulsified oil and pure water supply vessels.

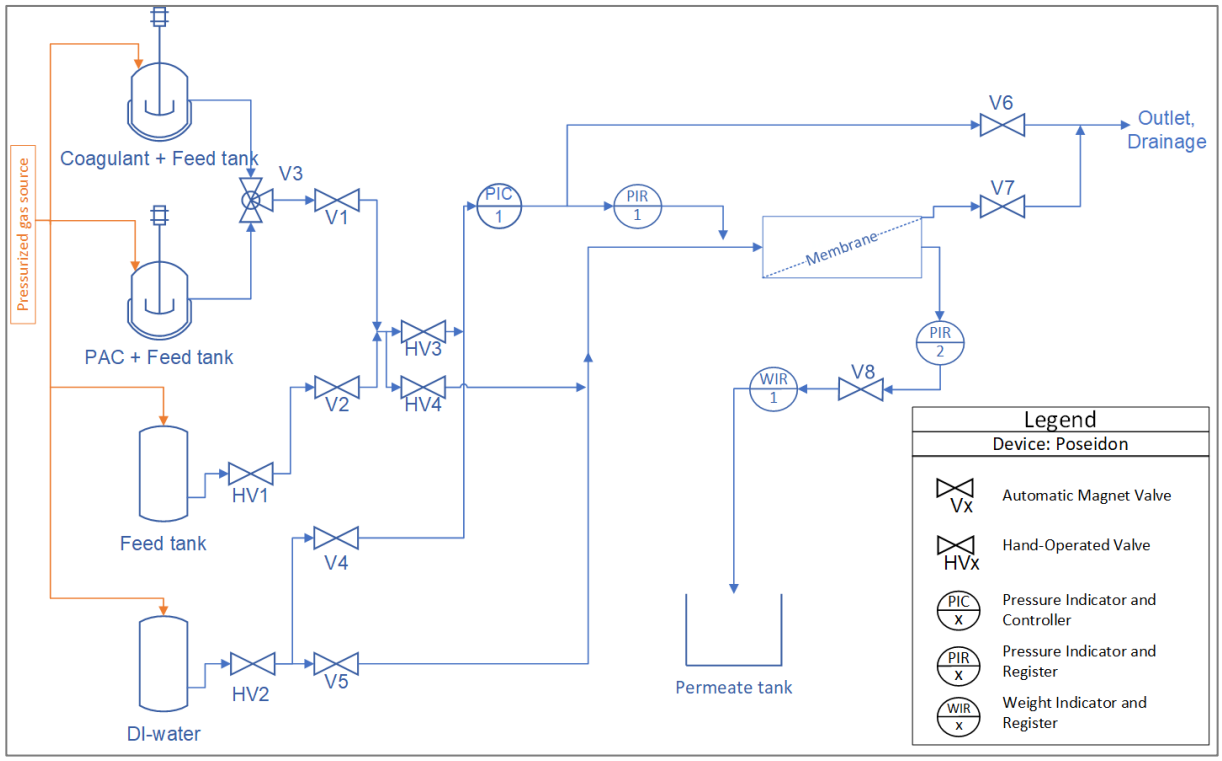

Figure 5: Schematic representation of the "Playground" bench-scale dead-end filtration unit operated at constant flow, modified for the synergistic combination of UF with the dosage of PAC and/or coagulants

This unit was supplied with magnetic valves and could therefore be operated automatically controlled by a self-written program. The measurements of the flow and the pressure at both feed and permeate sides of the membrane were registered within an interval of 5 sec.

3.7.1.3 Mini-plant fully automated filtration units (Poseidon and Neptunus)

Two mini-plant filtration units were implemented in this project, named as Poseidon and Neptunus, which were manufactured by Damecon-convergence, Netherlands. They are designed to test capillary membrane modules at a maximum flow rate of about 30 L/h for Poseidon and 200 L/h for Neptunus and a maximum pressure of 6 bar, as schematically represented in Figure 6.

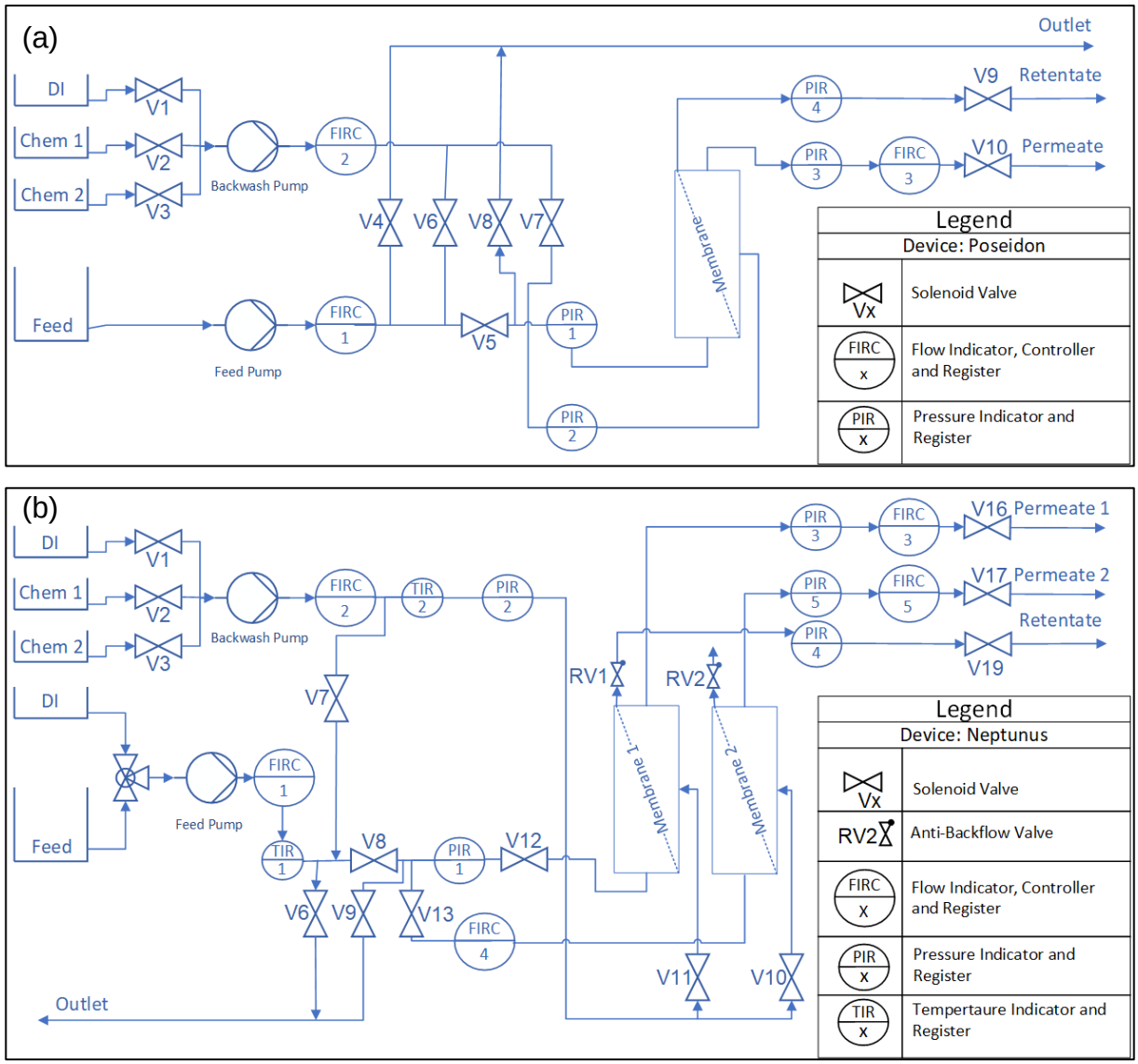

Figure 6: Schematic representation for (a) the Poseidon and (b) the Neptunus mini-plants dead-end filtration unit for constant flow rate

Both units were also supplied with magnetic valves and could therefore also be operated automatically controlled. The measurements of the flow meters and the pressure sensors were registered within an interval of 5 sec.

3.7.2 Filtration Experiments

3.7.2.1 Dead-end experiments using flat sheet membranes

Prior to filtration experiment, commercial flat sheet membranes were prepared using 50% ethanol solution overnight to eliminate manufacturing residuals and conservatives. Then, they were rinsed with pure water overnight to remove the ethanol. Pure water filtration at

constant pressure of 1 bar for 30 min was performed as pre-compaction. Then, pure water was filtered for 15 min at the intended filtration pressure, between 0.4 – 1 bar for determining the initial pure water permeability of the membrane. Thereafter emulsified oil samples were filtered at the same pressure as pure water until a total volume of 380 mL was collected at the permeate side.

3.7.2.2 Dead-end experiments using capillary membranes

Prior to filtration experiments, capillary membrane modules were rinsed to remove manufacturing residuals, bio-growth inhibitors and conservatives, and soaked overnight with NaOCl (50 ppm). Multiple-cycle dead-end filtration experiments with periodic hydraulic backwashing were conducted at constant flow rate employing either Poseidon or Neptunus filtration units. A schematic representation for the testing procedure is shown in Figure 7. As a default protocol, every mini-plant experiment started by filtering pure water at a flux of 100 L/(m²·h) for 15 min to determine initial pure water permeability. Thereafter, multiple filtration cycles were conducted at a constant flux of 100 L/(m²·h) for a total of six filtration cycles. Every filtration cycle lasted for 45 min, then it was followed by a hydraulic backwashing at a flux of 230 L/(m²·h) for 90 s. Finally, a short step of filtering pure water for testing the pure water permeability was carried out after each hydraulic backwash and before the subsequent filtration cycle.

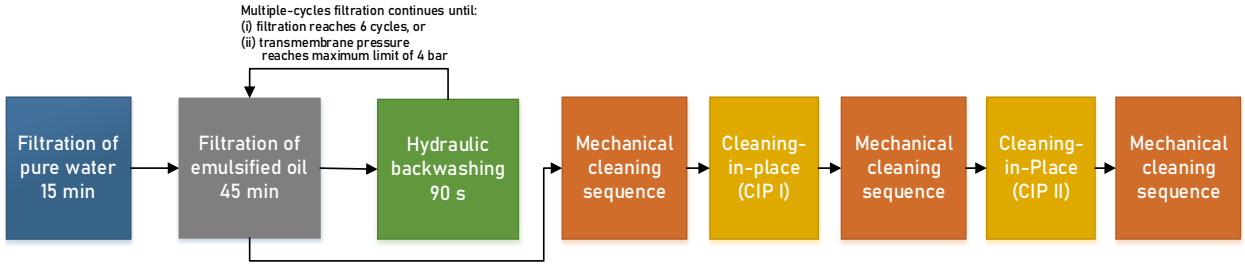

Figure 7: Schematic illustration of the default testing procedure for mini-plant multiple-cycles dead-end filtration tests employing lab-scale capillary membranes

Following the multiple-cycle filtration step, an alternating process of two chemical cleaning-in-place (CIP) steps and three mechanical cleaning sequences was applied for every membrane module as illustrated in Figure 7.Following the membrane manufacturer recommendation [136], CIP I was performed by flushing SDS solution of 1.2 g/L at flux of 120 L/(m²·h) for 10 min, then rinsing for 15 min, followed by flushing pure water at flux of

120 L/(m²·h) for 20 min. CIP II was performed using alkaline NaOCl solution of 200 mg/L Cl_2 at pH 12 at the same operating conditions of CIP I. The mechanical cleaning sequence comprised three pure water filtration steps at a flux of 100 L/(m²·h); each step lasted for 15 min and followed by a hydraulic backwashing at a flux of 230 L/(m²·h) for 90 s. Filtration experiments, in this report, were carried out following this described protocol unless other specification/parameters were mentioned. The separation performance was determined by measuring TOC, UV_{254} and PAHs for both feed and permeate at certain time intervals. Samples were collected during the first cycle (at 20 min and 40 min) and the second cycle (at 20 min).

3.7.2.3 Reference crossflow experiments using capillary membranes

Reference experiments were carried out in crossflow mode using the emulsified oils $E_{1,M}$ and $E_{2,U}$ at oil concentrations of 25 and 50 mg/L and constant SDS concentration of 60 mg/L. These experiments were conducted using Neptunus testing unit. The crossflow velocity and the feed pressure were set to 0.75 – 2.5 m/s and 0.6 bar, respectively. Every experiment was started with 30 min of pure water filtration to determine the initial pure water permeability, followed by 3 h of emulsified oil filtration. The permeate samples were collected after 30 min of filtration of emulsified oil and analyzed for TOC concentration to evaluate the separation efficiency of the membrane.

3.8 Hybrid UF tests with the dosage of PAC and/or coagulants

3.8.1 Hybrid UF tests using flat sheet membranes

Hybrid filtration experiments were carried out in which combinations of coagulation-UF, PAC-UF, and coagulation-PAC-UF were examined. First, reference standalone membrane filtration experiments were carried out, in which surfactant-free emulsified oils at concentration of 10 and 25 mg/L were employed. Both reference and hybrid experiments were performed using the manually operated unit at constant pressure condition. S100 and UP 150 flat sheet membranes were implemented.

In coagulations-based hybrid experiments, coagulant was dosed to the surfactant-free emulsified oil in the respective tank prior and the mixture was first subjected to a rapid mixing for 30 s at 300 rpm, then mixing speed was maintained at 50 rpm throughout the experiment.

In PAC-based hybrid experiments, PAC suspensions in pure water were filtered through the membrane, prior to the emulsified oil filtration, to form a PAC cake layer on the membrane surface. Then, pure water was filtered at 1 bar to measure the pure water permeability of the membrane. The emulsified oil was filtered at the same constant pressure of 1 bar until a total of 380 ml was collected.

In all experiments, the amount of filtered volume per unit time was measured to calculate the permeability. Samples of feed and permeate collected from every filtration cycle were characaterized in terms of TOC, UV_{254}, conductivity, pH and turbidity.

3.8.2 Hybrid UF tests using capillary membrane modules

To test the backwash efficiency for filtration experiments, hybrid UF experiments were additionally carried out using capillary membrane modules. Like those experiments with flat sheet membranes, reference experiments using standalone UF membranes were conducted using surfactant-free emulsified oil at concentration of 10 mg/L. Both reference and hybrid experiments were performed using Playground filtration unit at constant pressure condition. SM_1 and SM_2 capillary membrane modules were implemented. PAC and/or coagulant were/was dosed to the emulsified oil in the respective tank prior to the filtration. Coagulant tank was first subjected to a rapid mixing for 5 s at 300 rpm, then the mixing speed was maintained at 50 rpm throughout the experiment. PAC was stirred at 100 rpm along the experiment. Pure water was filtered at 0.4 bar to measure the pure water permeability. Then, the feed was filttered at the same constant pressure of 0.4 bar for either 30 or 45 min/cycle. Then, a backwash step of 90 s at constant pressure of 1 bar was performed. Samples from the permeate were collected after 20 min of the starting of the first filtration cycle and were chracterized in terms of TOC, UV_{254}, conductivity, pH and turbidity.

3.9 Semi-technical length and long-term hybrid filtration experiments

For examining the upscaling ability of the research results, lab-scale experiments were conducted using semi-technical length membrane modules with an active surface area of 0.22 m^2 or 0.055 m^2 when using LM or LM_2 membranes, respectively. The long-term experiments were performed using custom-designed testing system named “SRA filtration plant”. It can be operated at a constant flow rate up to 60 L/h and up to operation pressure

of 2.5 bars, as indicated in Figure 8. The unit is built of feed and backwash pumps, PID controllers and magnetic valves in addition to two dosing pumps, one for coagulant and one for PAC.

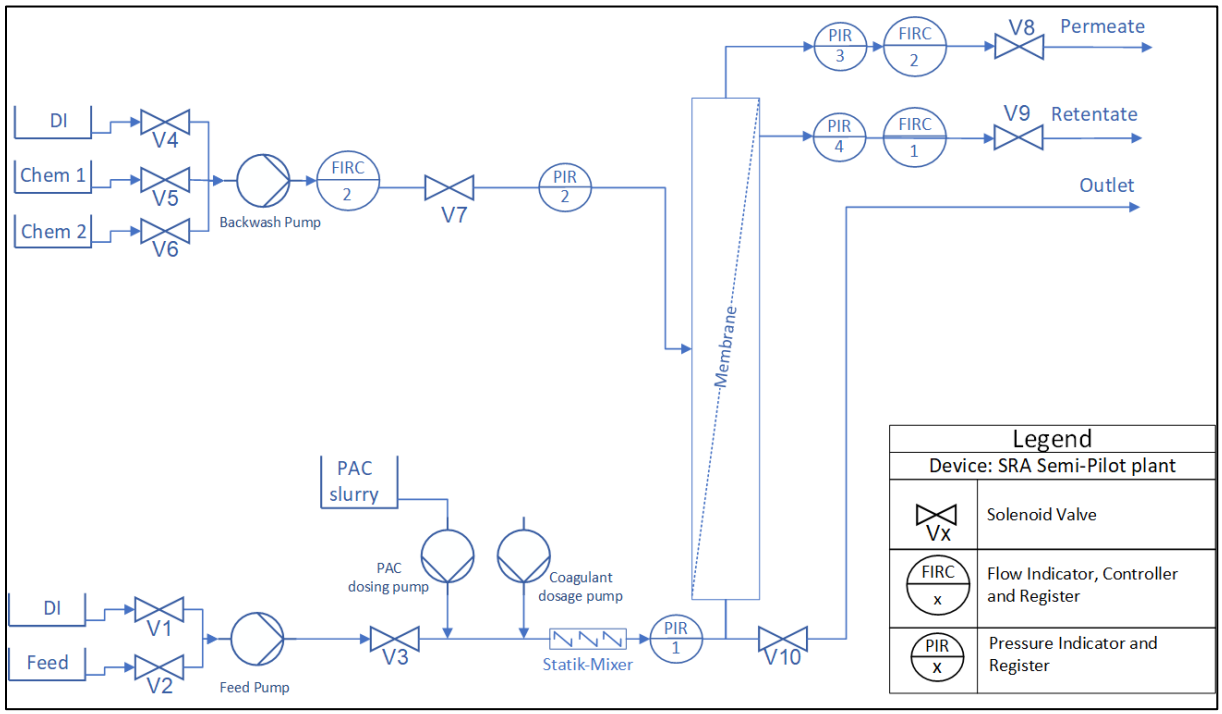

Figure 8: Schematic representation of the SRA dead-end filtration unit for constant flow rate

3.10 Statistical calculations and experimental design

3.10.1 Evaluation of membrane separation performance

The separation performance was determined by measuring turbidity, UV_{254}, TOC and in some cases PAH for both feed and permeate at certain time intervals. Retention ($\mathbb{R}$, %) was calculated according to Equation 1, where C_F and C_P represent the feed and permeate concentrations for the samples collected at the same time interval.

$$\mathbb{R}\% = \left(1 - \frac{C_P}{C_F}\right) \cdot 100\% \qquad \textbf{Equation 1}$$

3.10.2 Evaluation of membrane fouling

The membrane filtration performance was assessed by determining the filtered volume flow rate per unit time (Q) and the transmembrane pressure (TMP) along the filtration

course, which were then employed to calculate filtration flux (J) and membrane permeability (W) at a certain time following Equation 2 and Equation 3, respectively:

$$J\ (L/(m^2 \cdot h)) = \frac{Filtration\ rate}{membrane\ active\ surface\ area} = \frac{Q\ (L/h)}{A_m\ (m^2)} \qquad \textbf{Equation 2}$$

$$W\ (L/(m^2 \cdot \mathrm{h} \cdot \mathrm{bar})) = \frac{J\ (L/(m^2 \cdot h))}{TMP\ (bar)} \qquad \textbf{Equation 3}$$

Subsequently, unitless normalized permeability (W') during filtration experiment was determined by correlating the membrane permeability (W_t) at a certain filtration point t (one point was registered each 5 sec) to the initial pure water permeability (W_0) measured for every newly fresh membrane prior filtration by filtering DI at the testing conditions, as in Equation 4.

$$W' = \frac{W_t}{W_0} \qquad \textbf{Equation 4}$$

3.10.2.1 Extended fouling evaluation

For sections 4.3.1.2 and 4.3.1.3 the permeability recovery percentage ($PR\%$) after every filtration cycle was determined using Equation 5.

$$PR\% = \left(\frac{W_{t,BW}}{W_0}\right) \cdot 100\% \qquad \textbf{Equation 5}$$

Where $W_{t,BW}$ is the membrane permeability after every hydraulic backwashing step.

Most of the filtration experiments in sections 4.3.1.2 and 4.3.1.3 were repeated 2 – 5 times to investigate the results reproducibility. To evaluate the reproducibility quantitatively, the standard deviation of the normalized permeability for each registered measuring point i (σ_i) was calculated according to Equation 6. Thereafter, the average standard deviation of all points ($\sigma_{tot,av}$) was calculated according to Equation 7 and referred as "reproducibility indicator".

$$\sigma_i = \sqrt{\frac{\sum_{j=1}^{j=\mathrm{N}} (\boldsymbol{W'}_{i,j} - \boldsymbol{W'}_{i,av})^2}{N_i}} \qquad \textbf{Equation 6}$$

$$\sigma_{tot,av} = \frac{\sum_{i=1}^{i=n} \sigma_i}{n} \qquad \textbf{Equation 7}$$

whereas $W'_{i,j}$ is the normalized permeability at a certain time point i of a certain trial j, $W'_{i,av}$ is the average normalized permeability at a certain time point I, N is the number of repetitions for each filtration experiment, n is the number of points in every single experiment.

The status and growth of membrane fouling in hollow fiber PES membranes during multiple-cycle filtration of surfactant-free and surfactant-modified emulsified oils were analyzed from the permeability curves via determination of the total resistance after certain filtration cycle i ($R_{T,i}$, m^{-1}), and the total resistance after hydraulic backwashing ($R_{T,i,BW}$, m^{-1}) using Darcy's law (Equation 8and Equation 9).

$$R_{T,i} = \frac{1}{\mu\, W_i} \qquad \textbf{Equation 8}$$

$$R_{T,i,BW} = \frac{1}{\mu\, W_{i,BW}} \qquad \textbf{Equation 9}$$

W_i is the membrane permeability after filtration cycle i, $W_{i,BW}$ is the membrane permeability after hydraulic backwashing, and μ is fluid viscosity ($N{\cdot}s{\cdot}m^{-2}$). Subsequently, the distributive hydraulic reversible fouling resistance per cycle i ($R_{rev,i}$, m^{-1}) and the distributive hydraulic irreversible fouling resistance per one cycle i ($\Delta R_{irr,i}$, m^{-1}) were calculated using the resistance-in-series model (Equation 10 and Equation 11); the detailed procedure is described elsewhere [53].

$$R_{rev,i} = R_{T,i} - R_{T,i,BW} \qquad \textbf{Equation 10}$$

$$\Delta R_{irr,i} = R_{T,i,BW} - R_{T,i-1,BW} \qquad \textbf{Equation 11}$$

$R_{T,i-1,BW}$ is the total resistance after hydraulic backwashing for a previous filtration cycle $(i-1)$. While the cumulative hydraulic irreversible fouling ($R_{irr,i}$, m^{-1}) at certain filtration cycle i was calculated using Equation 12.

$$R_{irr,i} = R_{T,i,BW} - R_m \qquad \textbf{Equation 12}$$

R_m (m^{-1}) is the intrinsic resistance for a clean membrane determined using the initial pure water permeability.

3.10.3 Statistical experimental design

A series of experiments in dead-end operation mode were planned to examine the influence of filtration flux, filtration cycle duration, backwashing flux, backwashing duration, and post pure water filtration on the membrane performance and to determine the most-suited operating conditions (see section 4.3.1.8). Experiments were planned within the following operating parameters ranges: filtration fluxes in the range of 60 – 140 L/m²·h, filtration cycle durations in the range of 30 -60 min, backwashing fluxes in the range of 160 - 300 L/m²·h, backwashing duration in the range of 30 - 90 s, and post pure water filtration durations in the range of 0 - 10 min (with a flux equal to the filtration flux). An experimental plan was created using the design of experiment model, as described by Kleppmann (2016) for nonlinear relationships [137], resulting in a total of 46 experiments. The detailed list of experiments along with the respective recovery values are shown in Table 7.The experiments were conducted using surfactant-modified emulsions with oil concentration of 10 mg/L and SDS concentration of 0.48 g/L and SM membranes. The total fouling at the end of the experiment was utilized as the output parameter for these experiments, which was calculated as (initial pure water permeability - the permeability at the end of the last cycle) / initial pure water permeability in %.

Table 7: Detailed listing of the parameter values for the design of experiments. The experimental conditions were set using nonlinear 2-factorial design of experiment (DOE) for five parameters: i.e., filtration flux, filtration duration, backwash flux and pure water filtration duration as well as the respective recovery for each combination.

Exp. Nr.	Filtration flux (L/m²·h)	Filtration cycle duration (min)	Backwash flux (L/m²·h)	Backwash duration (s)	Pure water filtration duration (min)	Recovery (%)
Exp 01	60	30	160	30	3	86
Exp 02	140	30	160	30	3	88
Exp 03	60	60	160	30	3	93
Exp 04	140	60	160	30	3	94
Exp 05	60	30	300	30	3	82
Exp 06	140	30	300	30	3	86
Exp 07	60	60	300	30	3	91
Exp 08	140	60	300	30	3	93
Exp 09	60	30	160	90	3	77
Exp 10	140	30	160	90	3	84
Exp 11	60	60	160	90	3	88

Exp. Nr.	Filtration flux (L/m²·h)	Filtration cycle duration (min)	Backwash flux (L/m²·h)	Backwash duration (s)	Pure water filtration duration (min)	Recovery (%)
Exp 12	140	60	160	90	3	92
Exp 13	60	30	300	90	3	65
Exp 14	140	30	300	90	3	79
Exp 15	60	60	300	90	3	83
Exp 16	140	60	300	90	3	90
Exp 17	60	30	160	30	7	72
Exp 18	140	30	160	30	7	75
Exp 19	60	60	160	30	7	86
Exp 20	140	60	160	30	7	87
Exp 21	60	30	300	30	7	68
Exp 22	140	30	300	30	7	73
Exp 23	60	60	300	30	7	84
Exp 24	140	60	300	30	7	87
Exp 25	60	30	160	90	7	63
Exp 26	140	30	160	90	7	71
Exp 27	60	60	160	90	7	82
Exp 28	140	60	160	90	7	85
Exp 29	60	30	300	90	7	52
Exp 30	140	30	300	90	7	66
Exp 31	60	60	300	90	7	76
Exp 32	140	60	300	90	7	83
Exp 33	28.6	45	230	60	5	71
Exp 34	171.4	45	230	60	5	86
Exp 35	100	18.2	230	60	5	60
Exp 36	100	71.7	230	60	5	90
Exp 37	100	45	105	60	5	87
Exp 38	100	45	355	60	5	81
Exp 39	100	45	230	6.5	5	88
Exp 40	100	45	230	113.5	5	79
Exp 41	100	45	230	60	1.4	92
Exp 42	100	45	230	60	8.6	76
Exp 43	100	45	230	60	5	84
Exp 44	100	45	230	60	5	84
Exp 45	100	45	230	60	5	84
Exp 46	100	45	230	60	5	84

3.11 Environmental and economic assessment

To evaluate the feasibility of the developed strategies, a comparison was made with the crossflow operation, which served as the reference. As mentioned in section 2.4, in this

study, the focus was on examining the differences in dosed substances and electrical energy consumption. These differences formed the basis for assessing the environmental and economic feasibility of the enhanced dead-end methods. These parameters were presented and quantified in terms of cost and CFP.

3.11.1 Energy consumption of dead-end and crossflow operation of membranes

Pumps requires most of the energy for both crossflow and dead-end operation regimes. Those are feed and recirculation pumps for crossflow, and feed and backwash pumps for dead-end. The amount of energy consumed by a pump (EN) in what-hours can be calculated as the power in watts multiplied by the operation time in hours (t). Thereafter, E_s, the specific energy used per unit volume pumped by a single pump, measured in watt-hours per cubic meter (Wh/m³) by dividing the consumed energy by the net permeate flow the specific energy consumption of a single pump (EN_s) can be calculated as described by Equation 13 [138].

$$EN_s = \frac{EN}{\bar{Q}_P} = \frac{Power \cdot t}{\bar{Q}_P} = \frac{Q \cdot P}{\eta} \cdot \frac{t}{\bar{Q}_P} \qquad \textbf{Equation 13}$$

Where Q is the volumetric flow rate in cubic meters per second (m³/s), and P is the pressure that is delivered by the pump. $\bar{Q}_P$ represents the net permeate flow rate in cubic meters per second (m³/s) [138].

Furthermore, the specific energy consumption for crossflow considering an energy recovery from the pressure of the concentrate side was implemented can be calculated following Equation 14

$$EN_{S,CFW} = \frac{(\bar{Q}_F \cdot \bar{P}_F) - (\bar{Q}_C \cdot \bar{P}_C)}{3600 \cdot \eta_F \cdot \bar{Q}_P} \qquad \textbf{Equation 14}$$

Where $\bar{Q}_F$, $\bar{Q}_C$ and $\bar{Q}_P$ are the average feed flow rates of feed, concentrate and Permeate sides in m³/s, respectively. $\bar{P}_F$ and $\bar{P}_c$ are the average pressure values at the feed and concentrate sides in pascals, respectively. η_f is the efficiency of the feed pumps.

Similarly, the energy consumption of the dead-end modes is shown in Equation 15.

$$EN_{S,DE} = \frac{(\bar{Q}_F \cdot \bar{P}_F \cdot \Delta t_{Filt.}/3600 \cdot \eta_S) + (\bar{Q}_{BW} \cdot \bar{P}_{BW} \cdot \Delta t_{BW}/3600 \cdot \eta_S)}{\bar{Q}_P \cdot \Delta t_{Fill} - \bar{Q}_{BW} \cdot \Delta t_{BW}}$$ **Equation 15**

Where $\bar{Q}_{BW}$ is the mean BW flow rate in cubic meters per second (m³/s), $\bar{P}_{BW}$ is the mean pressure at the BW side, Δt_{Fill} and Δt_{BW} are the durations of the filtration and backwash steps in seconds, respectively, and η_S is the pump efficiency.

The specific energy consumption per cubic meter of permeate produced, E_S, was determined according to Equation 13. Subsequently, the energy consumption difference between crossflow and dead-end operation (ΔEN_S) was calculated using Equation 16.

$$\Delta EN_S = EN_{S,CFW} - EN_{S,DE}$$ **Equation 16**

Then, the difference in SDS dosage between crossflow and dead-end operation (ΔC_{SDS}) was calculated using Equation 17, considering that no SDS was dosed during crossflow operation.

$$\Delta C_{SDS} = C_{CFW} - C_{DE} = 0 - C_{DE} = -C_{DE}$$ **Equation 17**

Where C_{CFW} refers to the concentration of SDS in crossflow, while C_{DE} refers to the concentration of SDS dosed in dead-end operation.

The difference in the costs of crossflow and dead-end operation (ΔCost) can be calculated using Equation 18.

$$\Delta\text{Cost} = \text{Cost}_{CFW} - \text{Cost}_{DE}$$ **Equation 18**

Where Cost_{CFW} is the cost of crossflow operation and Cost_{DE} is the cost of dead-end operation. However, as the cost difference in this study is primarily due to the differences in energy consumption and SDS dosage ΔCost can be calculated using Equation 19.

$$\Delta\text{Cost} = \Delta\text{Cost}_E + \Delta\text{Cost}_{SDS}$$ **Equation 19**

ΔCost_{SDS} can be calculated using the difference in the dosage concentration (ΔC_{SDS} in g/L) and the cost of one gram of SDS (Cost_{SDS} in €/g), as indicated in Equation 20.

$$\Delta\text{Cost}_{SDS} = \Delta C_{SDS} \cdot \text{Cost}_{SDS}$$ **Equation 20**

$\Delta Cost_{EN}$ can be determined by calculating the difference in energy consumption between crossflow and dead-end operations, ΔEN, and multiplying it by the cost of the energy source ($Cost_{EN}$) as shown in Equation 21.

$$\Delta \mathrm{Cost}_E = \Delta EN \cdot \mathrm{Cost}_{EN} \quad \textbf{Equation 21}$$

The implemented environmental assessment methodology utilized the total CFP as the primary metric. CFP was chosen over Global Warming Potential (GWP) and Carbon Intensity (CI) to calculate the environmental impact of dead-end and crossflow modes. This choice is justified by capability of CFP to quantify the CO_2 equivalent (CO_2e) of both direct and indirect GHGs, thereby representing their combined impact in CO_2e units.

The difference in CFP between crossflow and dead-end operations, represented as ΔCFP, is calculated by subtracting the carbon footprint for dead-end mode (CFP_{DE}) and for crossflow mode (CFP_{CFW}), as described in Equation 22.

$$\Delta CFP = CFP_{CFW} - CFP_{DE} \quad \text{Equation 22}$$

Additionally, since the difference is primarily attributed to the variation in CFP resulting from energy consumption (ΔCFP_E) and SDS dosage (ΔCFP_{SDS}), ΔCFP can be calculated using Equation 23:

$$\Delta CFP = \Delta CFP_{EN} + \Delta CFP_{SDS} \quad \text{Equation 23}$$

ΔCFP_{SDS} can be calculated using Equation 24, where the dosage concentration (ΔC_{SDS}) in g/L is multiplied by the CFP_{SDS} per gram.

$$\Delta CFP_{SDS} = \Delta C_{SDS} \cdot CFP_{SDS} \quad \text{Equation 24}$$

ΔCFP_{EN} can be determined as the difference in energy consumption between crossflow and dead-end modes (ΔEN) multiplied by the CFP_{EN} of the applied energy source, as indicated in Equation 25.

$$\Delta CFP_{EN} = \Delta EN \cdot CFP_{EN} \quad \text{Equation 25}$$

Based on this calculation, if the value of ΔCFP is positive, it indicates that the CFP of crossflow mode is higher than that of dead-end mode. Conversely, if ΔCFP is negative, the CFP of dead-end mode is higher than that of crossflow mode.

Similarly, for ΔCost, if the value is positive, it signifies that the costs for crossflow operations are higher than those for dead-end operations. Conversely, if ΔCost is negative, the costs for dead-end operations are higher than those for crossflow operations.

4 Results and Discussions

4.1 Establishment of a standard protocol for the production of synthetic OWWE

4.1.1 Analysis of real PW sample

To determine the characteristics for real PW, a sample was obtained from an operator of an oil extraction well in Germany. The real PW sample was analyzed in terms of oil droplet size distribution. As the application of synthetic oil emulsions to be produced in this study was to mimic PW prior to tertiary treatment step, the droplet size measurement of the real PW sample was targeting sub-micron sized droplets only. This was realized by activating the option of “sub-micron only” in the operating software of the particle size analyzer. As depicted in Figure 9, the real PW sample exhibited oil droplet size distribution with d_{32}, $D_{10,N}$, $D_{90,N}$, $D_{10,V}$ and $D_{90,V}$ values of 0.67, 0.25, 0.64, 0.37 and 1.76 µm, respectively. The measured oil droplets sizes were comparable to the values reported in literature [30-35].

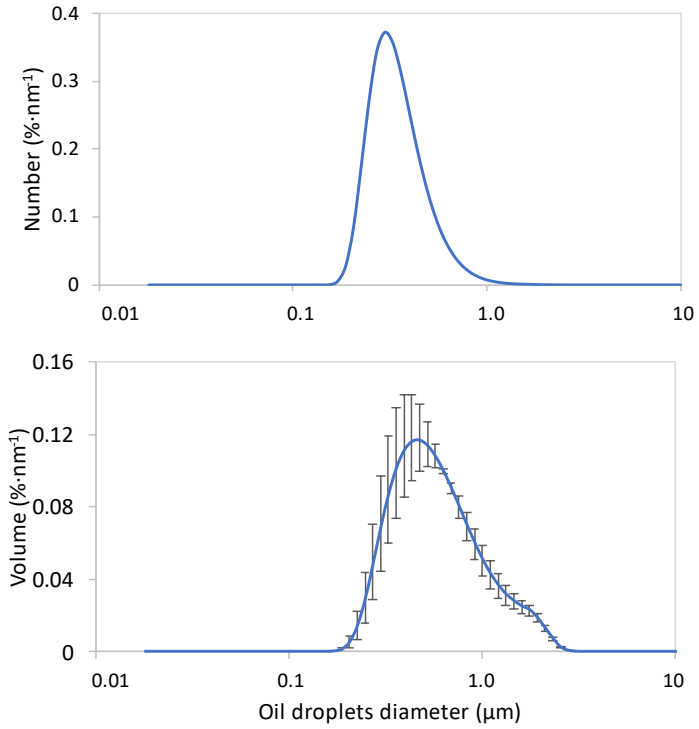

Figure 9: Differential number and volume size distributions for sub-micron oil droplets in real PW sample with min/max error bars

4.1.2 Preparation of HPH-based emulsified oil (E_1)

The produced HPH-based emulsified oil $E_{1,P}$ exhibited an oil droplet size distribution with $D_{50,N}$, $D_{50,V}$, $D_{90,v}$, and d_{32} of 1.37, 1.24, 2.43, and 0.94 µm, respectively. This emulsified oil type was already produced in a previous work aimed at testing the performance of surface-modified PES ultrafiltration membranes [56]. However, to investigate the influence of oil droplet size distribution on the membrane fouling mechanisms, model oil-in-water emulsions based on $E_{1,P}$ but with different oil droplet size distributions had to be produced. For generating different oil droplet size distribution profiles, it was important to control the energy input. This was accomplished through the adjustment of emulsification parameters, specifically the emulsification pressure P_E in conjunction with the number of emulsifications passes N_{PS} and O/W ratio.

As illustrated in Figure 10a, varying the emulsification pressure P_E at levels of 450, 1,000, 1,500, and 1,900 bar resulted in slight alterations in the oil droplet size distributions of the HPH-based emulsified oils E_1. Specifically, the mean droplet size $D_{50,N}$, exhibited a limited decrease measuring approximately 0.70, 0.71, 0.67, and 0.61 µm, respectively. This

observation indicates that elevating the emulsification pressure P_E did not yield a substantial reduction in the oil droplet size distribution. On the other hand, Figure 10b reveals the more significant impact of N_{PS}, at a constant P_E of 1,900 bar, on the oil droplet size distributions. Here, the increase in N_{PS} from 1 to 8 resulted in a reduction in the average oil droplets size. Specifically, d_{32} values were measured approximately to be 0.58, 0.41, 0.24, 0.23, and 0.18 µm, respectively, for 1, 2, 4, 6, and 8 passes. Furthermore, it was observed that other parameters, e.g., variation of O/W ratio prior to emulsification step had also a minor influence on the oil droplets sizes of the final product.

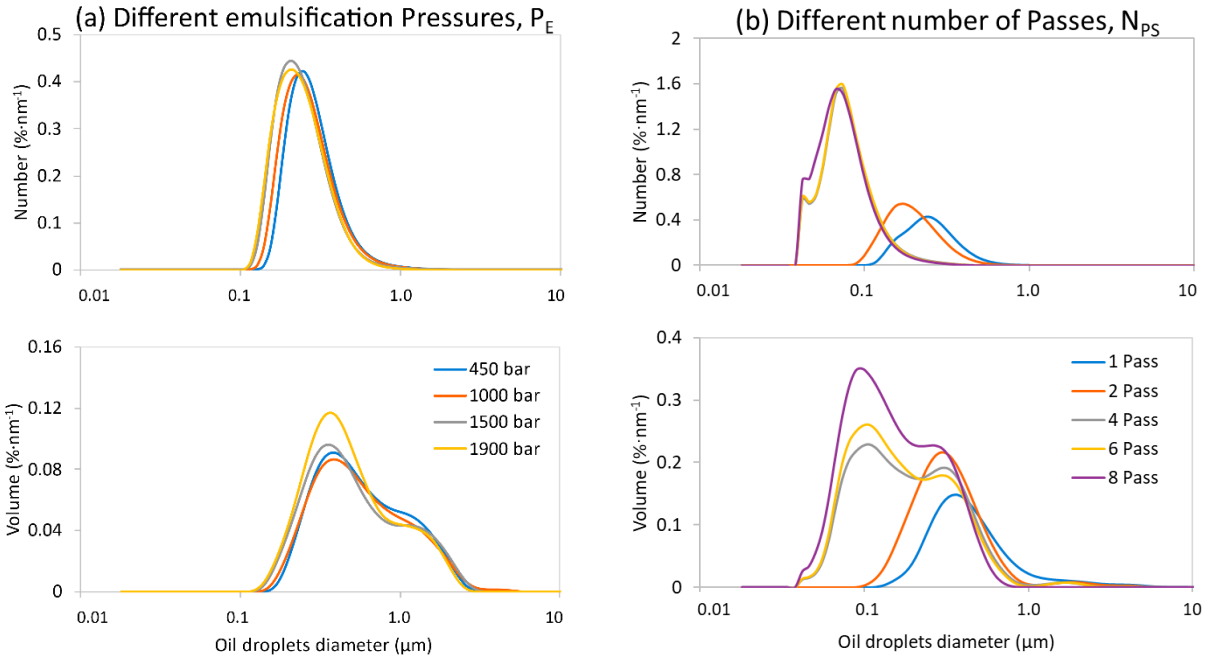

Figure 10: Differential number and volume size distributions for HPH-based emulsified oils E_1 at (a) different P_E of 450, 1,000, 1,500 and 1,900 bar for one pass, as well as (b) at different N_{PS} and P_E of 1,900 bar. O/W = 1/250

Following a series of adaptation trials, three chemically identical HPH-based emulsified oils E_1 with distinct oil droplet size distributions were successfully produced by employing certain values for O/W, P_E, and N_{PS}. As listed in Table 8, three HPH-based emulsified oils denoted as $E_{1,B}$, $E_{1,M}$ and, $E_{1,S}$, all exhibited a unique oil droplet size distribution, were effectively prepared through implementation of specific combinations of [O/W, P_E, N_{PS}], namely [1/250, 1,700, 1], [1/250, 1,700, 2], and [1/1,000, 1,700, 4], respectively. To achieve an emulsion with droplet size like $E_{1,S}$ using an O/W of 1/250, usually five to six passes were needed, this was reduced to four by reducing the O/W to 1/1,000, to save the required preparation time.

Table 8: Emulsification parameters for the preparation of HPH-based emulsified oils $E_{1,B}$, $E_{1,M}$, and $E_{1,S}$ along with oil droplet size distributions

Emulsified oil	O/W (V/V)	Pressure (bar)	Number of Passes	d_{32} (µm)	$D_{10,N}$ (µm)	$D_{90,N}$ (µm)	$D_{10,V}$ (µm)	$D_{90,V}$ (µm)
$E_{1,B}$	1/250	1,000	1	1.04	0.57	1.06	0.67	1.91
$E_{1,M}$	1/250	1,700	2	0.39	0.13	0.37	0.22	1.58
$E_{1,S}$	1/1,000	1,700	4	0.23	0.05	0.18	0.11	0.51

The stability and reproducibility of HPH-based emulsified oils E_1 with respect to the oil droplet size distribution were consistently observed. As an illustrative example, Figure 11 presents the oil droplet size distributions for a representative emulsified oil $E_{1,M}$ immediately after preparation as well as after the storage for two and six days. Notably, the emulsified oils $E_{1,M}$ exhibited d_{32} of 0.43, 0.42 and 0.43 µm, $D_{90,N}$ of 0.43, 0.43 and 0.44 µm and $D_{90,V}$ of 1.29, 1.31 and 1.33 µm for a freshly prepared sample, a two-days stored sample, and a six-days stored sample, respectively. The observed small variations in values were not significant. That certainly indicates the stability of the produced HPH-based emulsified oil over the course of six days.

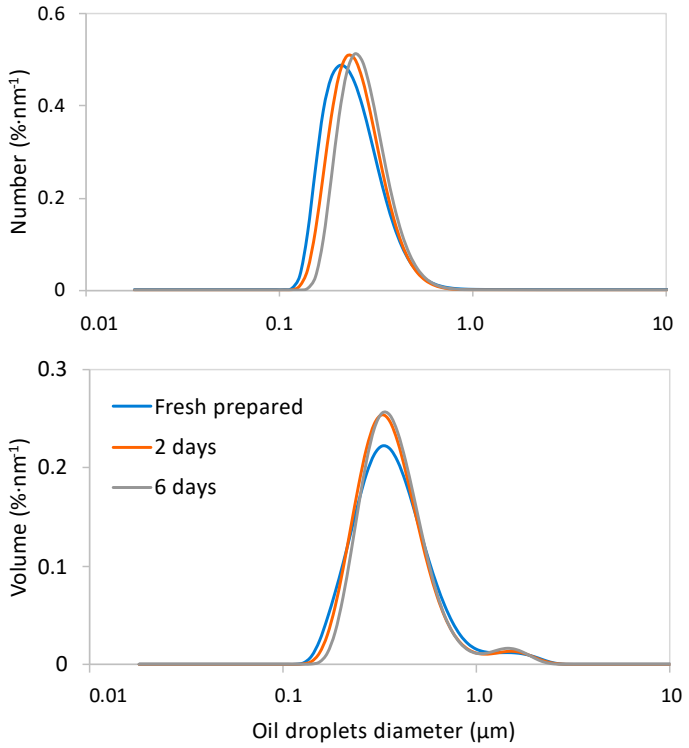

Figure 11: Oil droplet size distributions for three samples of a representative emulsified oil $E_{1,M}$ stored at different times. $E_{1,M}$ was prepared at O/W 1:250 and P_E 1,700 bar for 2 passes

Moreover, the reproducibility of emulsified oil $E_{1,M}$ was found to be highly consistent. As in Figure 12, the average differential volume distribution density was assessed for twelve preparation batches along with the corresponding standard deviations. The oil droplet size distribution profiles for these twelve preparation batches exhibited average values of d_{32}, $D_{10,N}$, $D_{90,N}$, $D_{10,V}$ and $D_{90,V}$ of 0.40, 0.12, 0.36, 0.22 and 1.63 µm, with standard deviations of 0.04, 0.04, 0.05, 0.02 and 0.51 µm, respectively. Analogously, all HPH-based emulsified oils exhibited high degree of reproducibility.

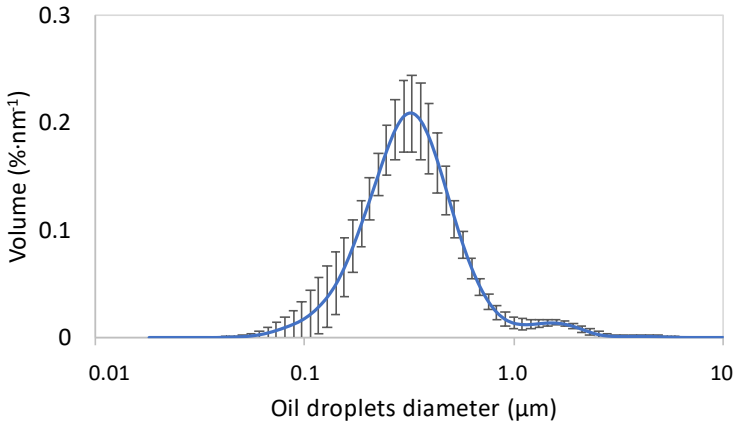

Figure 12: Average differential volume distribution density for twelve preparation batches for a representative emulsified oil $E_{1,M}$. Error bars indicate standard deviation

4.1.3 Preparation of US-based, emulsified oil (E_2)

The reference emulsified oil reported by Dardor et al. [60], R_{E2}, had an oil droplet size distribution of 1 - 63 µm, with mean, $D_{50,V}$, and $D_{90,V}$ values of 4.6, 2.31, and 6.4 µm, respectively, see Table 9. This procedure was reproduced and upgraded (cf. section 3.3.3) producing two emulsified oils $E_{2,P}$ and $E_{2,U}$, respectively. The oil droplet size distributions for $E_{2,P}$ and $E_{2,U}$ emulsified oils are shown in Table 9.

Table 9. Oil droplet size distributions for RE_2 (as reported [60], reproduced ($E_{2,P}$) and upgraded ($E_{2,U}$) emulsified oils

Sample	Mean (µm)	d_{32} (µm)	$D_{10,N}$ (µm)	$D_{50,N}$ (µm)	$D_{90,N}$ (µm)	$D_{10,V}$ (µm)	$D_{50,V}$ (µm)	$D_{90,V}$ (µm)
RE_2, Reference[1]	4.6	N.A.	N.A	N.A.	N.A	N.A	2.31	6.4
$E_{2,P}$, Reproduced	5.36	1.29	0.06	0.10	0.21	0.50	4.1	10.89
$E_{2,U}$, Upgraded	3.86	1.20	0.06	0.10	0.26	0.48	2.78	6.86

[1]Refereing to samples with low salinity in [60]

Figure 13 shows the oil droplet size distribution for two preparation batches of $E_{2,P}$; the size of oil droplets was 1.5 - 2 times the size of oil droplets in RE_2. This can be related to the different sources of crude oil, machinery, ambient conditions and human error. However, the method can be claimed to be successfully reproduced.

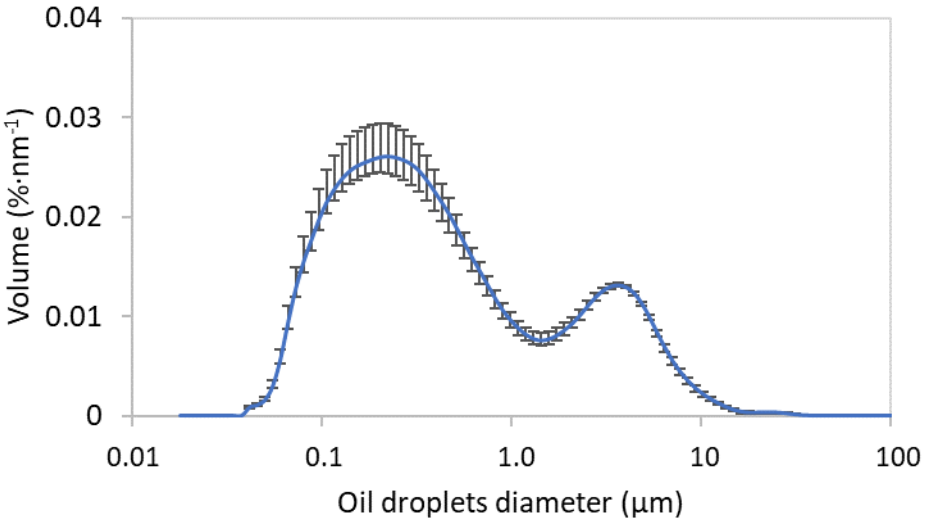

Figure 13: Average differential volume size distributions for two batches of $E_{2,P}$. Error bares represent min/max values

As shown in Figure 14, the oil droplet size distribution of $E_{2,U}$ is comparable to those of $E_{2,P}$ (cf Figure 13 and Table 9) and RE_2 (cf. Table 9) but with a high deviation. The $E_{2,U}$ batches had average values for $D_{10,V}$, $D_{50,V}$ and $D_{90,V}$ of 0.48, 2.78 and 6.86 µm compared to 0.50, 4.10 and 10.89 µm for $E_{2,P}$.

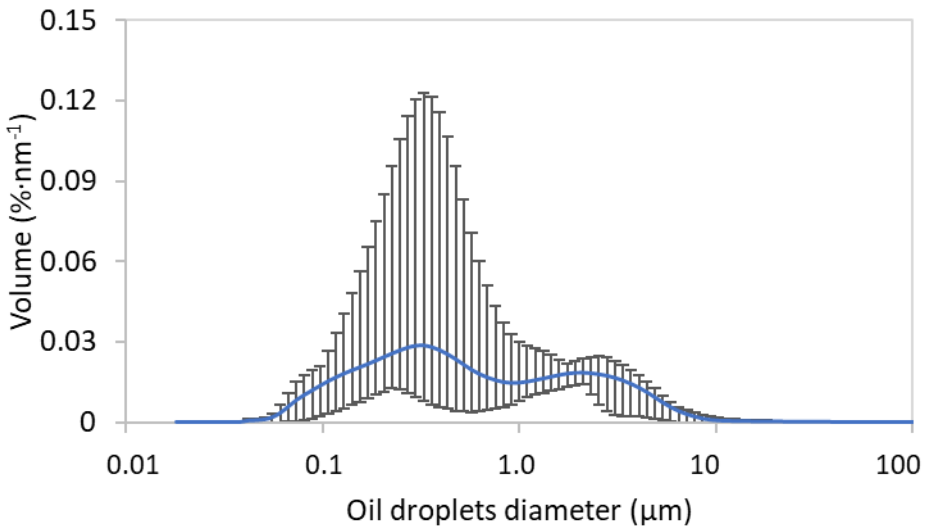

Figure 14: Differential volume size distribution for two batches of $E_{2,U}$. Error bars represent min/max values

As aforementioned in section 3.4.3, the preparation procedure for US-based emulsified oils included a step, where oil emulsion was allowed to settle in a separating funnel to simulate primary skimming or phase separation to remove free oil layer as is common in practice. Subsequently, controlling the oil emulsion composition was challenging. Table 10 shows TOC, UV_{254} absorbance, turbidity, conductivity, and pH values for RE_2 (as reported), $E_{2,P}$ and $E_{2,U}$ emulsions. It was noticed that $E_{2,P}$ exhibited lower TOC and turbidity values than in case of RE_2, but UV_{254} absorbance was higher. This might be essentially related to the different nature of crude oils, i.e., different portions of unsaturated hydrocarbons.

Table 10: TOC, UV_{254} absorbance, turbidity, conductivity, and pH for US-based emulsified oils. (±) represents standard error

Sample, Salinity	Nr. of trials	TOC (mg/L)	UV_{254} (m^{-1})	Turbidity (NTU)	EC (mS/cm)	pH
RE_2, Reference[1]	2	118 ±13	1.46 ±0.30	261	7.06 ±0.12	8.0 ±0.1
$E_{2,P}$, Reproduced	5	28.1 ±3.7	4.68 ±0.27	65 ±22	6.95 ±0.98	8.2 ±0.1
$E_{2,U}$, Upgraded	4	66.7 ±4.8	12.25 ±0.18	139±31	7.17 ±0.35	7.7 ±0.2

[1]Refereing to low salinity sample in [60]

Compared to $E_{2,P}$, $E_{2,U}$ exhibited higher TOC, UV_{254}, and turbidity values. This can be caused by the different types of ultrasonication (cf. Section 3.3.3). Bath ultrasonication provides constant energy input but can be influenced by water bath volume and container

type, while horn ultrasonication provides local energy input with direct contact with the sample. Subsequently, horn ultrasonication could disperse higher oil fractions, and consequently, much less free oil was separated during the settling step. This hypothesis is supported by the almost constant relationship of TOC to UV_{254} absorbance meaning that the organics composition was not changed by the upgrading process. On the other hand, conductivity and pH values were similar for all emulsified oils.

4.1.4 Assessment of the preparation methods

This assessment aimed at comparing HPH-based and US-based methods for the effective preparation of emulsified oils mimicking real PW samples and identifying the most suitable preparation method for the subsequent mini-plant membrane filtration experiments. Both methods were found to provide emulsified oils that fit our objectives.

4.1.4.1 Fouling behavior and separation performance of HPH- and US-based preparation methods

To keep the chemical composition of emulsified oils as similar as possible, SDS and salts were added at the same concentrations to both $E_{1,M}$ and $E_{2,U}$. Filtration experiments were conducted as explained in Section 3.7.2.3. Prior to oil filtration, hollow fiber membranes exhibited an initial pure water permeability of 400 - 500 L/(m^2·h·bar) in all experiments. As shown in Figure 15**,** filtration tests using $E_{1,M}$ and $E_{2,U}$ emulsified oils at two oil concentrations exhibited a moderate to sharp normalized permeability decline within the first 30 min of filtration, afterward almost consistent membrane performance was noticed in all experiments. $E_{1,M}$ and $E_{2,U}$ showed different fouling rates. $E_{1,M}$ with oil concentrations of 25 and 50 mg/L caused membrane performance decay of 60 % and 90 %, respectively. While less membranes fouling, performance decay of 30 % and 75 %, was observed for experiments using $E_{2,U}$ with oil concentrations of 25 and 50 mg/L, respectively. This can be attributed to the different oil droplets size distributions for $E_{1,M}$ and $E_{2,U}$, due to different emulsification techniques. For instance, the bigger oil droplets in $E_{2,U}$ seemed to cause less severe fouling than in case of $E_{1,M}$ with smaller oil droplets.

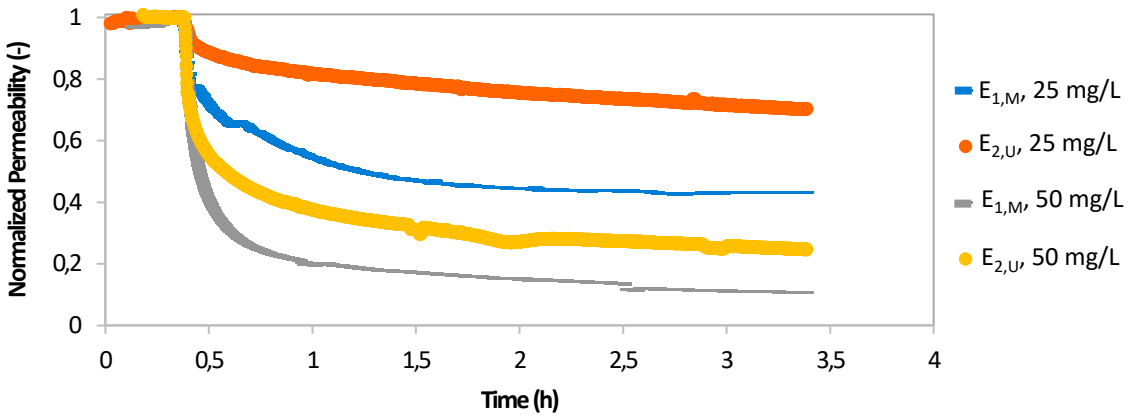

Figure 15: Normalized permeability curves for crossflow filtration experiments using $E_{1,M}$ and $E_{2,U}$ with oil concentrations of 25 and 50 mg/L

Additionally, the separation efficiency was assessed by analyzing TOC concentration in feed and permeate. The results revealed slight differences in TOC retention values. Average TOC retention values of 62 % and 56 % were measured for experiments using $E_{1,M}$ and $E_{2,U}$ with oil concentration of 25 mg/L, respectively. While average TOC of 56 % and 59 % measured for experiments using $E_{1,M}$ and $E_{2,U}$ with oil concentration of 50 mg/L, respectively. This indicates comparable membrane separation performance during experiments using both emulsified oil types. In earlier study, TOC retention for experiments using HPH-based emulsified oil (25 mg/L) without SDS and/or salts was reported to be about 97 % [30]. The lower TOC retention values measured here can be attributed to SDS portions that are not retained by the UF membrane [30].

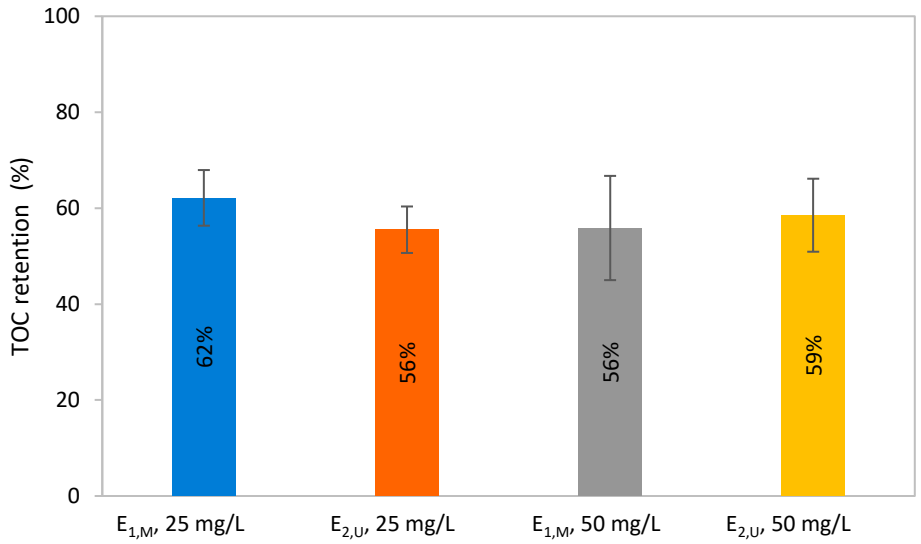

Figure 16: TOC retention measured during membrane filtration tests using $E_{1,M}$ and $E_{2,U}$ emulsified oil with oil concentrations of 25 mg/L and 50 mg/L

Overall, despite of different membrane fouling rates caused by $E_{1,M}$ and $E_{2,U}$, both emulsified oils were found to induce significant membrane fouling analogous to real PW. Therefore, both emulsified oils can be employed as synthetic PW for evaluating new separation techniques including membrane technology.

4.1.4.2 Assessment of preparation methods from a technical point of view

As summarized in Table 11, the HPH-based preparation method can offer several advantages, for instance, high reproducibility ensuring consistent product for multiple batches, and good control of emulsified oil composition facilitating effective adjustment to meet certain experiment requirements. This method is also capable of producing emulsified oils with various oil droplet size distributions, and generating stable surfactant-free emulsified oils that can be advantages for certain applications. However, it is important to consider one drawback that is the availability of HPH equipment along with high tear and wear rates. Thus, maintenance is often required several times per year posing budgetary constraints.

Table 11: Technical comparison of HPH-based and US-based methods

Method	HPH-based method (e.g., $E_{1,M}$)	US-based method (e.g., $E_{2,U}$)
Time required to prepare 20 L emulsified oil (25 mg/L as TOC)	~2 h @ O/W = 1:250, P_E = 1,700 bar and N_{PS} = 2	~7 h @ horn ultrasonication (for 2 min per 0.5 L batch)
Advantages	• High reproducibility • Better control of oil composition • Different oil droplet size distributions • Stable surfactant-free emulsified oil was possible	• More common and less complex equipment • Low maintenance costs
Disadvantages	• Complex equipment required • High maintenance costs	• Time consuming • Hard to control oil composition • low reproducibility regarding oil concentration • Emulsified oils with different oil droplets size cannot be achieved by adapting energy input • Stable surfactant-free emulsified oil was not possible

The US-based method can also offer some advantages. Ultrasonication is a rather common laboratory equipment, besides it needs less maintenance costs compared to HPH. Nonetheless, the application of US-based method beyond bench-scale preparations is a major limitation, since it is time-consuming. Compared to HPH, other downsides can include less controlling of emulsified oil composition, relatively lower reproducibility in terms of oil concentration, and less capability of producing emulsified oils with different oil droplet sizes via adjusting the energy input. Moreover, production of stable surfactant-free emulsified oil cannot be achieved so far. Therefore, decision regarding the most convenient method depends on the research objectives, application conditions, and the available lab facilities.

4.2 Understanding the main fouling mechanisms of dead-end operated PES UF membranes

4.2.1 Influence of oil droplet size distribution on fouling behavior of flat sheet membranes with different pore size distribution

4.2.1.1 Studying of membranes fouling behavior at constant flux condition

Three emulsified oil feeds, i.e. $E_{1,S}$, $E_{1,M}$ and $E_{1,B}$ were filtered through flat sheet membranes S800, S450 , S100 and IG, exhibiting pore size distributions of 0.8, 0.45, 0.1 and 0.02 µm. In this section, S800 and S450 were labeled as MF membranes, while S100 and IG were labeled as UF membranes. In general, a strong relationship was observed between membrane fouling behavior and average oil droplet size distribution. Permeability curves for filtration experiments using $E_{1,S}$, $E_{1,M}$ and $E_{1,B}$ through S800 and S450, are shown in Figure 17 A and B. Besides, the respective fouling mechanisms are indicated in Figure 17 C and D. In which it is noticed that $E_{1,S}$ and $E_{1,M}$ feeds caused higher permeability decline than in case of $E_{1,B}$, that might be explained by strong internal membrane fouling because of the low average oil droplet size in case of $E_{1,S}$ and $E_{1,M}$ compared to membrane pore diameters. Moreover, the chronological analysis of fouling mechanisms indicated that more than 90% of the decay in MF membrane performance during filtration of $E_{1,S}$ and $E_{1,M}$ was caused by pore blocking, i.e. intermediate and standard pore blocking.

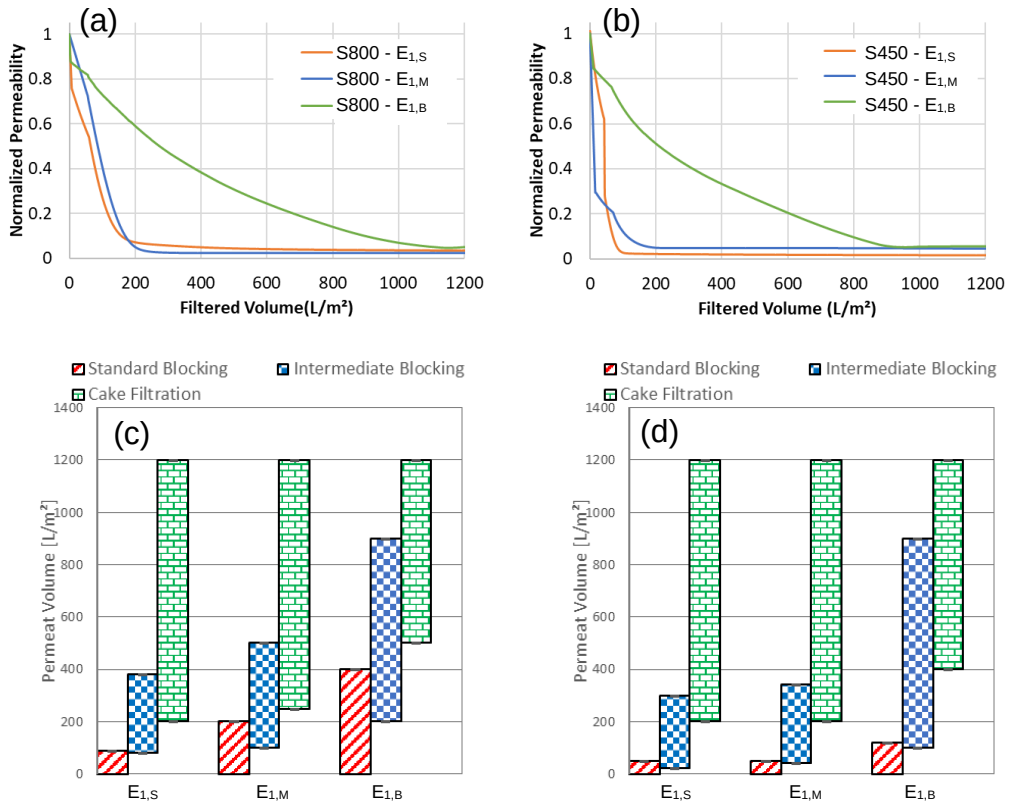

Figure 17: Normalized permeability curves (A and B) and the respective fouling chronological evolution (C and D) during the filtration of $E_{1,S}$, $E_{1,M}$ and $E_{1,B}$ using MF membranes S800 (A and C) and S450 (B and D) at constant flux of 1,300 L/(m²·h), one trial

Nevertheless, in case of UF membranes, i.e. S100 and IG, the permeability curves for filtration experiments using $E_{1,S}$, $E_{1,M}$ and $E_{1,B}$ through UF membranes (cf. Figure 18 A and B) and the respective fouling mechanisms (cf. Figure 18 C and D) indicated that only $E_{1,S}$ caused severe decline in the membrane permeability than in cases of $E_{1,M}$ and $E_{1,B}$, which supports certainly the hypothesis that feed solutions containing oil droplets smaller than / comparable to membrane pore diameters might lead to substantial decay in membrane performance due to severe internal membrane fouling.

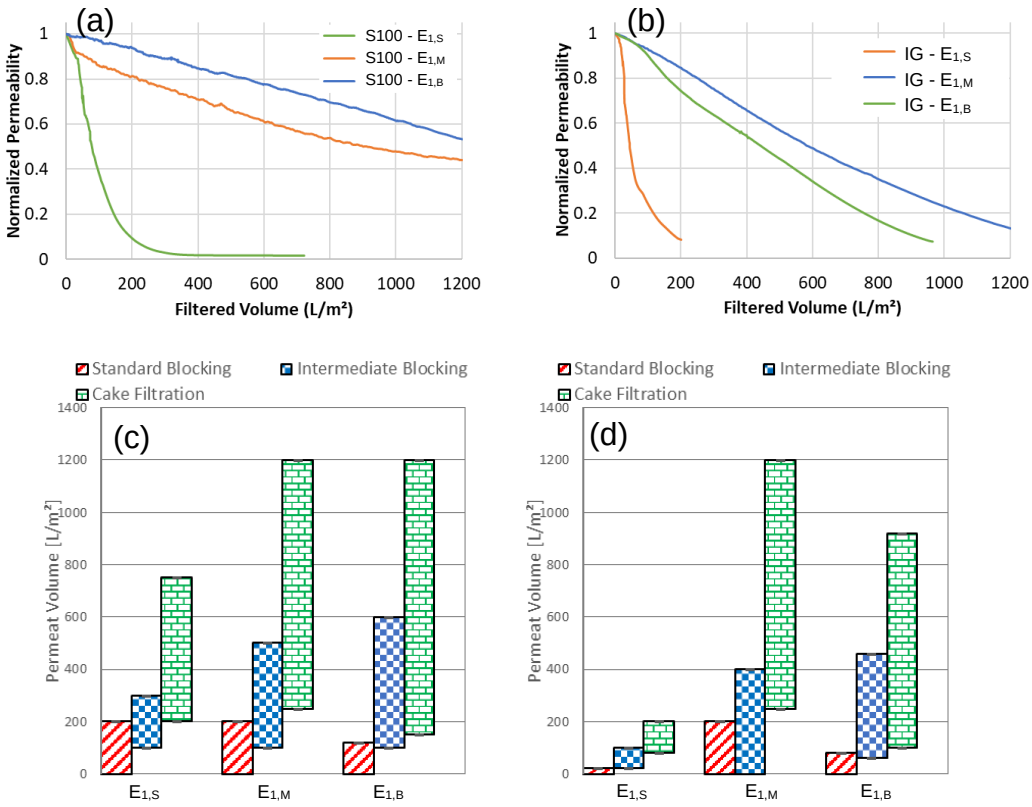

Figure 18: Normalized permeability curves (A and B) and the respective fouling chronological evolution (C and D) during the filtration of $E_{1,S}$, $E_{1,M}$ and $E_{1,B}$ using UF membranes S100 (A and C) and IG (B and D) at constant flux of 240 L/(m²·h), one trial

To ensure the reproducibility of the filtration experiments, those with S450 were repeated once again employing $E_{1,S}$, $E_{1,M}$, and $E_{1,B}$ as indicated in Figure 19. Results showed quite reproducible behaviors during filtration. Furthermore, experiments at constant pressure using $E_{1,M}$ through IG membranes and $E_{1,S}$, $E_{1,M}$ and $E_{1,B}$ through S450 membranes as well as S100 were repeated once again and were mostly reproducible.

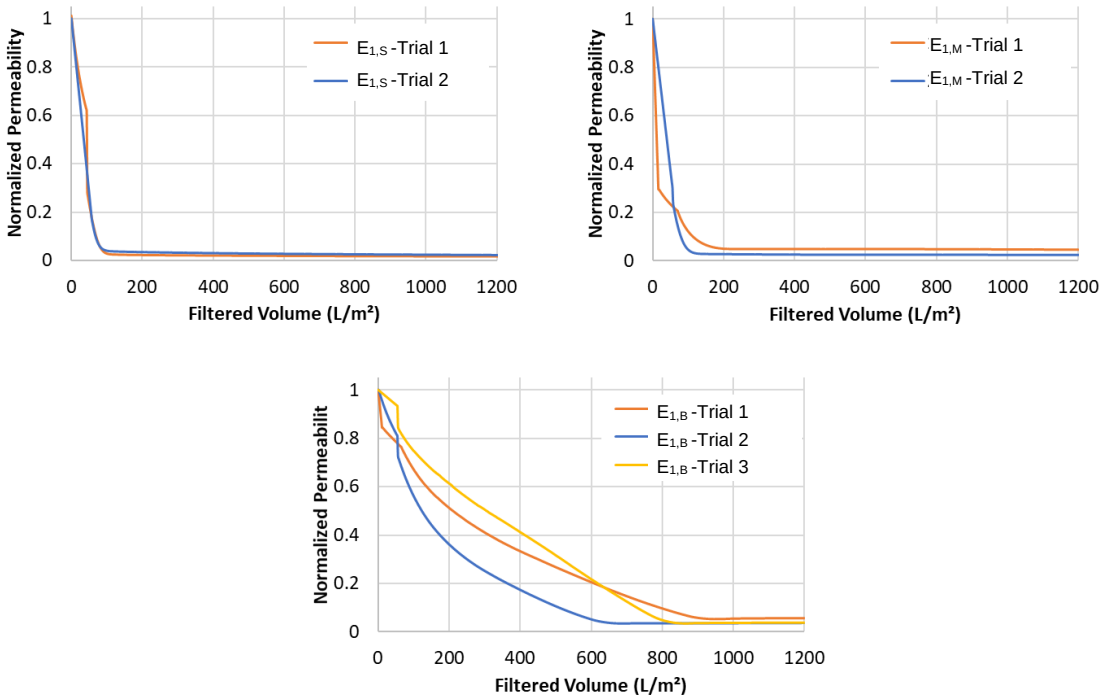

Figure 19: Reproducibility of filtration experiments of $E_{1,S}$, $E_{1,M}$ and $E_{1,B}$ through S450, two or three trials

4.2.1.1.1 Membrane morphology

The cross-sectional morphology of exemplary fouled MF membranes, S450, during filtration of three oil feed emulsions were analyzed and compared with pristine unfouled membranes. Scanning electron microscopy (SEM) micrograph for Pristine S450 showed that membrane exhibited a sponge-like isotropic structure without an active layer. In addition, SEM micrographs at higher magnification for pristine and fouled S450, after filtration of $E_{1,S}$, $E_{1,M}$ and $E_{1,B}$ feeds at oil content of 5 mg/L and constant flow rate, are shown in Figure 20.

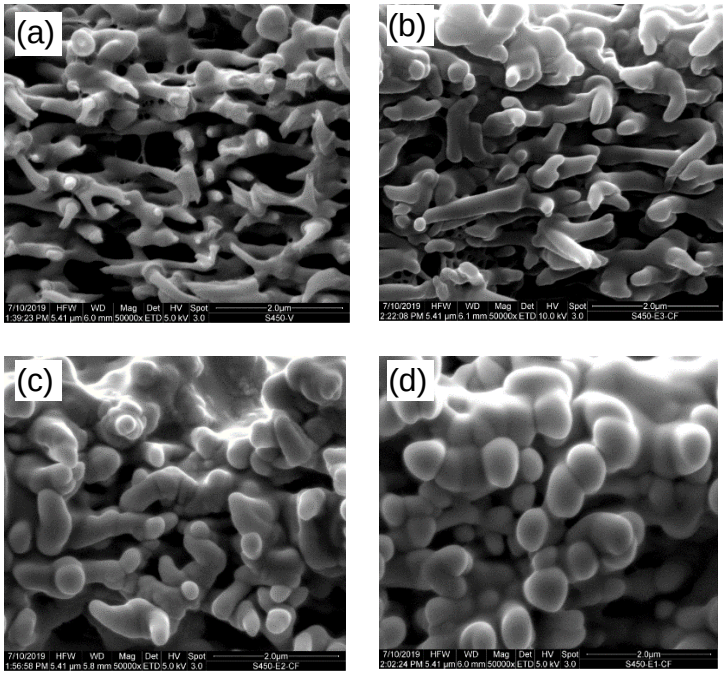

Figure 20: SEM micrographs for (A) Pristine S450 and fouled S450 during filtration of (B) $E_{1,B}$, (C) $E_{1,M}$ and (D) $E_{1,S}$ emulsified oils, Magnification: X 50,000

Interestingly membrane fouling was found to be associated with coating of membrane internal fiber structure by oil droplets causing proceeding contraction of internal pores, as can be seen in Figure 20. However, the extent of oil incorporation into the membrane structures is influenced by different oil droplet size distribution. Very limited oil coating was observed for membranes fouled after filtration of $E_{1,B}$ having larger oil droplet sizes. However, in case of $E_{1,M}$, more coating of membrane internal structure than in case of $E_{1,B}$ was found. Moreover, most severe fouling / intense oil incorporation was observed for fouled membranes by $E_{1,S}$, which has small oil droplet size. This supports well the earlier findings regarding the substantial influence of oil droplet size distribution and membrane average pore diameter on the membrane performance and fouling behavior.

4.2.1.2 Studying of membranes fouling behavior at constant pressure condition

In parallel, filtration experiments using the three emulsified oils were also conducted at 0.5 bar constant pressure condition. $E_{1,S}$, $E_{1,M}$ and $E_{1,B}$ feeds were filtered through S800, S450, S100 and IG membranes at constant operation pressure of 0.5 bar. The membrane performance curves, and fouling mechanism of MF membranes are introduced in Figure

21. In which, $E_{1,S}$ and $E_{1,M}$ caused stronger permeability decline than $E_{1,B}$, which is similar to what was noticed in constant flux experiments.

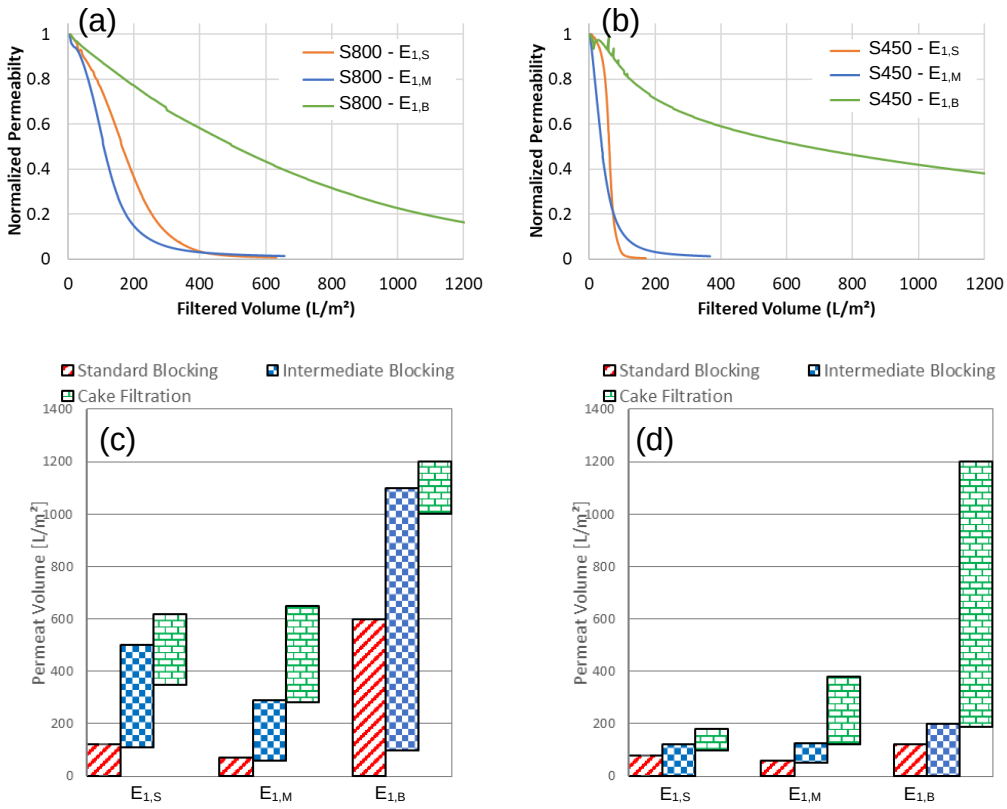

Figure 21: Normalized permeability curves (A and B) and the respective fouling chronological evolution (C and D) during the filtration of $E_{1,S}$, $E_{1,M}$ and $E_{1,B}$ using MF membranes S800 (A and C) and S450 (B and D) at constant pressure of 0.5 bar, one trial

Interestingly, in case of UF membranes, as indicated in Figure 22, which represent membrane permeability decline curves and the respective fouling mechanism for S100 and IG membranes, $E_{1,S}$ and $E_{1,M}$ also caused more decay in membrane performance than $E_{1,B}$. $E_{1,M}$ was expected to cause fouling behavior comparable to $E_{1,B}$ since they both contain oil droplets that are bigger than pores of UF membranes. This effect might be explained by considering that oil droplets are directly subject to a high constant pressure from the beginning which might push the drops into the pores of the still virgin membrane causing high fouling rate. With a constant flow, on the other hand, the new membrane is initially only subjected to low pressure. As a result, there is no penetration of oil droplets and the subsequent layer build-up prevents subsequent droplets from penetrating the pores.

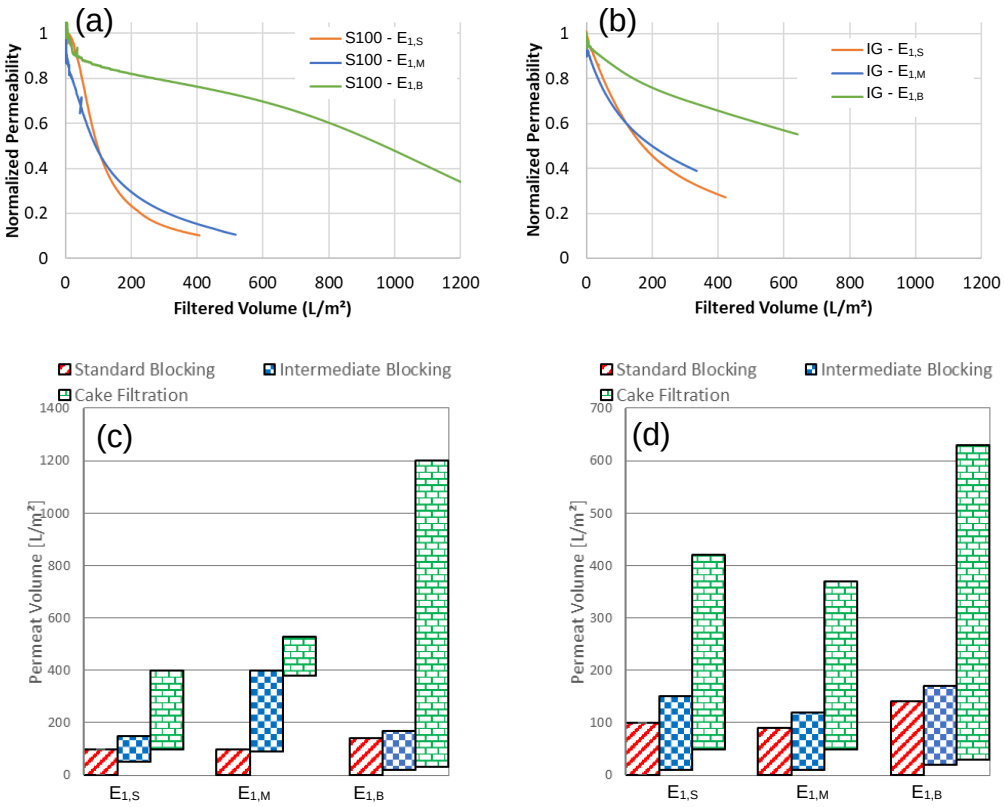

Figure 22: Normalized permeability curves (A and B) and the respective fouling chronological evolution (C and D) during the filtration of $E_{1,S}$, $E_{1,M}$ and $E_{1,B}$ using UF membranes S100 (A and C) and IG (B and D) at constant pressure of 0.5 bar, one trial

4.2.1.3 Influence of salt content on the filtration behavior

A set of experiments was carried out for testing the influence of different salt content in oily feed background water by filtering oily feeds prepared of $E_{1,S}$ emulsified oils with no salt, 0.5 M NaCl, 0.5 M $CaCl_2$, a mix of 0.5 M NaCl and $CaCl_2$, 1 M NaCl as well as ASW through S100 and S450. Furthermore, oil droplets size distribution was measured before and after adding salts. Results revealed that salts influence the stability of the oily feed, i.e., formation of larger drops has been noticed as shown in Figure 23.

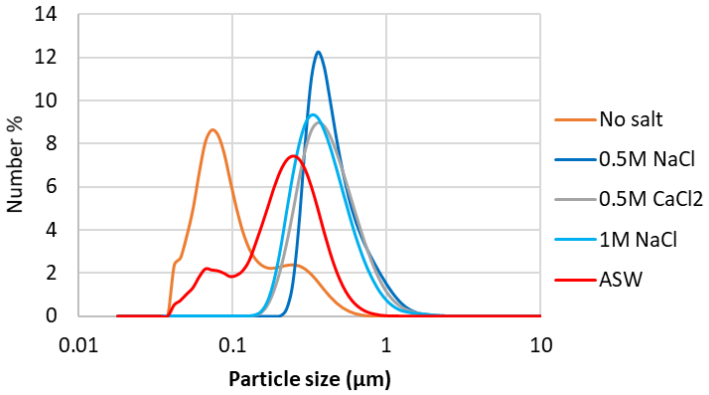

Figure 23: Droplet size distribution of oily feeds prepared of $E_{1,S}$ emulsified oils with no salt, 0.5 M NaCl, 0.5 M $CaCl_2$, 1 M NaCl and artificial sea water salts

Conductivity and Zeta potential of oily feeds are shown in Table 12. All feeds are negatively charged, and salt addition has decreased the absolute zeta potential.

Table 12: Conductivity and zeta potential of oily feeds prepared of E_1 emulsified oils with no salt, 0.5 M NaCl, 0.5 M $CaCl_2$, mix of 0.5 M NaCl and $CaCl_2$, 1 M NaCl and artificial sea water salts (ASW)

Sample	Conductivity in µS/cm	Zeta Potential in mV
$E_{1,S}$ – No Salt	60	- 45.0
$E_{1,S}$ – 0.5 M NaCl	46,160	- 23.3
$E_{1,S}$ – 0.5 M CaCl2	76,200	- 1.3
$E_{1,S}$ – 0.5 M Mix	112,500	- 1.4
$E_{1,S}$ – 1 M NaCl	92,600	- 15.4
$E_{1,S}$ – ASW	50,400	- 7.3

The permeability curves of $E_{1,S}$ oily feed filtered through S450 and S100 at constant flux of 240 and 1,300 L/m²·h are depicted in Figure 24 and Figure 25. The fouling behavior of emulsified oils through both membranes was previously addressed (see section 4.2.1.1). The strong permeability decline for both membranes and the fouling behavior was comparable for both membranes, in which they lost 90% of their permeability after filtering about 200 and 100 L/m² for S450 and S100, respectively.

However, the addition of salt led to an improvement in the performance of S450 (cf. Figure 24), i.e., less permeability decease was noticed. A 90% permeability loss only occurred

after filtering about 350, 500, 550 and 650 L/m² for 0.5 M $CaCl_2$, 0.5 M mix, ASW and 0.5 M NaCl, respectively.

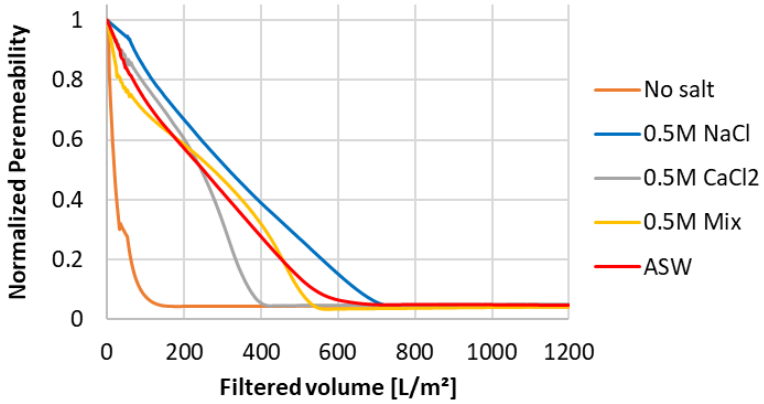

Figure 24: Normalized permeability decline of oily feeds prepared of $E_{1,S}$ emulsified oils with no salt, 0.5 M NaCl, 0.5 M $CaCl_2$, mix of 0.5 M NaCl and $CaCl_2$, 1 M NaCl and artificial seawater salts (ASW) filtered through S450

On the other hand, salts led to a more significant enhancement in the performance of S100, with ASW causing the smallest permeability decline of only about 10% after filtering 1,200 L/m², where the membranes were almost blocked when other oily feeds were employed.

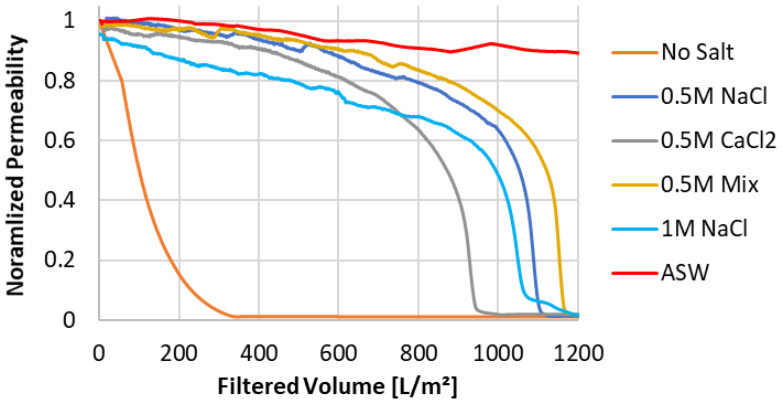

Figure 25: Normalized permeability decline of oily feeds prepared of $E_{1,S}$ emulsified oils with no salt, 0.5 M NaCl, 0.5 M $CaCl_2$, mix of 0.5 M NaCl and $CaCl_2$, 1 M NaCl and artificial seawater salts (ASW) filtered through S100

4.2.2 Contribution of water-soluble oil fraction in the membrane fouling

Before optimizing the treatment process, it was important to effectively separate and quantify the WSO in the model feed water (synthetic OWWE) and in the permeate water. Two

steps were carried out for this purpose: First, separation and quantitative determination of WSO, where separation was investigated with filtration of the model feed water through 0.1, 0.2 and 0.45 µm filters. Secondly, filtration tests with the permeates obtained to determine the contribution of WSO to membrane fouling.

4.2.2.1 Determination of dissolved oil fraction

In this project, two types of techniques were used to determine the dissolved oil fractions, one method using a fluorophotometer with emission excitation matrix, FEEM, according to the ASTM D5412-93 standard method, and another method using gas chromatography analysis performed in different ways.

4.2.2.1.1 Gas chromatography for determination of dissolved oil fraction

The PAH content of some emulsified oils samples was analyzed using two methods that applies the GC technique, one quantitative method that relied on measuring the samples at external laboratory and one half-quantitative method.

a. Quantitative GC method for determination of WSO

The raw crude oil implemented in this project was analyzed for the main 16 PAHs according to the EPA classifications using GC-FID method, in which the determination limit was 3 mg/L. The PAH contents are shown in Table 13. From the previous figures it can be noticed that naphthalene, phenanthrene, benzo[a]anthracene and pyrene are the dominant component among the main 16 PAHs.

Table 13: Composition of polycyclic aromatic hydrocarbon (PAH) in crude oil, measured using GC-FID, according to the EPA 16 PAH list; < 3 means that the value was below the limit of determination

PAH components	Conc. in mg/L	PAH components	Conc. in mg/L
Acenaphthene	<3	Acenaphthylene	<3
Dibenz[a,h]anthracene	<3	Anthracene	<3
Fluoranthene	<3	Benzo[a]anthracene	35
Fluorene	<3	Benzo[a]pyrene	<3
Indeno[1,2,3-c,d]pyrene	<3	Benzo[b]fluoranthene	<3
Naphthalene	620	Benzo[g,h,i]perylene	<3
Phenanthrene	150	Benzo[k]fluoranthene	<3
Pyrene	3	Chrysene	<3

On the other hand, model emulsified oil batches were characterized in terms of PAHs at GBA Gesellschaft für Bioanalytik mbH, Germany. Figure 26 shows the results of one sample for the 11 types of PAH that could be found in the model oil-emulsion at oil concentration of 10 mg/L as TOC, without SDS in concentrations higher the limit of determination.

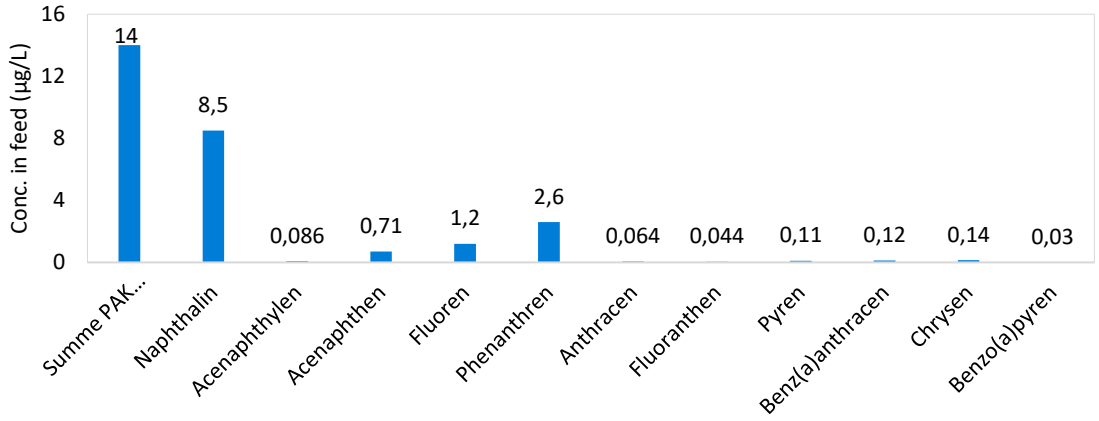

Figure 26: Concentration of 11 types of polycyclic aromatic hydrocarbons existing in the model oil-emulsion at 10 mg/L oil (as TOC) without SDS

Comparing these values to the raw oil analysis, cf. Table 13, similar values to for naphthalene and phenanthrene were also found the most dominant components. But benzo[a]anthracene and pyrene were found in lower concentrations, when compared to other components like fluorene and acenaphthene that were below to the detection limit in the raw oil analysis.

b. Semi-quantitative GC-MS method for the determination of WSO

Components of surfactant-free oil emulsions with oil concentration of 25 mg/L and the permeates of S450 and S200 membranes were analyzed with GC-MS and stir bar sorptive extraction using Gerstel-Twisters® as explained in section 3.4.1.1. Figure 27 shows the spectrum of surfactant-free oil emulsions with an oil concentration of 25 mg/L. Several intensity peaks were noticed. The maximum intensity was detected at a retention time of 6.71 min.

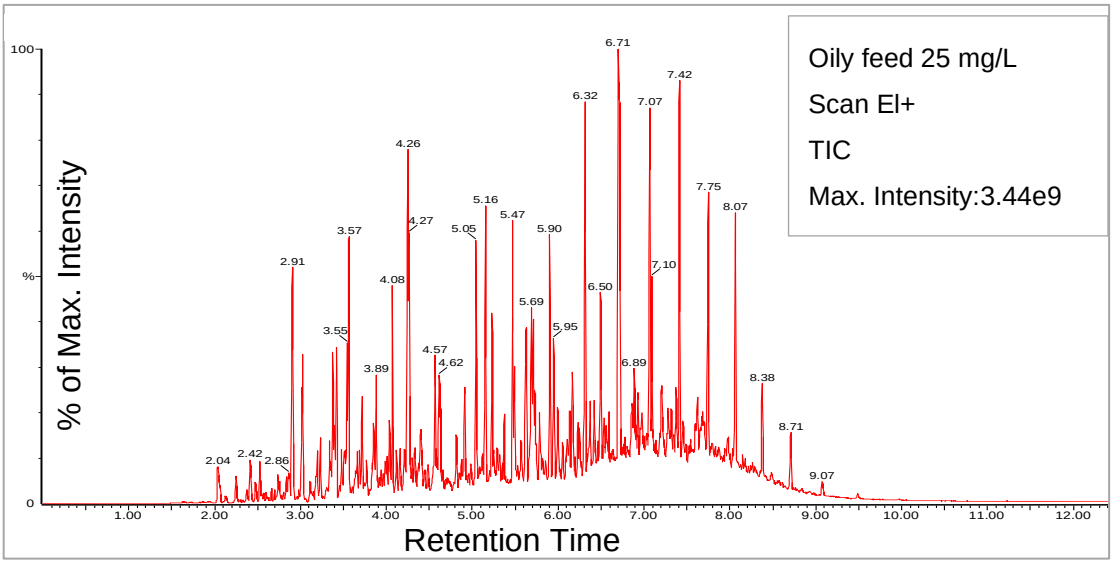

Figure 27: GC-MS analysis of surfactant-free emulsified oily feed with oil concentration of 25 mg/L as TOC

Further analysis of the chromatographic results included integrating the area of the main intensity peaks and a qualitative analysis by comparison with the NIST library. Components identified in the feed (among others) were methylcyclohexane, toluene, ethylbenzene, p-xylene, di-tert-butyl disulfide, methylnaphtalene, tetradecane, tetradecane, 2,6,10-trimethyl, pentadecane, 2,6,10,14-tetramethyl and nonadecan/heneicosane with a statistical probability of 71%, 38%, 65%, 38%, 46%, 30%, 34%, 17%, 25% and 13%, respectively. These compounds were chosen as “reference compounds” for further analysis due to their clearly separated peaks, sufficient intensities and their different molecular properties. It should be noted that the qualitative identification of longer aliphatic chains is statistically more uncertain than that of smaller aromatics because the pattern of the MS-fragments is less clear. As these compounds appear later in the chromatogram, i.e. they have longer retention times than smaller aromatics, the statistical probability values

decrease with increasing retention times. Figure 28 summarizes the chromatographic results of a four-fold chromatographic analysis of the oily feed.

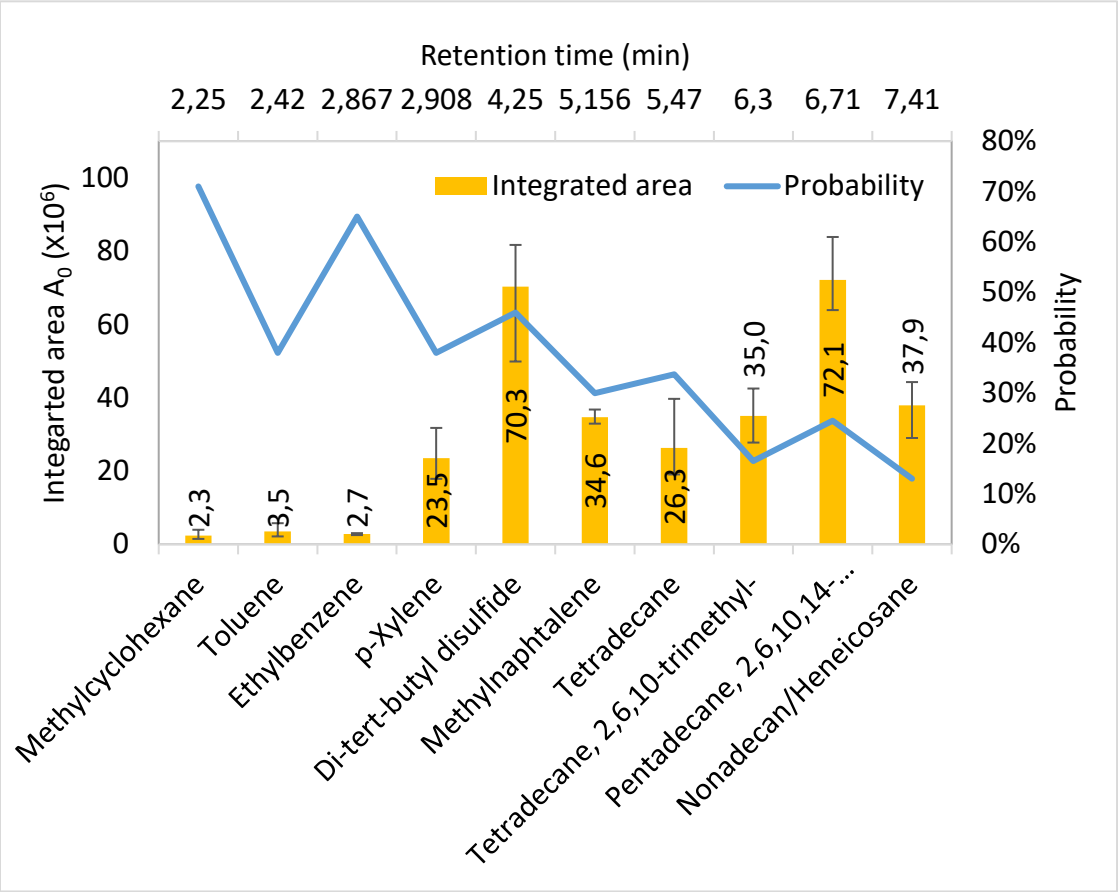

Figure 28: Reference components of surfactant-free emulsified oil that were detected with the GC-MS analysis with their respective retention time, integrated area of the intensity peak and probability of the detected component compared to the NIST library. Presented as average of four trials with the min. and max. error bars

Analysis of the permeates of S450 and S200 membranes after filtering surfactant-free emulsions with an oil concentration of 25 mg/L indicated different intensities at the peaks of the reference components as indicated in Figure 29.

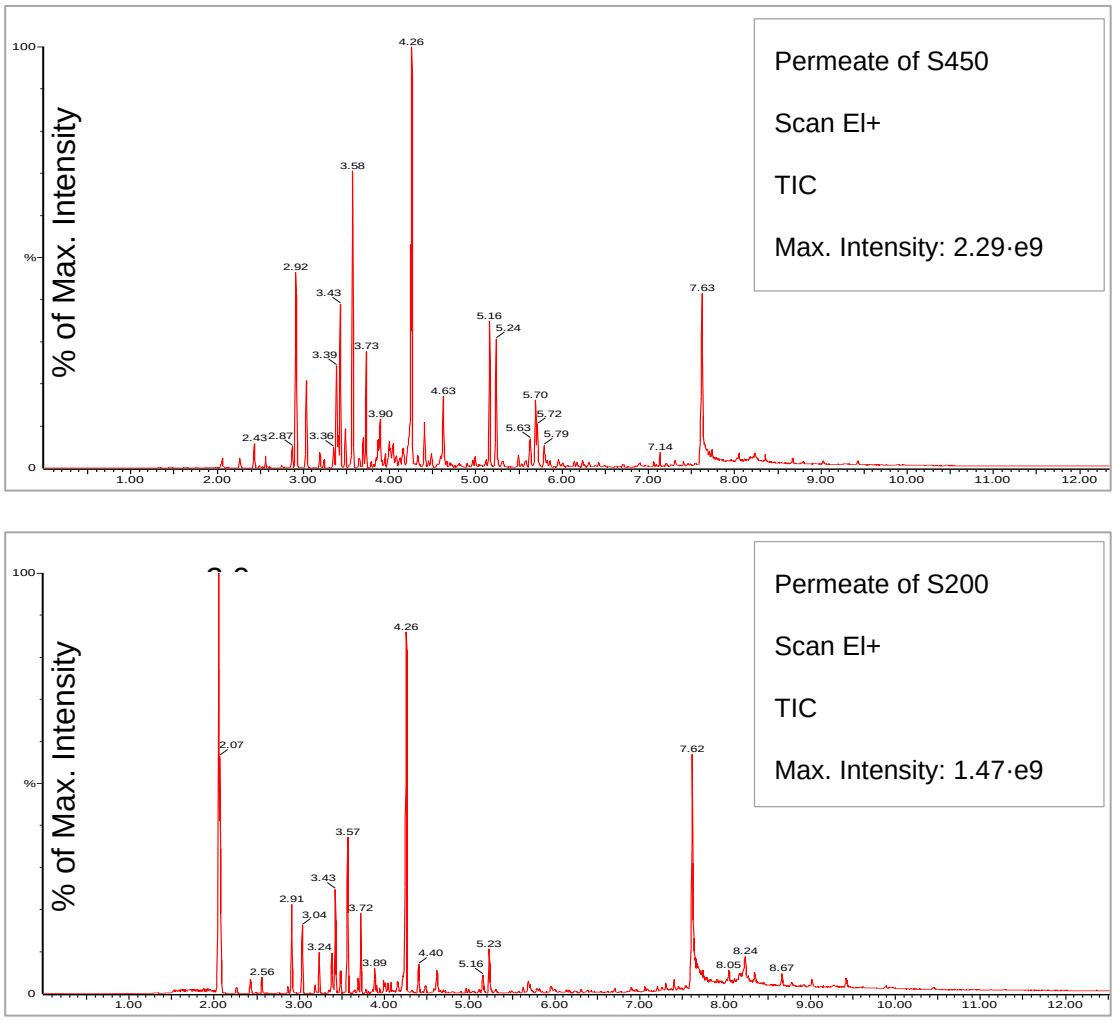

Figure 29: GC-MS analysis of the permeates of surfactant-free emulsified oily feed with oil concentration of 25 mg/L as TOC after being filtered through S450 and S200 membranes.

Furthermore, Figure 30 shows the so-called relative area A_i/A_0 which is the ratio of integrated area of the respective peaks (A_i) of the permeates of S450 and S200 membranes related to the reference integrated area of the intensity peak of the feed (A_0). In which, it can be noticed that some components like tetradecane, tetradecane, 2,6,10-trimethyl, pentadecane, 2,6,10,14-tetramethyl and nonadecan/heneicosane were completely removed by all three filter types. Other components, like di-tert-butyl disulfide, may penetrate the filters as they were detected in the permeate of both filters. Some components, like methylnaphtalene, were detected in the permeate of S450 with relative area about 30% of feed intensity, at low relative area <3% in permeate of S200. Other components

like methylcyclohexane, toluene, ethylbenzene, p-xylene were detected in the permeate of both S450 and S200.

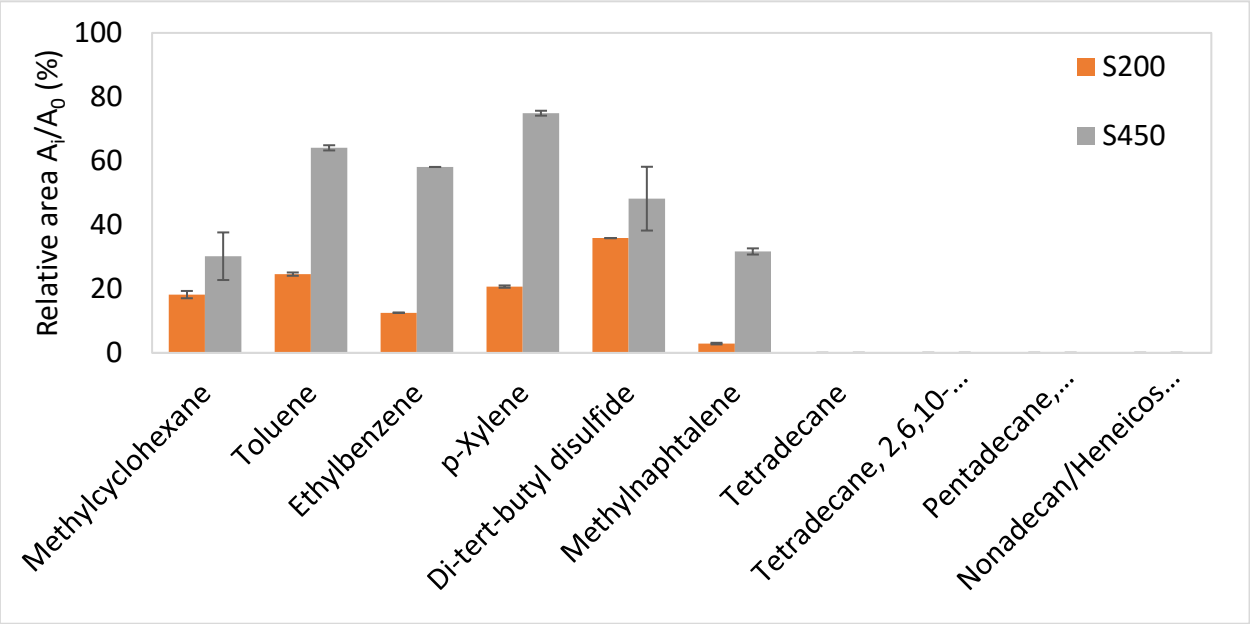

Figure 30: Relative area A_i/A_0, integrated area of intensity peaks (A_i) of the reference components in the permeate of S450 and S200 membranes related to the respective integrated area of the intensity peak of the feed (A_0). Presented as average of two trials with the min. and max. error bars

Figure 31 shows the relative area A_i/A_0 of the permeate of the S450 MF filter compared to the permeate of the SM UF membrane. Lower PAH concentrations were found in the permeate of the UF.

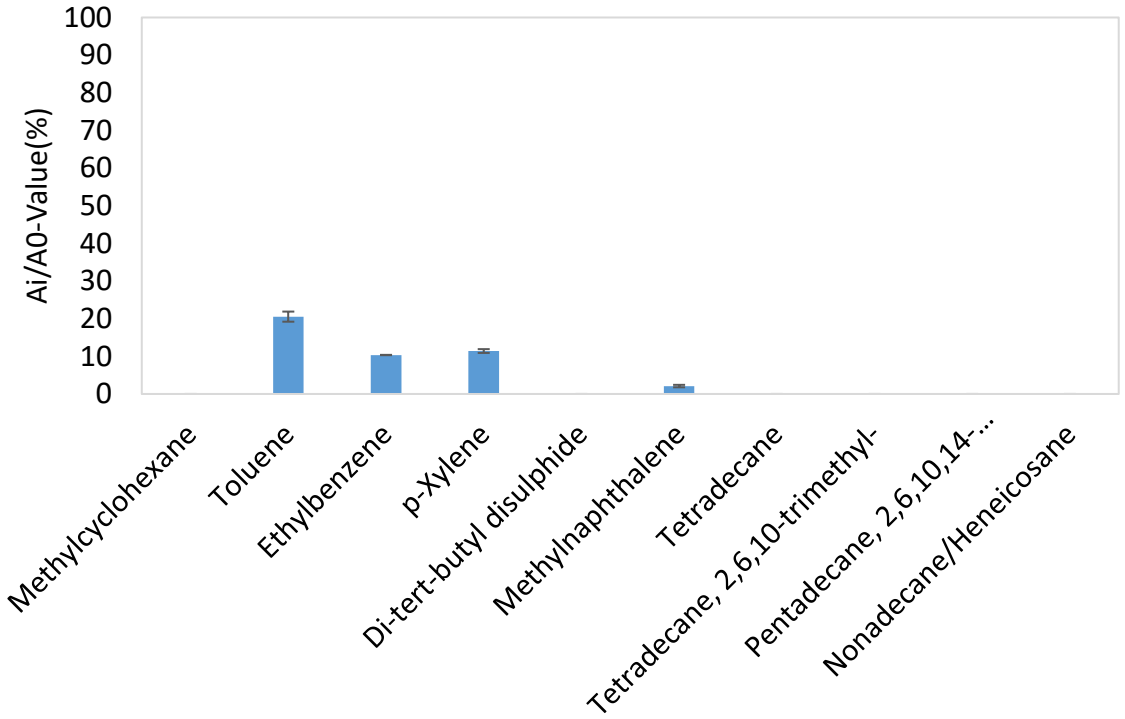

Figure 31: Relative area A_i/A_0, of the permeate of SM membranes, when filtering the permeates of S450 membranes through SM membrane.

4.2.2.1.2 Fluorophotometer with emission-excitation matrix (FEEM) for the determination of dissolved oil fraction following the ASTM D5412–93 method

The excitation and emission wavelength (λ_{ex} and λ_{em}) values for each type of the main 16 compounds of PAHs were determined from the literature [139-141], and listed in Table 14.

Table 14: The excitation and emission wavelength values for the main 16 compounds of PAHs

PAHs	λ_{ex}, nm	λ_{em}, nm	PAHs	λ_{ex}, nm	λ_{em}, nm
Acenaphthene	290	321	Chrysene	266	367
Acenaphthylene	323	394	Dibenz[a,h]anthracene	257	404
Anthracene	251	404	Fluoranthene	284	464
Benzo[a]anthracene	287	390	Fluorene	260	303
Benzo[a]pyrene	263	408	Indeno[1,2,3-c,d]pyrene	239	566
Benzo[b]fluoranthene	254	440	Naphthalene	275	321
Benzo[k]fluoranthene	248	436	Phenanthrene	248	349
Benzo[g,h,i]perylene	302	524	Pyrene	239	376

The model emulsified oil were prepared at oil concentrations of 1 - 50 mg/L as TOC, then they were analyzed as explained in section 3.4.1.2. The measurements were performed in triplicates, and the emission-intensity curves for emulsified oil samples were compared at every oil concentration. For instance, Figure 32 shows the emission-intensity curves for oil concentration of 5 mg/L TOC at excitation wavelength values of 290, 266, 260 and 275 nm, which are equivalent to acenaphthene, chrysene, fluorene and naphthalene, respectively. These curves showed maximum intensity at emission wavelength values of 320, 370, 305, and 320 nm respectively; emission wavelength values were rounded to the nearest 5 nm value since scanning intervals were set at 5 nm. The measurement exhibited good reproducibility for some PAH compounds, e.g., acenaphthene and fluorene, whereas the reproducibility for other PAH compounds, like chrysene and naphthalene was low.

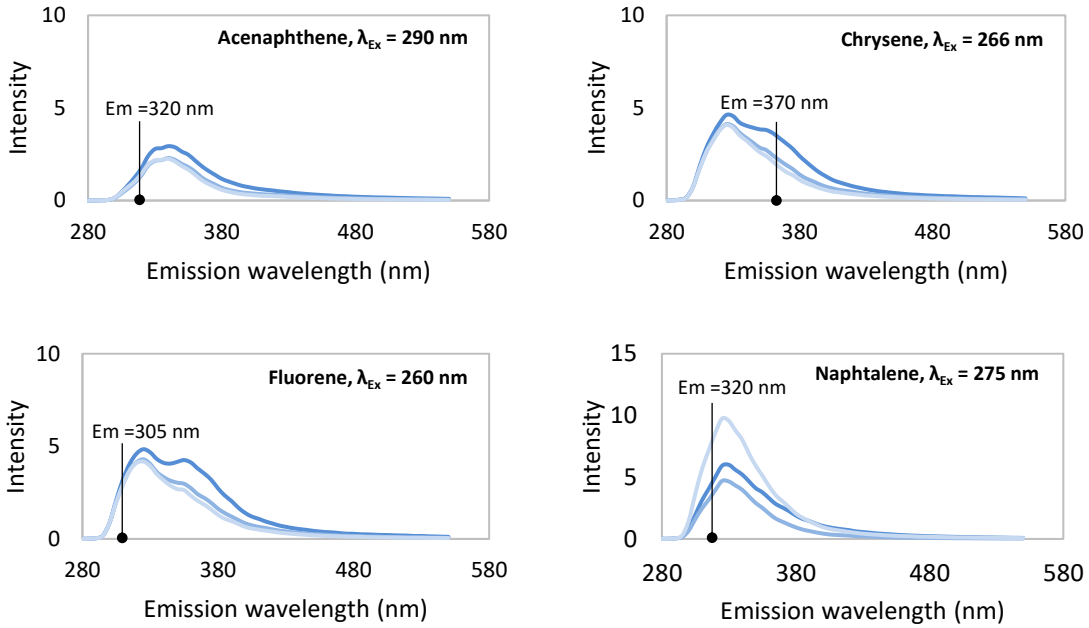

Figure 32: Emission-intensity curves for surfactant-free emulsified oil with oil concentration of 5 mg/L measured in triplicates at four excitation wavelength values of 290, 266, 260 and 275 nm that are assigned to acenaphthene, chrysene, fluorene and naphthalene

Furthermore, another set of measurements was conducted for emulsified oil samples with different oil concentrations in the range of 1 – 50 mg/L TOC concentrations. Every sample of certain oil concentration was divided into two portions; one portion was measured as it was, while 0.48 g/L of SDS was added to the second portion before measurement. This

SDS concentration was found in the process optimization analysis to be the most-suited surfactant concentration for surfactant-enhanced UF process (see section 4.3.1). The samples were analyzed for the concentration of the 16 PAH compounds. For instance, Figure 33 shows the emission-intensity curves for emulsified oils with different oil concentrations (1 – 50 mg/L) with and without surfactants at excitation wavelength of 290 and 239 nm (assigned to acenaphthene and pyrene, respectively). Emission- intensity values were observed to increase with increasing oil concentrations for both surfactant-free and surfactant-containing emulsified oil. Nevertheless, for all the analyzed 16 PAH compounds, samples prepared with SDS exhibited much less emission- intensity, almost the half, compared to surfactant-free emulsified oil samples. This indicates that SDS addition had a strong impact on the FEEM measurement; one possible reason is the effect of SDS addition on the extraction step of PAH compounds. A second possible reason is foam formation inside the emulsified oil sample that could strongly influence the sample homogeneity, and hence, influence the measurement.

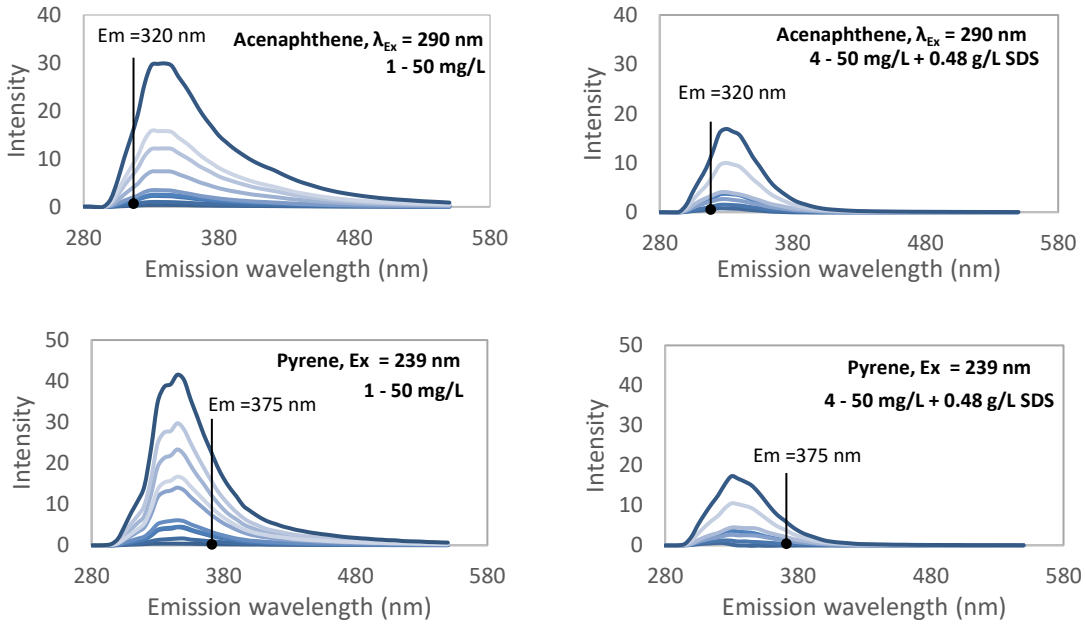

Figure 33: Emission-intensity curves for surfactant-free vs. surfactant-containing emulsified oil with different oil concentrations (1 – 50 mg/L TOC) at excitation wavelength values of 290 and 239 nm (assigned to acenaphthene and pyrene)

On the other hand, Figure 34 shows the concentrations of the 16 PAH compounds and total PAHs measured via GC-MS method (DIN 38407-39:2011-09) for emulsified oil with

oil concentrations of 5 and 10 mg/L TOC and different SDS concentrations (0, 0.12, 0.48 and 1.2 g/L). These analyses were carried in the labs of GBA Gesellschaft für Bioanalytik mbH, Germany. These results showed no strong deviation in the concentrations of PAH compounds due to SDS addition, which implies that the reduced emission-intensity in Figure 33 was mainly because of the influence of SDS on the measurement process.

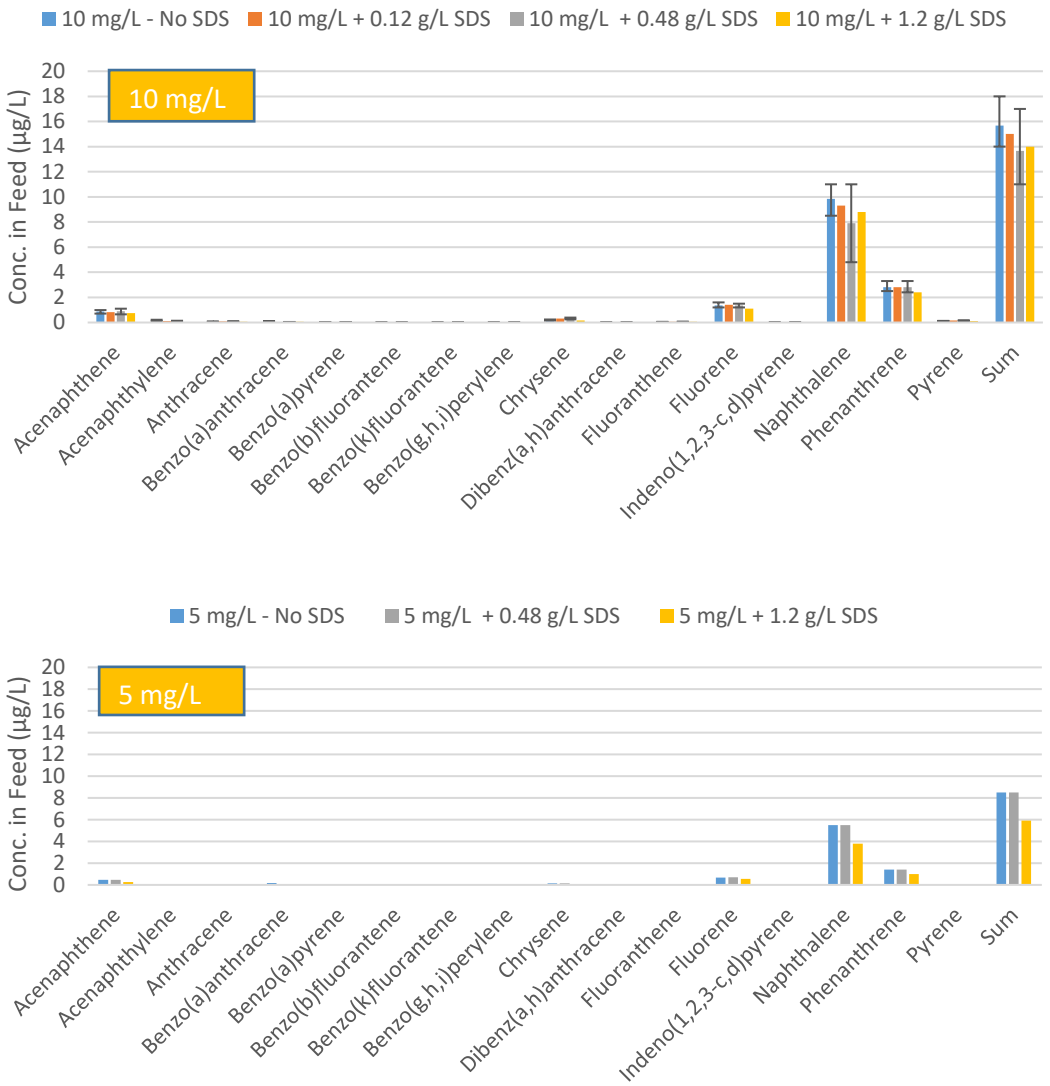

Figure 34: Concentrations of the main 16 PAH compounds in emulsified oil with oil concentrations of 5 and 10 mg/L TOC and different SDS concentrations (0, 0.12, 0.48 and 1.2 g/L)

Moreover, Figure 35 presents the relationship(s) between the TOC concentration in surfactant-free emulsified oil (in range of 1 – 50 mg/L) and the measured concentrations of total PAHs, naphthalene, phenanthrene and fluorene via GC-MS method. Linear

relationships were found for all the measured PAH compounds and TOC concentration (a very good R^2 of > 0.998).

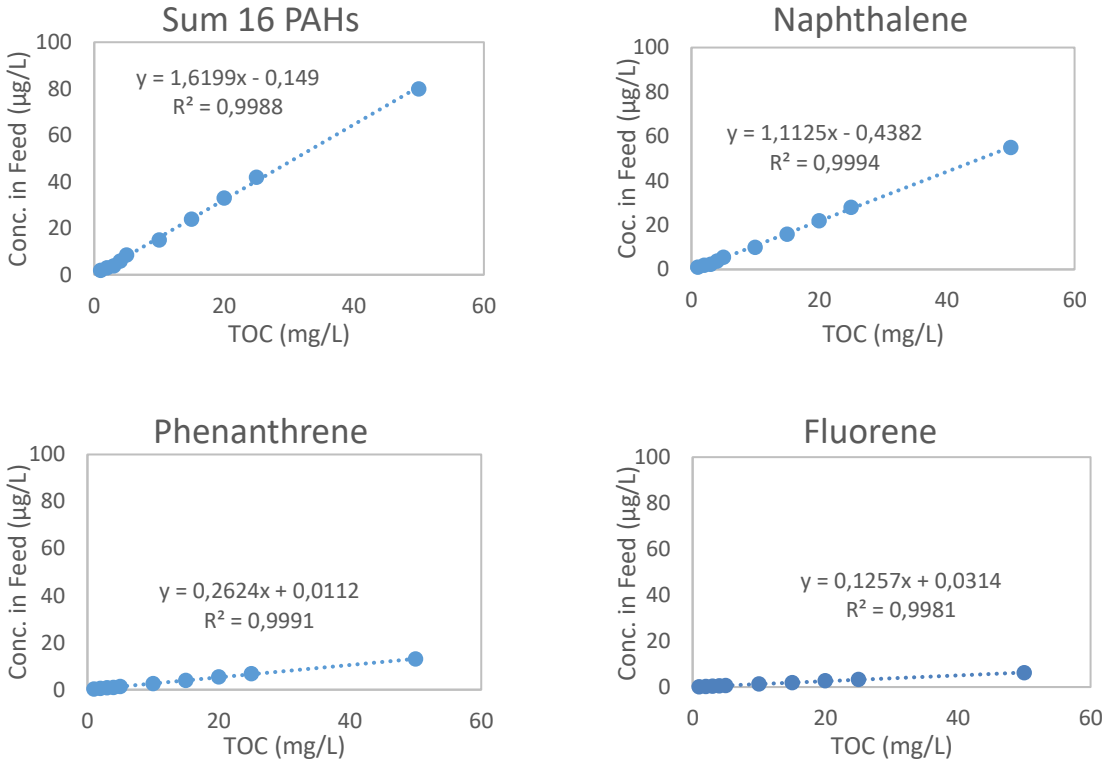

Figure 35: Relationship between TOC concentration in surfactant-free emulsified oil (1 – 50 mg/L) and the measured concentrations of total PAHs, naphthalene, phenanthrene and fluorene via GC-MS method

Additionally, the relationship(s) between the measured concentrations of PAH compounds using GC-MS method and emission-intensities measured by FEEM were examined; the curves are plotted in Figure 36. A linear relationship could also be found between the measured concentrations of PAHs via GC-MS method, and the emission-intensities measured via FEEM method. Nevertheless, the values for coefficient of determination (R^2) were less than in case of the relationship with TOC. In Figure 36, the total PAHs was plotted against the sum of emission-intensities of the main four components detected in the feed, namely naphthalene, phenanthrene, fluorene and acenaphthene.

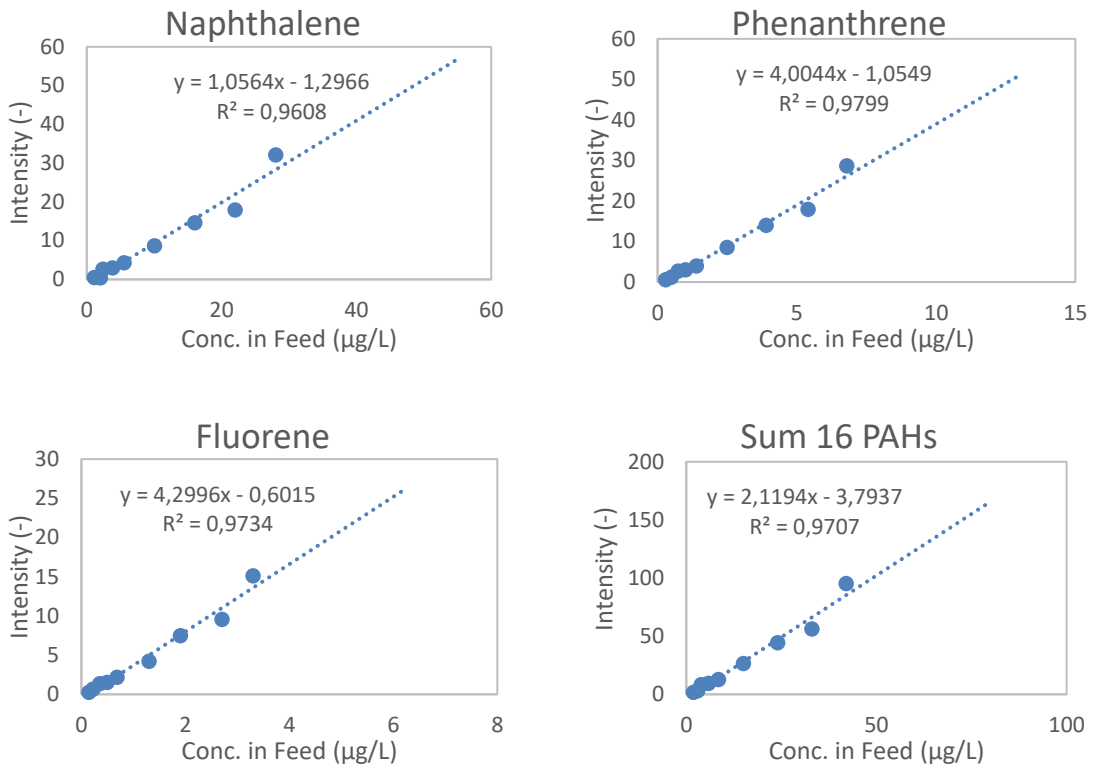

Figure 36: Relationship between the measured concentrations of total PAHs, naphthalene, phenanthrene and fluorene via GC-MS method and the respective emission-intensities for surfactant-free emulsified oil (1 – 50 mg/L)

4.2.2.2 Membrane fouling behavior due to dissolved oil fractions

Three PES membrane filters, S450, S200 and S100 were used for the separation of dissolved oil fraction from surfactant-free emulsified oil with two oil concentrations of 25 and 50 mg/L TOC. The S450 filter was used since it has a typical pore size employed for separation of dissolved organic compounds (for DOC determination), while S200 and S100 were chosen since measurement of oil droplet size distribution showed that emulsified oil contained small oil droplets in range of 0.1 µm. The permeates were then characterized in terms of oil droplet size distributions and compared with those of the original emulsified oil. Figure 37 shows both number- and volume-based size distributions of the emulsified oil with oil concentration 25 mg/L prior to filtration, measured by laser diffraction. Model emulsified oil was found to exhibit a relatively wide oil droplet size distribution in the range of 100 – 3,000 nm with a Sauter mean diameter d_{32} = 110 nm.

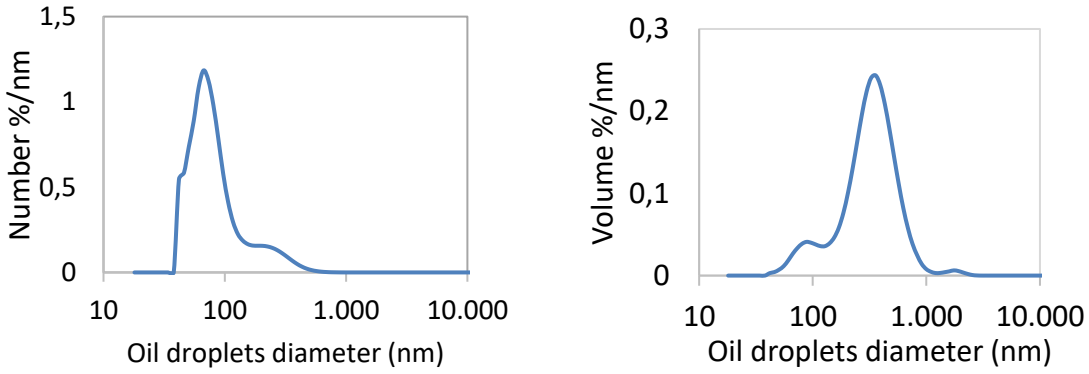

Figure 37: Differential number- (left) and volume-based oil droplet size distributions (right) for emulsified oil (25 mg/L) prior to separation of dissolved oil

Figure 38 shows the oil droplet size distributions for the permeates of S450 and S100 that were measured with the Zetasizer. The permeate of S450 showed different results for the three trials, yet the size distributions of the oil droplets were mostly below 250 nm. The permeate of S100 showed more reproducible oil size distributions with an average size of ~ 150 nm and maximum oil droplet size < 250 nm.

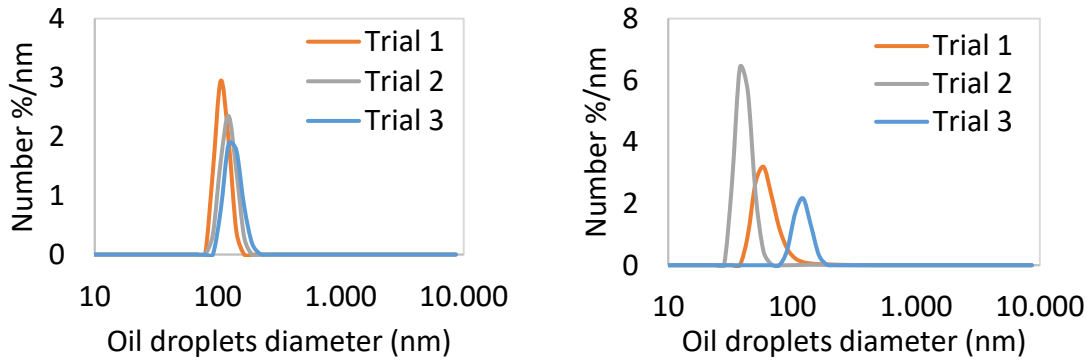

Figure 38: Differential volume-based oil droplet size distributions for permeates of S100 (left) and S450 (right) membrane filters over 3 trials

Nevertheless, the measured oil droplet sizes were expectedly larger than the average pore diameter of the membrane filters. This might be either related to a deformation of oil droplets or macroporous defects in the membrane filter. Subsequently, the pore size distributions of the membrane filters were measured using capillary flow permporometer (CFP-34RTG8A-X-6-LA, PMI). The measured pore size distributions for the membrane filters S450 and S100 are shown in Figure 39. The pore size distribution of S100 was found to exhibit two peaks (or two groups of membrane pores), one of ~ 150 nm and

macropores of ~ 290 nm. This might explain the measurement of oil droplets up to 250 nm in the permeate of S100. Besides, pore size distribution of S450 exhibited one peak around 700 nm, which does not match with the measured oil droplets below 250 nm in the permeate.

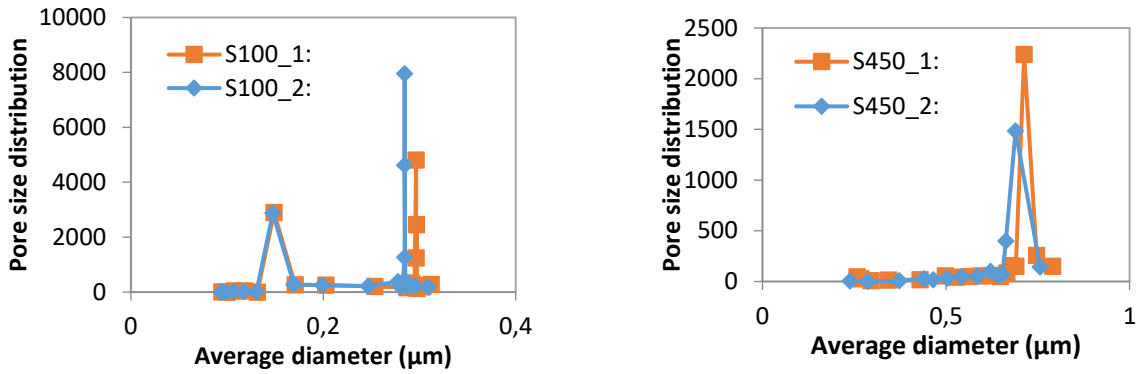

Figure 39: Differential pore size distribution of S450 and S100, 2 trials

Moreover, the permeates gained by the filtration using the different membrane filters were used as feed for the treatment with the SM_1 UF membrane module in single-cycle filtration experiments. Generally, much less performance decay was found compared to the treatment of emulsified oil, which may imply the role of the emulsified oil droplets (and coalescence) in the fouling mechanisms during filtration of surfactant-free emulsified oil. For instance, as indicated in Figure 40, treating the permeate of S450 by the UF membrane showed only a very low permeability decline from ~ 530 L/(m²·h·bar) to ~ 523 L/(m²·h·bar), i.e., the membrane lost only about 2 % of its initial permeability at the end of the filtration cycle. Further long-term fouling experiments using the three permeates and membranes with smaller surface area were conducted to get clearer insights into the contribution of water-soluble fractions in membrane fouling.

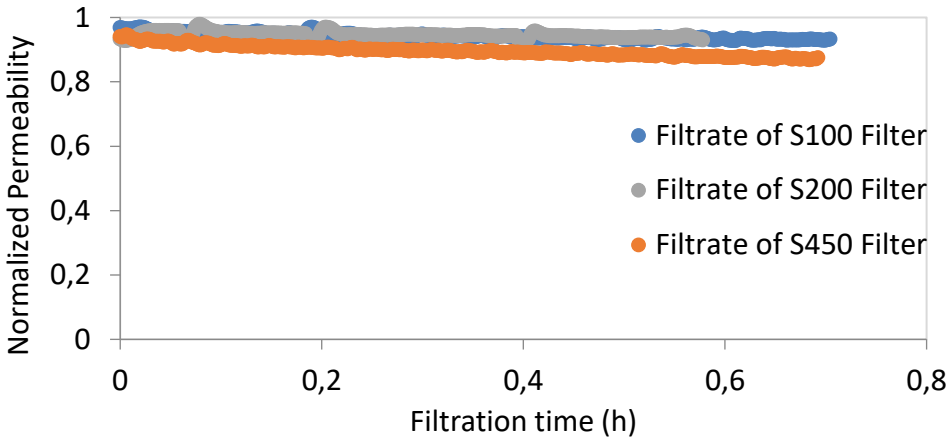

Figure 40: Normalized permeability of SM_1 membranes during single-cycle filtration experiment with the permeates of S100, S200 and S450 as feed

However, as indicated in Figure 41, extending the cycle duration to 5h did not indicate a significant permeability decline. As it was shown in section 4.2.2.1.1 that most of the dissolved oil fraction can pass through S450 (see Figure 30) this result emphasizes the finding that the dissolved oil fraction does not contribute significantly to membrane fouling.

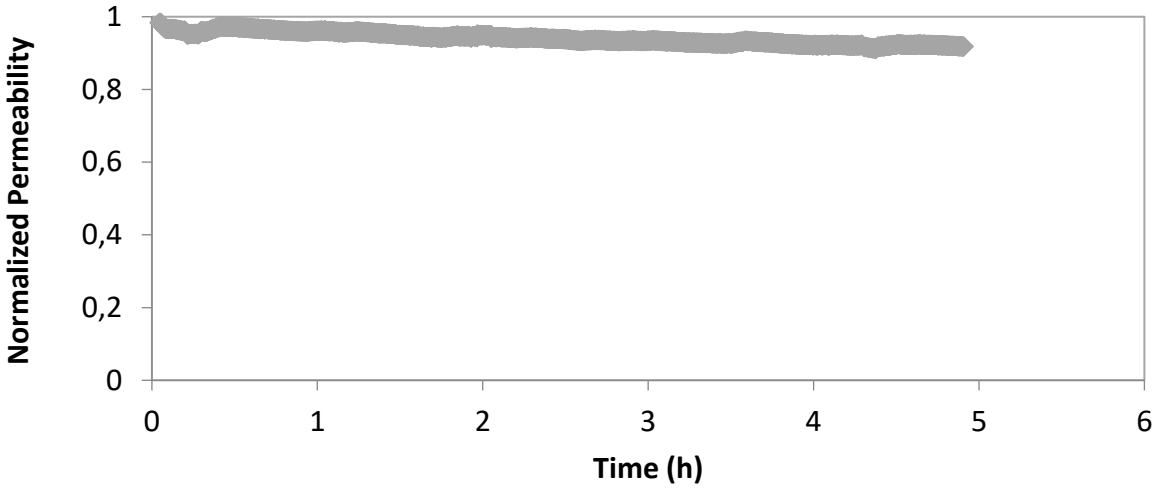

Figure 41: Normalized permeability of SM_1 UF membrane module during single-cycle filtration experiment of the permeate of S450 for an extended cycle duration

Modelling of fouling mechanisms due to dissolved oil fractions was not possible as no significant fouling could be detected.

4.2.3 Role of surfactant type on the fouling behavior of flat sheet membranes

More than 150 filtration experiments were performed using flat sheet membranes to gain better understanding of the effects of surfactants and co-surfactants in the model feed emulsions on UF membrane performance, as well as of the potential interactions between surfactants and flat sheet membranes. Various feeds compositions were tested, in which different types and concentrations of surfactants, with and without co-surfactant and salts, were investigated at the two oil concentrations of 5 and 10 mg/L. Most of these experiments were carried out using UP150 membranes under constant flux / pressure conditions. Table 15 lists the filtration experiment through UP150 membrane using complex oil-in-water emulsified oils (i.e., oil + surfactant) at constant flux, along with the number of trials (N), the average standard deviation of the normalized permeability for each registered measurement point i (according to equation Equation 6), the average pure water permeability and its respective standard deviation ($\sigma_{w0)}$.The results are presented and discussed in more detail in the following sub-sections.

Table 15: Results of emulsified oil filtration experiments using UP150 at constant flux, incl. number of trials (N), average standard deviation of normalized permeability for each measurement point, and average pure water permeability and its respective standard deviation

Exp. No.	Oil conc. (mg/L)	Surfactant type	Surfactant conc. relative to CMC	Co-surfactant	Salt	N	σ_{tot} (-)	W_0 (L/(m²·h·bar))	σ_{W_0} (L/(m²·h·bar))
1	10					3	0.045	675	23
2	-	SDS	0.2			2	0.024	1365	108
3	-	SDS	0.5			2	0.007	840	223
4	-	SDS	1			2	0.027	1093	102
5	-	Tween 20	0.2			2	0.078	929	238
6	-	Tween 20	0.5			2	0.031	1054	249
7	-	Tween 20	1			2	0.021	1153	145
8	-	CTAB	0.2			2	0.041	908	120
9	-	CTAB	0.5			2	0.013	985	86
10	-	CTAB	1			2	0.008	1014	295
11	-	SDS	0.2	X		3	0.083	1048	294
12		SDS	1	X		2	0.05	865	209
13	-	Tween 20	0.2	X		2	0.022	802	217
14		Tween 20	1	X		2	0.018	1006	22
15	-	CTAB	0.2	X		3	0.059	821	345
16	-	SDS	0.2		X	3	0.043	770	357
17		SDS	1		X	2	0.209	1173	24
18	-	Tween 20	0.2		X	2	0.103	759	341
19		Tween 20	1		X	2	0.015	948	117
20	-	CTAB	0.2		X	4	0.213	978	378
21	10	SDS	0.2			2	0.049	1306	101
22	10	SDS	0.5			2	0.033	778	338
23	10	SDS	1			2	0.024	911	237
24	10	Tween 20	0.2			2	0.016	721	236
25	10	Tween 20	0.5			3	0.021	982	496
26	10	Tween 20	1			2	0.013	806	188
27	10	CTAB	0.2			3	0.08	968	510
28	10	CTAB	0.5			2	0.013	1276	226
29	10	CTAB	1			2	0.106	667	438
30	10	SDS	0.2	X		3	0.115	910	317
31	10	SDS	1	X		2	0.032	973	23
32	10	Tween 20	0.2	X		2	0.011	797	411
33	10	Tween 20	1	X		2	0.005	1242	73
34	10	CTAB	0.2	X		4	0.131	951	345
35	10	SDS	0.2		X	3	0.085	893	257
36	10	SDS	1		X	2	0.005	1196	6
37	10	Tween 20	0.2		X	2	0.027	532	26
38	10	Tween 20	1		X	2	0.012	1012	37
39	10	CTAB	0.2		X	3	0.154	782	158

4.2.3.1 Filtration of surfactant-free emulsified oils

Reference experiments were carried out using surfactant-free emulsified oils. Figure 42 shows the normalized permeability for the reference experiments at constant flux operation and oil concentration of 10 mg/L. Figure 42 a shows the filtration curves of three trials and Figure 42 b shows the average curve of the three repetitions and the respective graph with min / max error bars. One can see that some trials were already aborted before reaching the 300 L/m² of filtered volume since the feed pressure exceeded the maximum allowed pressure of 3 bar. This also leads to an irregular shape of the average line at the final stage of the experiment (filtered volume V > 200 L/m²). As previously presented in Table 15, the average standard deviation σ_{tot} of this experiment was about 0.045, indicating an acceptable reproducibility of the test. Henceforward, to avoid the odd representation of average curves, only one representative filtration curve is presented instead for all upcoming experiments / results along with the respective average standard deviation as indicator to the reproducibility of the experiment.

As indicated in Figure 42 a and b, a steady decline in the normalized permeability was noticed due to strong membrane fouling in the three trials, such that membrane lost about 90 % of its performance at the end of the filtration experiment. As it was found in the investigations on the interplay of droplet size distribution and membrane pore size, cf. section 4.2.1, fouling of PES membranes can be explained by combined fouling mechanisms (standard blocking, intermediate blocking, and cake filtration). Such interactions were mostly figured to be derived by both relation between membrane pore size and oil droplet size distribution as well as hydrophobic -hydrophobic interactions (between oil and the membrane mater surfactant monomers adsorption onto membranes is often explained by either electrostatic interaction or hydrophobic association between surfactant molecules and the membrane sites [23, 38, 70]. Comparing the oil droplet size distribution of emulsified oils to the MWCO of the membrane (150 kDa, equivalent to pore size < 30 nm) indicates that the membrane should be able to retain oil droplets mainly via surface filtration; however, few small oil droplets can still pass and be retained inside the membrane matrix resulting in the aforementioned combined fouling mechanisms.

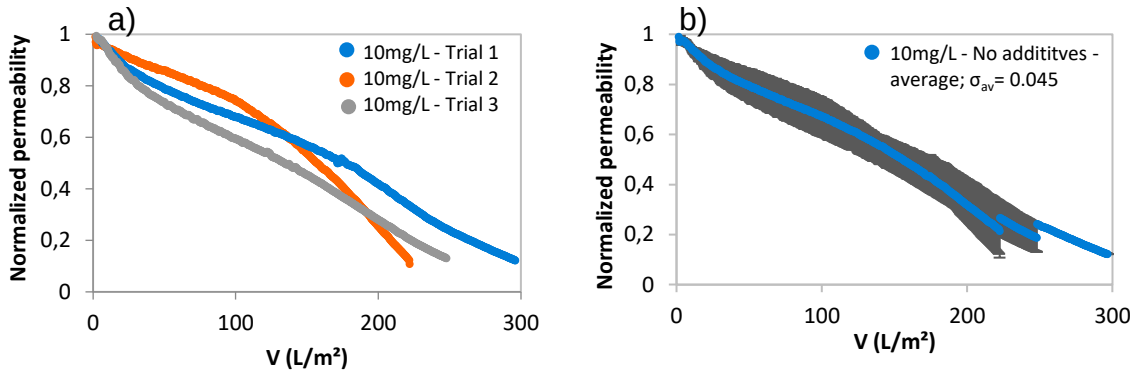

Figure 42: Normalized permeability of UP150 filtering 10 mg/L surfactant-free emulsified oils at a flux of 240 L/(m²·h) (a) for three trials (b) as average of the 3 trials with min/max errors

4.2.3.2 Filtration of oil emulsified oils stabilized by different surfactants

The normalized permeability for three reference filtration tests using oil-free surfactants (SDS, Tween 20 and CTAB) solutions, at concentration of 1 CMC are introduced in Figure 43a. For all surfactants, there was a rapid and sharp decrease in membrane permeability at the beginning of filtration, followed by a plateau. This behavior indicates usually the formation of a rapidly forming pore-blocking layer of surfactant molecules at the membrane surface, followed by the formation of a cake layer with no or very low resistance. However, due to the small size of the surfactants, it is more likely that a large portion of the surfactants will enter the membrane pores and adsorptively accumulate in the supporting structure of the membrane (membrane matrix), which is accompanied by a sharp increase in resistance. Once equilibrium has been reached, there is no further accumulation and the resistance does not increase any further. Nevertheless, in other experiments (compare Figure 43a, c and e), it was noticed that reducing the surfactant concentration to 0.5 CMC resulted in a smaller decrease of the membrane permeability, but a plateau was still observed. Decreasing the surfactant concentration to 0.2 CMC led to more consistent decline in membrane performance especially for CTAB and SDS (i.e., indicates no equilibrium or no complete coverage), while Tween 20 showed plateau at all concentrations. These observations support the hypothesis of the adsorptive fouling mechanism with the formation of an equilibrium loading in the matrix as a function of permeate concentration. This adsorptive fouling behavior also has been reported by other researchers, e.g., Trinh et al (2019) [40].

It can also be seen that the surfactants exhibit analogous fouling, or adsorption behavior, regardless of their different type (i.e., ionic or non-ionic), indicating that adsorption occurs via a hydrophobic-hydrophobic interaction between the relatively hydrophobic PES membrane and the hydrophobic tail of the surfactant molecules. The lower permeability decline in case of Tween 20 compared to SDS and CTAB could be due to its non-ionic character, which has a stronger affinity to hydrophobic substances. This finding is quite interesting, specially that it does not match any of the different effects of surfactants on membrane fouling that were introduced in the literature, for instance Trinh et al (2019) reported an increment, no effect and decline in the permeate flux of a microfiltration membranes when filtering CTAB, Tween 20 and SDS, respectively [40]. Matos et al (2016) claimed that more fouling was observed in ceramic membranes when filtering emulsions stabilized with surfactants carrying charges that are opposite to the membrane charge.

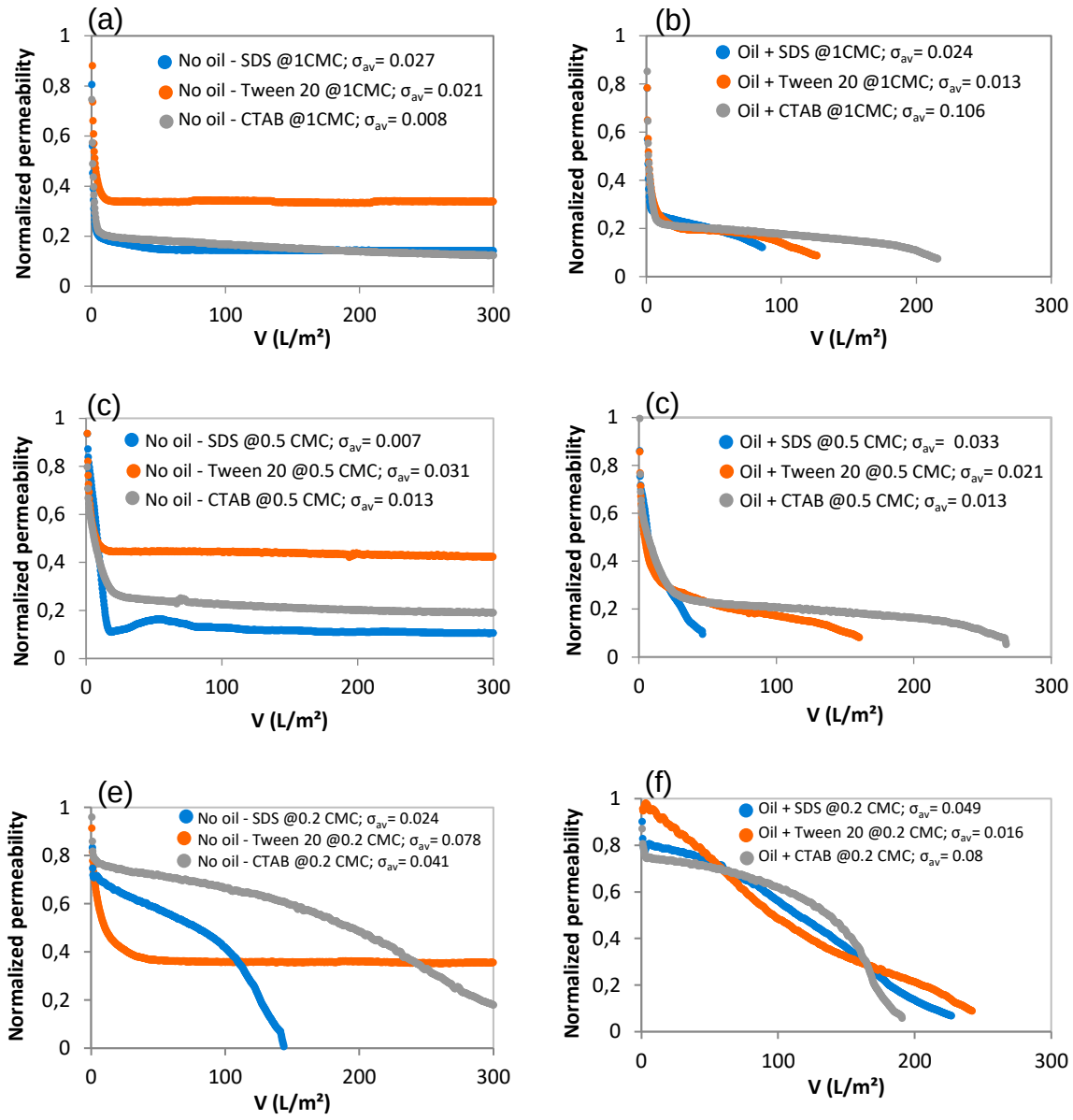

Figure 43: Normalized permeability of UP 150 operated at a flux of 240 L/(m²·h) filtering oil-free surfactant solutions at concentrations of (a) 1.0, (c) 0.5 and (e) 0.2 CMC and emulsified oil at 10 mg/L oil with surfactants at concentrations of (b) 1.0, (d) 0.5 and (f) 0.2 CMC

Filtration experiments using emulsified oils containing surfactants showed a fouling behavior that, at least in the early stage, is more comparable to reference experiments using oil-free surfactant solutions rather than reference experiments using surfactant-free emulsified oils. Figure 43b presents the normalized permeability for filtration experiments using complex oil emulsified oils containing oil at a concentration of 10 mg/L and surfactants at 1 CMC. Although more fouling by the oil occurs as the filtration progresses, as confirmed

by the termination of the filtration prior to the filtration of 300 L/m², this observation indicates that under the conditions and the higher surfactant concentration, fouling was influenced by the surfactants rather than the oil. Moreover, lower surfactant concentrations were found to cause generally lower membrane fouling (compare Figure 43b, d and f). Figure 43f reveals a lower normalized permeability decline at the early stage of filtration compared to the higher surfactant concentrations seen in Figure 43b and d.

Figure 44 presents the normalized permeability for filtration experiments using emulsified oils with the different SDS concentrations of 0.2, 0.5 and 1 CMC, at a fixed oil concentration of 10 mg/L, a constant flux of 240 L/m²·h (Figure 44a) and a constant pressure of 0.4 bar (Figure 44b).

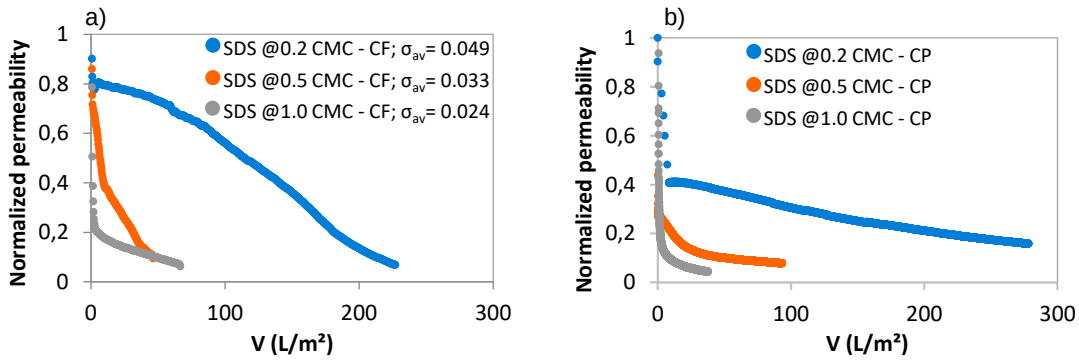

Figure 44: Normalized permeability of UP150 filtering emulsified oils at 10 mg/L containing SDS at concentrations of 0.2, 0.5 and 1 CMC at (a) constant flux (CF) of 240 L/(m²·h) and (b) constant pressure (CP) of 0.4 bar

Generally, normalized permeability declines for filtration experiments at 0.5 CMC were relatively close to those at 1 CMC. Analogues observations were seen for experiments at constant flux and constant pressure. On the other hand, at constant flux operation, emulsified oils with SDS at 0.2 CMC showed lower permeability decline than in case of 0.5 and 1 CMC, in which a sharp normalized permeability decline of 20 % was measured at the beginning of the filtration followed by a consistent gradual decline that reached 90% after filtering ~210 L/m². Such permeability decline was measured after filtering less than 50 L/m² in case of 0.5 and 1 CMC. When operating at constant pressure, similar trends were generally observed as in the constant flux experiments. Nevertheless, differences could be observed, especially at an SDS concentration of 0.2 CMC. For instance, a slightly steeper normalized permeability drop in the early filtration phase was observed in the

filtration experiments compared to the constant flux operation. Overall, the fouling behavior can be considered comparable for both operation modes, i.e., constant flux and constant pressure. Especially considering that the experiments of each operation mode were performed with different filtration setups. Thus, the further experiments focused on only constant flux operation because it is more commonly used in practice than constant pressure mode. Moreover, the morphology of fouled UP150 flat sheet membranes samples were analyzed using SEM and compared with pristine unfouled membranes. As a result SEM micrographs showed no significant alterations. This might indicate no oil penetration to the membrane matrices, i.e., most of membrane fouling (and performance decline) occurred due to surface fouling (oil and/or surfactant adsorption to the membranes surfaces). These observations contradict with earlier claims that a few small oil droplets might be able to pass into the membrane matrix.

4.2.3.3 Influence of co-surfactants and salts on the filtration of emulsified oils stabilized by different surfactants

The influences of emulsified oils containing co-surfactant and artificial seawater salts on UP150 were studied for the three types of surfactants. Figure 45 shows the normalized permeability for filtration experiments of oil-free surfactant solutions at concentration of 0.2 CMC containing 2-pentanol and ASW at concentration of 3.5 g/L, in Figure 45 a, c and e and with oil at 10 mg/L in Figure 45b, d and f. In the reference experiments using oil-free surfactant solutions, a slightly smaller decrease in the normalized permeability was observed with the addition of the co-surfactant (2-pentanol), which was more pronounced for SDS than for the other two surfactants. That might be related to the enhanced solubility of the surfactants in water, and hence, less adsorption on or in the membrane.

Dosing ASW at concentration of 3.5 g/L was found to change the fouling behavior and cause additional fouling in reference experiments in different ways. Less total fouling was noticed in case of SDS and slightly more fouling was noticed in case of Tween 20. Moreover, reference experiments with CTAB and ASW salt were not reproducible. This is due to the fact that CTAB hardly dissolved in water when ASW was added. It is known that salts reduce the solubility of surfactants in water and the CMC [142]. Micelle formation reduces the concentration of free surfactants and thus the equilibrium loading or fouling on or in the membrane. On the other hand, a micelle may well have a size in the range of

the small pores of a UF, which can lead to blocking of pores and thus to increased fouling. Corresponding reference experiments with flat sheet membranes and surfactant-free emulsified oils with salts were carried out, cf. section 4.2.3.1. The results showed that the dosage of salts was associated with lower membrane fouling, regardless of whether the salts were dosed in form of single salts, e.g., NaCl or $CaCl_2$, or as a mixture e.g. ASW. The interaction between SDS and ASW and their influence on the fouling behavior of capillary membranes by model oil-emulsions was also partly studied in previous work. It was observed that both SDS and ASW tend to reduce the membrane fouling. However, the interaction of SDS and ASW caused additional membrane fouling [56].

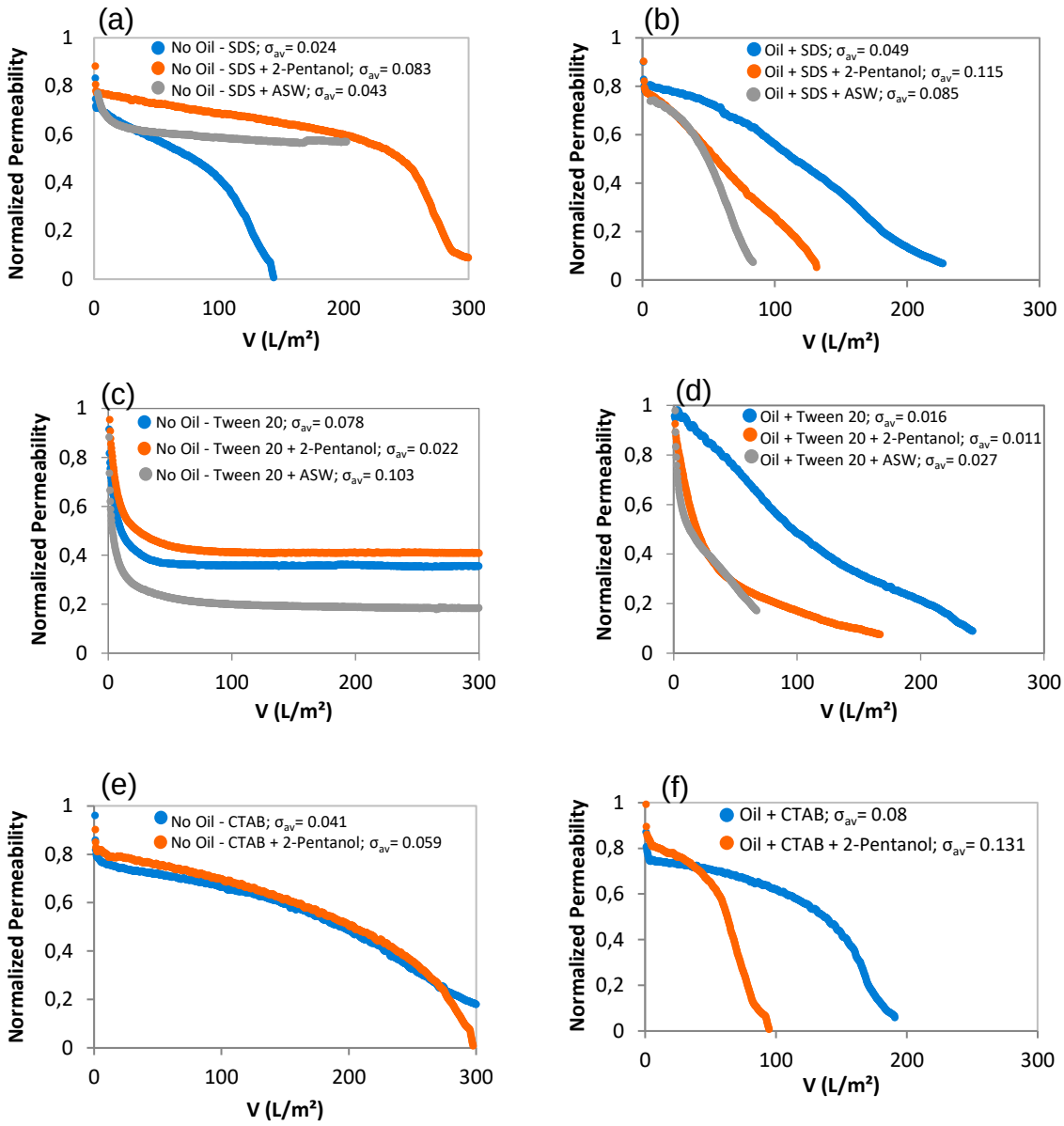

Figure 45: Normalized permeability of UP150 filtering surfactant, 2-pentanol and ASW at a flux of 240 L/m²·h. On the left side reference experiments with oil-free surfactant solutions using (a) SDS, (c) Tween 20 and (e) CTAB and on the right side those with emulsified oils with 10 mg/L oil and (b) SDS, (d) Tween 20 and (f) CTAB

Overall, one can conclude from bench-scale one-cycle filtration experiments using flat sheet membranes that dosing surfactants, co-surfactant and ASW exacerbate the membrane fouling of oil-emulsions at the employed experimental conditions. Stronger membrane fouling can be mainly interpreted by excessive adsorptive fouling by the surfactants on the membrane surface, and most likely inside internal porous structure because of the small surfactant molecular sizes (although not demonstrated in SEM analysis).

Interestingly, when a critical surfactant concentration is exceeded (approx. 0.5 CMC for 10 mg/L oil), the influence of surfactants on fouling already dominates at the beginning of filtration. In the further course of filtration, oil or fouling layer formation gains more and more influence.

It is important to note that no mechanical backwashing was performed in these experiments. Therefore, despite the important findings on the fundamental mechanisms from the studies with a flat sheet membrane, experiments with backwashable capillary membranes are inevitable.

4.3 Improvement of the PES UF dead-end process by testing different strategies

4.3.1 Surfactant-enhanced dead-end ultrafiltration for tertiary treatment of produced water

4.3.1.1 Characterization of surfactant-free and surfactant-modified emulsified oils

Prior to membrane filtration, surfactant-free and surfactant-modified emulsified oils were analyzed to examine the impact(s) of SDS on oil droplet size distribution. Three parameters were determined, d_{32}, $D_{90,V}$, and $D_{90,N}$. Table 16 presents values for the three characteristic parameters for representative emulsified oil samples including stock oil-in-water emulsion, surfactant-free 50 mg/L (as TOC) emulsified oil, in addition to surfactant-free and surfactant-modified 25 mg/L emulsified oils. Generally, the dilution process for stock emulsions was found to have no impact on the oil droplet size distribution, as indicated by comparable values for d_{32}, $D_{90,V}$, $D_{90,N}$ for surfactant-free emulsified oils with different oil contents, considering experimental error ranges. Surfactant-free emulsified oils were found to exhibit d_{32} of 300 - 400 nm, $D_{90,V}$ of 1,000 - 1,100 nm, and $D_{90,N}$ of 300 - 400 nm; hence, they can be classified as sub-micron sized emulsified oils as reported for PW after secondary treatment [18, 40, 41, 72].

The addition of SDS, in this study SDS_{VWR} was utilized unless something else is mentioned, was observed to decrease slightly the oil droplet size distribution compared to surfactant-free emulsified oil. This effect became relatively clear at higher SDS concentrations that may indicate a stabilization effect of the oil droplets. Analogous observations were reported for oil-in-water emulsions prepared from diesel and synthetic base oils using different types of surfactants [41, 72]. Nevertheless, in contrast to [41], no explicit

trends can be concluded for d_{32}, $D_{90,V}$, $D_{90,N}$ values with increasing SDS concentration. This might be mainly attributed to the different nature of the prepared oil-in-water emulsions in [41] (i.e., oil type, different surfactants, and bigger oil droplet size ranges). Besides, in the current study, application of high-pressure homogenizer was revealed to produce stable oil-in-water emulsified oils with sub-micron oil droplet size distribution; therefore, common effects of surfactants on the interfacial tension and oil droplets deformation / breakup are less likely to be remarkable here [23].

Table 16: Oil droplet size distributions for the stock oil-in-water emulsion as well as surfactant-free and surfactant-modified emulsified oils

Oil concentration (mg/L as TOC)	SDS (g/L)	d_{32} (nm)	$D_{90,V}$ (nm)	$D_{90,N}$ (nm)
Stock emulsion	-	362 ± 14*	1,057 ± 44	340 ± 20
50	-	375 ± 3	1,008 ± 23	315 ± 5
25	-	376 ± 9	1,026 ± 30	318 ± 20
25	0.024	374 ± 3	982 ± 61	306 ± 2
25	0.24	344 ± 3	849 ± 7	304 ± 23
25	0.48	347 ± 9	904 ± 62	265 ± 12

*standard deviation

SDS-modified emulsified oils with different oil contents of 5, 10, 25 and 50 mg/L (as TOC) and SDS concentrations of 0.024, 0.12, 0.24, 0.48 and 1.2 g/L were characterized with respect to UV_{254}-active substances, turbidity, total PAHs, conductivity, and zeta-potential. The results are listed in Table 17. Most importantly, SDS-modified emulsified oils exhibited higher negative zeta-potential values compared to surfactant-free emulsified oils. The measured negative zeta-potential for SDS-free emulsified oils (~43 mV, almost constant for all oil concentrations) might be attributed to the physically adsorbed OH^- from the medium. Nevertheless, the increased negative zeta-potential values for SDS-modified emulsified oils are mainly because of the adsorption of surfactant monomers. SDS molecules can be readily adsorbed onto the oil droplet interface at concentrations below CMC such that negatively charged polar groups are directed toward the continuous aqueous phase. For the same oil concentration, increasing SDS concentration was found to increase the zeta-potential toward more negative values; explicit increases were measured for emulsified oils with SDS concentrations ≥ 0.24 g/L. Increasing surface charges atop emulsified oil droplets is beneficial for increasing oil stability and preventing coalescence of oil

droplets in the bulk and during membrane filtration [23, 40]. Moreover, the turbidity values for SDS-modified emulsified oils exhibited an increase compared to the respective SDS-free emulsified oils (except in case of 50 mg/L oil), which might reflect the very-well dispersity and better stability of SDS-modified emulsified oil droplets.

Additionally, dosing of SDS was revealed to have no remarkable influence on the total PAHs contents, considering the experimental error ranges; differences were found to be related to the measurement process rather than the impact of SDS on the extraction of PAH substances. While addition of SDS was observed to significantly increase the conductivity for SDS-modified emulsified oils because of SDS itself as well as possible impurities (e.g., SO_4^{2-}, Cl^-). Furthermore, SDS-modified emulsified oils exhibited relatively higher UV_{254} absorbance values than the corresponding surfactant-free emulsified oils. This might be again related to the measurement difficulties; for instance, the tendency of foam formation with increasing SDS concentration. All surfactant-free and surfactant-modified emulsified oils prepared in this part of the study exhibited an average pH value of 7.41 ± 0.63.

Table 17: Characteristics for surfactant-free and surfactant-modified emulsion oil employed in this study

Oil conc. (mg/L)	SDS (g/L)	UV_{254} (m^{-1})	Turbidity (NTU)	Conductivity (µS/cm)	Total PAH (µg/L)	Zeta-potential (mv)
5	0.0	13.68 ± 0.5	13.1 ± 0.4	6.6 ± 1.3	11.75 ± 2.3	-43.4 ± 0.7
5	0.024	12.98 ± 0.06	14.1 ± 0.5	12.9 ± 2.3	N.A.[1]	-41.8 ± 0.6
5	0.12	13.74 ± 0.08	16.1 ± 0.6	37.8 ± 0.2	N.A.	-42.0 ± 0.6
5	0.24	14.28 ± 0.04	18.1 ± 0.7	65.8 ± 1.3	N.A.	-45.7 ± 0.6
5	0.48	14.89 ± 0.30	18.1 ± 1.0	134.4 ± 1.9	8.5	-54.0 ± 0.7
5	1.2	14.4 ± 0.08	14.1 ± 0.8	327.6 ± 1.0	5.9	-65.6 ± 0.9
10	0.0	29.51 ± 0.58	28.2 ± 0.7	4.9 ± 0.7	15.7 ± 1.0	-44.4 ± 0.9
10	0.024	28.44 ± 0.68	30.1 ± 0.8	11.0 ± 2.0	N.A.	-40.7 ± 0.6
10	0.12	27.54 ± 0.07	30.5 ± 1.8	35.5 ± 0.8	N.A.	-47.9 ± 0.5
10	0.24	27.18 ± 0.03	31.2 ± 1.1	64.7 ± 0.7	N.A.	-48.7 ± 0.5
10	0.48	29.78 ± 0.66	31.1 ± 0.8	134.4 ± 1.2	13.7 ± 1.4	-57.6 ± 0.6
10	1.2	27.37 ± 0.05	27.9 ± 1.5	324.1 ± 2.2	14	-68.3 ± 0.9
25	0.0	80.75 ± 2.3	73.4 ± 0.5	9.2 ± 2.0	42	-45.0 ± 0.6
25	0.48	85.50 ± 0.09	72.1 ± 3.5	140.6 ± 2.6	40	-65.9 ± 0.7
50	0.0	161.8 ± 0.52	149.2 ± 0.9	6.2 ± 0.4	80	-43.2 ± 0.6
50	0.48	163.5 ± 0.66	145.0 ± 5.6	129 ± 5.1	81	-66.8 ± 0.8

4.3.1.2 Reference filtration tests using oil-free surfactant solution and surfactant-free emulsified oil

Prior to mini-plant filtration tests using surfactant-modified emulsified oils, two sets of reference filtration experiments were performed at analogous operating conditions (i.e., constant flux dead-end multiple-cycle filtration with periodic hydraulic backwashing); one set with oil-free SDS solutions and another set with surfactant-free emulsified oils. These experiments aimed at investigating the fouling propensity (or adsorption ability) of each component as well as the individual impact(s) on SM capillary membrane performance at different initial concentrations.

4.3.1.2.1 Multiple-cycle filtration of oil-free SDS solution

A series of reference multiple-cycle dead-end filtration tests were conducted using oil-free SDS solutions with different initial concentrations below CMC (0.024, 0.12, 0.48 and 1.2 g/L, equivalent to 0.01, 0.05, 0.2 and 0.5 CMC, respectively). The normalized permeability curves for consecutive six filtration cycles with periodic hydraulic backwashing are presented in Figure 46. Filtration of oil-free SDS solutions at concentrations of 0.024, 0.12 and 0.48 g/L exhibited a limited normalized permeability decline at the very beginning of the first cycle (~ 10 %, 18 % and 20 %, respectively) followed by a long-pronounced plateau. The higher the SDS concentration the lower the plateau of normalized permeability, implying that a certain concentration-dependent equilibrium was reached. While filtration of 1.2 g/L SDS resulted in a substantial normalized permeability decline of about 80 % followed by a much shorter plateau until the end of the filtration cycle. Nevertheless, typical hydraulic backwashing was found to sufficiently restore the initial membrane performance (~ 100 %), irrespective of SDS concentration. The following filtration cycles, until the sixth cycle, showed almost the same pattern as the first cycle for all surfactant concentrations.

The consistent decrease in membrane permeability with increasing SDS concentration, but still below CMC, can be interpreted by the adsorption of SDS monomers (molecules) into the inner PES membrane structure and the consequent pores narrowing and/or reduced bulk porosity [41, 70, 72, 143]. The adsorption of surfactants on polymeric membranes is extensively studied in literature [17, 38, 68, 70, 72]. Adsorption of surfactant to membranes was found to result in two main effects, decay of permeate flux due to

decreasing of effective membrane pore diameter, and alteration of membrane surface characteristics because of surfactant-membrane interactions [41, 72].

When surfactant concentration is below CMC, surfactant monomers adsorption onto membranes is often explained by either electrostatic interaction or hydrophobic association between surfactant molecules and the membrane sites [38, 70]. In the present study, the adsorption of SDS molecules onto capillary membrane surface and pores can be explained by hydrophobic association between non-polar tail in SDS molecules and hydrophobic domains on PES, which increased with increasing SDS concentration until maintaining certain equilibrium that was represented by the plateau at the end of every filtration cycle (i.e., no further SDS molecules adhered to the membrane). The good / favored adsorption of SDS monomers on PES membranes was also reported by earlier studies [38, 69, 70]. Furthermore, many studies regarded adsorption of surfactants (at concentrations below CMC) as adsorption in monolayers, where two-step isotherm model developed by Zhu and Gu [38, 72, 144] is often adopted. Here, surfactant monomers are adsorbed as single molecules into the membrane matrix to form a monolayer, then surface micellization may occur upon increasing of surfactant concentration forming hemi-micelles [38, 143]. Nevertheless, the latter mechanism is unlikely to be applicable in the present study due to the low retention of SDS by SM capillary UF membrane, since SDS has low molecular-weight (~ 288.4 g/mole) and the radius of SDS micelles is reported to be ~ 2.5 nm [70, 145], while the nominal membrane pore diameter is 20 nm.

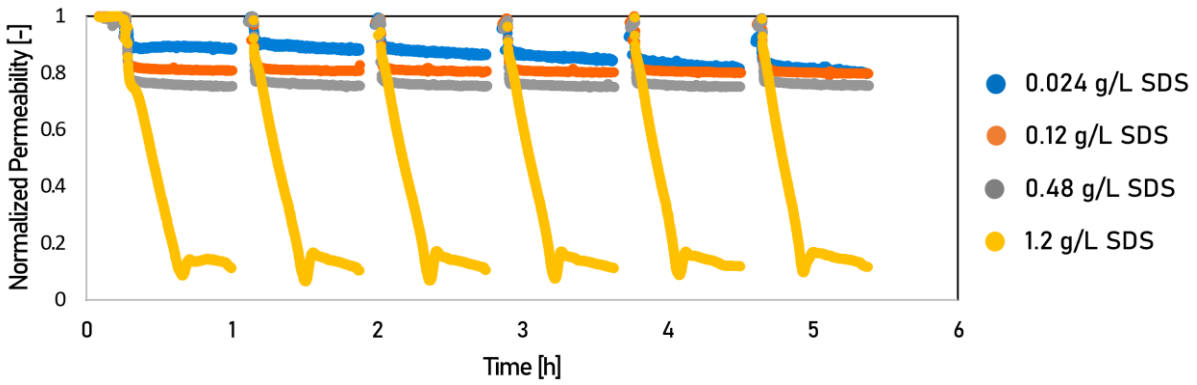

Figure 46: Normalized permeability curves for SM membranes in reference filtration tests with multiple-cycles at a constant flux of 100 L/(m²·h) using oil-free SDS solutions of different concentrations (0.024 - 1.2 g/L)

On the other hand, almost the complete recovery of PES membranes permeability by simple hydraulic backwashing, irrespective of SDS concentration and the extent of performance decay, may indicate that the adsorption of SDS monomers to the relatively hydrophilic PES membranes was obviously weak, although a kind of concentration-dependent equilibrium was observed. This behavior might be interpreted by the possibly repulsive interactions between the negative polar heads of SDS molecules and the negative charges atop PES membranes surface (due to the physically adsorbed hydroxide ions as indicated by zeta-potential measurements, cf. Table 17). Analogous findings were reported [41, 68]. For instance, molecular dynamic simulations by Ma et al. revealed that SDS molecules were least adsorbed by hydrophilic PVDF membrane due to the repulsive enthalpic interactions at very small SDS−membrane distances, notwithstanding the fact that dead-end filtration of SDS exhibited the worst flux decline (by enthalpic-driven adsorption) and the lowest retention [68]. This means that SDS molecules in the bulk first got attracted then repelled when they got too close to the membrane surface. Therefore, several studies reported better correlation between the extent of membrane fouling and the repulsive rather than attractive membrane-surfactant interactions [23, 40, 68].

4.3.1.2.2 Multiple-cycle filtration of surfactant-free emulsified oil

The second series of multiple-cycle reference filtration experiments was carried out employing surfactant-free emulsified oils with different crude oil concentrations of 5, 10 and 25 mg/L. Generally, substantial membrane performance decay was observed for dead-end filtration of surfactant-free emulsified oils with increasing oil concentration, as depicted in Figure 47. Multiple-cycle filtration tests using 5 mg/L surfactant-free emulsified oil showed a steady membrane performance decay along the experiment with an overall normalized permeability decline of 55 % measured at the end of the sixth cycle. One can also see almost constant normalized permeability decline rate over all filtration cycles with low hydraulic backwashing efficiency. Accordingly, the analysis of fouling resistances (see Figure 48) revealed that the distributive hydraulic irreversible fouling ($\Delta R_{irr,i}$) was almost constant but significantly higher than the distributive hydraulic reversible fouling ($R_{rev,i}$) in all filtration cycles, cf. Figure 48a; however, such difference was gradually decreasing for later cycles. The cumulative hydraulic irreversible fouling ($R_{irr,i}$) increased with a similar slope as the distributive reversible fouling ($R_{rev,i}$) but was also significantly higher.

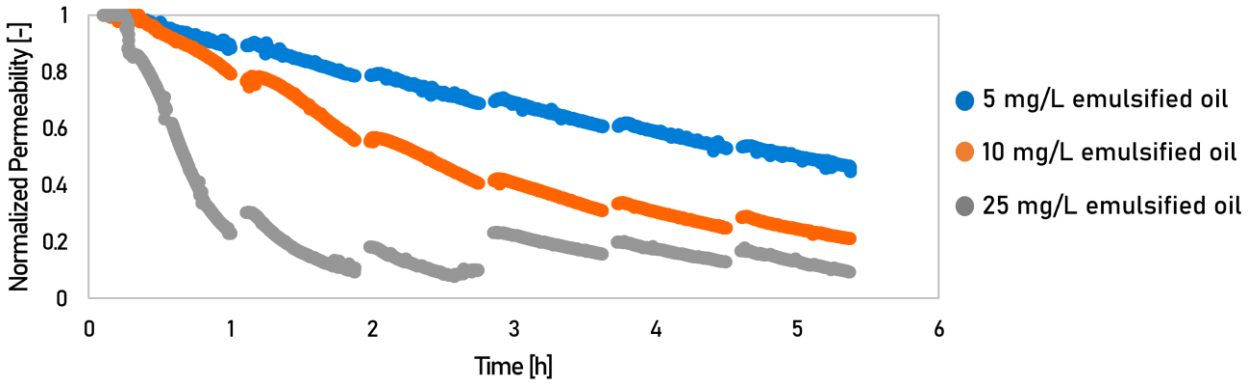

Figure 47: Normalized permeability curves for SM membranes in reference filtration tests with multiple-cycles at a constant flux of 100 L/(m²·h) using surfactant-free emulsified oils with different oil contents of 5, 10 and 25 mg/L

On the other hand, multiple-cycle filtration tests using surfactant-free 10 mg/L and 25 mg/L emulsified oils exhibited severer membrane performance decay with overall normalized permeability declines of ~ 80 % and ~ 90 %, respectively (cf. Figure 47). Additionally, more substantial performance decay was seen in the first three filtration cycles in both experiments compared to filtration using surfactant-free 5 mg/L emulsified oil. Whereas rather constant normalized permeability decay rates were observed over the last three filtration cycles in both experiments (i.e., 10 mg/L and 25 mg/L emulsified oils) that were comparable to that in case of 5 mg/L emulsified oil. Furthermore, analysis of fouling resistances revealed that the distributive hydraulic reversible fouling ($R_{rev,i}$) increased with increasing emulsified oil concentration (see Figure 48a-c), but the same was also true for the cumulative hydraulic irreversible fouling ($R_{irr,i}$). Nevertheless, the increase of distributive hydraulic irreversible fouling ($\Delta R_{irr,i}$) was less or even negative and converged for all emulsified oils, either with filtration progression or further filtration cycles. These observations imply that surfactant-free emulsified oils fouled PES capillary membranes via adsorption mechanism through hydrophobic-hydrophobic interactions between the hydrophobic oil and non-charged sites (or hydrophobic domains) on the membrane, which is concentration-dependent, i.e., the higher oil concentration the more oil adhesion to the membrane and the more performance decay. After certain filtration cycles, the adsorption equilibrium is more-or-less approached and cake filtration mechanism prevails resulting in a better hydraulic backwashing efficiency.

Overall, one can conclude that the oil adhesion to capillary PES membrane is influenced by certain hydraulic irreversible and hydraulic reversible effects. Hydraulic irreversible effects are mainly caused by the strong hydrophobic-hydrophobic interactions as well as the possible coalescence of the retained oil droplets in the membrane vicinity (that can block the access of backwashing water and deteriorate hydraulic backwashing efficiency). While the hydraulic reversible effects may be attributed to the charged membrane sites, where oil can be less adherent and better removable by typical hydraulic backwashing. Subsequently, severe irreversible fouling by surfactant-free emulsified oils at early filtration cycles can be explained by intensive oil adhesion to the membrane (to the non-charged hydrophobic sites), either by increasing oil concentration and/or filtration cycles, whereas, at certain loading during later filtration cycles, more reversible fouling and better hydraulic backwashing ability are rather ascribed to the weak (energetically less favorable) oil adhesion to the charged membrane sites.

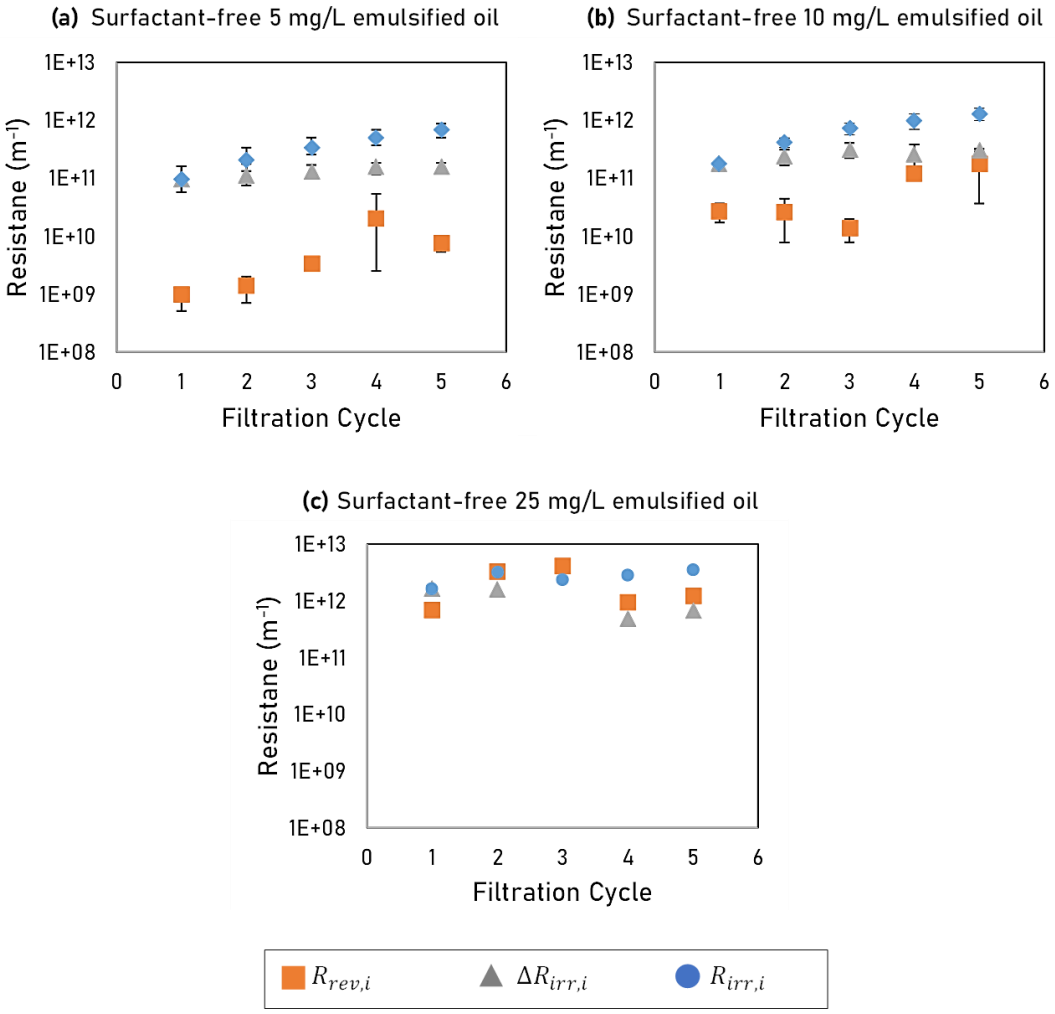

Figure 48: Distributive and cumulative fouling resistances for SM membranes during multiple-cycle reference filtration tests at a constant flux of 100 L/(m²·h) using surfactant-free emulsified oils with different oil contents of 5, 10 and 25 mg/L. The plotted data are the average fouling resistance values calculated from different repetitions. Error bars represent min/max values

4.3.1.3 Mini-plant filtration tests using emulsified oils stabilized by Tween 20

Mini-plant multiple filtration cycle experiments for testing the fouling behavior and backwash efficiency of SM membranes fouled by emulsified oils stabilized by Tween 20 were carried out. These experiments were conducted at oil concentration of 5 mg/L and Tween 20 concentrations of 0.2 and 0.5 CMC at a constant flux of 100 L/(m²·h). Significant irreversible membrane fouling was noticed at both Tween 20 concentrations. Figure 49 shows a significant drop of more than 60 % of the initial permeability, which could be restored by a maximum of 15 % by hydraulic backwashing. Such strong irreversible

fouling can be attributed to the non-ionic character of Tween 20, which caused too strong hydrophobic-hydrophobic interaction between the elongated lyophilic (non-ionic) tail in Tween 20 and the relatively hydrophobic membrane material. As a result, it was decided not to extend the investigations on the improvement of the membrane performance using Tween 20, and instead more attention was paid to the promising results obtained by adding SDS, see the following section 4.3.1.4.

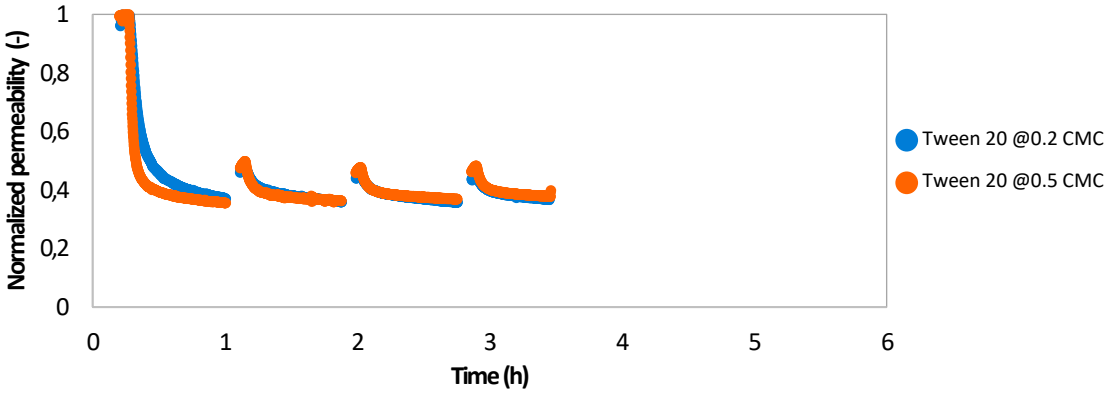

Figure 49: Normalized permeability for filtration of 5 mg/L emulsified oils containing Tween20 at concentrations of 0.2 and 0.5 CMC employing SM membranes at a constant flux of 100 L/(m²·h)

4.3.1.4 Mini-plant filtration tests using surfactant-modified emulsified oil: SDS-enhanced dead-end ultrafiltration

Numerous mini-plant multiple-cycle dead-end filtration tests using different sets of surfactant-modified emulsified oils with different oil contents (5 - 50 mg/L) and SDS concentrations (0.024 - 1.2 g/L) were conducted at conditions analogous to full-scale application to examine the reliability of SDS-enhanced dead-end ultrafiltration for the tertiary treatment of PW. The impacts of SDS dosing prior to membrane filtration on the fouling propensity of capillary PES membranes (cf. Sections 4.3.1.4.1 – 4.3.1.4.3 and 4.3.1.5) and their separation performance (cf. Section 4.3.1.6) were investigated. Here, the results of multiple-cycle filtration tests using surfactant-modified emulsified oils with oil contents of 5 mg/L and 10 mg/L are firstly discussed, afterward the best-suited conditions were applied for mini-plant experiments using surfactant-modified emulsified oils with the higher oil contents of 25 mg/L and 50 mg/L.

4.3.1.4.1 Filtration tests using SDS-modified 5 mg/L emulsified oil

Normalized permeability curves for capillary membranes during multiple-cycle dead-end filtration of SDS-modified emulsified oils with oil content of 5 mg/L and SDS concentrations of 0.024, 0.12, 0.24, 0.48 and 1.2 g/L are shown in Figure 50.

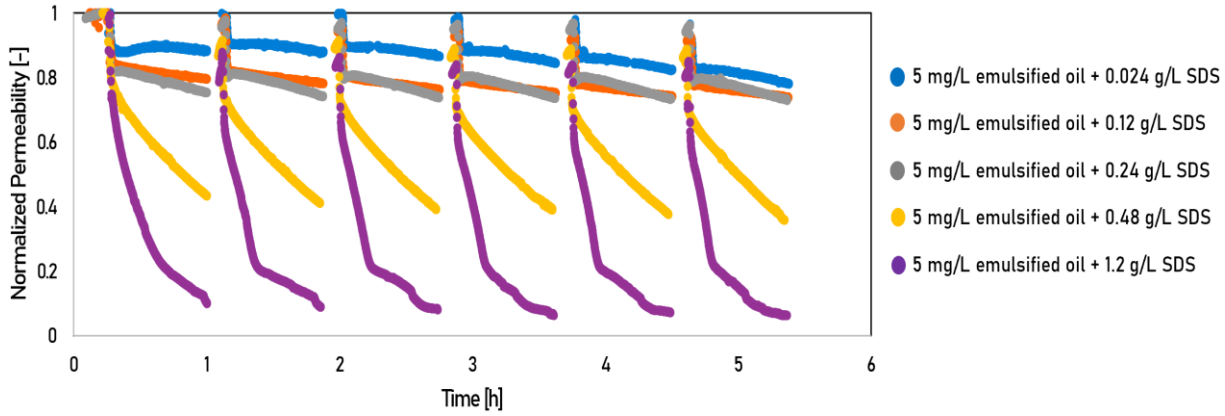

Figure 50: Normalized permeability curves for SM membranes during mini-plant filtration tests at a constant flux of 100 L/(m²·h) using SDS-modified 5 mg/L emulsified oils with different SDS concentrations (0.024 - 1.2 g/L)

Besides, permeability recovery (PR%) values are presented in Figure 51. The decline trends (patterns) of the normalized permeability appears much closer to those of multiple-cycle reference filtration tests using respective oil-free SDS solutions (i.e., almost similar decline rates, except for 0.48 g/L SDS, see Figure 46) rather than reference tests using surfactant-free 5 mg/L emulsified oil (cf. Figure 47). For instance, dead-end filtration of emulsified oils with SDS concentrations of 0.024, 0.12 and 0.24 g/L exhibited initial normalized permeability declines of 10 – 20 % followed by a near plateau (or sometimes with a very limited steady decline) that were substantially restored by typical hydraulic backwashing (i.e., PR% measured after the first cycle was 95%, 96% and 95%, respectively, cf. Figure 51).

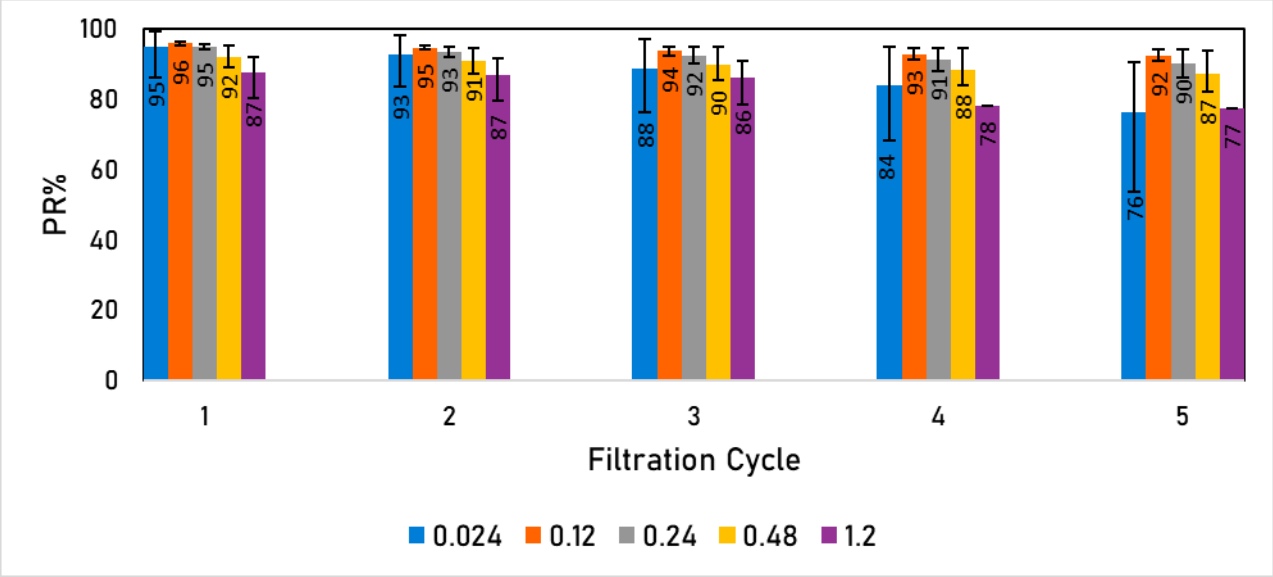

Figure 51: PR% values determined for multiple-cycle dead-end filtration tests at constant flux of 100 L/(m²·h) using SDS-modified 5 mg/L emulsified oils with different SDS concentrations (0.024 - 1.2 g/L)

Such normalized permeability decline behavior was repeatable for the subsequent filtration cycles until the sixth cycle, which was quite close to the behavior during reference tests using the same oil-free SDS concentrations. Therefore, one can claim that the surfactant impacts on the fouling behavior of capillary membranes in dead-end filtration were prevailing the oil effects. This implies that the membrane fouling by SDS-modified emulsified oil can by caused by two main phenomena, adsorption of SDS-modified emulsified oil droplets (i.e., negatively charged sub-micron oil droplets) onto PES membrane surface, and adsorption of excess SDS monomers into PES membrane matrix. This finding is supported by the severer normalized permeability declines per one cycle (up to 90 %) that were measured for SDS-modified emulsified oils with the higher SDS concentrations of 0.48 and 1.2 g/L. Nevertheless, since SDS adsorption on PES membranes was found to be weak or reversible (because of repulsive forces between negative charges on both SDS polar heads and charged membrane site), SDS dosing prior to membrane filtration was indeed beneficial for mitigating irreversible membrane fouling and significantly promoting hydraulic backwashing efficiency, as seen in Figure 50. Additionally, typical hydraulic backwashing at the end of first filtration cycle was able to restore 92 % and 88 % of the initial membrane performance for SDS-modified emulsified oil with SDS concentrations of 0.48 and 1.2 g/L, respectively. After the fifth filtration cycle (overall PR%), PR%

values were 87 % and 77 %, respectively compared to only 45% in case of surfactant-free 5 mg/L emulsified oil, cf. Figure 51 and Figure 55).

Moreover, the analysis of the fouling resistances for filtration tests using SDS-modified 5 mg/L emulsified oils (cf. Figure 52b-f) revealed that the distributive hydraulic reversible fouling ($R_{rev,i}$) increased with increasing SDS concentration and outperformed both distributive and cumulative irreversible fouling ($\Delta R_{irr,i}$ and $R_{irr,i}$, respectively) in all filtration cycles, compared to SDS-free 5 mg/L emulsified oil (cf. Figure 52a). The highest $R_{rev,i}$ values were determined for SDS-modified emulsified oil with 1.2 g/L SDS, cf. Figure 52f. Additionally, one can see that the gradual increasing trend for cumulative irreversible fouling ($R_{irr,i}$) values in case of SDS-free emulsified oil was replaced by rather consistent lower trends in all filtration tests using SDS-modified emulsified oils. Furthermore, in contrast to SDS-free emulsified oil, filtration tests using SDS-modified emulsified oils with SDS concentration ≥ 0.12 g/L (cf. Figure 52c-f) exhibited remarkable decreasing trends for $\Delta R_{irr,i}$ values.

By comparing the impacts of different SDS doses, one may conclude that both SDS concentrations of 0.24 g/L and 0.48 g/L can be effective for multiple-cycles dead-end filtration experiments with 5 mg/L emulsified oil since both concentrations were found to result in consistently promoted $R_{rev,i}$ values along with steadily reduced $\Delta R_{irr,i}$ values and rather constant $R_{irr,i}$ values (cf. Figure 52d and e). Nevertheless, SDS concentration of 0.48 g/L can be regarded as the most-suited dose because, compared to lower SDS concentrations, it effectively modified emulsified oil droplets negative surface charges (zeta-potential increased to - 54.0 ± 0.7 mV, cf. Table 17) what is beneficial for emulsified oil stability and preventing oil coalescence in the membrane vicinity during filtration [18, 23, 72].

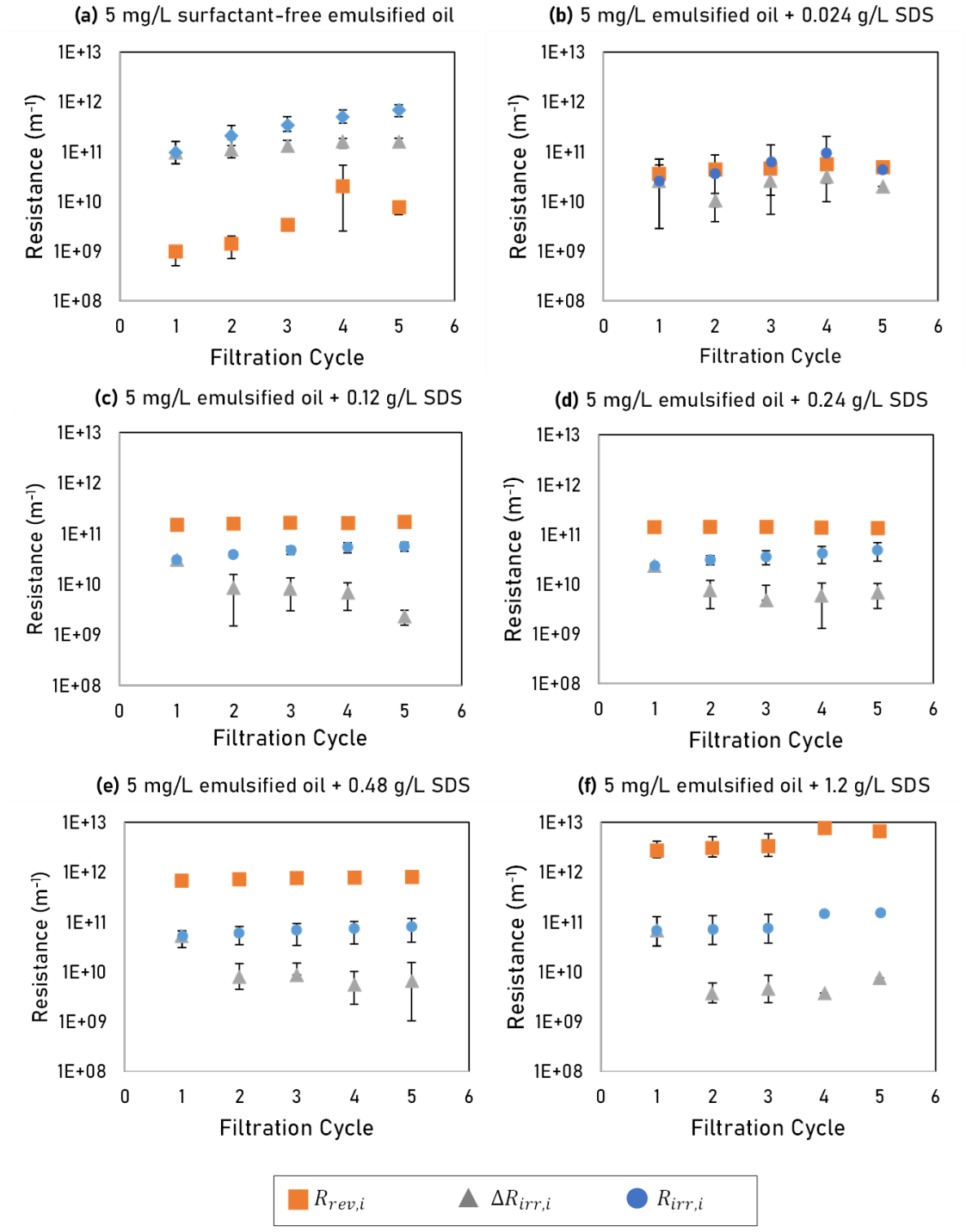

Figure 52: Distributive and cumulative fouling resistances for SM membranes during mini-plant dead-end filtration tests of SDS-modified 5 mg/L emulsified oil with SDS concentrations of 0.024, 0.12, 0.24, 0.48 and 1.2 g/L, compared to SDS-free emulsified oil. The plotted data are the average fouling resistance values calculated from different repetitions. Error bars represent min/max values

4.3.1.4.2 *Filtration tests using SDS-modified 10 mg/L emulsified oil*

Mini-plant filtration tests using SDS-modified emulsified oils at higher oil concentration of 10 mg/L were conducted employing analogous SDS concentrations range of 0.024 - 1.2 g/L; normalized permeability curves are presented in Figure 53.

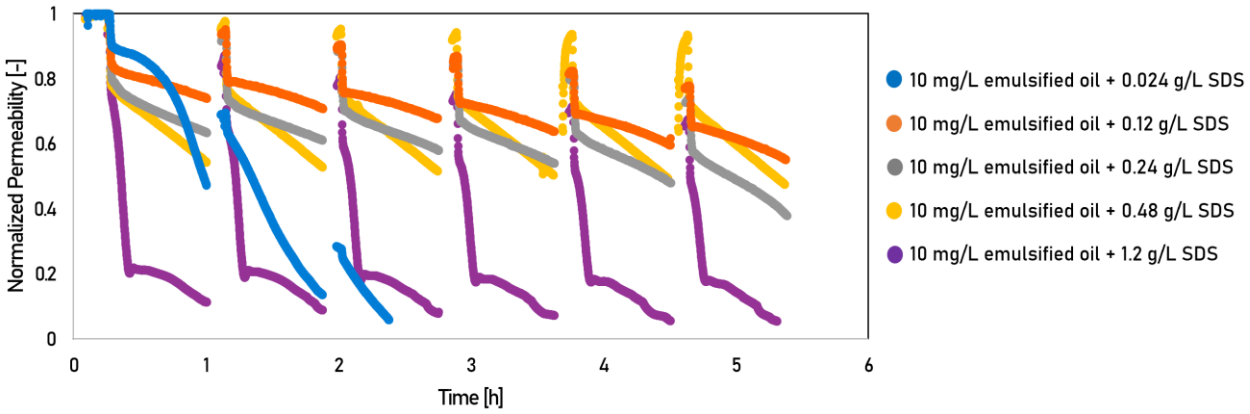

Figure 53: Normalized permeability curves for SM membranes during mini-plant filtration tests at constant flux of 100 L/(m²·h) using SDS-modified 10 mg/L emulsified oils with different SDS concentrations (0.024 - 1.2 g/L)

Besides, PR% values are presented in Figure 54. A substantially improved performance was generally found for most SDS doses. However, the lowest SDS concentration 0.024 g/L was insufficient to mitigate hydraulic irreversible fouling (as also revealed from Figure 56b); hydraulic backwashing could not restore severe performance decay caused in the first two filtration cycles (PR% after the second cycle was 33 %). Accordingly, the filtration test was aborted during the third cycle as the transmembrane pressure reached the maximum limit of 4 bar.

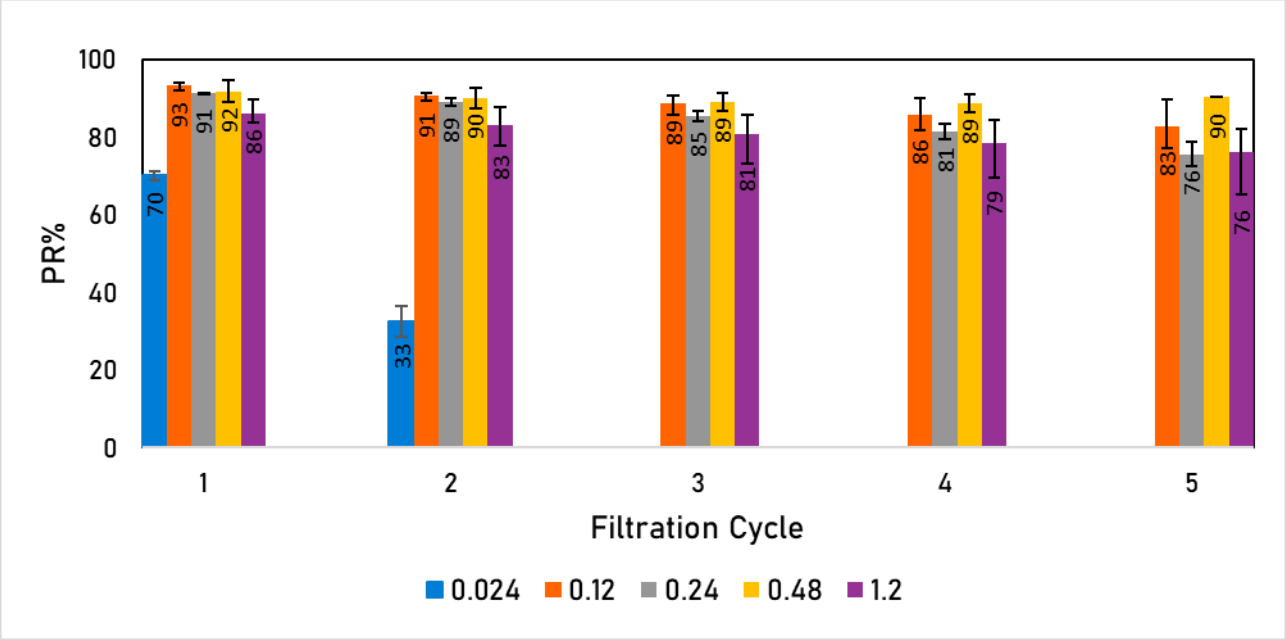

Figure 54: PR% values determined for multiple-cycle dead-end filtration tests at constant flux of 100 L/(m²·h) using SDS-modified 10 mg/L emulsified oils with different SDS concentrations (0.024 - 1.2 g/L)

Such observations were consistent with the low zeta-potential (low surface charges) measured for this SDS-modified emulsified oil type (cf. Table 17) that implies higher probability of oil coalescence in the membrane vicinity. Hence, one can claim that there is a certain SDS dose that should be maintained to obtain the desired enhanced membrane performance. Otherwise, modification of emulsified oil droplets is not sufficient, oil adhesion to membrane occurs extensively, and hence, typical hydraulic backwashing is not capable of restoring the membrane performance.

Moreover, filtrations of SDS-modified 10 mg/L emulsified oils with higher SDS concentrations (specially, 0.12 and 0.24 g/L) exhibited stronger performance decay per cycle, compared to 5 mg/L emulsified oils at analogous SDS concentrations, which can be attributed to the higher oil content. Besides, hydraulic backwashing efficiency for all SDS-modified 10 mg/L emulsified oils (except for SDS dose of 0.48 g/L) was generally less compared to SDS-modified 5 mg/L emulsified oils (cf. Figure 50). PR% values determined after the first cycle were 93 %, 91 %, 86 % for SDS-modified 10 mg/L emulsified oils with SDS concentrations of 0.12, 0.24, 1.2 g/L, respectively, while PR% values after the fifth cycle (overall PR%) were 83 %, 76 %, 76 %, respectively (cf. Figure 54). However, this was substantially enhanced performance when compared to reference tests using surfactant-free

10 mg/L emulsified oil (overall PR% of 34 %, cf. Figure 55). Overall, dead-end filtration of 10 mg/L emulsified oil with SDS concentration of 0.48 g/L exhibited the most consistent membrane performance with the highest hydraulic backwashing efficiency (PR% values were 92 % and 90 % after the first and the fifth cycle, respectively).

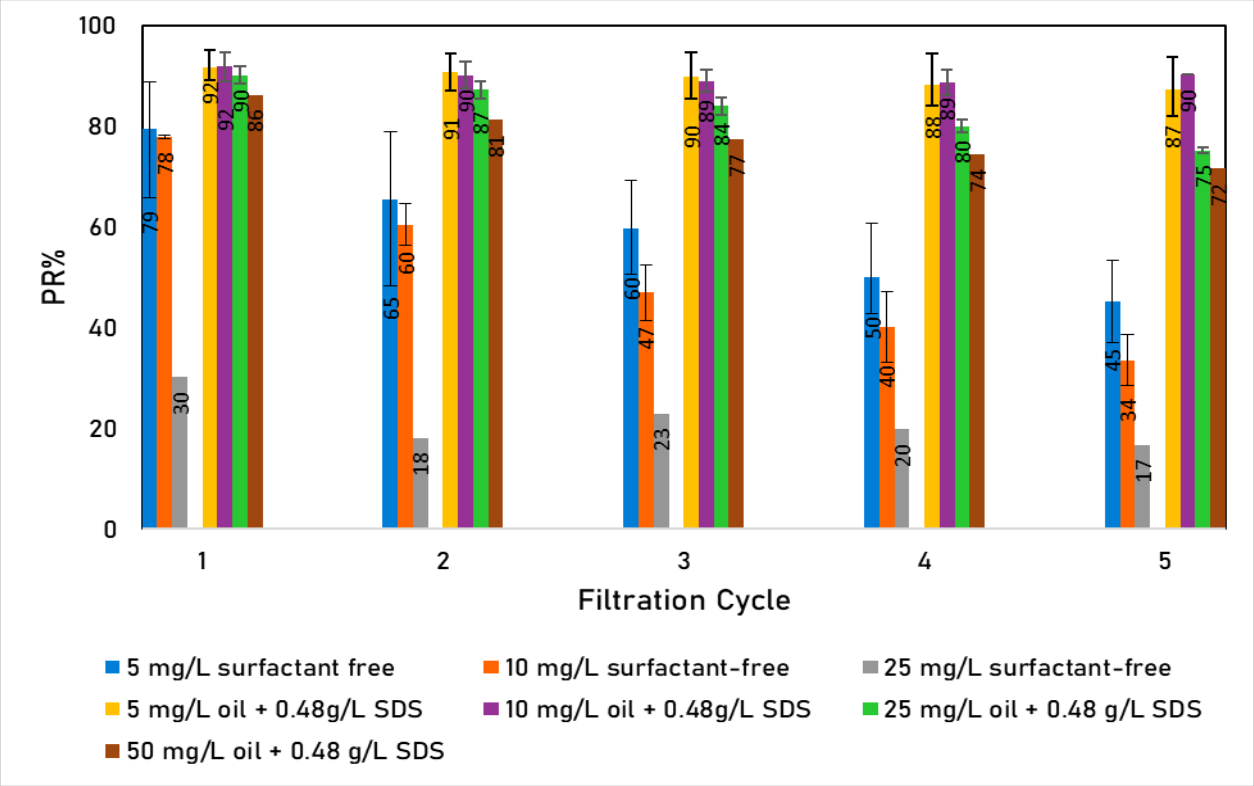

Figure 55: Overview on PR% values determined for multiple-cycle dead-end filtration tests at constant flux of 10 L/(m²·h) using SDS-free and SDS-modified emulsified oils with different oil concentrations (5 – 50 mg/L) and constant SDS concentrations of 0.48 g/L

Furthermore, the trends for distributive and cumulative fouling resistances supported the above findings, see Figure 56. All filtration tests using SDS-modified emulsified oils showed remarkably improved hydraulic reversible fouling per cycle ($R_{rev,i}$) compared to the surfactant-free reference test. Besides, $R_{rev,i}$ could outperform both irreversible fouling resistances $R_{irr,i}$ and $\Delta R_{irr,i}$ in all filtration cycles. Nevertheless, filtration of SDS-modified emulsified oil with 0.024 g/L SDS exhibited the highest hydraulic irreversible fouling resistances in two cycles (cf. Figure 56b) that was responsible for the automatic shutdown of the experiment due to severe membrane fouling. In contrast, increasing SDS concentration to 0.12 g/L and 0.24 g/L decreased the distributive hydraulic irreversible fouling

($\Delta R_{irr,i}$) to some extent; however, one can still see increasing trends for $R_{irr,i}$ in all filtration cycles, see Figure 56c and d, respectively. While filtration tests using SDS-modified emulsified oils with SDS concentrations of 0.48 g/L and 1.2 g/L exhibited almost consistent non-increasing trends for $R_{rev,i}$ and $R_{irr,i}$ in all cycles along with decreasing trend for $\Delta R_{irr,i}$ values. Nevertheless, considering SDS impacts on emulsified oil droplets surface charge (cf. Table 17) and capillary membranes performance, SDS concentration of 0.48 g/L was concluded to be the best-suited dose at the applied experimental conditions. Accordingly, this SDS concentration was furtherly examined for multiple-cycle dead-end filtration tests with higher oil concentrations of 25 mg/L and 50 mg/L.

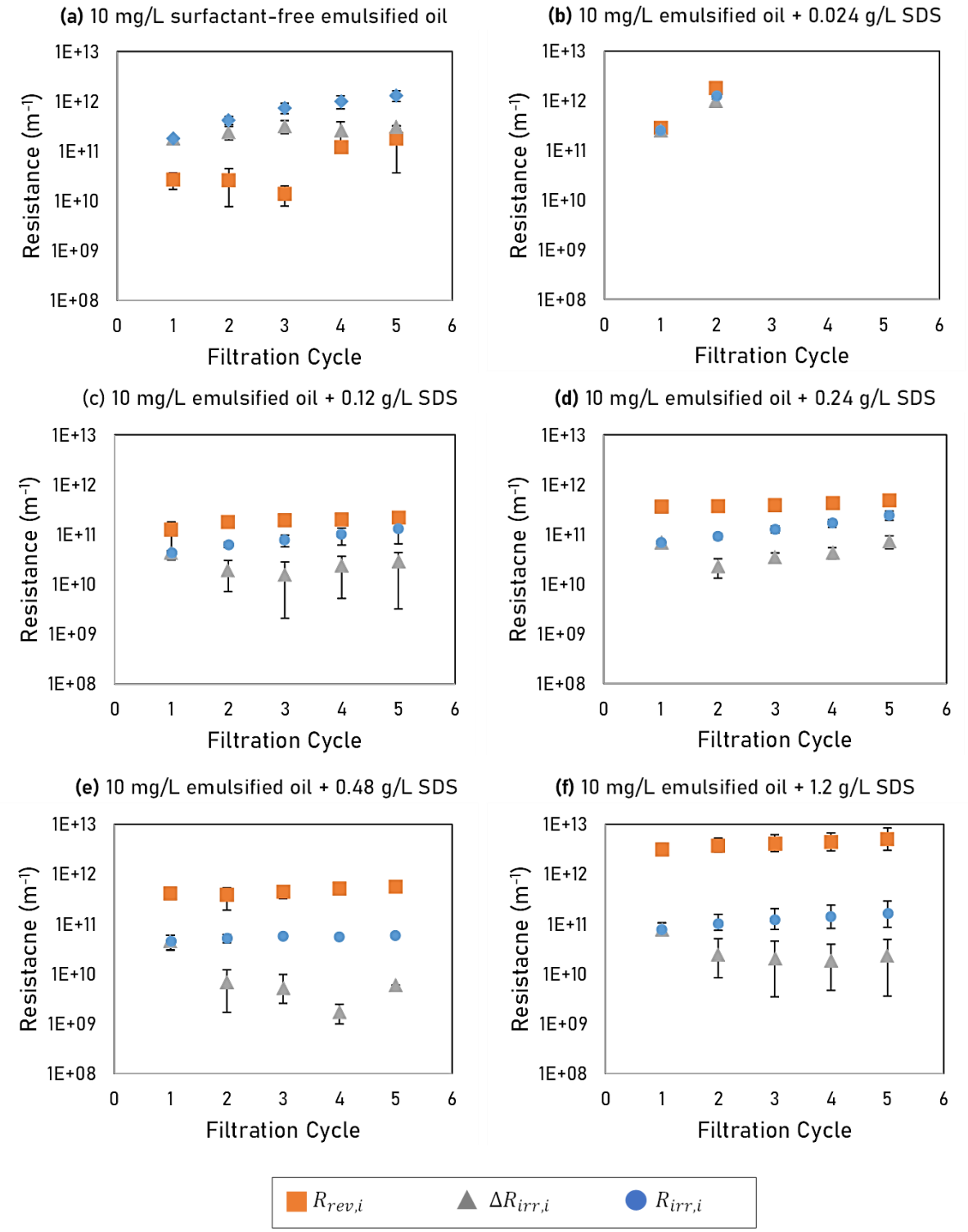

Figure 56: **Distributive and cumulative fouling resistances for SM membranes during mini-plant dead-end filtration tests of SDS-modified 10 mg/L emulsified oil with SDS concentrations of 0.024, 0.12, 0.24, 0.48 and 1.2 g/L, compared to SDS-free emulsified oil. The plotted data are the average fouling resistance values calculated from different repetitions. Error bars represent min/max values**

4.3.1.4.3 Filtration tests using SDS-modified emulsified oils with higher oil contents

Because of the quite different characteristics reported in literature for PW in the polishing step (e.g., oil concentration range of 10 – 100 mg/L), it was essential to examine the applicability of the developed SDS-enhanced dead-end ultrafiltration procedure for the treatment of emulsified oils with higher oil concentrations. The performance curves for capillary membranes in multiple-cycle dead-end filtration tests using SDS-modified emulsified oils with oil contents of 25 mg/L and 50 mg/L and constant SDS concentration of 0.48 g/L are presented in Figure 57a and b, respectively. Besides, permeability recovery (PR%) values are presented in Figure 55.

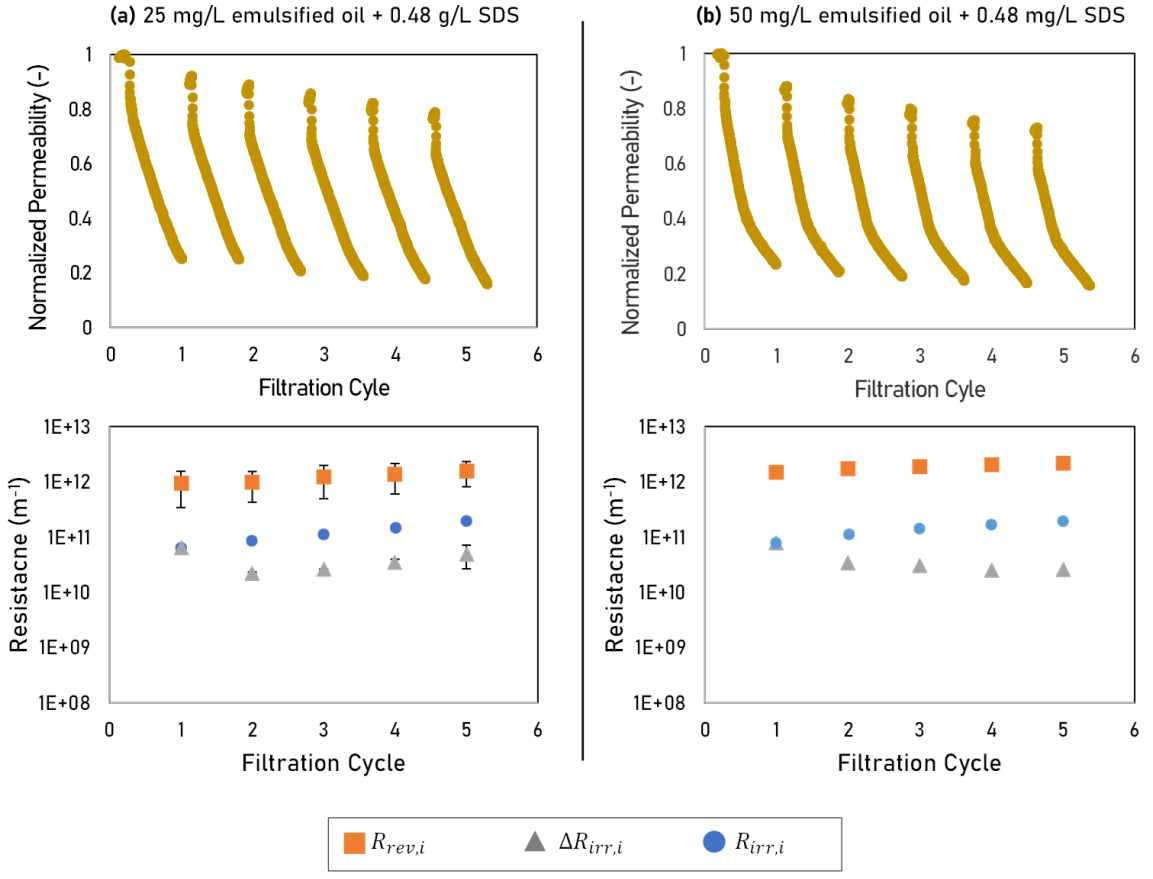

Figure 57: Normalized permeability curves as well as fouling resistances for SM membranes during mini-plant filtration tests at constant flux of 100 L/(m²·h) using SDS-modified emulsified oils with oil contents of 25 mg/L and 50 mg/L and constant SDS concentration of 0.48 g/L

Generally, severer normalized permeability declines per one cycle were observed for both dead-end filtration tests using SDS-modified 25 mg/L and 50 mg/L emulsified oils (~75 % and ~80 %, respectively) when compared with emulsified oils of 5 mg/L and 10 mg/L at the same SDS concentration. As explained earlier, the impacts of SDS on the normalized permeability decline curves were prevailing the oil effects; however, higher oil concentration, and thus more oil adsorption load to the membrane matrix, caused steeper decline rates and more hydraulic irreversible fouling. Interestingly, periodic typical hydraulic backwashing could successfully clean the oil fouling such that PR% values after the first filtration cycle were 90 % and 86 % for SDS-modified 25 mg/L and 50 mg/L emulsified oils, respectively, besides PR% values after the fifth filtration cycle (overall PR%) were 75 % and 72 %, respectively. This is a substantial enhancement compared to a quite low hydraulic backwashing efficiency ((overall PR%) of 17 %) in case of reference tests using surfactant-free 25 mg/L emulsified oil (cf. Figure 47); while multiple-cycle reference filtration tests using surfactant-free 50 mg/L emulsified oil was practically infeasible (experiment was automatically aborted within the first cycle). Furthermore, analysis of distributive and cumulative fouling resistances showed consistent increasing trends for distributive hydraulic reversible fouling ($R_{rev,i}$) for both experiments using SDS-modified 25 mg/L and 50 mg/L emulsified oils that outperformed irreversible fouling resistances, $R_{irr,i}$ and $\Delta R_{irr,i}$, cf. Figure 57. Additionally, distributive, and cumulative irreversible fouling ($\Delta R_{irr,i}$ and $R_{irr,i}$) in case of SDS-modified 25 mg/L emulsified oil were explicitly lower than those measured in case of surfactant-free 25 mg/L emulsified oil (cf. Figure 48c). In case of SDS-modified 50 mg/L emulsified oil, $R_{irr,i}$ values exhibited a rather consistent trend, while $\Delta R_{irr,i}$ values showed a decreasing trend, cf. Figure 57b.

When comparing such achieved performance with the most-relevant literature Teodosiu et al. [67] who investigated the influences of dead-end filtration conditions on the performance of PES UF membranes for the treatment of secondary refinery effluent with TOC concentration below 10 mg/L, a significant membrane fouling was reported such tha the membrane lost almost 50 % of its permeability after 1 h of filtration. Whereas in the current work, surfactant-enhanced dead-end ultrafiltration could achieve an overall PR% of 90 % after 5 filtration cycles of SDS-modified 10 mg/L emulsified oil and SDS concentration of 0.48 g/L, and an overall PR% of 72 % after 5 filtration cycles of emulsified oil with oil

concentration of 50 mg/L. This performance for commercial ready-to-use capillary PES membranes in multiple-cycle dead-end filtration tests using emulsified oils with oil contents up to 50 mg/L has not been so far reported in literature.

4.3.1.5 Understating the role of SDS in promoting membrane antifouling propensity in dead-end ultrafiltration of emulsified oils

Based on the knowledge gained, there are three proposed effects induced by SDS dosing prior to dead-end ultrafiltration of emulsified oils that are jointly responsible for the promoted hydraulic fouling reversibility and substantially improved mechanical backwashing efficiency, as illustrated in Figure 58.

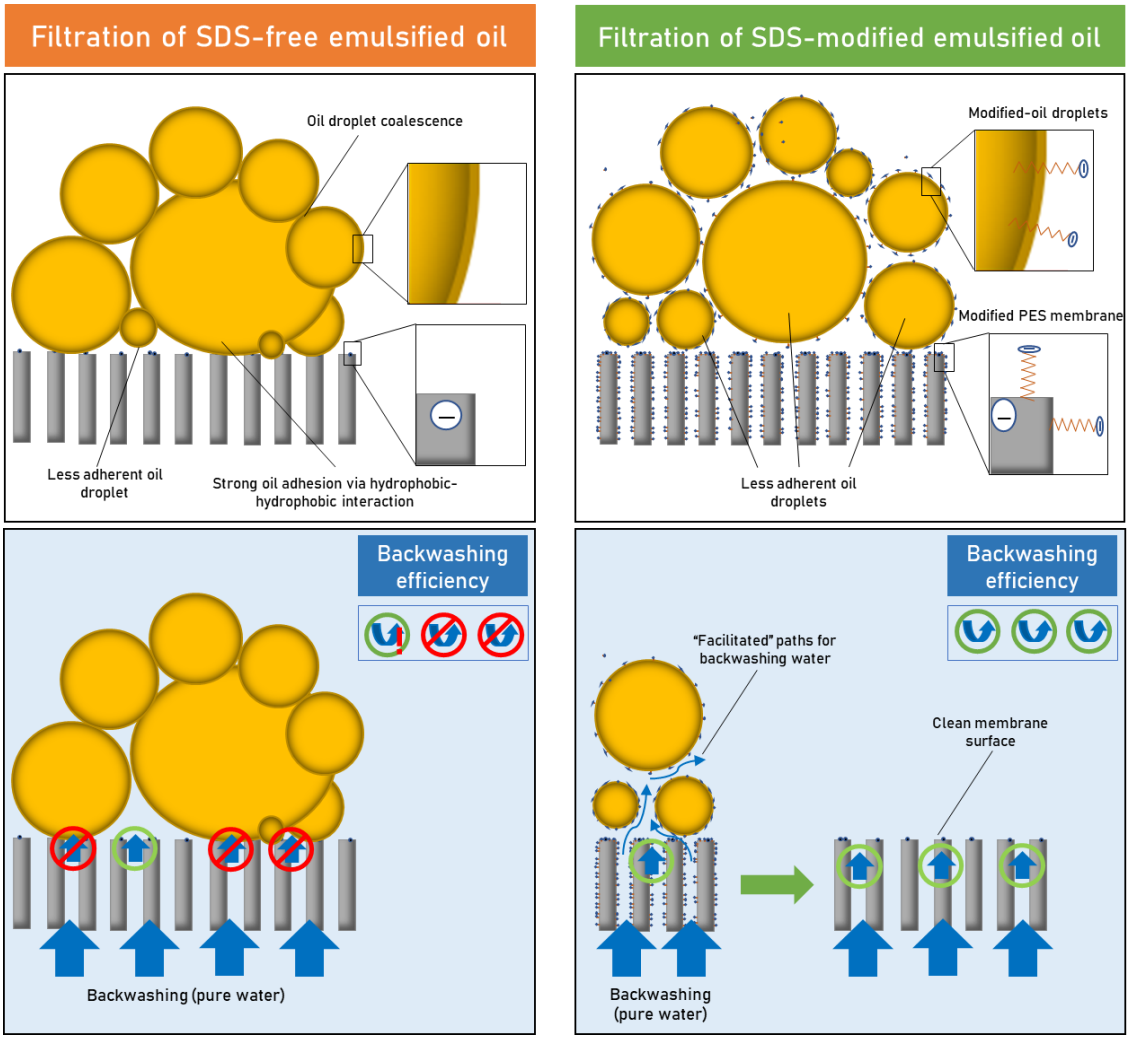

Figure 58: Representation for the proposed joint effects induced by SDS dosing prior to ultrafiltration that are responsible for the substantially improved membrane antifouling performance vs. strong membrane fouling caused by dead-end ultrafiltration of SDS-free emulsified oil

(i) Modification of emulsified oil characteristics via the adsorption of SDS molecules at the oil/water interface:

As discussed in Section 4.3.1.1 and presented in Table 17, SDS-modified oil droplets exhibited an increased negative zeta-potential values compared to surfactant-free emulsified oil. These negatively charged (or modified) oil droplets were found to be more stable and less susceptible to coalescence during membrane filtration (in the membrane vicinity). Moreover, they can be less adherent into the PES membrane matrix (that might be also modified by SDS) because of less (or prohibited) hydrophobic-hydrophobic interaction. These findings are consistent with recent literature [17, 23, 40, 41].

(ii) Modification of membrane surface characteristics via the adsorption of SDS monomers:

As revealed in Section 4.3.1.2.1, SDS monomers (below CMC) can be readily adsorbed into PES membrane matrix, and consequently, modify membrane surface characteristics by inducing negative charges that can minimize hydrophobic-hydrophobic interactions with the emulsified oil, i.e., a surfactant coating to the membrane to mitigate oil adhesion. The reliability of precoating mechanism was separately examined as a possible standalone mechanism for the observed superior membrane performance as presented in Figure 59. Nevertheless, the results showed that it cannot be solely responsible for the promoted fouling reversibility in the SDS-enhanced ultrafiltration process.

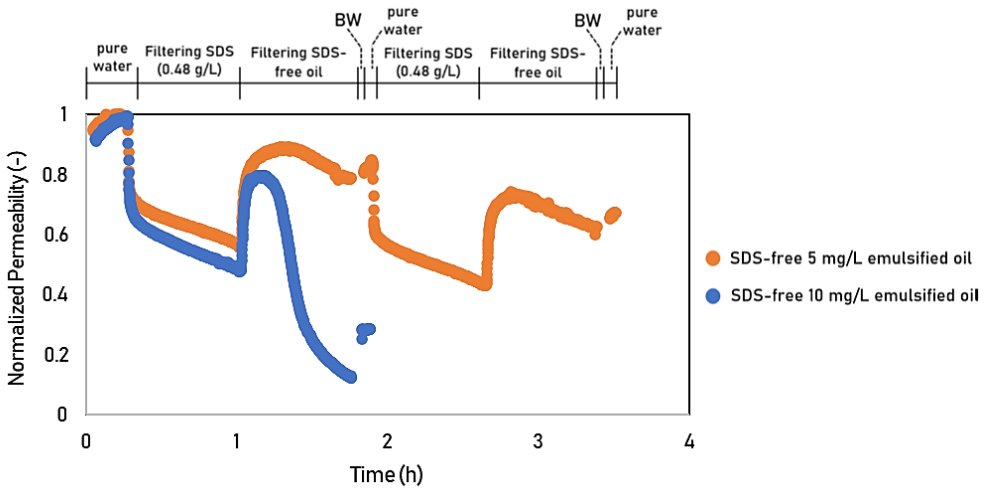

Figure 59: Normalized permeability curves for specially designed multiple-cycle dead-end filtration tests, starting with filtration of 0.48 g/L oil-free SDS solution at a constant flux of 100 L/(m²·h) followed by filtration of surfactant-free emulsified oils (5 mg/L or 10 mg/L)

(iii) Promoting the access of backwashing water via the adsorbed SDS molecules in the formed fouling layer (both adsorbed to membrane surface and emulsified oil droplets):

The adsorbed surfactant monomers in the composite fouling layer formed during the dead-end filtration of SDS-modified emulsified oils can decrease the interfacial surface tension between oil and water, offer “facilitated” paths for the backwashing water through the fouling layer, and consequently, promote the backwashing efficiency. Such facilitated access of backwashing water into the oil fouling layer and the superior hydraulic backwashing efficiency were found to be achievable only through the filtration of SDS-modified emulsified oils, while sequential filtrations of surfactant and emulsified oil (and *vice versa*) caused significantly less hydraulic backwashing efficiency.

The three effects are believed to contribute into the observed superior performance by SDS-enhanced ultrafiltration process. Nevertheless, since mini-plant filtration experiments using SDS-modified 5 mg/L and 10 mg/L emulsified oils revealed that there is a minimum SDS dose that should be maintained to obtain the desired enhanced membrane performance (cf. Sections 4.3.1.4.1and 4.3.1.4.2), one can conclude that modifications of emulsified oil droplets and the PES membrane by the SDS are the most influencing effects.

4.3.1.6 Removal efficiency of emulsified oil and polycyclic aromatic hydrocarbons

4.3.1.6.1 TOC removal of emulsified oils via SM membranes

The oil removal efficiency in multiple-cycle dead-end filtration of surfactant-free emulsified oils with different oil contents (5, 10 and 25 mg/L) was expressed in terms of TOC retention. The results are the average TOC retention values for three samples collected from the first two filtration cycles are presented in Figure 60. Generally, PES membranes were able to retain emulsified oil effectively; retention values of 87 %, 95 % and 97 % were determined for filtration tests of 5, 10, and 25 mg/L emulsified oils, respectively. Additionally, when comparing TOC retention values at different time intervals (i.e., within the first and second filtration cycles), no remarkable differences were found neither within the same filtration cycle nor after hydraulic backwashing.

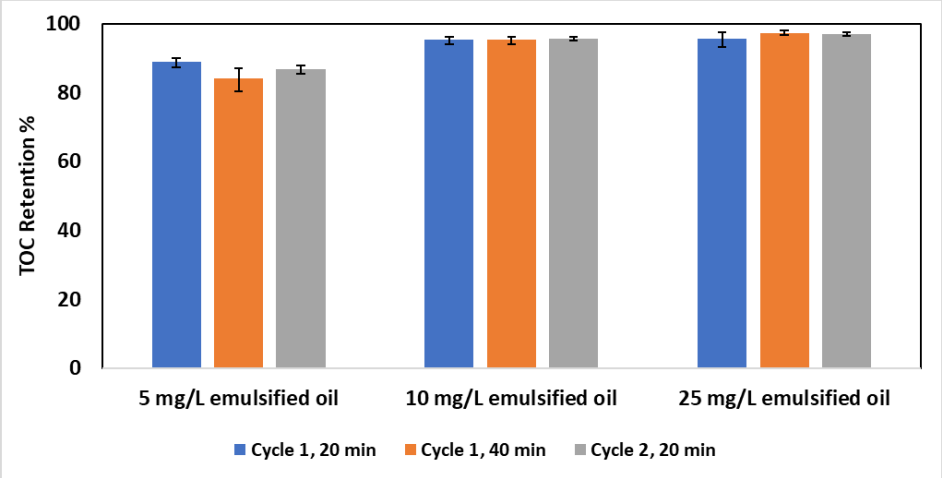

Figure 60: TOC retention for SM membranes at different time intervals, within the first two filtration cycles, in multiple-cycle dead-filtration tests using surfactant-free emulsified oils with different oil concentrations

Figure 61 introduces the TOC retention values during filtration tests using emulsified oils at oil concentrations of 5, 10 and 25 mg/L and SDS concentrations of 0, 0.05, 0.1, 0.2 and 0.5 CMC. Despite of its very positive impact on the fouling propensity, addition of SDS was found to significantly decrease the TOC retention, whereby the membrane retention decreased by increasing SDS dosage. It is hypothesized that the SDS is not retained by the membrane and thus increases the TOC concentration in the permeate.

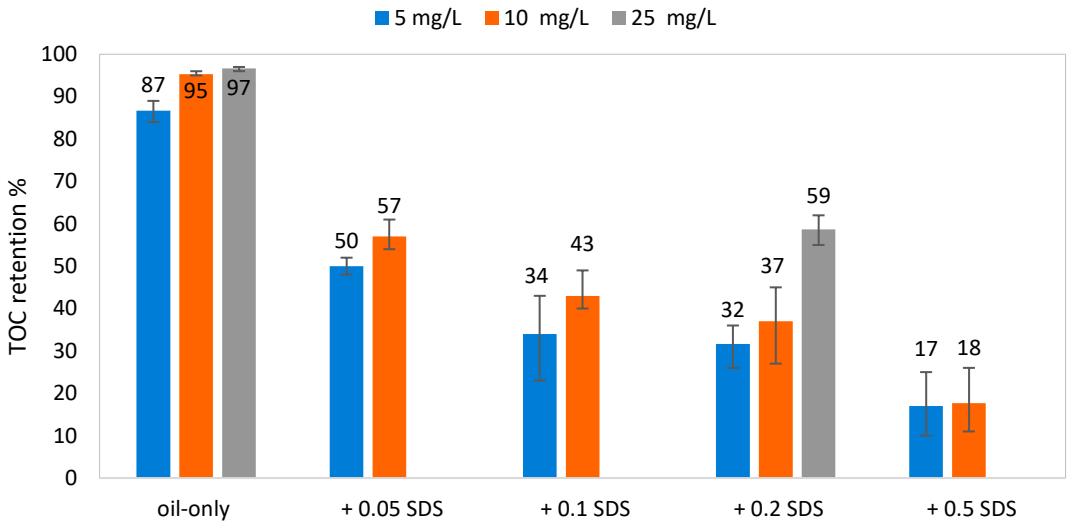

Figure 61: TOC retention of SM membranes for model oil-emulsions with different oil and SDS concentrations at a constant flux of 100 L/m²·h·bar. The presented values are the average of three samples collected at the beginning and the end of 1st cycle and at the beginning of 2nd cycle

Since the average oil droplet size distribution was much bigger than PES membrane pore diameter (cf. Table 16), the emulsified oil droplets are believed to be retained via a size-exclusion mechanism [23]. Nevertheless, since the measured TOC retention was always less than 100 %, one can claim that a portion of the emulsified oil droplets must be smaller than the membrane pore diameter or only a little larger since deformation of emulsified oil droplets into membrane pores was reported as a possible reason [23]. Overall, the oil removal measured for all filtration tests using SDS-free emulsified oils were consistent with global regulations for oil and grease discharge [9, 24], cf. section 2.3.1.

4.3.1.6.2 PAH elimination of emulsified oils via SM membranes

Removal efficiency of specific oil components, for instance, PAHs, in case of filtration tests of SDS-modified emulsified oils was determined. SDS-free 10 mg/L emulsified oil feed was first analyzed using GC-MS method, cf. Section 3.4.1.1. 11 PAH substances from the main 16 PAH substances (according to EPA) with concentrations higher than 0.01 µg/L (Limit of Detection) could be detected. Data were provided in section 4.2.2.1.1, Figure 26. Subsequently, the retention was determined for these 11 PAH substances during the filtration tests of SDS-modified 10 mg/L emulsified oils with SDS concentrations of 0.12, 0.24, 0.48 and 1.2 g/L. The removal data are plotted in Figure 62. Generally, apart from acenaphthylene, no significant alterations in the removal of PAHs were observed for the

filtration tests using SDS-modified emulsified oils compared to SDS-free emulsified oil (considering the measurement error). Accordingly, one can claim that dosing SDS prior to membrane filtration has no negative effects on the retention of emulsified oil components. Nevertheless, further research should be conducted on the removal of surfactant monomers that may not be retained by the ultrafiltration membrane at the employed surfactant concentrations (i.e., below CMC). One possible mechanism could be partial surfactant monomers retention via the adsorption on the retained oil droplets; however, this mechanism cannot be so far experimentally validated because of the limitation of the employed analytical tools.

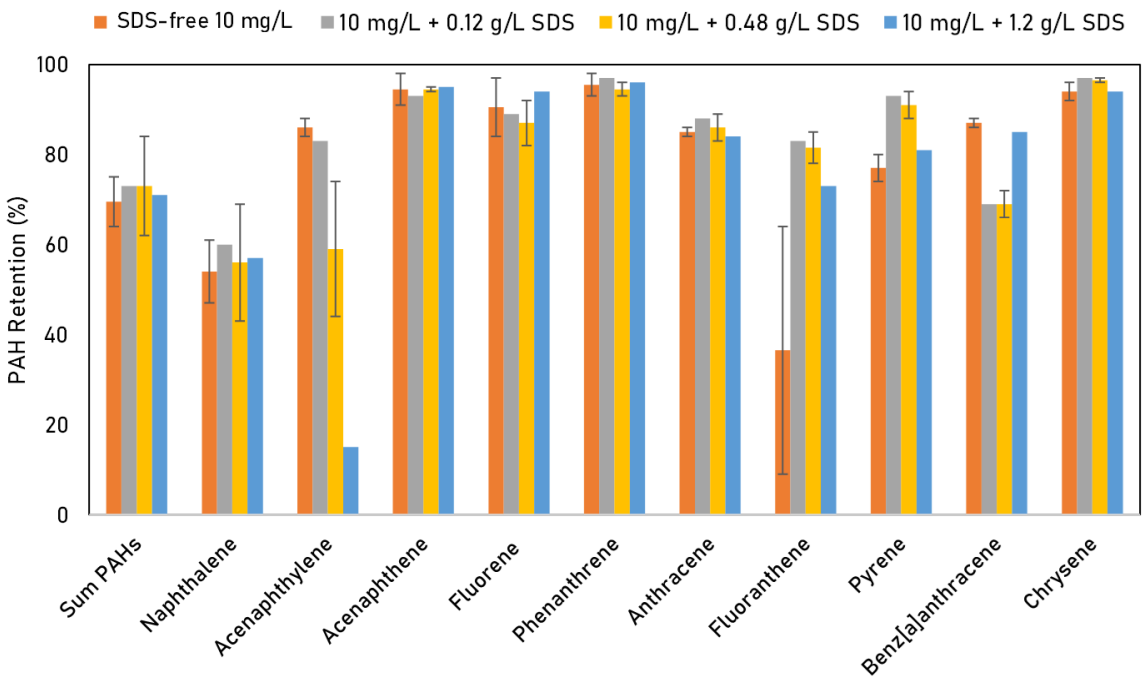

Figure 62: PAHs retention for SM membranes in multiple-cycle dead-filtration tests using surfactant-free and SDS-modified emulsified with oil content of 10 mg/L and SDS concentrations of 0.12, 0.24, 0.48 and 1.2 g/L

4.3.1.6.3 Quantitative determination of the SDS concentration in UF permeates

One of the challenges was to determine the SDS concentration in the permeate of the UF membrane. Within this work, based on literature review, four methods were examined for the quantification of the SDS. TOC [68], ion chromatography [129], conductivity [146], and spectrophotometric analysis [134], cf. section 3.4.2. Although these methods were

reported in the literature as successful ways for the SDS quantification, replicating them in our lab indicated some difficulties and drawbacks for each method.

a. TOC and ion chromatography

Due to the foam that is formed by SDS, TOC analysis was not accurate method for detecting the SDS content. The implemented ion chromatography method could not successfully detect the dodecyl sulfate and was significantly disturbed by the impurities present in the employed SDS.

b. SDS quantification using electrical conductivity

The electrical conductivity method reported by [146] was successfully replicated. A calibration curve was established as depicted in Figure 63. One can notice that conductivity rises with increasing SDS concentration, but the slope of the electrical conductivity plot exhibited a negative deviation when SDS concentration approached the CMC at 2.4 g/L. This can be explained by the lower mobility of the formed surfactant micelles (because of their bigger sizes) compared to the higher mobility of the surfactant monomers.

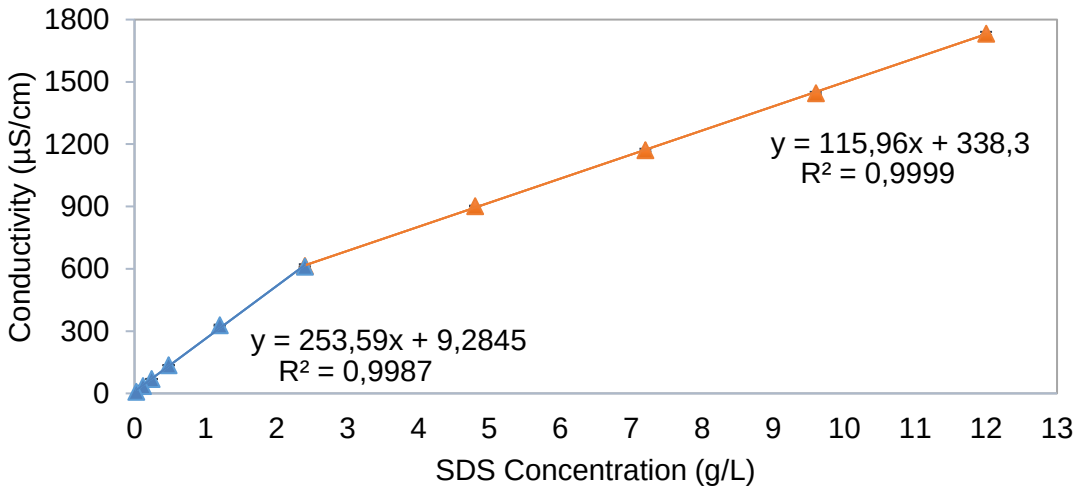

Figure 63: Calibration curve for the measured EC (µS/cm) against the SDS concentration (g/L)

Subsequently, this method was used for checking the SDS solubility (or quantifying SDS concentration in feed solutions), but it was not suitable for quantifying the SDS in the collected permeate samples, since the measured conductivity in the permeate may be prevailed by the unretained sodium ions despite of the possible (partial) retention / adsorption of dodecyl sulfate chains in the membrane matrix.

c. SDS quantification using Stains-all dye method

Another method was to implement Stains-all dye as explained in section 3.4.2. As depicted in Figure 64, UV values increased at wavelength of 453 nm by increasing SDS concentration. On the contrary, the UV values for wavelengths higher than 510 nm decreased by increasing the SDS concentration.

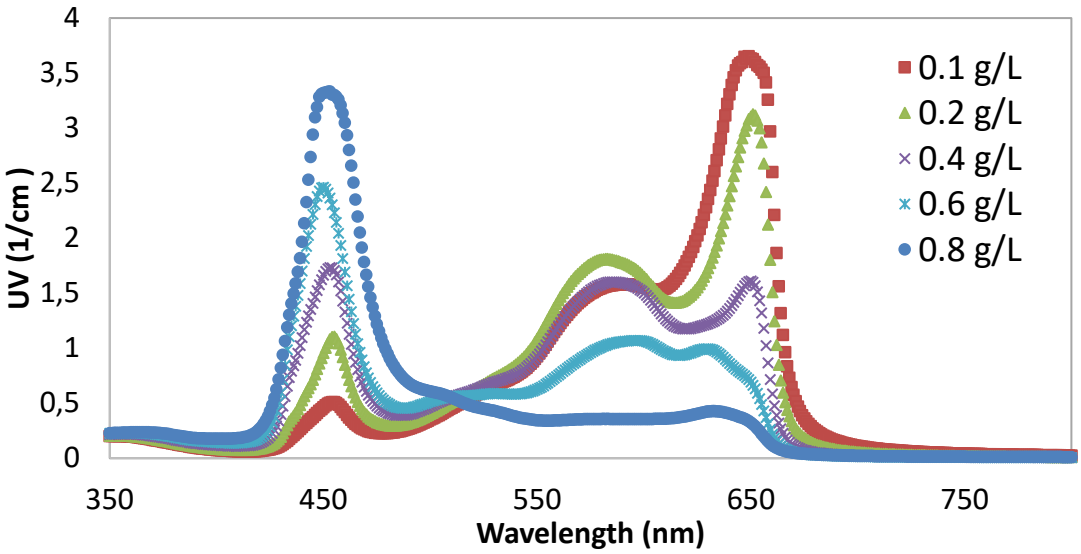

Figure 64: Spectral Absorption Coefficient (UV) at wavelengths 350 – 800 nm for SDS solutions at concentration of 0.1 – 0.8 g/L with the dye Stains-All

To determine the SDS concentration in the UF permeates, two calibration curves were established for SDS solutions that were prepared in two different background water matrices, ultrapure water as well as UF permeate (from filtration of surfactant-free emulsified oil at concentration of 10 mg/L). The calibration curves are presented in Figure 65a and b, respectively. Both calibration curves were obtained for SDS concentrations in the range of 0 - 100 mg/L with a step of 10 mg/L.

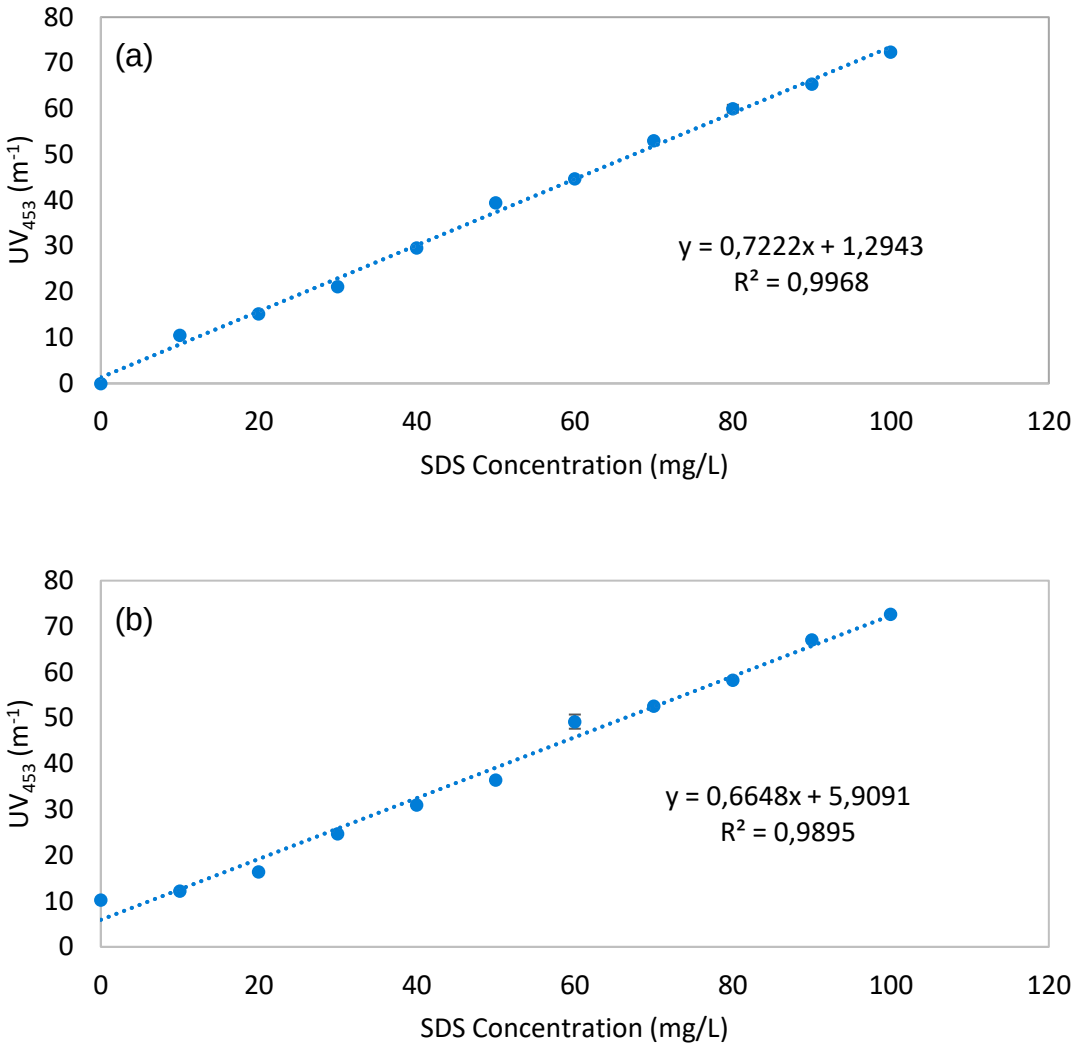

Figure 65: Calibration curve of measured UV_{453} (m^{-1}) against the SDS concentration (mg/L) for solutions prepared with two different background water matrices, ultrapure water (A) and permeate of 10 mg/L surfactant-free emulsified oil permeate through SM membrane (B)

4.3.1.6.4 SDS retention via SM membranes

Two filtration experiments were conducted using two feeds, oil-free SDS solution at concentration of 48 mg/L, and surfactant-modified emulsified oil at oil concentration of 10 mg/L and SDS concentration of 48 mg/L. Both feeds were filtered through SM membrane module at a constant flux of 100 L/(m^2·h). Permeate samples were collected after 1, 2, 3, 4, 5, 15, 30, and 45 min filtration intervals and analyzed for the SDS concentration. Results of SDS concentration in the permeates of both experiments are plotted in Figure 66a and b, respectively.

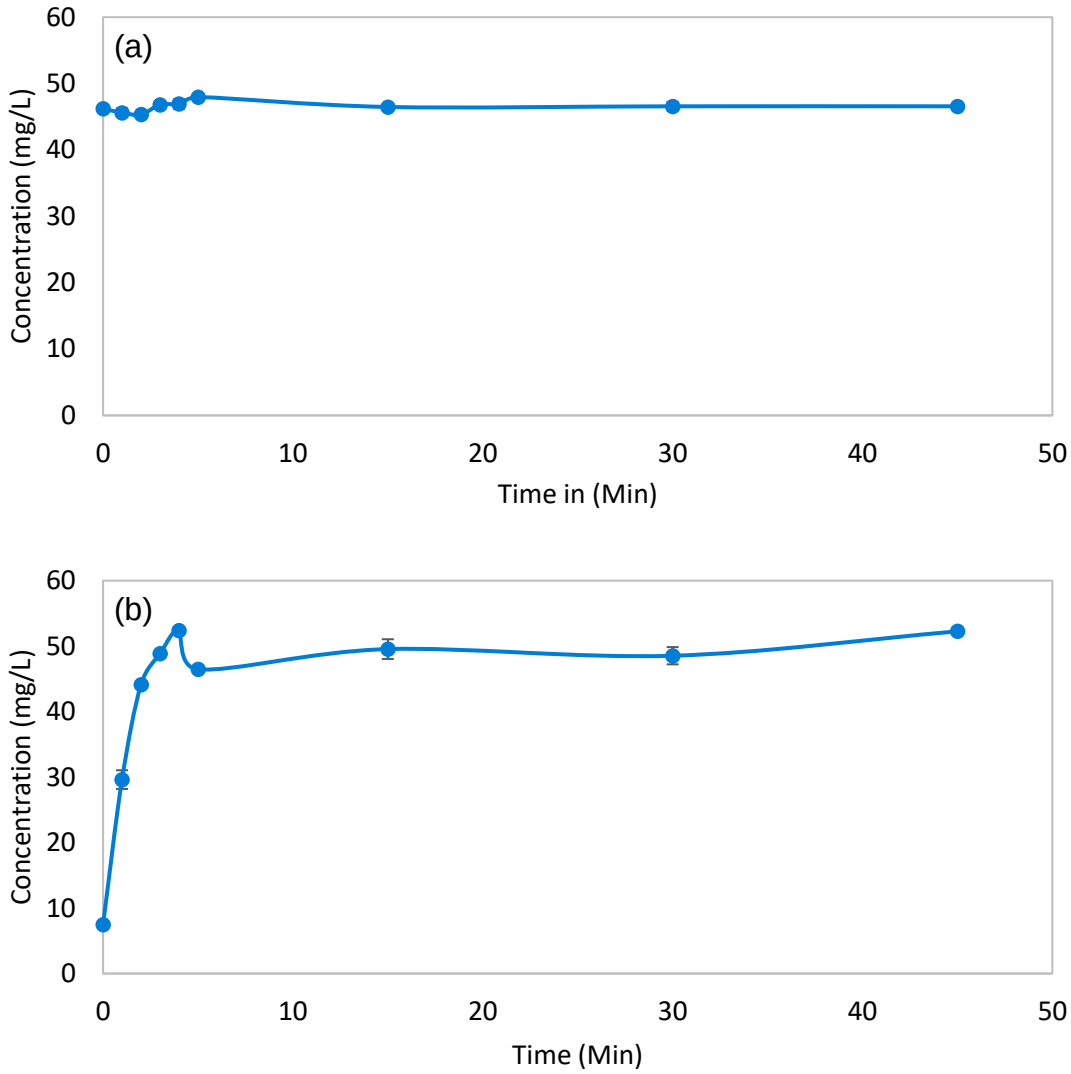

Figure 66: Quantified SDS (mg/L) in the UF permeate against the filtration time (min) for feed of 48 mg/L SDS without oil (A) and with emulsified oily feed at 10 mg/L as TOC (B) through SM membranes

Results from filtration experiments using oil-free SDS solution showed that the SDS concentration in permeate was almost equal to the feed concentration, indicating that no retention for SDS was achieved when oil-free SDS solution was filtered. On the other hand, different behavior was observed for surfactant-modified emulsified oil filtration. In the beginning of filtration experiments, partial retention of SDS was observed, then after almost 3 min of filtration, SDS concentration in the permeate was raised again to be close to its concentration in the feed. Such reduction (or partial SDS retention) should be attributed to SDS adsorption onto the retained emulsified oil droplets, which had positive effects on decreasing oil adhesion to the UF membrane and promotes fouling layer reversibility.

4.3.1.7 Influence of the quality of the applied SDS

In several experiments (over the course of the project), three types of SDS products were implemented, those are $SDS_{VWR,21}$, SDS_{VWR23} and SDS_{TS}, cf. section 3.1. Notable differences were observed in the fouling behavior of PES membranes during the filtration of SDS-modified emulsified oils and oil-free SDS solutions. Consequently, the impacts of SDS quality on the membrane performance was investigated.

4.3.1.7.1 Detailed characterization for SDS from different suppliers

Three analytical techniques were applied to examine the quality of $SDS_{VWR,23}$ and SDS_{TS}: elemental analysis, FTIR spectroscopy, and CMC measurement, cf. section . Unfortunately, at the time of conducting theses analysis there were no samples of $SDS_{VWR,21}$ remaining to be analyzed.

a. Elemental Analysis

To investigate the reasons behind the observed differences, an elemental analysis was conducted to determine the carbon, hydrogen, nitrogen, and sulfur content in both SDS_{TS} and $SDS_{VWR,23}$, cf. section 3.4.3. The measurements and the calculated theoretical values for pure SDS are presented in Figure 67**.**

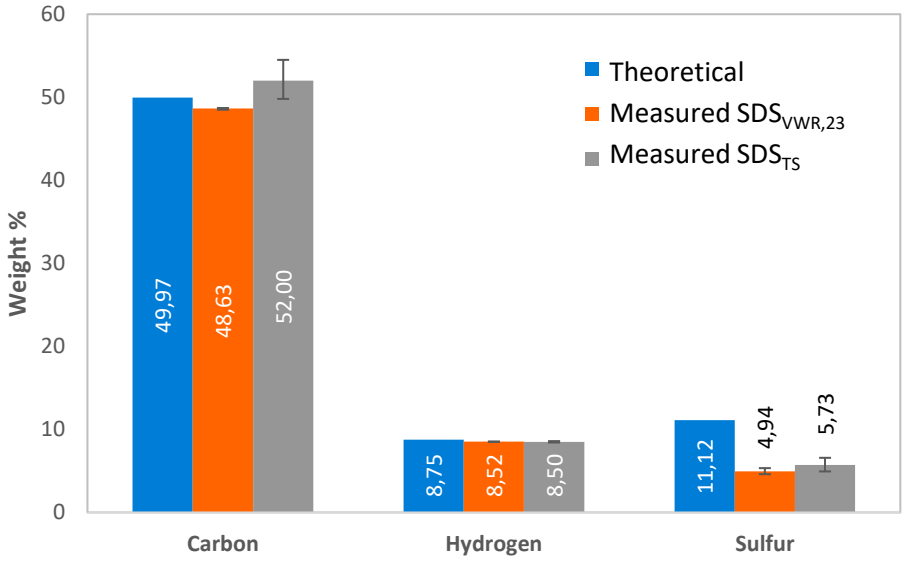

Figure 67: Measured and calculated theoretical values for a pure SDS, and measured values for $SDS_{VWR,23}$ and SDS_{TS} (Microanalytical Laboratory at University of Duisburg-Essen)

It can be observed that the measurements for $SDS_{VWR,23}$ were slightly more reproducible compared to SDS_{TS}, which exhibited higher fluctuations, bigger error values. However, it was also observed that neither SDS matched the theoretical values for pure SDS.

b. FT-IR analysis

The FT-IR analysis for both $SDS_{VWR,23}$ and SDS_{TS} samples was conducted to compare their chemical structures, with the results shown in Figure 68. Both SDS types exhibited typical FT-IR spectra: near 3,400 cm^{-1} equivalent to H–OH stretching, group of peaks near 2,900 cm^{-1} corresponding to CH_2 stretching, and characteristic peak near 1,200 cm^{-1} corresponding to S–O stretching. No significant differences in peaks intensities were noticed. This indicates both SDS products are contained of majorly SDS structures, while impurities are most likely responsible for the observed variations in the fouling behaviors of the membranes.

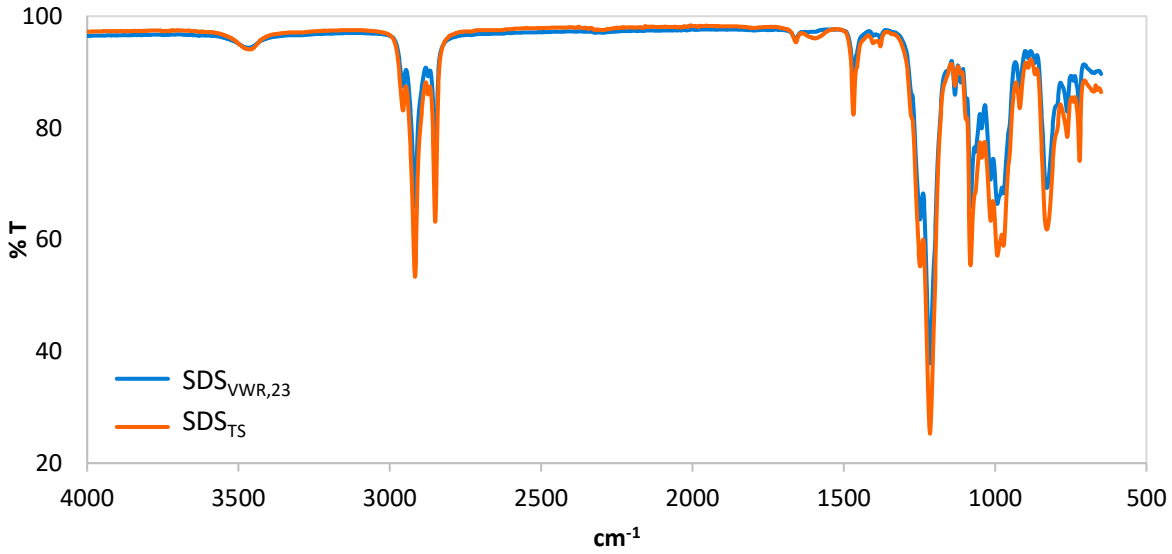

Figure 68: FTIR analysis for $SDS_{VWR,23}$ and SDS_{TS}

c. CMC analysis

To further investigate the effect of impurities in SDS products, the CMC value for both $SDS_{VWR,23}$ and SDS_{TS} was experimentally measured, alongside two reference SDS samples with purities of 95% and >99%, cf. section 3.4.3. The results of these measurements are presented in Table 18. The typical CMC value is reported to be approximately 2.3 g/L. Thus, the high-purity reference SDS (>99%, Ref. 2) actually shows exactly this CMC value, while the reference SDS with 95% purity (Ref. 1) exhibited a CMC value of 1.45 g/L.

Table 18: CMC measurement of SDS_{VWR} and SDS_{TS} together with two other reference SDS samples with purity of 95% and >99%

Material	CMC in g/L	Remarks
SDS >99% (Ref.2)	2.3	"Sodium dodecyl sulfate, for molecular biology, approx. 99%. Molecular biology tested", Sigma-Aldrich, Batch #078K0102
SDS 95% (Ref.1)	1.45	"Sodium dodecyl sulfate, Approx. 95% based on total alkyl sulfate content", Batch #019K0076
SDS_{TS}	1.88	Fine powder, color: white
$SDS_{VWR,23}$	2.33	Small granular, monodisperse, possibly spray-dried. Color: white, beige.

$SDS_{VWR,23}$ exhibited a CMC value of 2.33 g/L, which is close to the expected typical CMC value for pure SDS. In contrast, the measured CMC value of SDS_{TS} was 1.88 g/L, significantly deviating from the typical value and indicating the presence of impurities. Additionally, the surface tension of SDS_{TS} at the final concentration was noticeably higher than normal, which indicates the presence of surfactant impurities. Further, it was observed that at lower concentrations, the surface tension of SDS_{TS} decreased less sharply. This behavior can be attributed to the presence of fatty alcohols, which generally have a relatively low CMC and contribute to the unusual characteristics of SDS_{TS}.

4.3.1.7.2 Mini-plant filtration tests on SM membranes

Inconsistent membrane performance was observed during the filtration of different types of SDS, i.e. $SDS_{VWR,21}$ $SDS_{VWR,23}$ and SDS_{TS}. For instance, Figure 69a and b present two sets of filtration experiments of oil-free SDS solutions made of $SDS_{VWR,21}$ and $SDS_{VWR,23}$. It was noticed that Different membranes performance can be clearly seen.

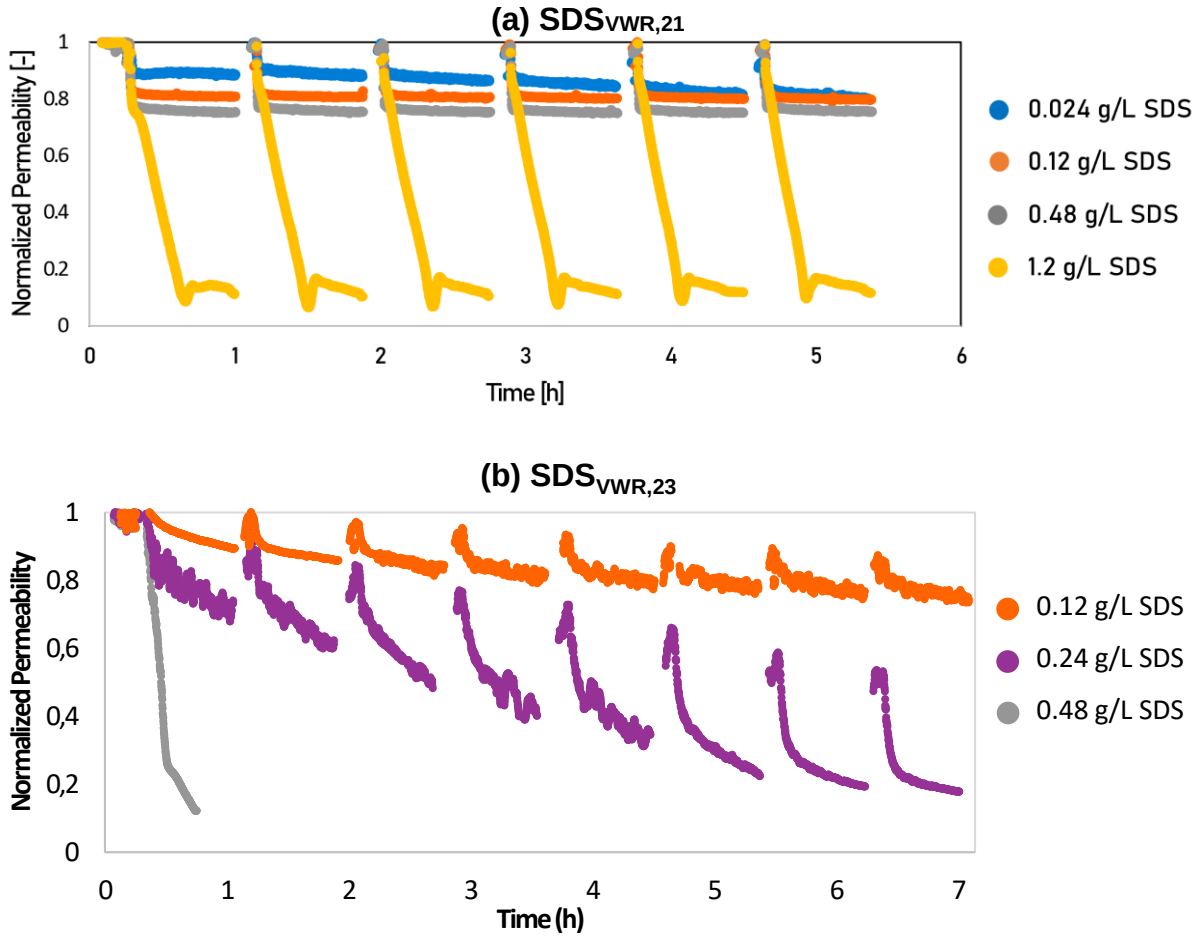

Figure 69: Normalized permeability curves for SM membranes in filtration tests with multiple-cycles at a constant flux of 100 L/(m²·h) using oil-free SDS solutions of different concentrations (0.024 - 1.2 g/L) made of (A) $SDS_{VWR,21}$ and (B) $SDS_{VWR,23}$,

In the first set of experiments (Figure 69a), the membrane permeability was completely restored after each backwash for all tested concentrations. But this was not noticed in the second set (Figure 69b), a certain irreversible fouling remained after each backwash for all three tested concentrations. On the other hand, different fouling rates were observed within the filtration cycles. For example, in the second set the membrane lost about 18% and 20% of its peremability in the first set for 0.12 g/L and 0.48 g/L at the end of the first cycle, those were 11% and 75% in the second set, respectively.

Similarly, two sets of filtration experiments with surfactant-modified emulsified oils and oil concentration of 10 and 25 mg/L and 0.48 g/L were conducted with $SDS_{VWR,21}$ and $SDS_{VWR,23}$,. As indicated in Figure 70, higher fouling rate within the cycle could be noticed when using the $SDS_{VWR,23}$ compared to $SDS_{VWR,21}$. For example, the membrane lost about

45% and 75% at the end of first cycle for 10 and 25 mg/L with $SDS_{VWR,21}$ but these both over 95% with $SDS_{VWR,23}$. Also, higher permeability recovery was noted after each back-wash with $SDS_{VWR,21}$.

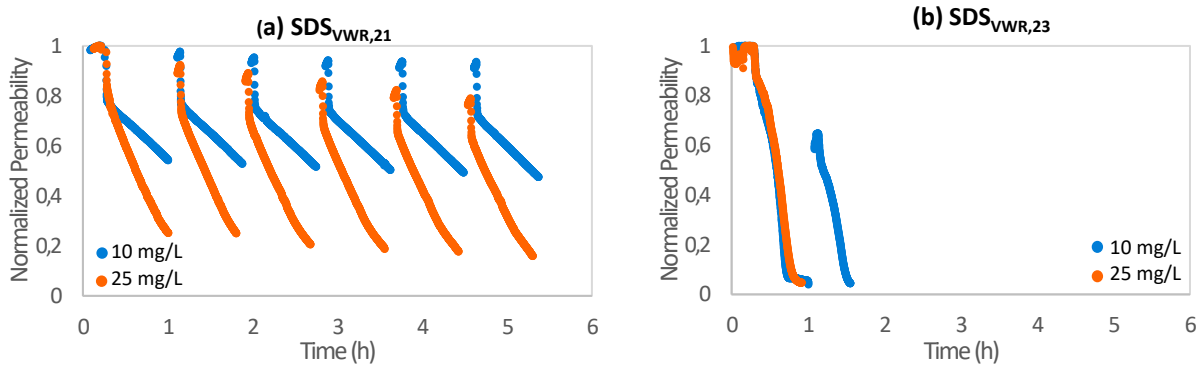

Figure 70: Normalized permeability curve for filtering surfactant-modified emulsified oil with10 mg/L and 25 mg/L both with 0.48 g/L of (A) $SDS_{VWR,21}$ and (B) $SDS_{VWR,23}$. One trial each

On the other hand, two experiments were conducted using SM membranes as well, in which SDS_{TS} at concentration of 0.24 g/L was implemented. One experiment was conducted using oil-free SDS solutions and the other one using SDS-modified emulsified oil at oil concentration of 10 mg/L. As indicated in Figure 71, both experiments suffered from very sever permeability decline, so that the membrane lost over 95% of its permeability within the first cycle. Thereafter both experiments were aborted as when the pressure exceeded the maximum allowed pressure of 4 bar.

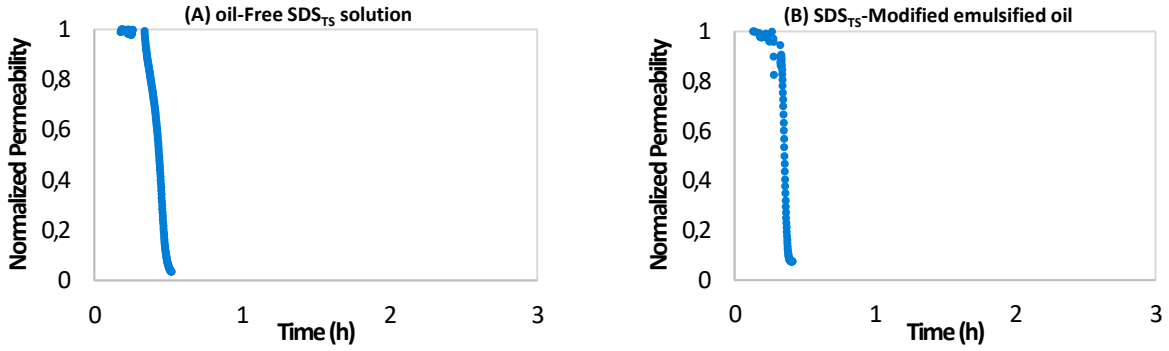

Figure 71: Normalized permeability curve for filtering (A) oil-free SDS_{TS} solutions and (B) SDS_{TS}-modified emulsified oil with oil concentration of 10 mg/L, both at SDS concentration of 0.24 g/L through SM membranes, one trial each

This different behavior of SDS_{TS}, compared to $SDS_{VWR,23}$ can be attributed to the presence of impurities, likely fatty alcohols, as indicated by the elemental and CMC analyses. This finding further emphasizes that the SDS-enhanced dead-end ultrafiltration method is highly sensitive and strongly intolerant to deviations in the experimental setup, such as variations in SDS quality.

4.3.1.7.3 Mini-plant filtration tests on SX membranes

One possible reason for the inconsistent behavior of filtering $SDS_{VWR,21}$ and $SDS_{VWR,23}$ could be potential differences in the Membrane batches implemented in 2021 and 2023. For that further investigations were carried out on the SDS-enhanced dead-end ultrafiltration method. In which another PES UF membrane type from different manufacturer were tested, namely X-Flow membranes, cf. section3.2.2.

Figure 72a and b illustrate the normalized permeability curves for mini-plant filtration experiments using oil-free SDS solutions and surfactant-modified emulsified oil with oil concentration of 10 mg/L, both made with $SDS_{VWR,23}$ at concentration of 0.24 g/L through SX membranes, respectively.

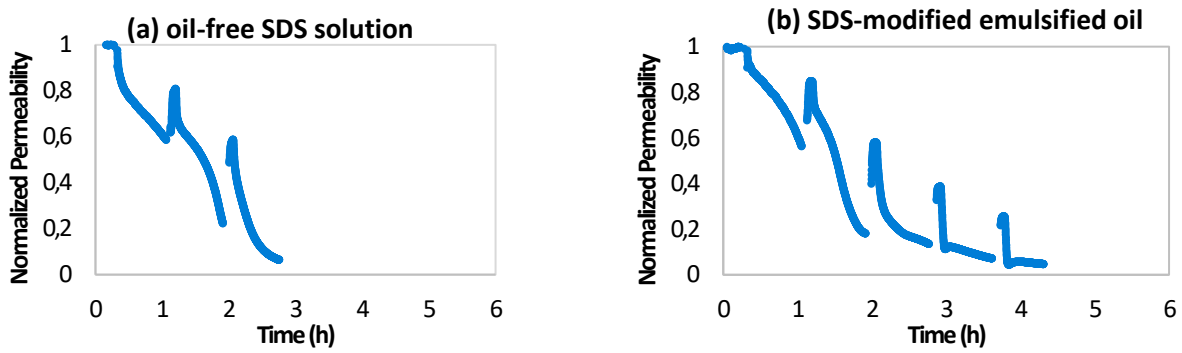

Figure 72: Normalized permeability curve for filtering (a) oil-free SDS solutions and (b) SDS-modified emulsified oil with oil concentration of 10 mg/L, both made with $SDS_{VWR,23}$ at concentration of 0.24 g/L through SX membranes, one trial each

Despite the differences in permeability decline rates within the cycle and the recovery rate after backwash, the overall filtration trends observed with SX membranes were comparable to those with SM membranes. These differences can be attributed to variations in the manufacturing processes, such as blending techniques or membrane post-treatment, as well as deviations in SDS quality.

Similarly, two experiments were conducted using SX membranes with SDS_{TS} at a concentration of 0.24 g/L. One experiment utilized oil-free SDS solutions, while the other involved SDS-modified emulsified oil with an oil concentration of 10 mg/L. As shown in **Figure 73**, both experiments experienced severe permeability decline, with the membranes losing over 95% of their permeability within the first cycle. Consequently, both experiments were aborted when the pressure exceeded the maximum allowable limit of 4 bar.

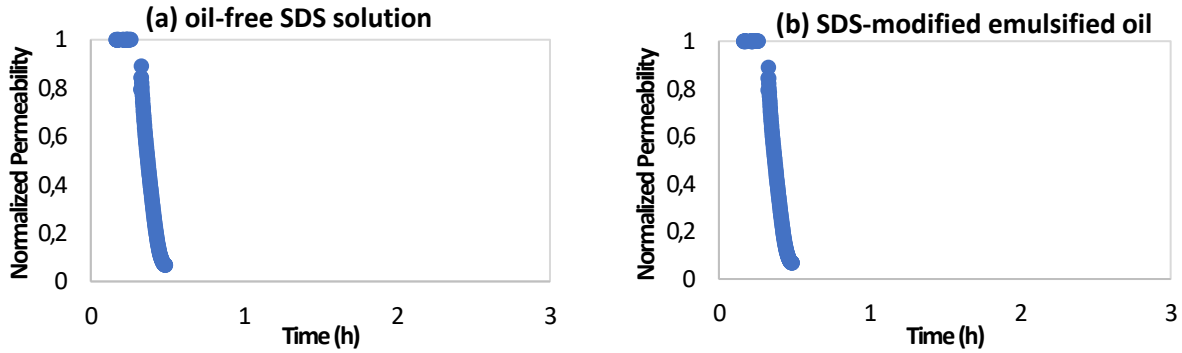

Figure 73: Normalized permeability curve for filtering (a) oil-free SDS_{TS} solutions and (b) SDS_{TS}-modified emulsified oil with oil concentration of 10 mg/L, both at SDS concentration of 0.24 g/L through SX membranes, one trial each

However, it was not possible to conduct experiments implementing $SDS_{VWR,21}$ and SX membranes because no $SDS_{VWR,21}$ samples were remaining or possible to procure. So that the not favorable filtration behavior of SDS solutions and SDS-modified emulsified oils reported in the section 4.3.1.7 are very likely related to the deficits in the SDS quality but not of the SX or SM membranes.

4.3.1.8 Influence of filtration conditions on the efficiency of surfactant-enhanced dead-end ultrafiltration

Based on the findings reported in W-UFO II regarding the surfactant-enhanced dead-end ultrafiltration method, further investigations were planned to examine the influence of filtration conditions on the efficiency of the developed method. This included a total of 70 experiments conducted under varying operational conditions, specifically: filtration flux, filtration duration, BW flux, BW duration, and the duration of the pure water filtration step following the BW. These experiments aimed to optimize the listed parameters by evaluating their impact on the efficiency of the surfactant-enhanced dead-end ultrafiltration process. This was planned to be carried out with the help of a statistical experimental plan to test filtration fluxes in the range of 60 – 140 L/(m²·h), filtration cycle durations in the range of 30 -60 min, backwashing fluxes in the range of 160 - 300 L/(m²·h), backwashing duration in the range of 30 - 90 s, and post pure water. filtration durations in the range of 0 - 10 min (with a flux equal to the filtration flux). This results in 46 experiments. Thereafter, about 10 – 15 further experiments were planned to validate the output of the experimental design. In addition to about 10 experiments for optimizing the dosing conditions. So that, a total of about 70 experiments was dedicated to this part, i.e. these two subtasks, in the proposed plan, see WP2, subtasks b and c, page 22 in W-UFO III^{+} proposal.

During the execution of the project, over 100 experiments were carried out in relation to this subtask. This was realized using three filtration units: Poseidon, Neptunus and Playground, and using three types of membrane modules: SM, SM_2 and SX. However, as previously mentioned in section 4.3.1.7, the surfactant-enhanced dead-end ultrafiltration method was sensitive to alternations in the experimental set up, mainly the quality of the SDS applied. This unforeseen significant fluctuations in the materials and the related variations in performance parameters necessitated an adjustment and expansion of the experimental plan. We decided to suspend the development of mathematical relationships

through statistical experimental design and instead conduct more individual experiments with direct parameter comparisons to reliably capture trends. This caused additional workload and material costs. For example, Table 19 shows a list of 17 experiments that were carried out using Playground filtration unit out of the 46 planned experiments according to the design of experiment, see section 3.10.3. The total fouling at the end of the experiment was utilized as the output parameter for these experiments. All experiments in this section, i.e., section 4.3.1.8 were conducted utilizing $SDS_{VWR,23}$.

Table 19: A list of experiments completed in accordance with the statistical experimental plan with central composite design and the associated filtration flux, filtration cycle duration, backwash flux, backwash duration, and pure water filtration including experiments done on playground, number of successful cycle and total fouling.

Experiment number	Filtration flux ($L/m^2 \cdot h$)	Filtration cycle duration (min)	Backwash flux ($L/m^2 \cdot h$)	Backwash duration (sec)	pure water filtration (min)	Nr. of successful cycle	Total fouling
EXP 01	60	30	90	30	3	6	79%
EXP 02	140	30	90	30	3	3	75%
EXP 03	60	60	90	30	3	3	81%
EXP 05	60	30	230	30	3	6	41%
EXP 06	140	30	230	30	3	1	85%
EXP 07	60	60	230	30	3	3	57%
EXP 08	140	60	230	30	3	1	86%
EXP 09	60	30	90	90	3	6	42%
EXP 10	140	30	90	90	3	6	69%
EXP 11	60	60	90	90	3	3	82%
EXP 13	60	30	230	90	3	6	71%
EXP 14	140	30	230	90	3	6	65%
EXP 15	60	60	230	90	3	3	44%
EXP 16	140	60	230	90	3	1	80%
EXP 17	60	30	90	30	7	6	47%
EXP 19	60	60	90	30	7	3	58%
EXP 23	60	60	230	30	7	3	
EXP 43	100	45	160	60	5	4	58%
EXP 46	100	45	160	60	5	4	76%

To study the effect of filtration flux on membrane fouling, the filtration curves of two experiments, EXP 01 and EXP 02, were compared. EXP 01 and EXP 02 were conducted at filtration flux of 60 and 140 L/(m²·h), respectively. Both experiments were performed at filtration cycle duration of 30 min, BW flux of 90 L/(m²·h), BW duration of 30 s, pure water duration of 3 min. In these two experiments oily feed at oil concentration of 10 mg/L and SDS concentration of 0.48 g/L was filtered through SM_1. As depicted in Figure 74, EXP 01 completed 6 cycles. In which, the permeability decreased in the first cycle to reach 39% of the initial permeability, but the following BW recovered the permeability up to 81%. At the end of the 6th filtration cycle, the membrane lost about 79% of its initial permeability. While EXP 02 stopped during the BW of the third filtration cycle as the pressure exceeded the pre-set limit of 3 bar. In which, the permeability decreased in the first cycle and reached 70% of the initial permeability, but the following BW recovered the permeability up to 79%. At the end of the 3rd filtration cycle, the membrane lost about 77% of its initial permeability.

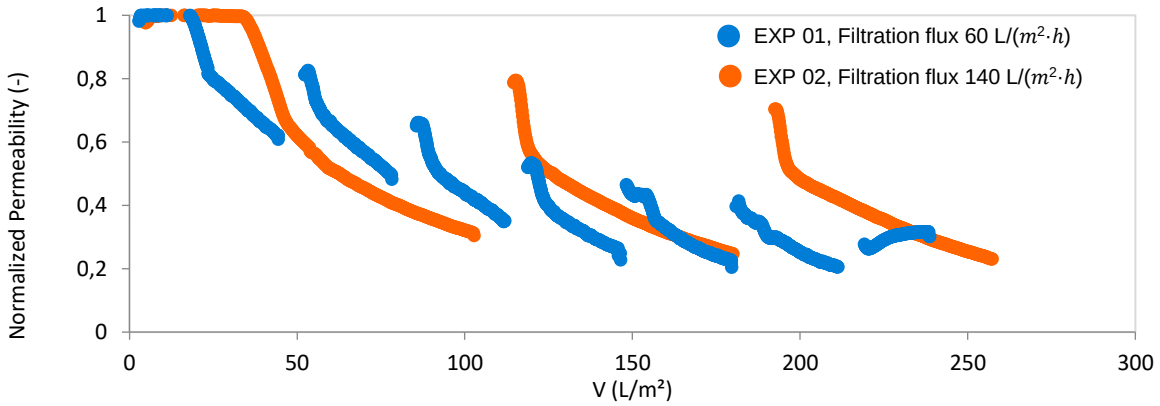

Figure 74: Filtration curves for EXP 01 and EXP 02 with filtration flux of 60 and 140 L/(m²·h), respectively. Both experiments were performed at filtration duration of 30 min, BW flux of 90 L/(m²·h), BW duration of 30 sec, Pure water duration of 3 min, as well as oily feed at oil concentration of 10 mg/L and SDS concentration of 0.48 g/L through SM_1 membranes

From these two experiments, one can see that higher filtration flux had some advantages. Although the same fouling was reached at the same filtered volume of 100 L/m², but the decreased number of BW steps led to higher recovery rate. Also, the BW was more effective after the first cycle of higher flux experiment. However, most of the other tests that were conducted at high flux stopped mostly after the first, second or in the best cases at the third cycle. Increasing the flux leads to accelerated accumulation (higher loading) of

foulants onto the membrane surface that can lead to plugging of the liquid passages and hence the drastic decrease of the permeability.

To study the effect of filtration cycle duration on the membrane fouling, the filtration curves of two experiments, EXP 01 and EXP 03, were compared. EXP 01 and EXP 03 were conducted at filtration cycle duration of 30 and 60 min, respectively. Both experiments were performed at filtration flux of 60 L/(m²·h), BW flux of 90 L/(m²·h), BW duration of 30 sec, Pure water duration of 3 min. In these two experiments oily feed at oil concentration of 10 mg/L and SDS concentration of 0.48 g/L was filtered through SF membrane modules. As depicted in Figure 75, EXP 03 completed 3 cycles. In which, the permeability decreased in the first cycle to reach 70% of the initial permeability, but the following BW recovered the permeability up to 53%. At the end of the 3rd filtration cycle, the membrane lost about 83% of its initial permeability.

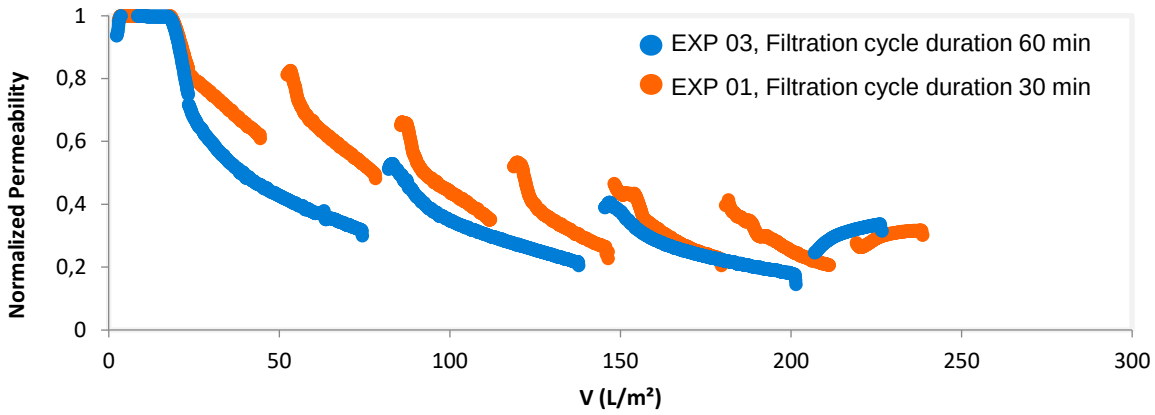

Figure 75: Filtration curves for EXP 03 and EXP 01 with filtration cycle duration of 60 and 30 min, respectively. Both experiments were performed at filtration flux of 60 L/(m²·h), BW flux of 90 L/(m²·h), BW duration of 30 s, pure water duration of 3 min, as well as oily feed at oil concentration of 10 mg/L and SDS concentration of 0.48 g/L through SM_1 membranes.

From these two experiments, one can conclude that increasing the filtration cycle duration from 30 min to 60 min led to an increase in the total fouling by 6%.

The filtration curves of two experiments, EXP 10 and EXP 14, were compared to investigate the effect of filtration flux on the membrane fouling. EXP 10 and EXP 14 were conducted at BW flux of 90 and 230 L/(m²·h), respectively. Both experiments were performed at filtration cycle duration of 30 min, filtration flux of 140 L/(m²·h), BW duration of 90 s, pure water duration of 3 min. In these two experiments oily feed at oil concentration of

10 mg/L and SDS concentration of 0.48 g/L was filtered through SF membrane modules. As depicted in Figure 76, EXP 10 completed 6 cycles. In which, the permeability decreased in the first cycle to reach 65% of the initial permeability, but the following BW recovered the permeability up to 81%. At the end of the 6th filtration cycle, the membrane lost about 72% of its initial permeability. EXP 14 completed 6 cycles. In which, the permeability decreased in the first cycle to reach 61% of the initial permeability, but the following BW recovered the permeability up to 89%. At the end of the 6th filtration cycle, the membrane lost about 67% of its initial permeability.

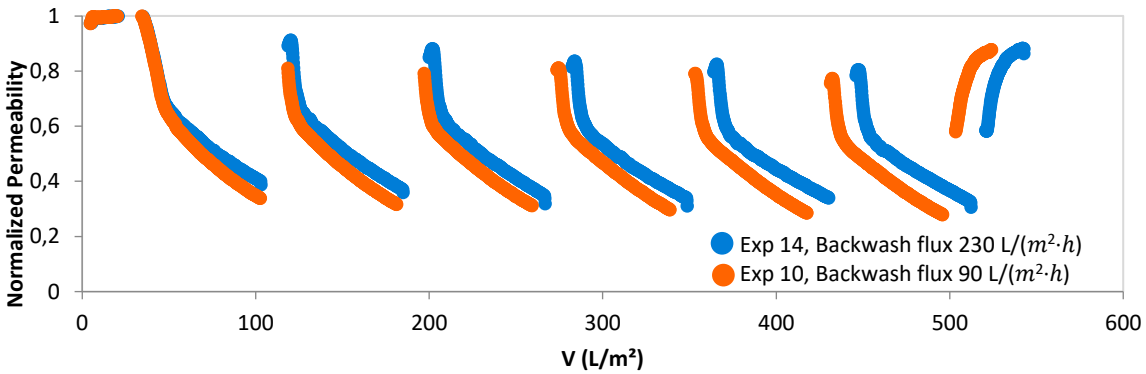

Figure 76: Filtration curves for EXP 10 and EXP 14 with BW flux 90 and 230 L/(m²·h), respectively. Both experiments were performed at filtration flux of 140 L/(m²·h), filtration cycle duration 30 min, BW duration of 90 s, pure water duration of 3 min, as well as oily feed at oil concentration of 10 mg/L and SDS concentration of 0.48 g/L through SM_1 membranes.

From these two experiments, one can conclude that the effect of backwash flux on the membrane fouling was indeed minor, as the increase in backwash flux led to an increase about 4% on the membrane permeability at the end cycle of the filtration.

To investigate the effect of BW duration on the membrane fouling, the filtration curves of two experiments, EXP 11 and EXP 03, were compared. EXP 11 and EXP 03 were conducted at BW duration of 90 and 30 s, respectively. Both experiments were performed at filtration cycle duration of 60 min, filtration flux of 60 L/(m²·h), BW flux of 90 L/(m²·h), pure water duration of 3 min. In these two experiments oily feed at oil concentration of 10 mg/L and SDS concentration of 0.48 g/L was filtered through SF membrane modules. As depicted in Figure 77, EXP 11 completed 3 cycles. In which, the permeability decreased in the first cycle to reach 81% of the initial permeability, but the following BW recovered the

permeability up to 48%. At the end of the 3rd filtration cycle, the membrane lost about 83% of its initial permeability.

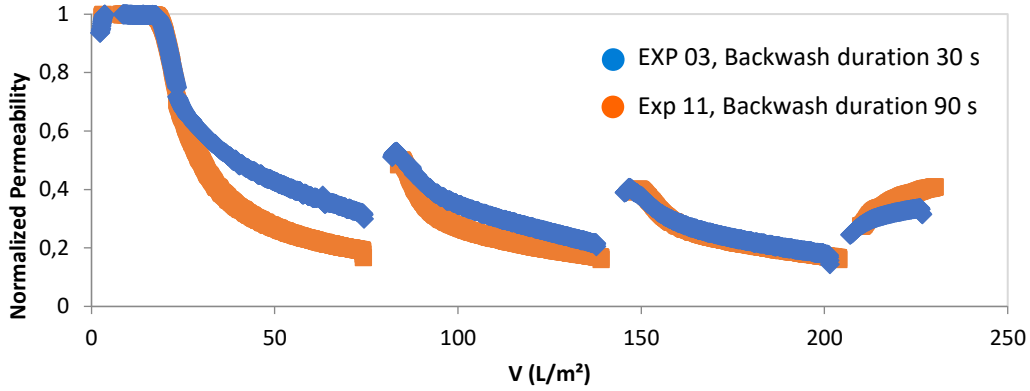

Figure 77: Filtration curves for EXP 11 and EXP 03 with BW duration of 90 and 30 s, respectively. Both experiments were performed at filtration flux of 60 L/(m²·h), filtration cycle duration of 60 min, BW flux of 90 L/(m²·h), pure water duration of 3 min, as well as oily feed at oil concentration of 10 mg/L and SDS concentration of 0.48 g/L through SM_1 membranes.

From these two experiments, one can conclude that there was no significant impact of increasing backwash duration on the membrane fouling, since, in both experiments, the two membranes behaved almost identically, and they exhibited the same performance decay in the last cycle of filtration.

Similarly, the filtration curves of EXP 03 and EXP 19 were compared to elaborate the effect of pure water filtration on the membrane fouling, EXP 03 and EXP 19 were conducted at pure water filtration duration of 3 and 7 min, respectively. Both experiments were performed at filtration flux of 60 L/(m²·h), filtration cycle duration of 60 min, BW flux of 90 L/(m²·h), BW duration of 30 s. In these two experiments oily feed at oil concentration of 10 mg/L and SDS concentration of 0.48 g/L. As depicted in Figure 78**,** EXP 19 completed 3 cycles. In which, the permeability decreased in the first cycle to reach 49% of the initial permeability, but the following BW recovered the permeability up to 68%. At the end of the 3rd filtration cycle, the membrane lost about 59% of its initial permeability.

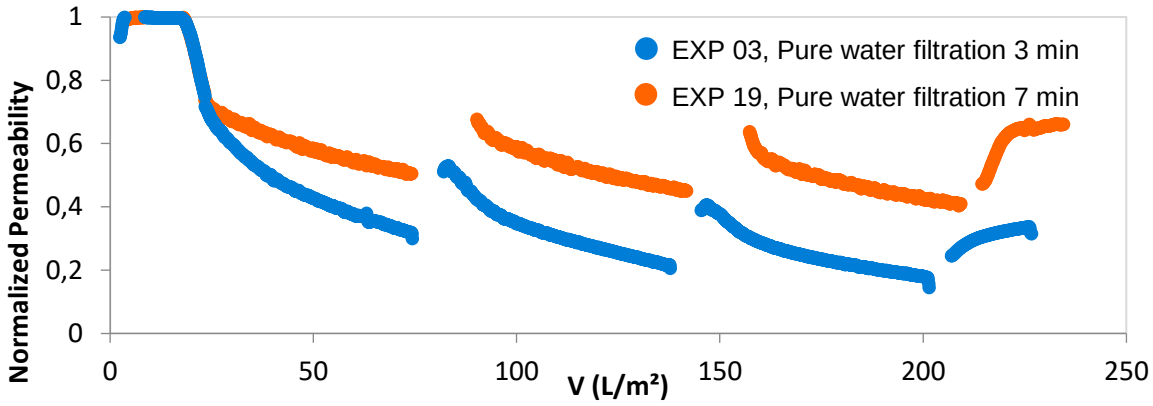

Figure 78: Filtration curves for EXP 03 and EXP 19 with pure water duration of 3 and 7 min, respectively. Both experiments were performed at filtration flux 60 L/(m²·h), filtration cycle duration of 60 min, BW flux of 90 L/(m²·h), BW duration of 30 s, as well as oily feed at oil concentration of 10 mg/L and SDS concentration of 0.48 g/L through SM_1 membranes

From these two experiments, one can conclude that the increase in pure water filtration after every filtration cycle led to an improved membrane performance such that the overall membrane fouling was reduced by about 24%. This results also should be taken with caution, as the membrane fouling behavior in the first cycle was not identical in both experiments.

In conclusion, it was noted that tests conducted under the applied conditions in this section, i.e., section 4.3.1.8, demonstrated no enhancement in performance when altering the filtration fluxes, filtration cycle durations, backwashing fluxes, backwashing duration and post pure water after backwash. This lack of improvement is likely attributable to the previously discussed issues with the surfactant-enhanced dead-end UF process, as resulting from variations in SDS quality, as detailed in section 4.3.1.7.

4.3.2 Hybrid UF processes with PAC dosing and/or coagulants

4.3.2.1 Adsorption kinetic experiments

To investigate the adsorption behavior, a series of adsorption kinetic experiments were performed with three commercially available granular activated carbon products, ABG-H, HMA-B and ORG-K, made from the different raw materials wood, anthracite, and coconut shells, respectively. First, the granular activated carbon products were milled into PAC with a comparable particle size ($D_{50,V}$ = 5 ~ 8 µm). As shown in Figure 79, at 50 mg/L

dosage rate of PAC, the PACs removed 75%, 58%, and 53% of the UV_{254} of the oil emulsion at concentration of 25 mg/L an input concentration of 65 – 70 m^{-1} as UV_{254}.

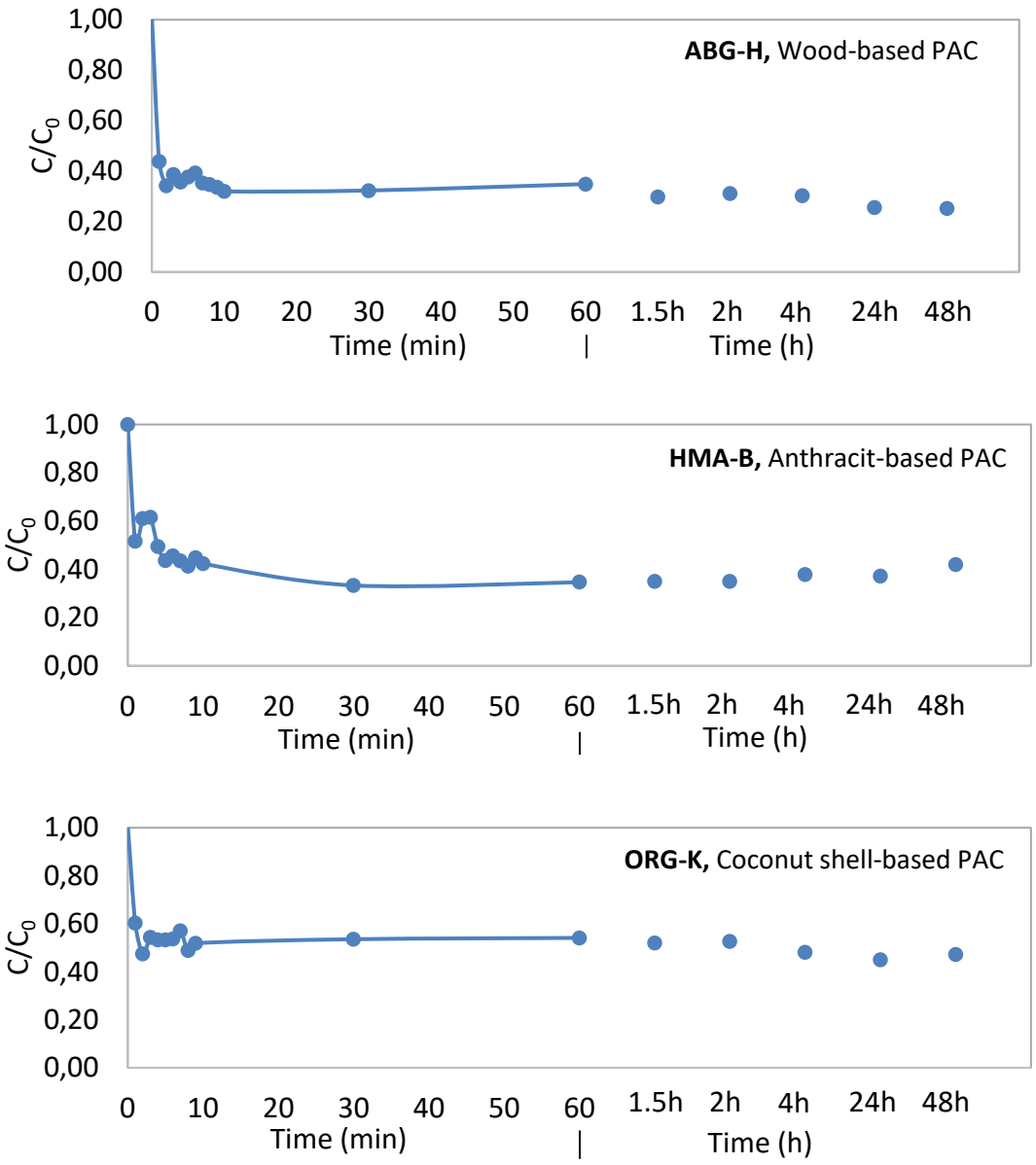

Figure 79: Results of adsorption kinetic experiments of ABG-H, HMA-B and ORG-K PACs, presented as UV_{254} concentration in the permeate (C) related to the feed concentration(C_0) over time

The differences in the removal of UV_{254} using the three PACs are comparable to the removal of UV_{254} when the same PACs are applied to municipal wastewater (68%, 55%, and 37% at an input concentration of 27 m^{-1}). The three PACs differ mainly in their surface area formed by meso- and macropores (822, 424 and 279 m^2/g). The micropore surface area of the three PACs, on the other hand, is comparatively similar at 787, 741, and

888 m²/g, respectively, or exhibits a different sequence. The removal of oil compounds identified as UV_{254} is therefore can be expected, based on these results, to occur either on the outer surface or in the meso- and macropores of PAC. However, due to the irreproducible adsorption behavior on the PAC during the adsorption isotherms experiments, see following section 4.3.2.2, it is more likely that the adsorption to occur on the outer surface of the PAC, rather than inside the pores.

4.3.2.2 Adsorption isotherms experiments

A set of experiments were carried out to obtain the adsorption isotherm and to define the minimum required dose of PAC to achieve the highest possible oil removal. As described in Section 0, the PAC concentration varied first in the range of 1-100 mg/L with a step of 10 mg/L. The removal of oil in terms of UV_{254} are depicted in Figure 80. The results of these experiments showed that all PAC behaves similar with a strong increase of the elimination at low dosage up to 10 mg/L and then decreasing elimination rate with increasing dosage. Up to a dosage of 50 mg/L, the elimination of ORG-K is about 10 % better than that of the other PAC types. Above a PAC dosage of 50 mg/L, elimination remains constant at around 80% for all PAC types.

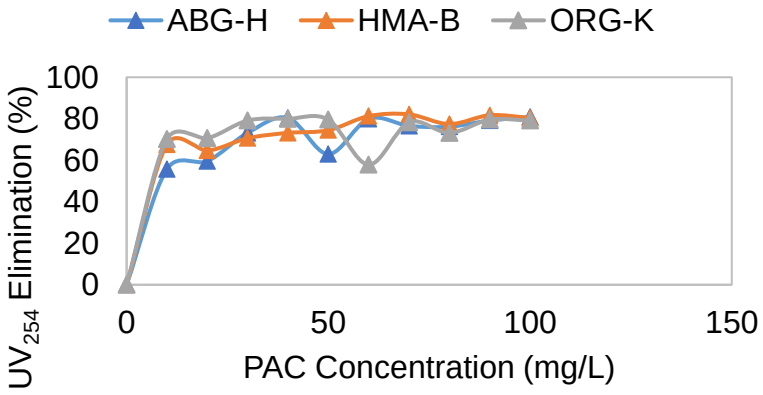

Figure 80: UV_{254} elimination in percentage against the direct dosed concentrations of three PACs, ABG-H, HMA-B and ORG-K to the emulsified oil of 25 mg/L as TOC, one trial each

It seems that the oil sample has about 20% components that are not adsorbable, so it is a multi-component system. Furthermore, the PAC types differ slightly in their maximum loading at PAC dosing quantities below 10 mg/L. Contrary to the results from the kinetics tests, ORG-K has the best elimination in this dosing range with ca. 70%.

However, repeating these experiments resulted in very high fluctuations, as indicated in Figure 81a, b and c, which presents the four-fold adsorption isotherms for the three PACs ABG-H, HMA-B and ORG-K, respectively. All experiments tested a PAC-dosage of 10 - 100 mg/L except for ABG-H - Trial 4, in which the PAC-dosage was extended to cover from 5 to 400 mg/L. In general, no clear trend can be drawn out of these isotherms. This can be attributed to the fact that crude oil contains several components, and the final isotherm is expected to be a multi-component isotherm.

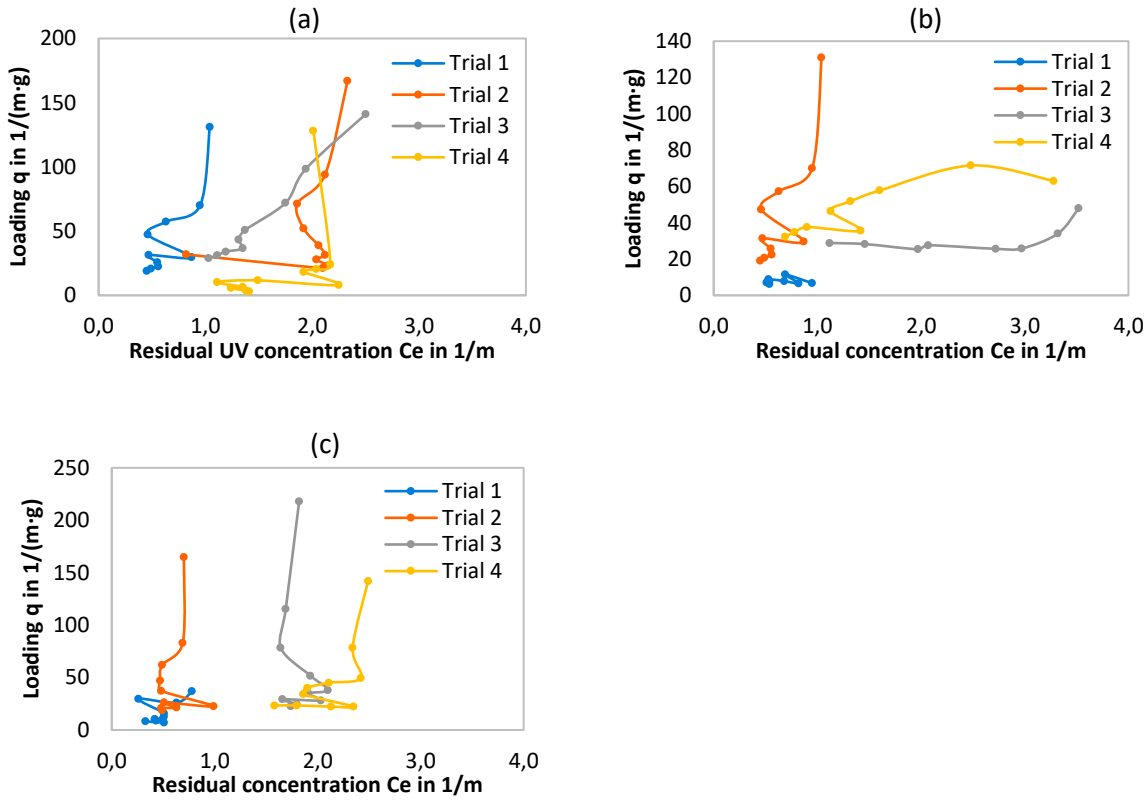

Figure 81: UV_{254} adsorption isotherms for the three different PAC, (a) ABG-H, (b) HMA-B and (c) ORG-K, four trials each

Due to the very similar behavior of the three PAC types, it is assumed that the main adsorption takes place on the outer surface of the activated carbon and only a negligible capacity of the large inner surface of the PAC is used. It is assumed that the oil droplets are adsorbed on the outer surface and coalesce with the next droplets faster than they can diffuse into the interior of the PAC. As a result, the large oil droplets also block the access of smaller oil components to the inner structure of the PAC.

To investigate this phenomenon, two experiments were conducted simultaneously. The first experiment was conducted with the permeate of the emulsified oil that was filtered through a filter with pore size of 0.45 µm. The second experiment was conducted with a non-prefiltered emulsified oil. The results are indicated in Figure 82. A higher elimination was achieved with the pre-filtered emulsified oil, as fewer droplets can adsorb on the outer surface in this case.

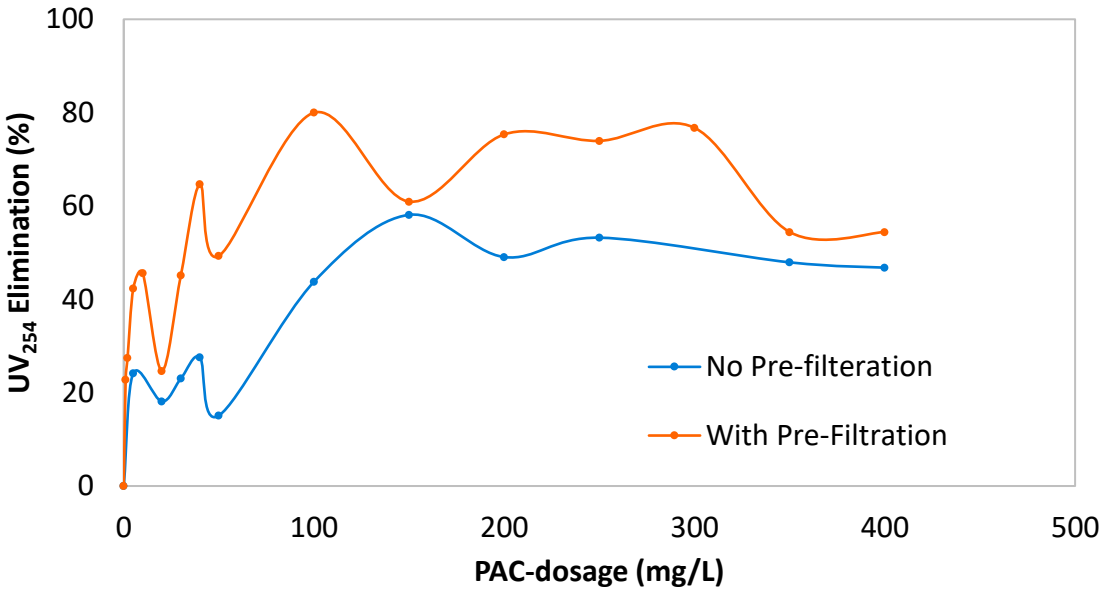

Figure 82: UV_{254} elimination in percentage against the direct dosed concentrations of ABG-H PAC to emulsified oil of 25 mg/L as TOC that is prefiltered through filter of 0.45 µm and not pre-filtered, one trial each

In summary it could be shown that PAC is effective in removing oil from emulsified oil, but no significance difference could be noticed between the three types of PAC in terms on the removal efficiency. Based on these results, a PAC dosage of 20 mg/L. Here, one may argue that PAC concentration of 10 mg/L could also be sufficient, as it removed more than 50% of UV_{254} active substances in the oil. However, with the addition of extra 10 mg/L (i.e., 20 mg/L), the elimination of DOC substances was increased by 20%. Considering this observation, further experiments were chosen to be carried out using ABG-H at dosing concentration of 10 and 20 mg/L.

4.3.2.3 Coagulation/Flocculation experiments

To determine the optimum coagulation/flocculation parameters for better membrane performance and oil removal, a series of typical jar-test coagulation experiments (according

to W 218 DVGW [135]) were carried out with different commercial iron- and aluminum-based inorganic coagulants (0 - 12 mg/L for iron and 0 - 6 mg/L for aluminum). As presented in Figure 83, the aluminum-based coagulant showed little to no removal for the oil at all coagulant dosing concentrations, whereas the iron-based coagulant was able to remove about 20% of the DOC even at a dosing concentration of about 1 mg/L. However, increasing the dosing concentration did not result in a further significant change in oil removal. Similar to the adsorption tests, there appears to be an oil fraction that cannot be flocculated.

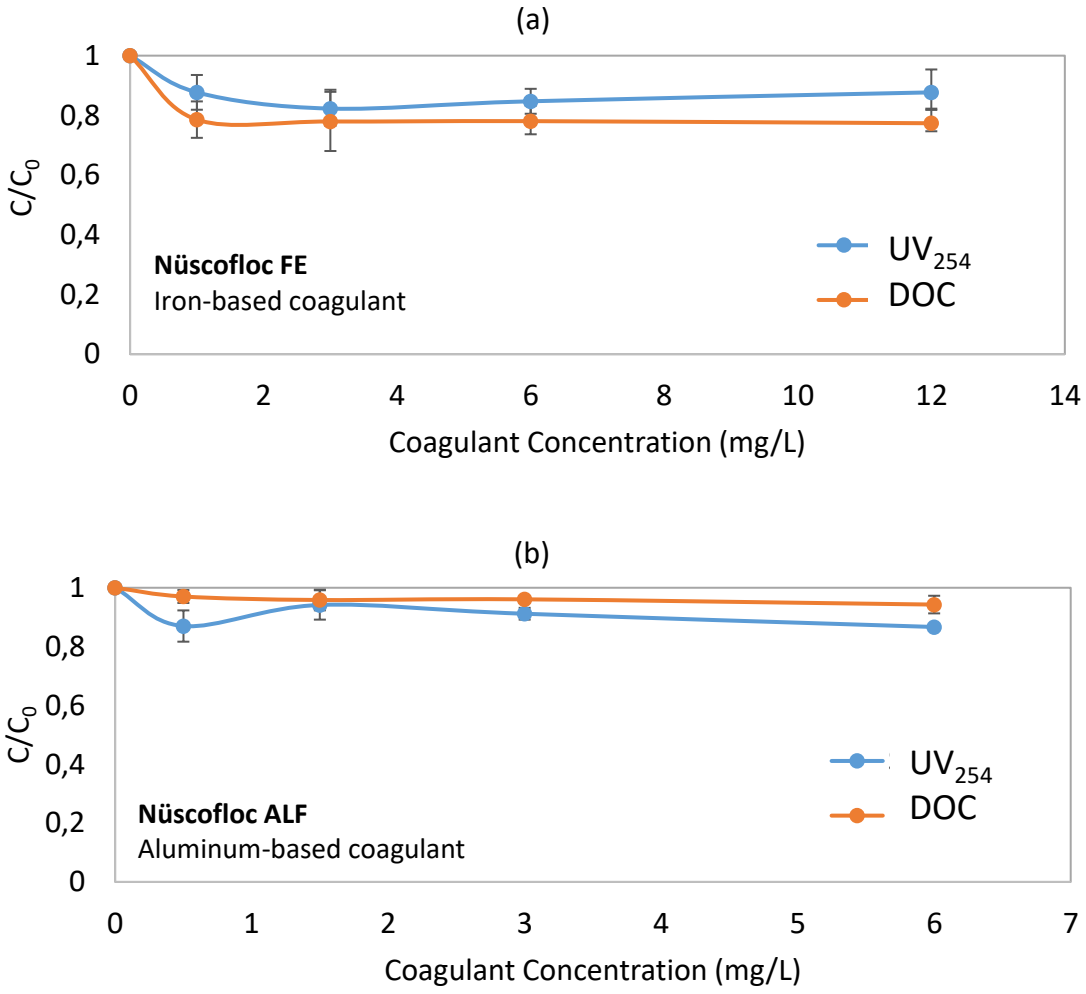

Figure 83: Relative concentrations of oil as DOC and UV_{254} in the supernatant of the coagulation/flocculation experiments (C) related to the feed concentration(C_0) for (a) Nüscofloc FE as iron-based coagulant and (b) Nüscofloc ALF as aluminum-based coagulant. Presented as average of two trials with the min. and max. error bars.

For the further studies on the synergistic combination of UF with coagulants, the iron-based coagulant was chosen as it showed better oil removal than the aluminum-based one. The dosage of the iron-based coagulant was set to 1 – 2 mg/L, as this concentration was sufficient to achieve an additional oil removal of about 20% with respect to DOC and UV_{254}.

4.3.2.4 Filtration tests using S100 flat sheet MF membranes

Figure 84a, b, c and d show the normalized permeability curves against the specific filtered volume per membrane area (V) in L/m² for filtration experiments of standalone S100, combination of coagulation-S100, PAC-S100 and coagulation-PAC-S100, respectively. All filtration experiment were performed at constant pressure of 1 bar with surfactant-free emulsified oil with an oil concentration of 25 mg/L as TOC.

The reference filtration experiment (i.e., PAC-free and coagulant-free) aimed at testing membrane fouling caused by only emulsified oil. As indicated in Figure 84a, the respective permeability loss was approximately 35%, 95%, 99.2%, and 99.6% after a filtration of 20, 50, 100, and 250 L/m², respectively.

Further filtration experiments were carried out to investigate the individual impacts of coagulant dosing on the membrane fouling behavior. These experiments were performed with an additional digital mixer mounted in the feed pressure vessel (that was the same coagulation reactor) to apply rapid mixing at 200 rpm for 30 s and then the continuous mixing at 50 rpm for the whole filtration cycle. After feed pH stabilization with NaOH at 1 M, iron-based coagulant, Nüscofloc FE, was dosed at 1 mg/L, as the findings from the preliminary experiments, cf. section 4.3.2.3. Results are depicted in Figure 84b. In the first trial the membrane lost approximately 49%, 71%, and 88% of its permeability after a filtration of 50, 100, and 250 L/m², and around 39%, 59%, and 81% in the second trial.

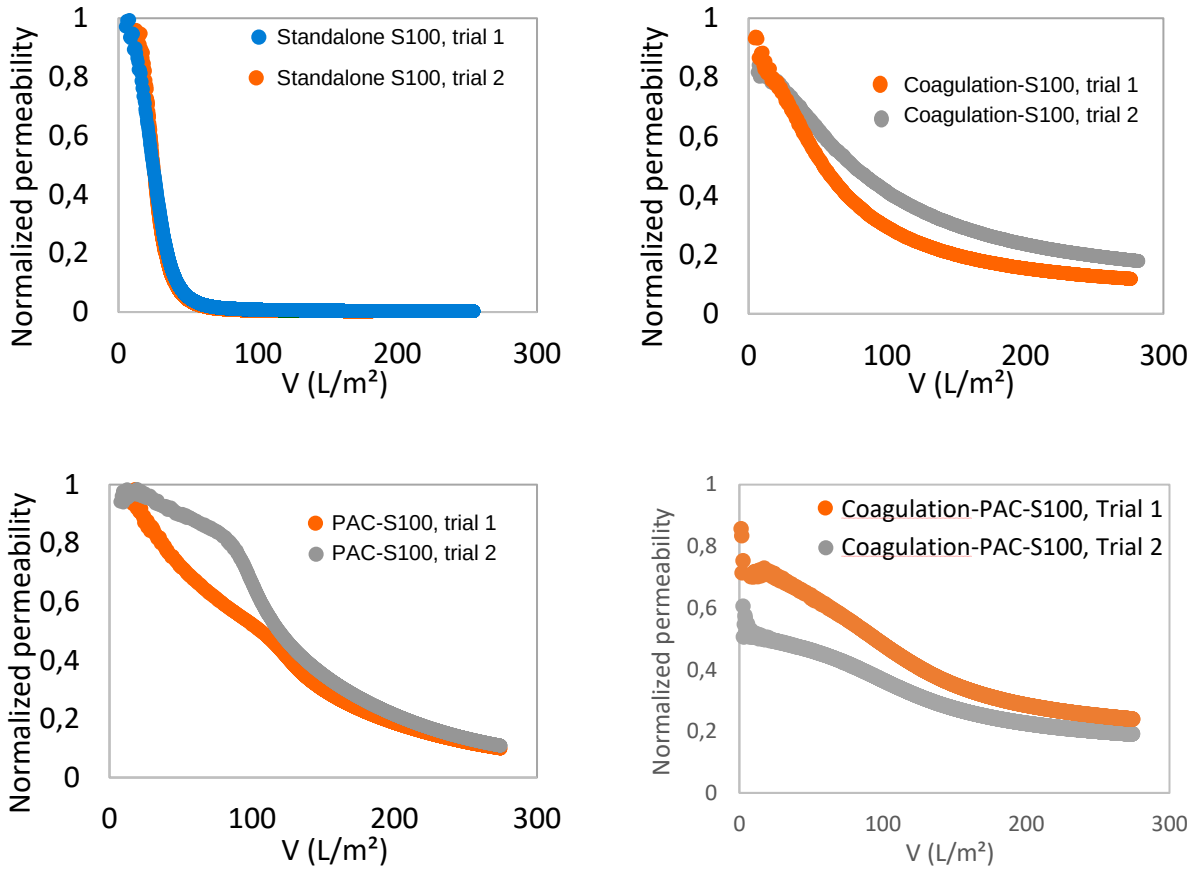

Figure 84: Normalized permeability curve of the dead-end filtration experiments on standalone S100, combination of coagulation-S100, PAC-S100 and coagulation-PAC-S100 for emulsified oils of 25 mg/L as TOC at constant pressure of 1 bar

Figure 84c shows results of the filtration experiments carried out with PAC dosing. PAC suspensions were filtered through the membrane with pure water, prior to the emulsified oil filtration, allowing them to form a cake layer on the membrane. The membrane lost only about 28%, 48%, and 78% of its permeability after a filtration of 50, 100, and 250 L/m², respectively, in the first trial and approximately 11%, 33%, and 78% in the second trial. This shows that the PAC-S100 combination led to decreased fouling even compared to the coagulation-S100 operation. This might be explained by the accumulation of the oil droplets on the PAC surface rather than on the membrane leading to reduction of the oil amount that reaches the membrane and hence the emerged fouling.

Two last experiments were conducted to investigate the fouling behavior of emulsified oil by the addition of PAC and coagulation. The PAC-dosage was set to 10 mg/L, and the

iron dosage was 1 mg/L. The corresponding filtration curves are presented in Figure 84d. In the first trial the membrane lost about 55%, 64%, and 81% of its permeability after a filtration of 50, 100, and 250 L/m², respectively, and around 38%, 53%, and 76% in the second trial.

The results show that the use of PAC and/or coagulation in the feed of an MF significantly reduces the fouling of the membranes compared to the application of MF alone. Under the conditions tested, PAC-MF resulted in less fouling than coagulation-MF. Although the combined PAC-coagulation-MF showed slightly higher fouling at the beginning of the trial, it resulted in the lowest fouling rate at the end of the trial period.

4.3.2.5 Filtration tests using UP150 flat sheet UF membranes

Figure 85a, b, c and d show the normalized permeability curves against the specific filtered volume per membrane area (V) in L/m² for filtration experiments of standalone UP150, combination of coagulation-UP150, PAC-UP150 and coagulation-PAC-UP150, respectively. All filtration experiment were performed at constant pressure of 1 bar with surfactant-free emulsified oil with an oil concentration of 25 mg/L as TOC.

The reference filtration experiment (i.e., PAC-free and coagulant-free) aimed at testing membrane fouling caused by only emulsified oil. As indicated in Figure 85a, the respective permeability loss was approximately 84%, 87%, and 99.4% after a filtration of 50, 100, and 250 L/m². Further filtration experiments were carried out to investigate the individual impacts of coagulant dosing on the membrane fouling behavior. These experiments were performed in the same way then described in section 4.3.2.4. Nüscofloc FE was dosed in a concentration of 1 mg/L. Results are depicted in Figure 85b. In the first trial the membrane lost approximately 45%, 54%, and 60% of its permeability after a filtration of 50, 100, and 250 L/m², respectively, and approximately 45%, 54%, and 78% in the second trial.

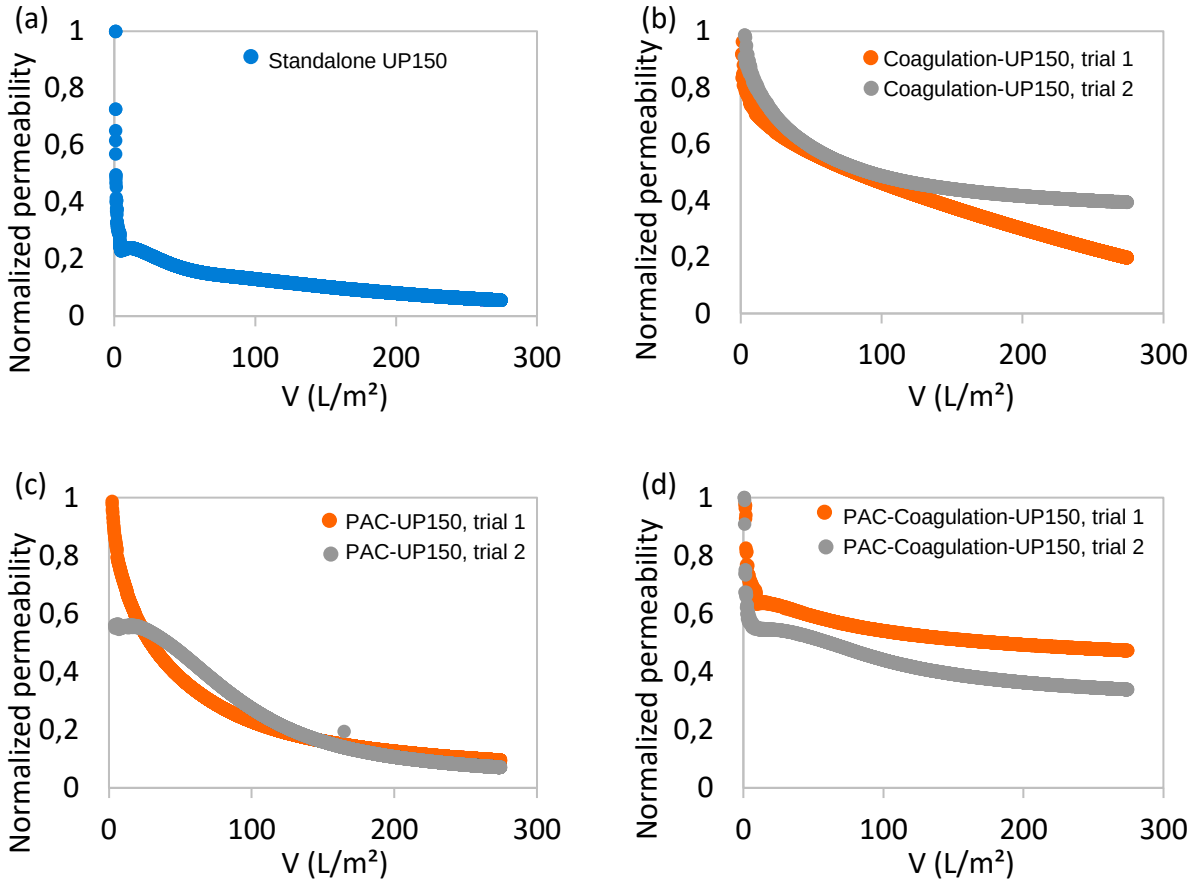

Figure 85: Normalized permeability curve of the dead-end filtration experiments on standalone UP 150, combination of coagulation- UP 150, PAC-UP 150 and coagulation-PAC- UP 150 membranes for emulsified oils of 25 mg/L as TOC at constant pressure of 1 bar

Figure 85c shows results of the filtration experiments carried out with PAC dosing. In the first trial, the membranes lost about 64%, 78%, and 90% of its permeability after a filtration of 50, 100, and 250 L/m², respectively, and approximately 56%, 74%, and 90% in the second trial. The two final experiments were conducted to investigate the fouling behavior of oily feed modified by the dosage of PAC and coagulation. The PAC-dosage was 10 mg/L, and the coagulation dosage was 1 mg/L. As represented in **Figure 85d,** the membrane lost about 42%, 47%, and 53% of its permeability after in the first trial a filtration of 50, 100, and 250 L/m², respectively, and approximately 49%, 57%, and 64% in the second trial.

The results demonstrated that the application of PAC and/or coagulation prior to a UF significantly reduced fouling compared to the use of UF alone. Unlike the tested MF, the coagulation-UF resulted in less fouling than the PAC-UF and the PAC-coagulation-UF exhibited the lowest fouling rate. The difference between MF and UF membranes can be attributed to the larger pore size of MF which may allow small-formed flocs to cause pore blockage. The best results with the combination of PAC and coagulation in both MF and UF could be due to the gradual development of a protective layer over the membrane, which in case of MF prevents small flocs from penetrating and blocking the pores.

4.3.2.6 Filtration tests on SM membranes

After investigating the influence of PAC dosage and/or coagulation prior to flat sheet S100 and UP150 membranes, the next objective was to assess the improvement in backwash efficiency. To achieve this, a series of filtration experiments were conducted on capillary SM_1 membranes at a constant pressure of 0.4 bar. Each experiment commenced with testing the pure water permeability for 15 minutes, followed by several cycles of filtering emulsified oils at a concentration of 10 mg/L. The experiments were conducted in four combinations: standalone SM membrane, PAC-SM, coagulation-SM, and PAC-coagulation-SM, with each cycle followed by a one-minute backwash step at a pressure of 1 bar. The cycles were repeated three times unless otherwise specified. Finally, the pure water permeability was measured at the end of the experiments to determine the total fouling. In these experiments, Nüscofloc FE was applied as coagulant at concentration of 1 mg_{FE}/L. Three PACs, ABG-H, HMA-B and ORG-K, were dosed into the feed tank at concentration of 10 mg/L and stirred at 100 rpm before beeing filtered as a layer onto the membrane. The coagulation-PAC-SM tests were realized by alternating the coagulant- or PAC-containing feed each three minutes, starting with the coagulant.

Figure 86 shows the normalized permeability curves for the reference experiment with surfactant-free emulsified oil only. The membrane lost about 25 – 40%, 35 – 50% and 45 – 55% of its permeability at the end of first, second and third filtration cycle, respectively. The backwash could not restore any significant portion of the membrane permeability.

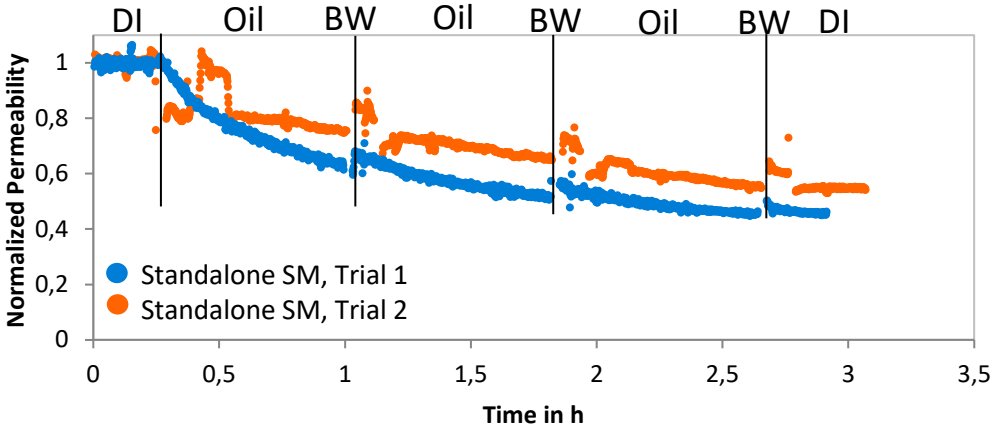

Figure 86: Normalized permeability curve for reference experiment for filtering surfactant-free emulsified oil of 10 mg/L as TOC at constant pressure of 0.4 bar through SM_1 membranes. BW for one minute at 1 bar. Two trials.

Figure 87 presents three trials of filtration experiments using the coagulation-SM combination. The first observation is that the permeability decline within each cycle was very limited, approximately 1-4%. Exceptions included the first cycle of the third trial and two sudden drops in the membrane permeability; one occurring after BW in the first trial and another in the middle of the third cycle during the second trial. In each of the two sudden drop instances, the membrane lost about 10-15% of its permeability, likely due to the blockage of one of the membrane capillaries. The blockage of only one capillary would have a significant effect, as only seven capillaries were used in these tests.

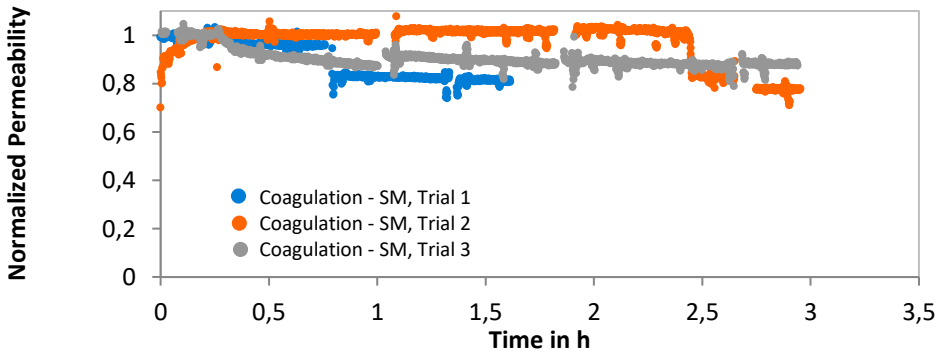

Figure 87: Normalized permeability curve for filtering surfactant-free emulsified oil of 10 mg/L as TOC at constant pressure of 0.4 bar with a combination of coagulation – PAC – SM_1 with ABG-H PAC at dosage of 10 mg/L, Nüscofloc FE coagulant at dosage of 1 mg/L

Figure 88a, b and c present the normalized permeability curves for the combination of PAC-SM_1 experiments with 10 mg/L of ABHG-H, HMA-B and ORG-K PAC. Figure 88a shows that two trials with ABG-H were conducted with one and two cycles. The membrane lost about 20% of its permeability at the end the experiments. The BW was not able to restore any significant amount of the permeability. Figure 88b and c show the filtration curves for the hybrid PAC-SM system using HMA-B and ORG-K. Several sudden drops and jumps in permeability can be observed. The reason behind this phenomenon is not completely clear, but it is expected to be due to partial or complete blockage of the capillaries during the filtration process. This variability complicates the comparison of the fouling rates, but a general trend can still be discerned. In general, the membrane lost approximately 20% and 30% of its permeability within each cycle for HMA-B and ORG-K, respectively. The backwash was partially effective in restoring some portion of the permeability, but the complete performance was not fully recovered.

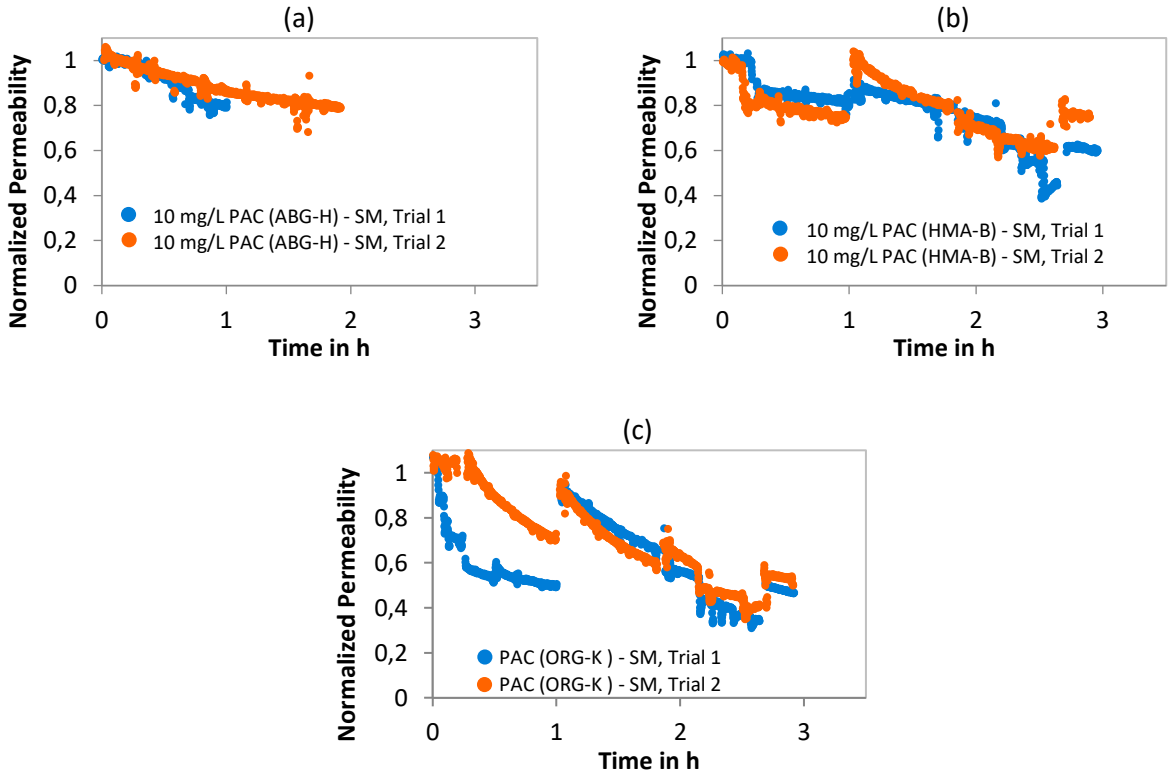

Figure 88: Normalized permeability curve for filtering surfactant-free emulsified oil of 10 mg/L as TOC at constant pressure of 0.4 bar with a combination of PAC-SM_1 with 10 mg/L (a) ABG-H, (b) HMA-B and (c) ORG-K PAC

Figure 89 presents the results of filtration experiments using the coagulation-10 mg/L PAC (ABG-H)-SM combination. The membrane experienced a permeability loss of approximately 13-15%, 13-17%, and 14-28% at the end of the first, second, and third cycles, respectively. The backwash was unable to restore the membrane permeability. Overall, the hybrid coagulation-PAC-SM system demonstrated better performance than the PAC-SM system but was not superior to the coagulation-SM system. Consequently, subsequent experiments with capillary membranes on a semi-technical scale were decided to be conducted using coagulation-UF without the dosage of PAC, cf. section 4.4.3.

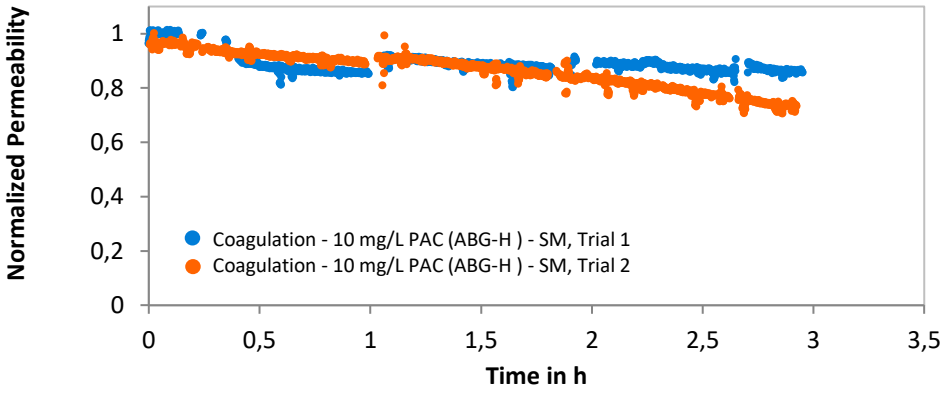

Figure 89: Normalized permeability curves for filtering surfactant-free emulsified oil of 10 mg/L as TOC at constant pressure of 0.4 bar with hybrid operation of coagulation – PAC – SM_1 experiments with ABG-H PAC at dosage of 10 mg/L, Nüscofloc FE coagulant at dosage of 1 mg/L

4.3.2.7 Influence of hybrid operation of PAC and/or coagulation-UF on the elimination performance of SM membranes

To investigate the influence of PAC and/or coagulant dosage on UV_{254} elimination, one feed sample and two or three permeate samples were collected and analyzed for UV_{254} absorbance. **Figure 90** presents the UV_{254} elimination results for standalone SM and hybrid operations of PAC-SM, coagulation-SM, and coagulation-PAC-SM systems.

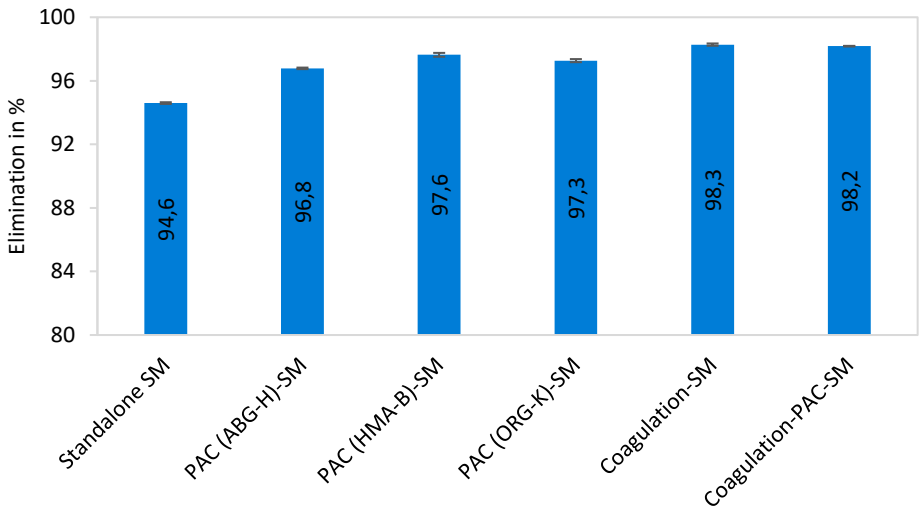

Figure 90: Elimination performance represented as percentage retention of UV_{254} for standalone S100, PAC-S100, coagulation-S100 and PAC-coagulation-S100

The standalone SM retained 94.6% of UV_{254}-active compounds. Dosing PAC prior to SM increased the elimination to 96.8%, 97.6%, and 97.3% for ABG-H, HMA-B, and ORG-K, respectively. Dosing the coagulant alone or in combination with ABG-H PAC increased the elimination to 98.3% and 98.2%, respectively.

The better elimination in coagulant dosing compared to PAC may be related to the improved size exclusion after coagulant dosing, as the coagulant helps to form larger oil droplets or clusters of small droplets. In addition, the ability of PAC to adsorb all oils is limited as adsorption occurs mainly on the outer surface of the PAC particles.

4.4 Assessment of the developed strategies:

To assess the feasibility of the developed strategies, a comparative analysis was conducted using crossflow operation as the reference standard. As detailed in section 3.11, this study focused on evaluating the differences in dosed substances and electrical energy consumption. These differences were pivotal for determining the environmental and economic viability of the improved dead-end methods. The parameters were presented and quantified in terms of cost and CFP.

4.4.1 Economic assessment (cost)

To estimate the difference in the energy consumption, between the crossflow operation and the surfactant-enhanced UF dead-end operation methods, the specific energy consumption per each cubic meter of produced permeate was calculated for each process as it was indicated in section 3.11.

4.4.1.1 Energy consumption of crossflow UF operation

Four filtration experiments in which surfactant-free emulsified oils were filtered at concentrations of 10, 25 and 50 mg_{TOC}/L with SM membranes at CFV 2.5 m/s or 0.75 m/s were analyzed again to evaluate the specific energy consumption for crossflow operation. As indicated in Figure 91, experiments at CFV of 2.5 m/s showed a total fouling of approximately 15%, 57%, and 89% at the end of the experiments for oil concentrations of 10, 25, and 50 mg/L, respectively. The fourth experiment implemented an oil concentration of 50 mg/L at a CFV of 0.75 m/s, in which reducing the CFV to 0.75 m/s had no significant impact on the fouling behavior.

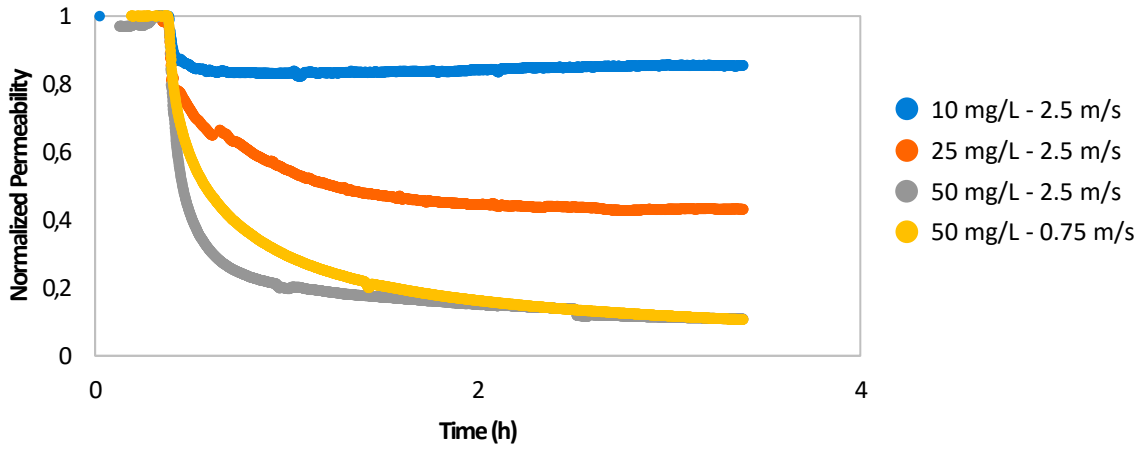

Figure 91: Normalized permeability of filtering emulsified oil with10 mg/L, 25 mg/L and 50 mg/L at CFV of 2.5 m/s compared with Normalized permeability of filtering emulsified oil with 50 mg/L at CVF of 0.75 m/s

Figure 92 presents the calculated E_S values for these four experiments assuming an η_F of 0.6 or 0.8 and that an energy recovery is implemented on the concentration side. It was observed that higher specific energy consumption was associated with higher oil

concentrations. Assuming a pump efficiency factor of η_F of 0.8, approximately 788, 1,430 and 1,599 Wh/m³ were needed for feed containing oil at concentrations of 10, 25, and 50 mg/L, respectively. Although no significant difference in fouling behavior was observed when the CFV was reduced to 0.75 m/s, but a substantial decrease in energy consumption was evident, amounting to 442 Wh/m³.

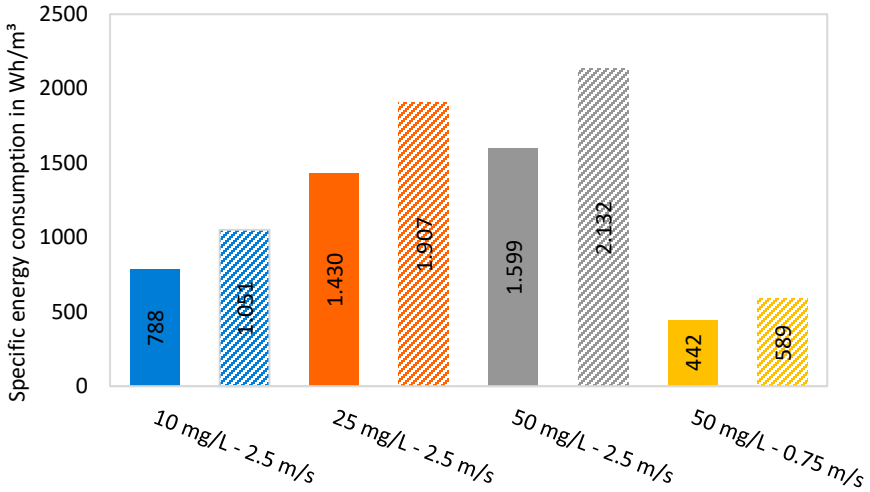

Figure 92: Specific energy consumption of crossflow experiments with emulsified oils at concentration of 10, 25 and 50 mg_{TOC}/L at CFV of 2.5 m/s. Calculated for η_F = 0.8 (solid-colored) and 0.6 (hatched)

The lower efficiency factor η_F = 0.6 resulted in increased energy consumption, with values of 1,051, 1,907 and 2,132 Wh/m³ for experiments conducted at CFV of 2.5 m/s with feed concentrations of 10, 25, and 50 mg/L, respectively.

4.4.1.2 Energy consumption of surfactant enhanced dead-end UF operation

The economic assessment of the surfactant-enhanced dead-end UF was conducted based on the experiments demonstrating the best reproducible performance. For that the results from five experiments were selected and analyzed for economic sustainability calculation. These five experiments comprised three trials with an oil concentration of 10 mg/L and SDS concentrations of 0.12, 0.48, and 1.2 g/L. Along with two other trials that were conducted implementing oil concentrations of 25 and 50 mg/L, both conducted with an SDS concentration of 0.48 g/L, as depicted in Figure 93.

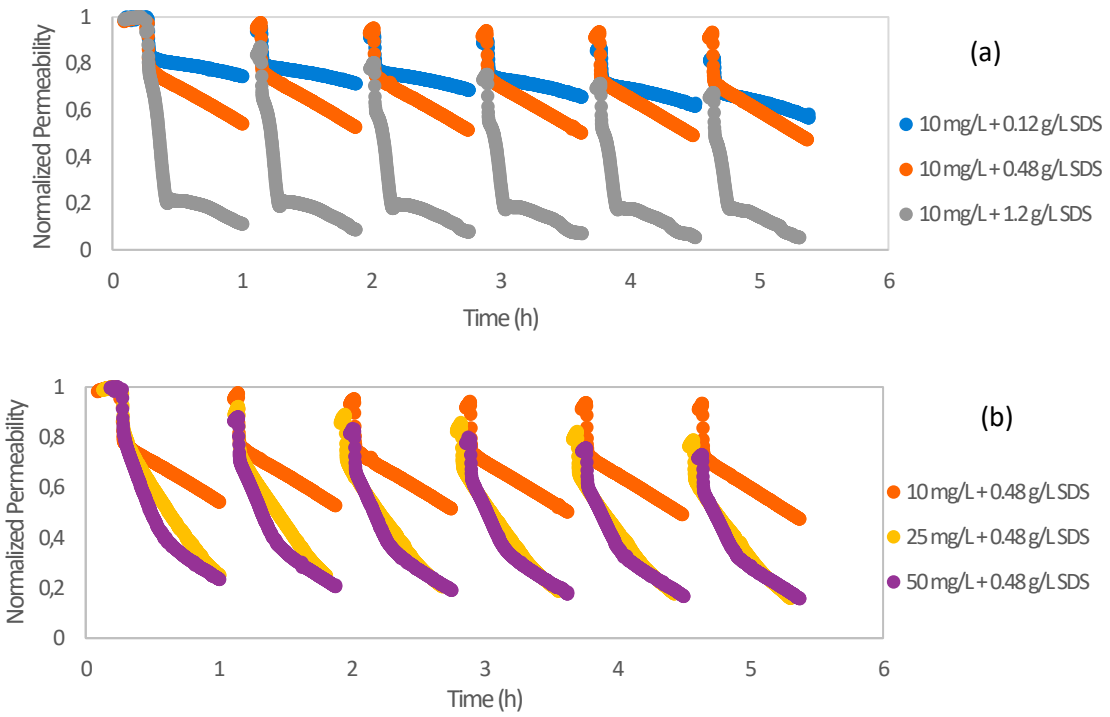

Figure 93: Normalized permeability of filtering surfactant-modified emulsified oils (a) at oil concentration of 10 mg/L with SDS concentrations of 0.12, 0.48 and 1.2 g/L and (b) at oil concentrations of 10, 25 and 50 mg/L with SDS concentration of 0.48 mg/L

Figure 94 illustrates the specific energy consumption of the surfactant-enhanced dead-end ultrafiltration experiments presented in Figure 93. EN_S was calculated for two pump efficiency values of 0.8 and 0.6. For experiments with an oil concentration of 10 mg/L and SDS dosages of 0.12, 0.48, and 1.2 g/L, E_S were 10, 9.6, and 37 Wh/m³, respectively, for a pump efficiency of 0.8, and 13.4, 12.8, and 49.8 Wh/m³ for a pump efficiency of 0.6. For oil concentrations of 25 and 50 mg/L with an SDS dosage of 0.48 g/L, E_S were 16.1 and 16.8 Wh/m³ for a pump efficiency of 0.8, and 21.5 and 22.3 Wh/m³ for a pump efficiency of 0.6.

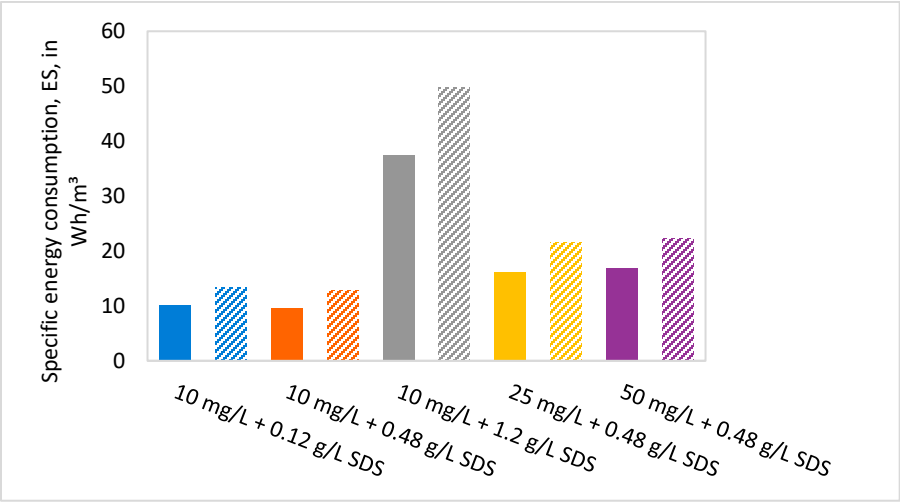

Figure 94: Specific energy consumption of surfactant-enhanced dead-end UF experiments with surfactant-enhanced emulsified oils at a concentration of 10 mg/L with SDS concentration of 0.12, 0.48 and 1.2 g/L and an oil concentration of 25 and 50 mg/L with SDS concentration of 0.48 g/L. Calculated for η_F = 0.8 (solid-colored) and 0.6 (hatched)

Two representative experiments, one for each operation mode, were selected for further EN_s calculation. The first experiment, labeled EXP_{CFW}, was conducted using crossflow mode with an oil concentration of 10 mg/L and CFV of 2.5 m/s. The second experiment, labeled EXP_{DE}, was conducted using dead-end mode with the same oil concentration but an SDS dosage of 0.48 g/L. Table 20 provides more detailed operation conditions of each one of these experiments.

Table 20: Detailed operation conditions and the respective parameters included for EN_s calculations in UF dead-end and crossflow modes.

Parameter	EXP_{DE}	EXP_{CFW}	Unit
Operation mode	Dead-end	Crossflow	
Oil concentration	10	10	mg/L
SDS dosage	0.48	-	g/L
Membrane active surface area	515	103	cm²
Average feed flow	5.15	80	L/h
Average permeate flow	5.15	3.1	L/h
Average concentrate flow	-	76.9	L/h
Permeate Flux	100	304	L/(m²·h)
Crossflow velocity	-	2.5	m/s
Average BW flux	230	-	L/(m²·h)
Average feed pressure	0.241	1.47	bar
Average Concentrate pressure	-	0.6	bar
Average Backwash pressure	0.35	-	bar

Parameter	EXP_{DE}	EXP_{CFW}	Unit
EN_S	9.6	788	Wh/m³

Based on the values from Table 20, the ΔEN and ΔC_{SDS} is calculated as follows:

$$\Delta EN_S = EN_{S,CFW} - EN_{S,DE} = 788\ \mathrm{Wh/m^3} - 9.6\ \mathrm{Wh/m^3} \approx 778\ \mathrm{Wh/m^3}$$

$$\Delta C_{SDS} = C_{CFW} - C_{DE} = 0 - C_{DE} = -C_{DE} = -0.48\ g/L$$

These values were used in the further assessment.

4.4.1.3 Cost balance between surfactant-enhanced dead-end and crossflow ultrafiltration

The cost of SDS depends on various factors, such as the source of SDS (petrochemicals, oleochemicals, etc.), its production lifecycle, and the production site or location. Table 21 shows the price for 1 kg of SDS from three marketplaces for suppliers of industrial level, namely: Alibaba, Made-in-china and Global Sources. The best price per 1 kg of SDS that was found on these marketplaces was 0.65, 0.83 – 1.3 and 0.83 – 1.57 €/kg, which corresponds to a minimum ordered quantity of 20, 20 and 5 ton, respectively.

Table 21: Price for 1 kg of SDS from three marketplaces for suppliers of industrial level

Marketplace	SDS price		Minimum order quantity
	$/Kg	€/kg	(Tons)
Alibaba	0.7	0.65	20 T
Global Sources	0.89 - 1.5	0.83 - 1.39	20 T
Made-in-china	0.89 - 1.7	0.83 - 1.57	5 T

Considering an average price of 1.1 € per kg, the cost difference due to the SDS dosage can be calculated as follows:

$$\Delta Cost_{SDS} = \Delta C_{SDS} \cdot Cost_{SDS} = -0{,}48\ g/L \cdot 1.1\ €/kg = -0.264\ €/m^3$$

The cost balance between the crossflow and surfactant enhanced dead-end UF operation was calculated as described in section 3.11. The two main factors still needed to be defined are the unit price of energy and the unit price of SDS. The electricity price depends on the location and the source of energy. Table 22 lists the electricity price, the respective value for $\Delta Cost_{EN}$ considering an energy consumption of 0.758 kWh/m³ and the ΔCost considering an average SDS cost of 0.264 €/m³ for Germany. Saudi Arabia, Egypt and Sweden.

Table 22: Electricity price, the respective value for $\Delta Cost_{EN}$ considering an energy consumption of 0.778 kWh/m³ and the ΔCost considering an average SDS cost of 0,264 €/m³ for Germany. Saudi Arabia, Egypt and Sweden.

Country	Electricity price in €/kWh	$\Delta Cost_{EN}$ in €/m³	ΔCost in €/m³
Germany	0.1178	0.092	-0.172
Saudi Arabia	0.069	0.054	-0,210
Egypt	0.037	0.029	-0,235
Sweden	0.07	0.055	-0,209

It can be observed that ΔCost is negative, where $|\Delta Cost_{EN}| < |\Delta Cost_{SDS}|$. This indicates that the costs associated with the SDS dosage in the dead-end operation are higher than the cost compared to the crossflow operation. In conclusion, the SDS dosage cost is more than three times higher than the energy cost difference, resulting in the fact that even reducing the SDS dosage, e.g., to 0.24 g/L, the surfactant-enhanced dead-end ultrafiltration process will still be economically unfeasible.

4.4.2 Environmental assessment

The surfactant-enhanced dead-end filtration was compared to the crossflow operation regarding sustainability and environmental impact.

4.4.2.1 The carbon footprint for electrical energy and SDS

Based on the literature review about the CFP value of the produced energy, cf. section 3.11, for further calculations, the average CFP value for EU in 2022 was considered and used, i.e., CFP_{EN}= 0.251 kg CO_2e/kWh.

Calculating the CFP for SDS was found to be more challenging than for electrical energy. Despite the widespread use of SDS, there is a notable lack of quantitative data regarding its environmental impacts. Generally, petrochemical and oleochemical surfactants are preferred over biosurfactants due to their cost-effectiveness. However, the environmental impact of these surfactants, including increased greenhouse gas emissions, is significant. SDS derived from renewable resources, such as oleochemicals, contributes less to global warming if produced sustainably.

An estimation value was defined and compared based on a literature review. Referring to the case study of surfactant chain production of Sodium Lauryl Ether Sulfate containing 3 mol of ethylene oxide (SLES 3EO) reported by Nogueira et al. (2019) [125], an

estimation was made based on the “cradle-to-gate” life cycle assessment approach and ISO 14067 guidelines for an SLES 3EO surfactant. SLES 3EO was selected as a reference surfactant due to its similarity with the targeted SDS surfactant in terms of product system boundaries and relevant unit processes, as discussed in the literature review. The CFP (specified as GWP in the reference) of producing one ton of SLES 3EO was reported to be about 1,870 kg CO_2e/t. The CFP associated with the production of ethylene oxide was reported as 239 kg CO_2e/t. In this study, the CFP_{SDS} was therefore calculated to be 1,590 kg CO_2e/t. The CFP_{SDS} has higher value comparing to the CFP values of other chemicals, such as NaOH and NaOCl, that are typically used for chemical cleaning during membrane operation. The CFP values for NaOH and NaOCl are about 1,000 kg CO_{2eq}/t and 410 kg CO_{2eq}/t, respectively [147].

4.4.2.2 CFP comparison between surfactant-enhanced dead-end and crossflow ultrafiltration

The CFP difference between crossflow and dead-end resulting from the energy consumption can be calculated as follows:

$$\Delta CFP_{EN} = \Delta EN \cdot CFP_{EN} = 0.778\ kWh/m^3 \cdot 0.251\ \mathrm{kgCO2e/kWh} = 0{,}195\ kg\ \mathrm{CO2eq/m^3}$$

The CFP difference due to the SDS dosage can be calculated as follows:

$$\Delta CFP_{SDS} = \Delta C_{SDS} \cdot CFP_{SDS} = -0{,}48\ g/L \cdot 1.59\ \mathrm{kg\ CO2eq/kg\ SDS} = 0.763\ kg\ \mathrm{CO2eq/m^3}$$

And thus, the total CFP difference is:

$$\Delta CFP = \Delta CFP_{EN} + \Delta CFP_{SDS} = 0{,}195\ kg\ \mathrm{CO2e/m^3} - 0.763\ kg\ \mathrm{CO2e/m^3}$$
$$= -0.568\ kg\ \mathrm{CO2e/m^3}$$

A similar observation as for the ΔCost can also be made for the ΔCFP, namely that the difference indicates a negative value. This implies that the CFP associated with surfactant-enhanced dead-end UF operation exceeds that of the crossflow operation. Furthermore, the use of SDS results in the release of over four times the amount of carbon compared to the additional energy required in crossflow. Hence, it is apparent that the surfactant-enhanced dead-end approach has a more significant environmental impact.

4.4.3 Experiments relevant to practice

To assess the scalability of the results obtained, selected experiments were carried out with membrane modules that have a similar length to the real modules, a larger surface area and a longer time span. Figure 95 shows the permeability of filtering surfactant-free emulsified oils at oil concentration of 10 mg/L through pristine LM_2 modules. This was conducted as standalone UF in dead-end regime at constant flux of 100 L/(m²·h). The experiment started by filtering pure water for 15 min, then emulsified oils were filtered for 30 min followed by hydraulic BW step. The membrane showed an average permeability of about 435 L/(m²·h·bar) and suffered almost no fouling during the first cycle. This might be attributed to dilution effect caused by the residual pure water in the feed pipes before getting replaced with emulsified oil. But the permeability declined below 350 L/(m²·h·bar) at the end of the second cycle and the following BW could restore no significant amount of the permeability. A sharper decline in the permeability was noticed during the third, fourth and fifth cycles, in which the membrane permeability dropped to about 267, 147 and 53 L/(m²·h·bar), respectively. The membrane lost about 88% of its permeability after less than 3 hours, which is higher than the fouling rate that was noticed in similar experiments that were carried out with SM modules. For comparison, the membrane in Figure 47, cf. section 4.3.1.2.2, lost about 60% of its permeability after 3 hours.

However, the experiment was not conducted continuously; the experiment paused at several time points, indicated as points A-E in Figure 95. The filtration was first paused after approximately 2.9 hours (Timepoint A) due to the pressure exceeding the maximum allowed limit of 2.5 bar. Significant fouling necessitated manual CIP of the membrane. This was accomplished by rinsing with a 1.2 g/L SDS solution for 15 minutes, followed by a 10-minute rinse with pure water. Data from this step were not recorded.

Subsequently, a chemical cleaning process was initiated (Timepoint B). The initial membrane permeability was measured at approximately 170 L/(m²·h·bar). The first CIP with a 1.2 g/L SDS solution restored the membrane permeability to approximately 200 L/(m²·h·bar). A second CIP with a 200 mg/L NaOCl solution further increased the permeability to approximately 210 L/(m²·h·bar) by the end of the cleaning step (Timepoint C).

Filtration with emulsified oil at a concentration of 10 mg/L was then resumed. The membrane permeability showed a slight decrease over the first three cycles, reaching values of approximately 200, 200, and 195 L/(m²·h·bar), respectively. However, a significant increase in fouling was observed during the fourth, fifth, and sixth cycles, with final permeabilities of approximately 155, 85, and below 50 L/(m²·h·bar), respectively. The experiment was subsequently halted after 11 hours (Timepoint D) due to the pressure again exceeding the maximum allowable limit. A subsequent cleaning step was ineffective and did not restore any of the membrane permeability.

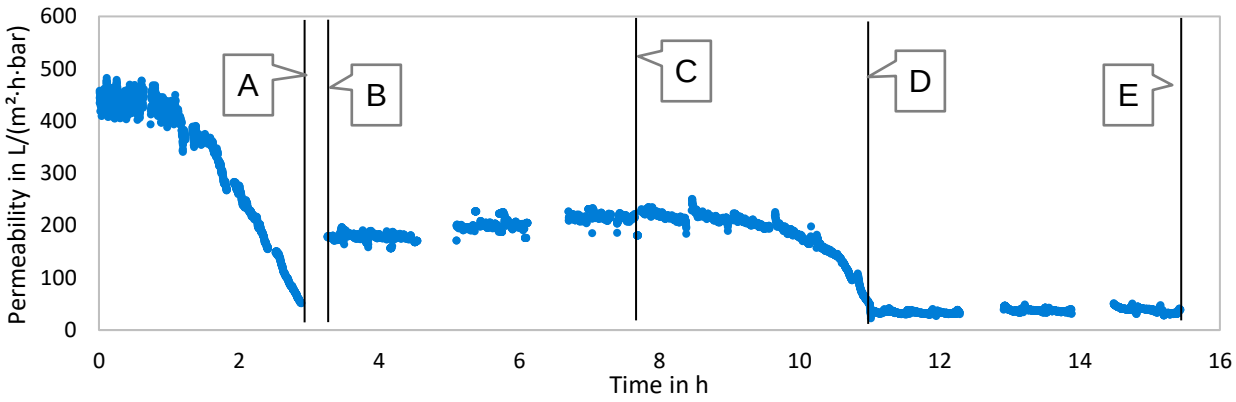

Figure 95: Permeability of filtering surfactant-free emulsified oils at oil concentration of 10 mg/L through LM$_2$ membranes as standalone UF at constant flux of 100 L/(m²·h)

In another experiment, surfactant-modified emulsified oils were filtered through the LM membrane modules. SDS$_{VWR,23}$ was added at a concentration of 0.48 g/L. As indicated in Figure 96, the initial membrane permeability, measured during the filtration of pure water, was approximately 390 L/(m²·h·bar). Upon switching to emulsified oil, the membrane permeability immediately decreased to 355 L/(m²·h·bar).

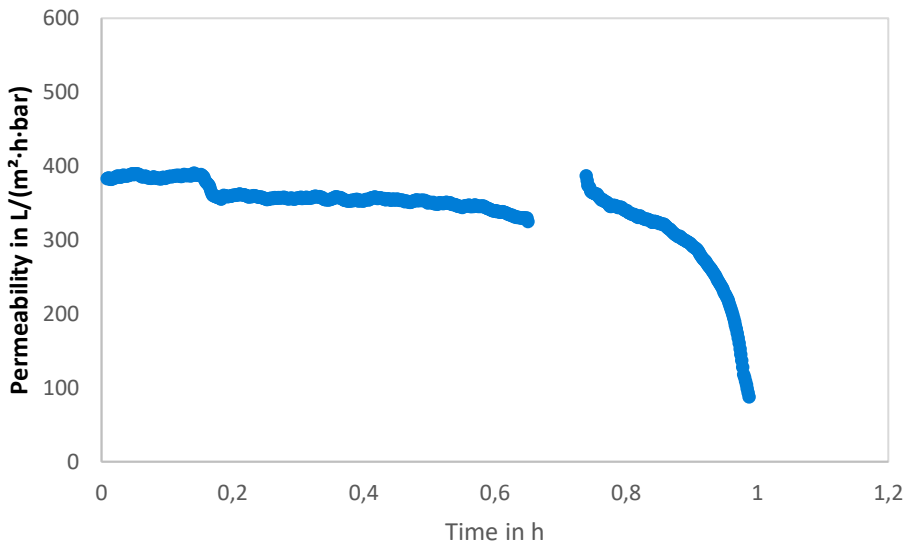

Figure 96: Permeability of filtering surfactant-modified emulsified oils at oil concentration of 10 mg/L and SDS concentration of 0.48 g/L through LM module as standalone UF at constant flux of 100 L/(m²·h)

Subsequently, the permeability curve plateaued, with a slight decline observed during the later stages of the filtration cycle, resulting in a final permeability of 325 L/(m²·h·bar). BW effectively restored the membrane permeability to approximately 385 L/(m²·h·bar).

In the subsequent filtration cycle, the membrane permeability again rapidly decreased to about 350 L/(m²·h·bar) within the first minute. This was followed by a moderate fouling rate, with permeability decreasing to 275 L/(m²·h·bar) after 10 minutes. The fouling rate then escalated significantly, causing the permeability to fall below 50 L/(m²·h·bar) after approximately 15 minutes, so that the experiment stopped due to exceeding the maximum allowed pressure.

Figure 97 compares the membranes operation as standalone UF and as hybrid coagulant-UF with a coagulant dose of 1 mg/L of Nüscofloc FE. The surfactant-free emulsified oil at oil concentration of 10 mg/L were filtered through two pristine LM_2 modules. Both were conducted in dead-end regime at constant flux of 100 L/(m²·h). The first experiment was previously discussed and depicted in Figure 95. In the second experiment, which involved hybrid coagulation-UF operation, the membrane demonstrated a slightly higher average initial permeability of approximately 470 L/(m²·h·bar). Slight fouling, occurring at different rates, was observed in each cycle. For instance, during the second cycle, the membrane experienced a permeability decline of about 7%, resulting in an average permeability of

approximately 440 L/(m²·h·bar) by the end of the cycle. The permeability also dropped to around 385 L/(m²·h·bar) and 350 L/(m²·h·bar) after 6 and 12 hours, which corresponds to the total fouling of about 18% and 26% respectively.

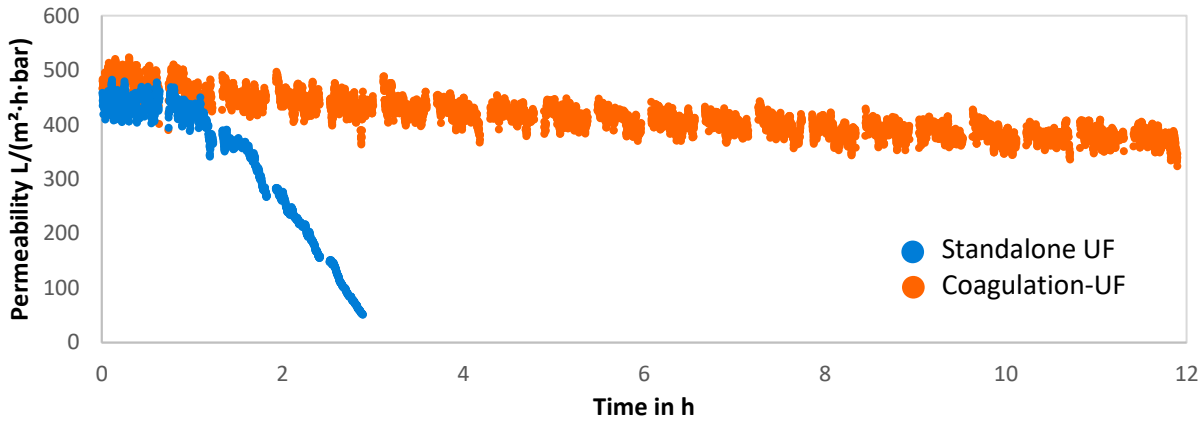

Figure 97: Permeability of filtering surfactant-free emulsified oils at oil concentration of 10 mg/L through LM_2 modules as standalone UF or hybrid coagulant-UF. Nüscofloc FE was dosed as 1 mg/L. Both experiments werde done at constant flux of 100 L/(m²·h)

Backwashing was not effective in significantly restoring membrane permeability. This fouling rate is comparable to that observed in experiments with SM modules, as depicted in Figure 87 (section 4.3.2.6), where the membrane lost between 1-4% of its permeability within a 45-minute filtration cycle.

The experiment was extended to approximately 5.5 days (Figure 98). However, it could also not be carried out continuously and the experiment paused at several time points, indicated as points A-D in Figure 98. Timepoints A, B, and C correspond to brief experimental stops due to temporary pressure spikes exceeding the maximum allowed pressure. The experiment resumed immediately after these events without further actions.

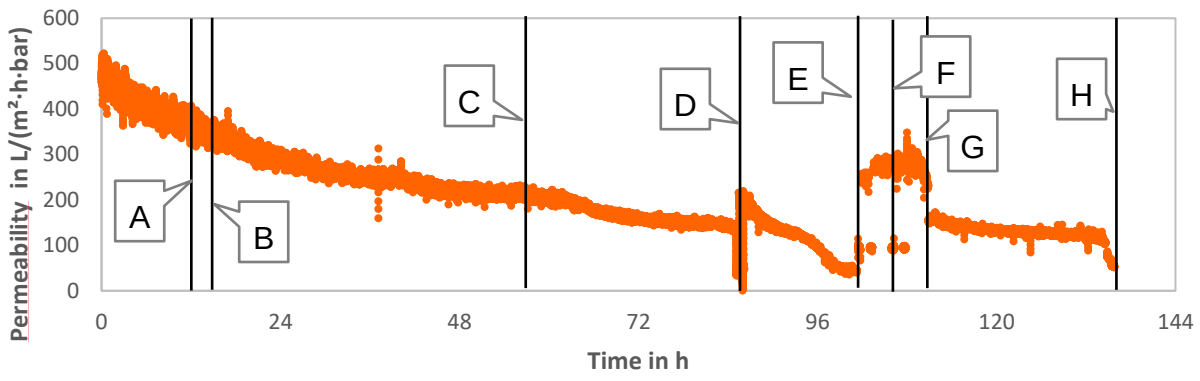

Figure 98: Permeability of filtering surfactant-free emulsified oils at oil concentration of 10 mg/L through LM_2 module as hybrid coagulant-UF. Nüscofloc FE was dosed as 1 mg/L, flux was set constant to 100 L/(m²·h)

Membrane performance showed a steady permeability decline, with average values dropping to approximately 290, 240, 200, and 140 L/(m²·h·bar) after 24, 40, 60, and 80 hours, respectively. At around 86 hours (Timepoint D), a technical failure in the coagulation dosage pump led to a sharp permeability decline and pressure increase above the 2.5 bar limit, causing an automatic experiment abort. The membrane rested for about 12 hours before the issue was noticed. Several backwash steps partially restored permeability, and the experiment resumed with a permeability of about 200 L/(m²·h·bar).

Notably, the fouling rate increased post-resumption; permeability dropped from 200 to 140 L/(m²·h·bar) in less than four hours (Timepoints 86 to ~90 hours), a decline that previously took about 20 hours (Timepoints 60 to 80 hours). After 100 hours, the experiment stopped at timepoint E due to severe fouling, with permeability dropping below 50 L/(m²·h·bar) and pressure again exceeding 2.5 bar. A chemical cleaning at timepoint E (104.5 hours) restored permeability to 300 L/(m²·h·bar). A second chemical cleaning (Timepoint F) did not further improve permeability. Subsequent filtration of emulsified oil led to an immediate permeability decline to about 160 L/(m²·h·bar) followed by a steady decrease to 110 L/(m²·h·bar) after 134 hours, at which point the experiment stopped due to increased fouling and permeability falling below 50 L/(m²·h·bar).

The performance of coagulation-UF was tested using membrane with bigger surface area, i.e., LM module with surface area of 0.23 m³. Figure 99 shows permeability of two experiments for filtering surfactant-free emulsified oils at oil concentration of 10 mg/L. Filtration was done with LM modules as hybrid coagulation-UF with a coagulant dose of 1 mg/L of

Nüscofloc FE at constant flux of 100 L/(m²·h) for three cycles followed by two CIP steps with NaOCl at chlorine concentration of 200 mg/L and SDS at concentration of 1.2 g/L. In the first trial, the membrane permeability was recorded at approximately 470 L/(m²·h·bar) during pure water filtration. This value decreased to 415 L/(m²·h·bar), but subsequent BW restored the permeability to 455 L/(m²·h·bar).

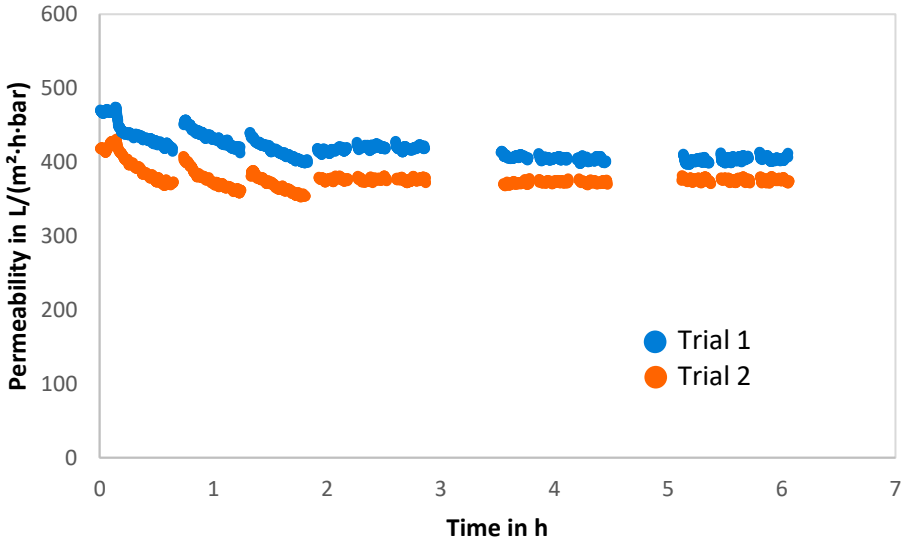

Figure 99: Permeability of filtering surfactant-free emulsified oils at oil concentration of 10 mg/L through LM module as hybrid coagulation-UF at constant flux of 100 L/(m²·h) for three cycles followed by two CIP steps with NaOCl at chlorine concentration of 200 mg/L and SDS at concentration of 1.2 g/L. Two trials

By the end of the second cycle, the permeability had dropped to around 410 L/(m²·h·bar) and was restored to about 440 L/(m²·h·bar) following BW, eventually declining to approximately 398 L/(m²·h·bar) by the end of the third cycle. Chemical cleaning performed afterward was ineffective in restoring the irreversible fouling. The second trial exhibited a similar trend to the first trial. This fouling rate is higher than that observed in the experiments with SM modules, as depicted in, where the membrane lost between 1-4% of its permeability within a 45-minute filtration cycle.

The experiments demonstrate that coagulation dosing prior to UF membrane treatment effectively reduces the fouling rate and slightly enhances backwash efficiency, leading to improved overall membrane performance. These findings were validated at various scales, indicating good scalability of the results.

5 Conclusion

The W-UFO research project aimed to establish an efficient pressure-driven membrane-based treatment method for the purification of PW using polymeric ultrafiltration membranes. This method is intended as a polishing step in the treatment process of oily wastewater effluents. Over the last four year this research project has made significant progress in addressing the four key topics set out to investigate. Every topic has yielded valuable insights and advancements, contributing to the broader field of study. The conclusions are presented in respect to the hypothesis that were made in section 1.4:

5.1 Establishment of a standard protocol for the production of synthetic OWWE.

a. Reference HPH-based and US-based methods for the preparation of synthetic emulsified oils were successfully reproduced. HPH-based method was more reliable, than US-based method, for the preparation of stable and reproducible emulsified oils with controlled characteristics. Nevertheless, the complex instrumentation and maintenance costs were the main challenges.

b. HPH-based method can be employed to effectively produce a sufficient quantity of stable emulsified oil with controlled oil composition and oil droplets size distribution for the lab-scale mini-plant membrane experiments.

c. Emulsions that were produced using both methods exhibited characteristics similar to PW prior to tertiary treatment step.

d. Emulsified oils with similar chemical compositions but produced via different emulsification methods were found to cause different membrane fouling behaviors that were related to different oil droplets size distributions.

5.2 Understanding the main fouling mechanisms of dead-end operated PES UF membranes

a. The performance of UF and MF membranes as well as the nature of fouling mechanisms were emphasized to be substantially influenced by the interrelation between oil droplet size distribution and membrane pore size distribution.

b. In case of the used MF membranes (with pore sizes larger than droplet size of oily emulsions), fouling mechanisms were dominated by standard pore blocking

at early stage of filtration, afterward, more contribution of intermediate blocking and cake filtration mechanisms were observed. This indicates that the severe decay in MF performance should be mainly related to internal membrane fouling. This conclusion was additionally supported by SEM analysis of fouled MF membranes, where oil droplets were seen to penetrate and coat the internal membrane structure. In case of the used UF membranes (with pore size smaller than droplet size of oily emulsions), fouling mechanisms were rather prevailed by intermediate and cake filtration fouling models, which means that fouling of more dense membranes by produced water should be interpreted in terms of surface fouling rather than internal pore blocking if pore size is sufficiently small.

c. Our experiments revealed that dissolved crude oil components, i.e., WSO, had no significant contribution into the fouling of SM membrane by emulsified oils under the tested conditions

5.3 Improvement of the PES UF dead-end process by testing different strategies

5.3.1 Surfactant-enhanced dead-end UF

a. Bench-scale filtration experiments with flat sheet membranes revealed that the addition of surfactants increased the membrane fouling under the given conditions. This is likely due to adsorptive fouling by the surfactants on the membrane surface and within its porous structure. In contrast, the addition of salts was found to disturb the stability of emulsified oils and resulting in bigger oil droplets, and consequently, oil droplet size distributions with bigger droplets are highly expected in case of real saline produced water. Subsequently, saline oily feeds caused less membrane fouling. Co-surfactants were found to have no significant effect on the fouling rate at the tested conditions.
b. It was noticed that the surfactants exhibited analogous fouling, or adsorption behavior, on PES UF membranes regardless of their different type. The effect of the surfactant's concentration was more emphasized.
c. Ultrafiltration of sub-micron sized surfactant-free emulsified oil caused severe hydraulic irreversible fouling due to strong oil adhesion to non-charged membrane

sites such that initial membrane performance could not be restored via typical hydraulic backwashing.

d. Adsorption of SDS monomers onto emulsified oil droplets increased remarkably negative surface charges that promoted oil droplets stability during filtration of SDS-modified emulsified oils and prevented coalescence in the membrane vicinity.
e. SDS monomers were readily adsorbed into PES membrane matrix causing a strong concentration-dependent normalized permeability decline that was completely hydraulically backwashable.
f. Compared to surfactant-free emulsified oil, improved membranes performance along with substantially enhanced hydraulic backwashing efficiency was observed during dead-end filtration of surfactant-modified emulsified oils. Nevertheless, it was found that a minimum SDS dose should be maintained to obtain the desired enhanced membrane performance. The developed SDS-ultrafiltration procedure allowed multiple-cycle dead-end filtration of emulsified oils (with oil content up to 50 mg/L) using commercial ready-to-use capillary PES membranes substantially enhanced hydraulic backwashing efficiency that was not practically feasible for surfactant-free emulsified oils.

   However, the method suffered from high sensitivity regarding the quality of the applied SDS. This led to significant drop in the backwasheability of the accumulated fouling layer on the membrane during the filtration of surfactant-modified emulsified oils.
g. Our experiments on optimizing operational conditions, including filtration flux, filtration duration, BW flux, and BW duration, did not lead to enhanced membrane performance. This may be attributed to the SDS type used (i.e., $SDS_{VWR,23}$), which proved ineffective in restoring membrane performance through BW.

5.3.2 Hybrid UF process: PAC-UF, coagulation-UF, and PAC-coagulation-UF

a. Significant portion of the oil components from the emulsified oils were adsorb on the PAC (up to 75%), a certain non-adsorbable part could be noticed. The adsorption most likely follows a multi-component adsorption isotherm. However, the adsorption isotherm could not be determined. A high fluctuation in the elimination rate could be observed during adsorption isotherm experiments.

b. Adsorbable components were assumed adsorbed on the outer surface of the PAC particles. No significant difference could be noticed when using different PAC types. An isotherm equilibrium could be noticed after 24 hours.

c. Dosing iron-based and aluminum-based coagulants enhanced the oil elimination from the emulsions, which is expected mainly to be attributed to an increase the oil coalescence between oil droplets. Iron-based coagulant exhibited higher elimination rates than the aluminum based one.

d. Dosing PAC prior to UF membranes did not significantly reduce the fouling or enhance the backwash efficiency. Dosing coagulant prior to UF membranes reduced the fouling rate but did not improve the backwash efficiency. Dosing both PAC and Coagulation prior to UF reduced the fouling but could not outperform the coagulation-UF operation.

e. Dosing PAC slightly improved the separation performance of the membrane compared to standalone UF membrane, on the other hand dosing coagulation alone or combined with PAC prior UF exhibited better separation performance.

5.4 Assessment of the developed strategies

a. The developed surfactant-enhanced dead-end UF prosses was found to be sensitive for minor deviations in the quality of the applied SDS surfactant.

b. Higher carbon footprint was calculated for the surfactant-enhanced dead-end UF compared to the crossflow operation.

c. The developed surfactant-enhanced dead-end UF was found less economically feasible than the crossflow operation mode due to high costs associated to the SDS.

d. Test on different scales, i.e., different membrane length, surface area and for different running time, indicated good reproducibility of the acquired coagulation-UF results and thus good scalability.

6 Outlook

Based on the findings of the W-UFO research project, several areas for further improvement could be identified:

- Effective Cleaning Strategies: Establish effective cleaning strategies, including testing different cleaning agents, protocols, and intervals. Determine the critical permeability level below which cleaning efficiency is significantly reduced preventing sustainable membrane operation.
- Coagulation-UF Operation Feasibility: Investigate the feasibility of coagulation-UF operation with coagulants of varying quality or from different suppliers, and with membranes from different manufacturers.
- Influence of PAC Size: Study the effect of PAC size on its efficiency in removing oil components, reducing PES-UF membrane fouling, and increasing membrane backwashability.
- Alternative Adsorbers: Given that oil adsorption on PAC mainly occurs on the outer surface, conduct filtration experiments with non-activated carbon or other adsorbents.
- Filtration Experiments with SDS: Perform filtration experiments using high-quality SDS, like the type used in the CMC analysis (section 4.3.1.7).

These recommendations and identified research areas highlight the potential for improving the efficiency and sustainability of membrane treatment processes for oily produced water.

7 References

1. Cooper, C.M., et al., *Oil and Gas Produced Water Reuse: Opportunities, Treatment Needs, and Challenges.* ACS ES&T Engineering, 2022. **2**(3): p. 347-366.
2. Emmons, R.V., et al., *Unraveling the Complex Composition of Produced Water by Specialized Extraction Methodologies.* Environmental Science & Technology, 2022. **56**(4): p. 2334-2344.
3. Igunnu, E.T. and G.Z. Chen, *Produced water treatment technologies.* International Journal of Low-Carbon Technologies, 2014. **9**(3): p. 157-177.
4. Ray, J.P. and F.R. Engelhardt, *PRODUCED WATER, Technological/Environmental Issues and Solutions.* 1992.
5. Je, Y., *Membrane technologies for water treatment and reuse in the gas and petrochemical industries*, in *Advances in membrane technologies for water treatment : materials, processes and applications*, A. Basile, A. Cassano, and N.K. Rastogi, Editors. 2015, Elsevier, Woodhead Publishing: Amsterdam.
6. Dickhout, J.M., et al., *Produced water treatment by membranes: A review from a colloidal perspective.* Journal of Colloid and Interface Science, 2017. **487**: p. 523-534.
7. Neff, J., K. Lee, and E. Deblois, *Produced Water: Overview of Composition, Fates, and Effects*. 2011. p. 3-54.
8. Chew, J.W., J. Kilduff, and G. Belfort, *The behavior of suspensions and macromolecular solutions in crossflow microfiltration: An update.* Journal of Membrane Science, 2020. **601**: p. 117865.
9. Jiménez, S., et al., *State of the art of produced water treatment.* Chemosphere, 2018. **192**: p. 186-208.
10. John M. Walsh, P., CETCO Energy Services, Inc.; , A.S. James Vanjo-Carnell, and C.E.S. Jarid Hugonin, Inc., *Understanding water soluble organics in upstream production systems.* SPE-International, 2014.
11. John A. Veil, et al., *A White Paper Describing Produced Water from Production of Crude Oil, Natural Gas, and Coal Bed Methane.* Produce Water White Paper, 2004.
12. Olajire, A.A., *Recent advances on the treatment technology of oil and gas produced water for sustainable energy industry-mechanistic aspects and process chemistry perspectives.* Chemical Engineering Journal Advances 4, 2020.

13. Redman, A.D., et al., *Quantifying the concentration of crude oil microdroplets in oil-water preparations.* Environ Toxicol Chem, 2012. **31**(8): p. 1814-22.
14. Bostick, D.T., H. Luo, and B. Hindmarsh, *Characterization of Soluble Organics in Produced Water.* OAK RIDGE NATIONALLABORATORY, 2002.
15. Fakhru'l-Razi, A., et al., *Review of technologies for oil and gas produced water treatment.* J Hazard Mater, 2009. **170**(2-3): p. 530-51.
16. Liu, Y., et al., *A review of treatment technologies for produced water in offshore oil and gas fields.* Sci Total Environ, 2021. **775**: p. 145485.
17. Lin, Y.-M. and G.C. Rutledge, *Separation of oil-in-water emulsions stabilized by different types of surfactants using electrospun fiber membranes.* Journal of Membrane Science, 2018. **563**: p. 247-258.
18. Lu, D., T. Zhang, and J. Ma, *Ceramic Membrane Fouling during Ultrafiltration of Oil/Water Emulsions: Roles Played by Stabilization Surfactants of Oil Droplets.* Environmental Science & Technology, 2015. **49**(7): p. 4235-4244.
19. Adham, S., et al., *Membrane applications and opportunities for water management in the oil & gas industry.* Desalination, 2018. **440**: p. 2-17.
20. Cabrera, S.M., et al., *Performance evaluation of an industrial ceramic nanofiltration unit for wastewater treatment in oil production.* Water Research, 2022. **220**: p. 118593.
21. Veil, J.A., et al., *A white paper describing produced water from production of crude oil, natural gas, and coal bed methane*. 2004, Argonne National Lab., IL (US).
22. Duraisamy, R.T., A.H. Beni, and A. Henni, *State of the Art Treatment of Produced Water*, in *Water Treatment*, W. Elshorbagy and R.K. Chowdhury, Editors. 2013, InTech: Rijeka. p. Ch. 09.
23. Tummons, E., et al., *Membrane fouling by emulsified oil: A review.* Separation And Purification Technology, 2020. **248**: p. 116919.
24. Fakhru'l-Razi, A., et al., *Review of technologies for oil and gas produced water treatment.* Journal of Hazardous Materials, 2009. **170**(2): p. 530-551.
25. Ahmad, T., C. Guria, and A. Mandal, *A review of oily wastewater treatment using ultrafiltration membrane: A parametric study to enhance the membrane performance.* Journal of Water Process Engineering, 2020. **36**.
26. Sobolciak, P., et al., *Materials and Technologies for the Tertiary Treatment of Produced Water Contaminated by Oil Impurities through Nonfibrous Deep-Bed Media: A Review.* Water, 2020. **12**(12): p. 3419.

27. Judd, S., et al., *The size and performance of offshore produced water oil-removal technologies for reinjection.* Separation and Purification Technology, 2014. **134**: p. 241-246.

28. Salahi, A., et al., *Asymmetric polyethersulfone ultrafiltration membranes for oily wastewater treatment: Synthesis, characterization, ANFIS modeling, and performance.* Journal of Environmental Chemical Engineering, 2015. **3**(1): p. 170-178.

29. Xu, J., et al., *Polyoxadiazole hollow fibers for produced water treatment by direct contact membrane distillation.* Desalination, 2018. **432**: p. 32-39.

30. Idrees, H., et al., *Surfactant-enhanced dead-end ultrafiltration for tertiary treatment of produced water.* Separation and Purification Technology, 2023. **311**: p. 123225.

31. Stewart, M. and K. Arnold, *Part 1 - Produced Water Treating Systems*, in *Produced Water Treatment Field Manual*, M. Stewart and K. Arnold, Editors. 2011, Gulf Professional Publishing: Boston. p. 1-134.

32. Ahmad, T., C. Guria, and A. Mandal, *Optimal synthesis, characterization and antifouling performance of Pluronic F127/bentonite-based super-hydrophilic polyvinyl chloride ultrafiltration membrane for enhanced oilfield produced water treatment.* Journal of Industrial and Engineering Chemistry, 2020. **90**: p. 58-75.

33. Badrnezhad, R. and A.H. Beni, *Ultrafiltration membrane process for produced water treatment: experimental and modeling.* Journal of Water Reuse and Desalination, 2013. **3**(3): p. 249-259.

34. Reyhani, A. and H. Mashhadi Meighani, *Optimal operating conditions of micro- and ultra-filtration systems for produced-water purification: Taguchi method and economic investigation.* Desalination and Water Treatment, 2016. **57**(42): p. 19642-19654.

35. Beh, J.J., et al., *Development of high water permeability and chemically stable thin film nanocomposite (TFN) forward osmosis (FO) membrane with poly(sodium 4-styrenesulfonate) (PSS)-coated zeolitic imidazolate framework-8 (ZIF-8) for produced water treatment.* Journal of Water Process Engineering, 2020. **33**: p. 101031.

36. Bolto, B., et al., *A Review on Current Development of Membranes for Oil Removal from Wastewaters.* Membranes, 2020. **10**(4): p. 65.

37. Munirasu, S., M.A. Haija, and F. Banat, *Use of membrane technology for oil field and refinery produced water treatment—A review.* Process Safety and Environmental Protection, 2016. **100**: p. 183-202.

38. Shi, L.X., et al., *Roles of surfactants in pressure-driven membrane separation processes: a review.* Environmental Science and Pollution Research, 2019. **26**(30): p. 30731-30754.

39. Virga, E., et al., *Theory of oil fouling for microfiltration and ultrafiltration membranes in produced water treatment.* Journal of Colloid and Interface Science, 2022. **621**: p. 431-439.

40. Trinh, T.A., et al., *Microfiltration of oil emulsions stabilized by different surfactants.* Journal of Membrane Science, 2019. **579**: p. 199-209.

41. Matos, M., et al., *Surfactant effect on the ultrafiltration of oil-in-water emulsions using ceramic membranes.* Journal of Membrane Science, 2016. **520**: p. 749-759.

42. Salahi, A., et al., *PES and PES/PAN Blend Ultrafiltration Hollow Fiber Membranes for Oily Wastewater Treatment: Preparation, Experimental Investigation, Fouling, and Modeling.* Advances in Polymer Technology, 2015. **34**(3).

43. Miller, D.J., et al., *Comparison of membrane fouling at constant flux and constant transmembrane pressure conditions.* Journal of Membrane Science, 2014. **454**: p. 505-515.

44. Kapavarapu, M.S.R.S., et al., *Economic Analysis of Membrane-Based Separation of Biocatalyst: Mode of Operation and Stage Configuration.* Industrial & Engineering Chemistry Research, 2022. **61**(19): p. 6682-6692.

45. Padaki, M., et al., *Membrane technology enhancement in oil–water separation. A review.* Desalination, 2015. **357**: p. 197-207.

46. Tanudjaja, H.J., et al., *Membrane-based separation for oily wastewater: A practical perspective.* Water Research, 2019. **156**: p. 347-365.

47. Huehmer, R., *MF/UF Pretreatment in Seawater Desalination: Applications and Trends*. 2009.

48. Iqbal, A., et al., *Importance and Significance of UF/MF Membrane Systems in Desalination Water Treatment*, in *Desalination*, Y. Taner, Editor. 2017, IntechOpen: Rijeka. p. Ch. 10.

49. Abushawish, A., et al. *Desalination Pretreatment Technologies: Current Status and Future Developments*. Water, 2023. **15**, DOI: 10.3390/w15081572.

50. Lohmann, R., et al., *Are Fluoropolymers Really of Low Concern for Human and Environmental Health and Separate from Other PFAS?* Environmental Science & Technology, 2020. **54**(20): p. 12820-12828.

51. Carlson, J.M. and J. Doyle, *Complexity and robustness.* Proceedings of the National Academy of Sciences, 2002. **99**(suppl_1): p. 2538-2545.

52. Federsel, H.-J., *Chemical Process Research and Development in the 21st Century: Challenges, Strategies, and Solutions from a Pharmaceutical Industry Perspective.* Accounts of Chemical Research, 2009. **42**(5): p. 671-680.

53. Laksono, S., et al., *Fouling scenarios in hollow fiber membranes during mini-plant filtration tests and correlation to microalgae-loaded feed characteristics.* Chemical Engineering Journal, 2021. **420**: p. 127723.

54. Tadros, T.F., *Emulsions: Formation, Stability, Industrial Applications*. 2016: Walter de Gruyter GmbH & Co KG.

55. Ebrahimi, M., et al., *Development and production of oil-in-water vehicles — sub-micron emulsion using tubular ceramic membranes.* Desalination, 2008. **224**(1): p. 40-45.

56. Idrees, H., et al., *Surface Modification of Ready-to-Use Hollow Fiber Ultrafiltration Modules for Oil/Water Separation.* Chemie Ingenieur Technik, 2021. **93**(9): p. 1408-1416.

57. Ebrahimi, M., et al., *Evaluation of the fouling potential of ceramic membrane configurations designed for the treatment of oilfield produced water.* Separation Science and Technology, 2018. **53**(2): p. 349-363.

58. Ebrahimi, M., et al., *Investigations on the use of different ceramic membranes for efficient oil-field produced water treatment.* Desalination, 2010. **250**(3): p. 991-996.

59. Ebrahimi, M., et al., *Characterization and application of different ceramic membranes for the oil-field produced water treatment.* Desalination, 2009. **245**(1): p. 533-540.

60. Dardor, D., et al., *Protocol for Preparing Synthetic Solutions Mimicking Produced Water from Oil and Gas Operations.* ACS Omega, 2021. **6**(10): p. 6881-6892.

61. Kumar, S., C. Guria, and A. Mandal, *Synthesis, characterization and performance studies of polysulfone/bentonite nanoparticles mixed-matrix ultra-filtration membranes using oil field produced water.* Separation and Purification Technology, 2015. **150**: p. 145-158.

62. Abdel-Aty, A.A.R., et al., *Superior separation of industrial oil-in-water emulsions utilizing surface patterned isotropic PES membranes.* Separation and Purification Technology, 2023. **311**: p. 123286.

63. Abdel-Aty, A.A.R., et al., *High performance isotropic polyethersulfone membranes for heavy oil-in-water emulsion separation.* Separation and Purification Technology, 2020. **253**: p. 117467.

64. Lai, G.S., et al., *Novel mixed matrix membranes incorporated with dual-nanofillers for enhanced oil-water separation.* Separation and Purification Technology, 2017. **178**: p. 113-121.

65. Ahmad, T., C. Guria, and A. Mandal, *Optimal synthesis of high fouling-resistant PVC-based ultrafiltration membranes with tunable surface pore*

size distribution and ultralow water contact angle for the treatment of oily wastewater. Separation and Purification Technology, 2021. **257**: p. 117829.

66. Stoller, M., *On the effect of flocculation as pretreatment process and particle size distribution for membrane fouling reduction.* Desalination, 2009. **240**(1): p. 209-217.
67. Teodosiu, C.C., et al., *Evaluation of secondary refinery effluent treatment using ultrafiltration membranes.* Water Research, 1999. **33**(9): p. 2172-2180.
68. Ma, Y., et al., *Investigation of Surfactant–Membrane Interaction Using Molecular Dynamics Simulation with Umbrella Sampling.* ACS ES&T Engineering, 2021. **1**(10): p. 1470-1480.
69. Kosiol, P., et al., *Determination of pore size distributions of virus filtration membranes using gold nanoparticles and their correlation with virus retention.* Journal of Membrane Science, 2017. **533**: p. 289-301.
70. Majewska-Nowak, K., I. Kowalska, and M. Kabsch-Korbutowicz, *Ultrafiltration of SDS solutions using polymeric membranes.* Desalination, 2005. **184**(1): p. 415-422.
71. Tanudjaja, H.J. and J.W. Chew, *Assessment of oil fouling by oil-membrane interaction energy analysis.* Journal of Membrane Science, 2018. **560**: p. 21-29.
72. Shi, L., et al., *Ultrafiltration of oil-in-water emulsions using ceramic membrane: Roles played by stabilized surfactants.* Colloids and Surfaces A: Physicochemical and Engineering Aspects, 2019. **583**: p. 123948.
73. Zhao, C., et al., *Application of coagulation/flocculation in oily wastewater treatment: A review.* Science of The Total Environment, 2021. **765**: p. 142795.
74. Zhong, J., X. Sun, and C. Wang, *Treatment of oily wastewater produced from refinery processes using flocculation and ceramic membrane filtration.* Separation and Purification Technology, 2003. **32**(1): p. 93-98.
75. Rasouli, Y., M. Abbasi, and S.A. Hashemifard, *Investigation of in-line coagulation-MF hybrid process for oily wastewater treatment by using novel ceramic membranes.* Journal of Cleaner Production, 2017. **161**: p. 545-559.
76. Almojjly, A., et al., *Removal of oil from oil-water emulsion by hybrid coagulation/sand filter as pre-treatment.* Journal of Water Process Engineering, 2018. **26**: p. 17-27.
77. Ozbey-Unal, B., et al., *Treatability studies on optimizing coagulant type and dosage in combined coagulation/membrane processes for table olive*

processing wastewater. Journal of Water Process Engineering, 2018. **26**: p. 301-307.

78. Abbasi, M., M. Reza Sebzari, and T. Mohammadi, *Enhancement of Oily Wastewater Treatment by Ceramic Microfiltration Membranes using Powder Activated Carbon.* Chemical Engineering & Technology, 2011. **34**(8): p. 1252-1258.
79. Rasouli, Y., M. Abbasi, and S. Hashemifard, *Oily wastewater treatment by adsorption-MF hybrid process using PAC, natural zeolite powder and low cost ceramic membranes.* Water Science and Technology, 2017. **76**: p. wst2017247.
80. Kose-Mutlu, B., et al., *Influence of powdered and granular activated carbon system as a pre-treatment alternative for membrane filtration of produced water.* Journal of Chemical Technology & Biotechnology, 2017. **92**(2): p. 283-291.
81. Zhang, J.C., et al., *Feasibility investigation of refinery wastewater treatment by combination of PACs and coagulant with ultrafiltration.* Desalination, 2005. **174**(3): p. 247-256.
82. Cordes, E.E., et al., *Environmental Impacts of the Deep-Water Oil and Gas Industry: A Review to Guide Management Strategies.* Frontiers in Environmental Science, 2016. **4**.
83. Klemz, A.C., et al., *Oilfield produced water treatment by liquid-liquid extraction: A review.* Journal of Petroleum Science and Engineering, 2021. **199**: p. 108282.
84. Bandlien, E., et al., *Water Management in Oil and Gas Operations: Industry Practice and Policy Guidelines for Developing Countries*. International Development in Focus. 2024: The World Bank. 234.
85. Zheng, J., et al., *Offshore produced water management: A review of current practice and challenges in harsh/Arctic environments.* Marine Pollution Bulletin, 2016. **104**(1): p. 7-19.
86. Ivo, O. and L. Imsland, *Framework for produced water discharge management with flow-weighted mean concentration based economic model predictive control.* Computers & Chemical Engineering, 2021. **157**: p. 107604.
87. Nwokoma, D. and K. Dagde, *Performance evaluation of produced water quality from a nearshore oil treatment facility.* Journal of Applied Sciences and Environmental Management, 2012. **16**(1): p. 27-33.
88. Tummons, E.N., *Oil droplet behavior at the membrane surface during filtrationof oil-water emulsions*. 2016, Michigan State University. p. 199.

89. Costa, T.C., et al., *Evaluation of the technical and environmental feasibility of adsorption process to remove water soluble organics from produced water: A review.* Journal of Petroleum Science and Engineering, 2022. **208**: p. 109360.

90. Liang, Y., et al., *Chapter Fourteen - Special Focus on Produced Water in Oil and Gas Fields: Origin, Management, and Reinjection Practice*, in *Formation Damage During Improved Oil Recovery*, B. Yuan and D.A. Wood, Editors. 2018, Gulf Professional Publishing. p. 515-586.

91. Eldos, H.I., et al., *Characterization and assessment of process water from oil and gas production: A case study of process wastewater in Qatar.* Case Studies in Chemical and Environmental Engineering, 2022. **6**: p. 100210.

92. Amakiri, K.T., et al., *Review of oilfield produced water treatment technologies.* Chemosphere, 2022. **298**: p. 134064.

93. Ekins, P., R. Vanner, and J. Firebrace, *Zero emissions of oil in water from offshore oil and gas installations: economic and environmental implications.* Journal of Cleaner Production, 2007. **15**(13): p. 1302-1315.

94. OSPAR-Commision. *The North-East Atlantic Environment Strategy, Strategy of the OSPAR Commission for the Protection of the Marine Environment of the North-East Atlantic 2010–2020*. Agreement 2010-03 2010; Available from: https://www.ospar.org/convention/strategy/previous-strategies.

95. OSPAR-Commision. *Strategy of the OSPAR Comission for the Protection of the Marine Environment of the North-East Atlantic 2030*. Agreement 2021-02 2021; Available from: https://www.ospar.org/convention/strategy/implementation-plan.

96. Jiang, W., et al., *Analysis of Regulatory Framework for Produced Water Management and Reuse in Major Oil- and Gas-Producing Regions in the United States.* Water, 2022. **14**(14): p. 2162.

97. Seager, R., et al., *Whither the 100th Meridian? The Once and Future Physical and Human Geography of America's Arid–Humid Divide. Part I: The Story So Far.* Earth Interactions, 2018. **22**(5): p. 1-22.

98. Nwosi-Anele, A. and O. Iledare, *Produced Water Treatment Methods and Regulations: Lessons from the Gulf of Mexico and North Sea for Nigeria.* American Journal of Engineering Research, 2016. **5**: p. 46-57.

99. Nwilo, P.C. and O.T. Badejo, *OIL SPILL PROBLEMS AND MANAGEMENT IN THE NIGER DELTA.* International Oil Spill Conference Proceedings, 2005. **2005**(1): p. 567-570.

100. Amakiri, K.T., et al., *Physicochemical assessment and treatment of produced water: A case study in Niger delta Nigeria.* Petroleum Research, 2023. **8**(1): p. 87-95.

101. Owolabi, A. and P. Adesida, *ASSESSMENT OF THE PHYSICOCHEMICAL CHARACTERISTICS OF PRODUCED WATER IN SELECTED FLOW-STATIONS IN DELTA STATE, NIGERIA.* JOURNAL OF ENGINEERING AND ENGINEERING TECHNOLOGY, 2022.

102. Isehunwa, S. and S. Onovae, *Evaluation of produced water discharge in the Niger-Delta.* 2011.

103. Veil, J., *US produced water volumes and management practices in 2012*, in *Groundwater Protection Council*. 2015.

104. Yazdan, M.M.S., et al., *Review on the Evaluation of the Impacts of Wastewater Disposal in Hydraulic Fracturing Industry in the United States.* Technologies, 2020. **8**(4): p. 67.

105. Scanlon, B.R., et al., *Can we beneficially reuse produced water from oil and gas extraction in the U.S.?* Science of The Total Environment, 2020. **717**: p. 137085.

106. Conrad, C.L., et al., *Fit-for-purpose treatment goals for produced waters in shale oil and gas fields.* Water Research, 2020. **173**: p. 115467.

107. Popoola, L.T., et al., *Oilfield produced water assessment from onshore treatment facilities in Niger Delta: Water quality susceptibility and suitability for soil irrigation* South African Journal of Chemical Engineering, 2023. **45**(1): p. 127-135.

108. Chen, C.-Y., et al., *Non-conventional water reuse in agriculture: A circular water economy.* Water Research, 2021. **199**: p. 117193.

109. Mueller, J., Y. Cen, and R.H. Davis, *Crossflow microfiltration of oily water.* Journal of Membrane Science, 1997. **129**(2): p. 221-235.

110. Darvishzadeh, T. and N.V. Priezjev, *Effects of crossflow velocity and transmembrane pressure on microfiltration of oil-in-water emulsions.* Journal of Membrane Science, 2012. **423-424**: p. 468-476.

111. Wright, L.A., S. Kemp, and I. Williams, *'Carbon footprinting': towards a universally accepted definition.* Carbon Management, 2011. **2**(1): p. 61-72.

112. Scrucca, F., et al., *Carbon Footprint: Concept, Methodology and Calculation*, in *Carbon Footprint Case Studies: Municipal Solid Waste Management, Sustainable Road Transport and Carbon Sequestration*, S.S. Muthu, Editor. 2021, Springer Singapore: Singapore. p. 1-31.

113. Uusitalo, V., et al., *Carbon Footprint*, in *Encyclopedia of Sustainable Management*, S. Idowu, et al., Editors. 2020, Springer International Publishing: Cham. p. 1-7.

114. Wiedmann, T. and J. Minx, *A Definition of Carbon Footprint.* CC Pertsova, Ecological Economics Research Trends, 2008. **2**: p. 55-65.

115. IPCC, *Global Warming potential* 2013.

116. Yang, X. and B. Su, *Impacts of international export on global and regional carbon intensity.* Applied Energy, 2019. **253**: p. 113552.

117. Moro, A. and L. Lonza, *Electricity carbon intensity in European Member States: Impacts on GHG emissions of electric vehicles.* Transp Res D Transp Environ, 2018. **64**: p. 5-14.

118. Scarlat, N., M. Prussi, and M. Padella, *Quantification of the carbon intensity of electricity produced and used in Europe.* Applied Energy, 2022. **305**: p. 117901.

119. Carboncloud.com. 2024.

120. Meinrenken, C.J., et al., *The Carbon Catalogue, carbon footprints of 866 commercial products from 8 industry sectors and 5 continents.* Scientific Data, 2022. **9**(1): p. 87.

121. Alvarez-Gaitan, J.P., et al., *Consequential cradle-to-gate carbon footprint of water treatment chemicals using simple and complex marginal technologies for electricity supply.* The International Journal of Life Cycle Assessment, 2014. **19**(12): p. 1974-1984.

122. Francke, I.C.M. and J.F.W. Castro, *Carbon and water footprint analysis of a soap bar produced in Brazil by Natura Cosmetics.* Water Resources and Industry, 2013. **1-2**: p. 37-48.

123. Asio, J.R.G., et al., *Sodium lauryl sulfate and its potential impacts on organisms and the environment: A thematic analysis.* Emerging Contaminants, 2023. **9**(1): p. 100205.

124. Nunes, R.F. and A.C.S.C. Teixeira, *An overview on surfactants as pollutants of concern: Occurrence, impacts and persulfate-based remediation technologies.* Chemosphere, 2022. **300**: p. 134507.

125. Nogueira, A.R., et al., *Environmental and energetic effects of cleaner production scenarios on the Sodium Lauryl Ether Sulfate production chain.* Journal of Cleaner Production, 2019. **240**: p. 118203.

126. Rodríguez, M. and Y. Pena-Boquete, *Carbon intensity changes in the Asian Dragons. Lessons for climate policy design.* Energy Economics, 2017. **66**: p. 17-26.

127. EEA, E.e.a. *Greenhouse gas emission intensity of electricity generation* 2023 Sep., 13 [cited 2024 Mai, 22]; Available from: https://www.eea.europa.eu/data-and-maps/daviz/co2-emission-intensity-14#tab-chart_7.

128. Bruzzoniti, M.C., R.M. De Carlo, and C. Sarzanini, *Determination of sulfonic acids and alkylsulfates by ion chromatography in water.* Talanta, 2008. **75**(3): p. 734-739.

129. Hoeft, C.E. and R.L. Zollars, *Direct Determination of Anionic Surfactants Using Ion Chromatography.* Journal of Liquid Chromatography, 1994. **17**(12): p. 2691-2704.

130. Kunitani, M.G. and L.M. Kresin, *Analysis of alkyl sulfates in protein solutions by isocratic and gradient ion chromatography.* Analytical Biochemistry, 1989. **182**(1): p. 103-108.

131. Chai, Y., et al., *Mechanistic study of drag reduction in turbulent pipeline flow over anionic polymer and surfactant mixtures.* Colloid and Polymer Science, 2019. **297**(7): p. 1025-1035.

132. Ghosh, P. and A. Mandal, *Sodium dodecyl sulfate in water: greener approach for the synthesis of quinoxaline derivatives.* Green Chemistry Letters and Reviews, 2013. **6**(1): p. 45-54.

133. Rusconi, F., et al., *Quantification of Sodium Dodecyl Sulfate in Microliter-Volume Biochemical Samples by Visible Light Spectroscopy.* Analytical Biochemistry, 2001. **295**(1): p. 31-37.

134. Rupprecht, K.R., et al., *A precise spectrophotometric method for measuring sodium dodecyl sulfate concentration.* Analytical Biochemistry, 2015. **486**: p. 78-80.

135. DVGW, *Arbeitsblatt W 218. Flockung in der Wasseraufbereitung - Flockungstestverfahren*. 1988, DVGW Deutsche Vereinigung des Gas- und Wasserfachs e.V.: Bonn.

136. Inge-Dupont, *DuPont™ IntegraTec™ P Series PES-UF ModulesT-Rack™ and Modules for Open Platform, Process and Design Manual,*. 6 ed. 2022, Germany: Inge Dupont.

137. Kleppmann, W., *Versuchsplanung: Produkte und Prozesse optimieren*. 2016: Hanser, Carl.

138. Arun Shankar, V.K., et al., *A comprehensive review on energy efficiency enhancement initiatives in centrifugal pumping system.* Applied Energy, 2016. **181**: p. 495-513.

139. Driskill, A.K., et al., *Monitoring polycyclic aromatic hydrocarbon (PAH) attenuation in Arctic waters using fluorescence spectroscopy.* Cold Regions Science and Technology, 2018. **145**: p. 76-85.

140. Lage-Yusty, M., et al., *Resolution of 13 Polycyclic Aromatic Hydrocarbons by Constant-wavelength Synchronous Spectrofluorometry.* Analytical Sciences, 2005. **21**(10): p. 1203-1206.

141. Brum, D.M., R.J. Cassella, and A.D. Pereira Netto, *Multivariate optimization of a liquid–liquid extraction of the EPA-PAHs from natural contaminated waters prior to determination by liquid chromatography with fluorescence detection.* Talanta, 2008. **74**(5): p. 1392-1399.

142. Wan, L.S.C. and P.K.C. Poon, *Effect of salts on the surface/interfacial tension and critical micelle concentration of surfactants.* Journal of Pharmaceutical Sciences, 1969. **58**(12): p. 1562-1567.

143. Nguyen, L.A.T., M. Schwarze, and R. Schomäcker, *Adsorption of non-ionic surfactant from aqueous solution onto various ultrafiltration membranes.* Journal of Membrane Science, 2015. **493**: p. 120-133.

144. Zhu, B.-Y., T. Gu, and X. Zhao, *General isotherm equation for adsorption of surfactants at solid/liquid interfaces. Part 2. Applications.* Journal of the Chemical Society, Faraday Transactions 1: Physical Chemistry in Condensed Phases, 1989. **85**(11): p. 3819-3824.

145. Malyukin, V.Y., S.L. Efimova, and K. Kemnitz, *Spectroscopy of intermolecular interaction in the system: dye-sodium dodecylsulfate micelles.* Journal of Luminescence, 2001(94–95): p. 239–242.

146. Mateus, M.V., et al., *Molecular Interactions and Modeling of Anionic Surfactant Effect on Oxygen Transfer in a Cylindrical Reactor.* Environmental Engineering Science, 2018. **36**(2): p. 180-185.

147. Alvarez-Gaitan, J., et al., *A hybrid life cycle assessment of water treatment chemicals: An Australian experience.* The International Journal of Life Cycle Assessment, 2013. **18**.

8 Appendices

8.1 List of Abbreviations

Abb.	Unit	Description
A_i /A_0	-	Relative integrated area of the respective peaks/ integrated area of the reference peaks in GC-MS Analysis
API		Oil–water separator named after the American Petroleum Institute
ASW		Artificial seawater salt
BOD	mg/L	Biological Oxygen Demand
BTEX		Benzene, toluene, ethylbenzene, and xylene
BW		Hydraulic backwash
C	g/L	Concentration
CF		Constant Flux
CFP	kg CO_{2eq}	Carbon footprint
CI		Carbon Intensity
CIP		Cleaning-in-place
CMC	g/L	Critical micelle concentration
COD	mg/L	Chemical oxygen demand
CP		Constant Pressure
CTAB		Cetyltrimethylammonium bromide, cationic surfactant
$D_{10,N}$	µm	Diameter where 10% of the number distribution has a smaller particle size
$D_{10,V}$	µm	Diameter where 10% of the volume distribution has a smaller particle size
$D_{50,N}$	µm	Median droplet size of number distribution; Diameter where 50% of the number distribution has a smaller particle size
$D_{50,V}$	µm	Median droplet size of volume distribution; Diameter where 50% of the volume distribution has a smaller particle size
$D_{90,N}$	µm	Diameter where 50% of the number distribution has a smaller particle size
$D_{90,V}$	µm	Diameter where 50% of the volume distribution has a smaller particle size
DI		Pure water
DOC	mg/L	Dissolved organic content
DOE		Design of experiment
E_1		HPH-based emulsified oil
$E_{1,S}$		HPH-based emulsified oil with small droplet size
$E_{1,M}$		HPH-based emulsified oil with middle droplet size
$E_{1,B}$		HPH-based emulsified oil with big droplet size
$E_{2,P}$		Reproduced US-based emulsified oil
$E_{2,U}$		Upgraded US-based emulsified oil
EN	kWh	Energy consumed by a pump
EN_s	kWh/m^3	Specific energy consumption
EPA		United States environmental protection agency
FT-IR		Fourier transform infrared
HCA		Cogulant; Poly dimethyl diallyl propyl ammonium chloride

HPH		High-pressure homogenizer
J	L/(m²·h)	Filtration flux
MF		Microfiltration
N	-	Number of trials
N_{PS}	-	Number of emulsification passes
NEAES		North-East Atlantic Environment Strategy
NF		Nanofiltration
OWWE		Produced water after primary and secondary treatment stages
OSPAR		The convention for the protection of the marine environment of the north-east Atlantic
P	bar	Pressure
PE	bar	Emulsification pressure
PAC		Powdered activated carbon
PACL		Polyaluminum chloride, coagulant
PAH		Polycyclic aromatic hydrocarbon
PAN		Polyacrylonitrile
PES		Polyethersulfone
PR%	%	Permeability recovery percentage
PSF		Polysulfone
PVDF		Polyvinylidene fluoride
PW		Produced water
Q	L/h	Volume flow rate
$\boldsymbol{R_i}$	m^{-1}	Resistance
$\mathbb{R}$	%	Retention
RE_2		Reference US-based emulsion
RO		Reverse osmosis
SDS		Sodium dodecyl sulfate
SEM		Scanning electron microscopy
SLES		Sodium Lauryl Ether Sulfate
TC	mg/L	Total carbon
TDS	mg/L	Total dissolved solids
TMP	bar	Transmembrane pressure
TOC	mg/L	Total organic carbon
TOG	mg/L	Total oil and grease
TSS	mg/L	Total suspended solids
UF		Ultrafiltration
US		Ultrasound
USA		United States of America
UVi	m^{-1}	Ultraviolent spectral absorption coefficient, where i represents the measurement wavelength in nm
V	L/m²	specific filtered volume per membrane area
W, Wt	L/(m²·h·bar)	Membrane permeability, membrane permeability at certain time t
W'	-	Normalized permeability
W_0	L/(m²·h·bar)	Initial pure water permeability
WP		Workpackage
WSO		Water-soluble oil fraction

$W_{t,BW}$	L/(m²·h·bar)	Membrane permeability after every hydraulic backwashing step
η_F	-	The pump's yiels
λ_{ex}	nm	Excitation wavelength in FEEM analysis
λ_{em}	nm	Emission wavelength in FEEM analysis
σ_i	-	Standard deviation of the normalized permeability for each registered measuring point
σ_{tot}	-	Average standard deviation the normalized permeability of all points
σ_{W0}	L/(m²·h·bar)	Standard deviation of the initial membrane pure water permeability

8.2 List of Figures

Figure 1: Environmental impact factors of produced water discharge 30

Figure 2: Carbon intensity in gCO_{2eq}/kWh of electricity generation over years for different European countries..... 40

Figure 3: Schematic representation of the bench-scale dead-end filtration unit for flat-sheet membranes operated manually at constant pressure 48

Figure 4: Schematic representation of the "Playground" bench-scale dead-end filtration unit operated at constant flow..... 49

Figure 5: Schematic representation of the "Playground" bench-scale dead-end filtration unit operated at constant flow, modified for the synergistic combination of UF with the dosage of PAC and/or coagulants..... 50

Figure 6: Schematic representation for (a) the Poseidon and (b) the Neptunus mini-plants dead-end filtration unit for constant flow rate..... 51

Figure 7: Schematic illustration of the default testing procedure for mini-plant multiple-cycles dead-end filtration tests employing lab-scale capillary membranes ... 52

Figure 8: Schematic representation of the SRA dead-end filtration unit for constant flow rate 55

Figure 9: Differential number and volume size distributions for sub-micron oil droplets in real PW sample with min/max error bars..... 64

Figure 10: Differential number and volume size distributions for HPH-based emulsified oils E_1 at (a) different P_E of 450, 1,000, 1,500 and 1,900 bar for one pass, as well as (b) at different N_{PS} and P_E of 1,900 bar. O/W = 1/250..... 65

Figure 11: Oil droplet size distributions for three samples of a representative emulsified oil $E_{1,M}$ stored at different times. $E_{1,M}$ was prepared at O/W 1:250 and P_E 1,700 bar for 2 passes 66

Figure 12: Average differential volume distribution density for twelve preparation batches for a representative emulsified oil $E_{1,M}$. Error bars indicate standard deviation 67

Figure 13: Average differential volume size distributions for two batches of $E_{2,P}$. Error bares represent min/max values 68

Figure 14: Differential volume size distribution for two batches of $E_{2,U}$. Error bars represent min/max values 69

Figure 15: Normalized permeability curves for crossflow filtration experiments using $E_{1,M}$ and $E_{2,U}$ with oil concentrations of 25 and 50 mg/L 71

Figure 16: TOC retention measured during membrane filtration tests using $E_{1,M}$ and $E_{2,U}$ emulsified oil with oil concentrations of 25 mg/L and 50 mg/L 72

Figure 17: Normalized permeability curves (A and B) and the respective fouling chronological evolution (C and D) during the filtration of $E_{1,S}$, $E_{1,M}$ and $E_{1,B}$ using MF membranes S800 (A and C) and S450 (B and D) at constant flux of 1,300 L/(m²·h), one trial 75

Figure 18: Normalized permeability curves (A and B) and the respective fouling chronological evolution (C and D) during the filtration of $E_{1,S}$, $E_{1,M}$ and $E_{1,B}$ using UF membranes S100 (A and C) and IG (B and D) at constant flux of 240 L/(m²·h), one trial 76

Figure 19: Reproducibility of filtration experiments of $E_{1,S}$, $E_{1,M}$ and $E_{1,B}$ through S450, two or three trials 77

Figure 20: SEM micrographs for (A) Pristine S450 and fouled S450 during filtration of (B) $E_{1,B}$, (C) $E_{1,M}$ and (D) $E_{1,S}$ emulsified oils, Magnification: X 50,000 78

Figure 21: Normalized permeability curves (A and B) and the respective fouling chronological evolution (C and D) during the filtration of $E_{1,S}$, $E_{1,M}$ and $E_{1,B}$

using MF membranes S800 (A and C) and S450 (B and D) at constant pressure of 0.5 bar, one trial 79

Figure 22: Normalized permeability curves (A and B) and the respective fouling chronological evolution (C and D) during the filtration of $E_{1,S}$, $E_{1,M}$ and $E_{1,B}$ using UF membranes S100 (A and C) and IG (B and D) at constant pressure of 0.5 bar, one trial 80

Figure 23: Droplet size distribution of oily feeds prepared of $E_{1,S}$ emulsified oils with no salt, 0.5 M NaCl, 0.5 M $CaCl_2$, 1 M NaCl and artificial sea water salts 81

Figure 24: Normalized permeability decline of oily feeds prepared of $E_{1,S}$ emulsified oils with no salt, 0.5 M NaCl, 0.5 M $CaCl_2$, mix of 0.5 M NaCl and $CaCl_2$, 1 M NaCl and artificial seawater salts (ASW) filtered through S450 82

Figure 25: Normalized permeability decline of oily feeds prepared of $E_{1,S}$ emulsified oils with no salt, 0.5 M NaCl, 0.5 M $CaCl_2$, mix of 0.5 M NaCl and $CaCl_2$, 1 M NaCl and artificial seawater salts (ASW) filtered through S100 82

Figure 26: Concentration of 11 types of polycyclic aromatic hydrocarbons existing in the model oil-emulsion at 10 mg/L oil (as TOC) without SDS 84

Figure 27: GC-MS analysis of surfactant-free emulsified oily feed with oil concentration of 25 mg/L as TOC 85

Figure 28: Reference components of surfactant-free emulsified oil that were detected with the GC-MS analysis with their respective retention time, integrated area of the intensity peak and probability of the detected component compared to the NIST library. Presented as average of four trials with the min. and max. error bars 86

Figure 29: GC-MS analysis of the permeates of surfactant-free emulsified oily feed with oil concentration of 25 mg/L as TOC after being filtered through S450 and S200 membranes. 87

Figure 30: Relative area A_i/A_0, integrated area of intensity peaks (A_i) of the reference components in the permeate of S450 and S200 membranes related to the

respective integrated area of the intensity peak of the feed (A_0). Presented as average of two trials with the min. and max. error bars 88

Figure 31: Relative area A_i/A_0, of the permeate of SM membranes, when filtering the permeates of S450 membranes through SM membrane. 89

Figure 32: Emission-intensity curves for surfactant-free emulsified oil with oil concentration of 5 mg/L measured in triplicates at four excitation wavelength values of 290, 266, 260 and 275 nm that are assigned to acenaphthene, chrysene, fluorene and naphthalene..... 90

Figure 33: Emission-intensity curves for surfactant-free vs. surfactant-containing emulsified oil with different oil concentrations (1 – 50 mg/L TOC) at excitation wavelength values of 290 and 239 nm (assigned to acenaphthene and pyrene) 91

Figure 34: Concentrations of the main 16 PAH compounds in emulsified oil with oil concentrations of 5 and 10 mg/L TOC and different SDS concentrations (0, 0.12, 0.48 and 1.2 g/L)..... 92

Figure 35: Relationship between TOC concentration in surfactant-free emulsified oil (1 – 50 mg/L) and the measured concentrations of total PAHs, naphthalene, phenanthrene and fluorene via GC-MS method 93

Figure 36: Relationship between the measured concentrations of total PAHs, naphthalene, phenanthrene and fluorene via GC-MS method and the respective emission-intensities for surfactant-free emulsified oil (1 – 50 mg/L) 94

Figure 37: Differential number- (left) and volume-based oil droplet size distributions (right) for emulsified oil (25 mg/L) prior to separation of dissolved oil..... 95

Figure 38: Differential volume-based oil droplet size distributions for permeates of S100 (left) and S450 (right) membrane filters over 3 trials..... 95

Figure 39: Differential pore size distribution of S450 and S100, 2 trials..... 96

Figure 40: Normalized permeability of SM_1 membranes during single-cycle filtration experiment with the permeates of S100, S200 and S450 as feed 97

Figure 41: Normalized permeability of SM_1 UF membrane module during single-cycle filtration experiment of the permeate of S450 for an extended cycle duration 97

Figure 42: Normalized permeability of UP150 filtering 10 mg/L surfactant-free emulsified oils at a flux of 240 L/(m²·h) (a) for three trials (b) as average of the 3 trials with min/max errors 101

Figure 43: Normalized permeability of UP 150 operated at a flux of 240 L/(m²·h) filtering oil-free surfactant solutions at concentrations of (a) 1.0, (c) 0.5 and (e) 0.2 CMC and emulsified oil at 10 mg/L oil with surfactants at concentrations of (b) 1.0, (d) 0.5 and (f) 0.2 CMC 103

Figure 44: Normalized permeability of UP150 filtering emulsified oils at 10 mg/L containing SDS at concentrations of 0.2, 0.5 and 1 CMC at (a) constant flux (CF) of 240 L/(m²·h) and (b) constant pressure (CP) of 0.4 bar 104

Figure 45: Normalized permeability of UP150 filtering surfactant, 2-pentanol and ASW at a flux of 240 L/m²·h. On the left side reference experiments with oil-free surfactant solutions using (a) SDS, (c) Tween 20 and (e) CTAB and on the right side those with emulsified oils with 10 mg/L oil and (b) SDS, (d) Tween 20 and (f) CTAB 107

Figure 46: Normalized permeability curves for SM membranes in reference filtration tests with multiple-cycles at a constant flux of 100 L/(m²·h) using oil-free SDS solutions of different concentrations (0.024 - 1.2 g/L) 112

Figure 47: Normalized permeability curves for SM membranes in reference filtration tests with multiple-cycles at a constant flux of 100 L/(m²·h) using surfactant-free emulsified oils with different oil contents of 5, 10 and 25 mg/L 114

Figure 48: Distributive and cumulative fouling resistances for SM membranes during multiple-cycle reference filtration tests at a constant flux of 100 L/(m²·h) using surfactant-free emulsified oils with different oil contents of 5, 10 and 25 mg/L. The plotted data are the average fouling resistance values calculated from different repetitions. Error bars represent min/max values 116

Figure 49: Normalized permeability for filtration of 5 mg/L emulsified oils containing Tween20 at concentrations of 0.2 and 0.5 CMC employing SM membranes at a constant flux of 100 L/(m²·h) 117

Figure 50: Normalized permeability curves for SM membranes during mini-plant filtration tests at a constant flux of 100 L/(m²·h) using SDS-modified 5 mg/L emulsified oils with different SDS concentrations (0.024 - 1.2 g/L) 118

Figure 51: PR% values determined for multiple-cycle dead-end filtration tests at constant flux of 100 L/(m²·h) using SDS-modified 5 mg/L emulsified oils with different SDS concentrations (0.024 - 1.2 g/L)..... 119

Figure 52: Distributive and cumulative fouling resistances for SM membranes during mini-plant dead-end filtration tests of SDS-modified 5 mg/L emulsified oil with SDS concentrations of 0.024, 0.12, 0.24, 0.48 and 1.2 g/L, compared to SDS-free emulsified oil. The plotted data are the average fouling resistance values calculated from different repetitions. Error bars represent min/max values 121

Figure 53: Normalized permeability curves for SM membranes during mini-plant filtration tests at constant flux of 100 L/(m²·h) using SDS-modified 10 mg/L emulsified oils with different SDS concentrations (0.024 - 1.2 g/L) 122

Figure 54: PR% values determined for multiple-cycle dead-end filtration tests at constant flux of 100 L/(m²·h) using SDS-modified 10 mg/L emulsified oils with different SDS concentrations (0.024 - 1.2 g/L)..... 123

Figure 55: Overview on PR% values determined for multiple-cycle dead-end filtration tests at constant flux of 10 L/(m²·h) using SDS-free and SDS-modified emulsified oils with different oil concentrations (5 – 50 mg/L) and constant SDS concentrations of 0.48 g/L 124

Figure 56: Distributive and cumulative fouling resistances for SM membranes during mini-plant dead-end filtration tests of SDS-modified 10 mg/L emulsified oil with SDS concentrations of 0.024, 0.12, 0.24, 0.48 and 1.2 g/L, compared to SDS-free emulsified oil. The plotted data are the average fouling resistance values calculated from different repetitions. Error bars represent min/max values 126

Figure 57: Normalized permeability curves as well as fouling resistances for SM membranes during mini-plant filtration tests at constant flux of 100 L/(m²·h) using SDS-modified emulsified oils with oil contents of 25 mg/L and 50 mg/L and constant SDS concentration of 0.48 g/L 127

Figure 58: Representation for the proposed joint effects induced by SDS dosing prior to ultrafiltration that are responsible for the substantially improved membrane antifouling performance vs. strong membrane fouling caused by dead-end ultrafiltration of SDS-free emulsified oil 129

Figure 59: Normalized permeability curves for specially designed multiple-cycle dead-end filtration tests, starting with filtration of 0.48 g/L oil-free SDS solution at a constant flux of 100 L/(m²·h) followed by filtration of surfactant-free emulsified oils (5 mg/L or 10 mg/L) 131

Figure 60: TOC retention for SM membranes at different time intervals, within the first two filtration cycles, in multiple-cycle dead-filtration tests using surfactant-free emulsified oils with different oil concentrations 132

Figure 61: TOC retention of SM membranes for model oil-emulsions with different oil and SDS concentrations at a constant flux of 100 L/m²·h·bar. The presented values are the average of three samples collected at the beginning and the end of 1st cycle and at the beginning of 2nd cycle 133

Figure 62: PAHs retention for SM membranes in multiple-cycle dead-filtration tests using surfactant-free and SDS-modified emulsified with oil content of 10 mg/L and SDS concentrations of 0.12, 0.24, 0.48 and 1.2 g/L 134

Figure 63: Calibration curve for the measured EC (µS/cm) against the SDS concentration (g/L) 135

Figure 64: Spectral Absorption Coefficient (UV) at wavelengths 350 – 800 nm for SDS solutions at concentration of 0.1 – 0.8 g/L with the dye Stains-All 136

Figure 65: Calibration curve of measured UV_{453} (m^{-1}) against the SDS concentration (mg/L) for solutions prepared with two different background water matrices, ultrapure water (A) and permeate of 10 mg/L surfactant-free emulsified oil permeate through SM membrane (B) 137

Figure 66: Quantified SDS (mg/L) in the UF permeate against the filtration time (min) for feed of 48 mg/L SDS without oil (A) and with emulsified oily feed at 10 mg/L as TOC (B) through SM membranes 138

Figure 67: Measured and calculated theoretical values for a pure SDS, and measured values for $SDS_{VWR,23}$ and SDS_{TS} (Microanalytical Laboratory at University of Duisburg-Essen) 139

Figure 68: FTIR analysis for $SDS_{VWR,23}$ and SDS_{TS} 140

Figure 69: Normalized permeability curves for SM membranes in filtration tests with multiple-cycles at a constant flux of 100 L/(m²·h) using oil-free SDS solutions of different concentrations (0.024 - 1.2 g/L) made of (A) $SDS_{VWR,21}$ and (B) $SDS_{VWR,23}$, ... 142

Figure 70: Normalized permeability curve for filtering surfactant-modified emulsified oil with10 mg/L and 25 mg/L both with 0.48 g/L of (A) $SDS_{VWR,21}$ and (B) $SDS_{VWR,23}$. One trial each 143

Figure 71: Normalized permeability curve for filtering (A) oil-free SDS_{TS} solutions and (B) SDS_{TS}-modified emulsified oil with oil concentration of 10 mg/L, both at SDS concentration of 0.24 g/L through SM membranes, one trial each..... 144

Figure 72: Normalized permeability curve for filtering (a) oil-free SDS solutions and (b) SDS-modified emulsified oil with oil concentration of 10 mg/L, both made with $SDS_{VWR,23}$ at concentration of 0.24 g/L through SX membranes, one trial each 145

Figure 73: Normalized permeability curve for filtering (a) oil-free SDS_{TS} solutions and (b) SDS_{TS}-modified emulsified oil with oil concentration of 10 mg/L, both at SDS concentration of 0.24 g/L through SX membranes, one trial each 145

Figure 74: Filtration curves for EXP 01 and EXP 02 with filtration flux of 60 and 140 L/(m²·h), respectively. Both experiments were performed at filtration duration of 30 min, BW flux of 90 L/(m²·h), BW duration of 30 sec, Pure water duration of 3 min, as well as oily feed at oil concentration of 10 mg/L and SDS concentration of 0.48 g/L through SM_1 membranes..... 148

Figure 75: Filtration curves for EXP 03 and EXP 01 with filtration cycle duration of 60 and 30 min, respectively. Both experiments were performed at filtration flux of 60 L/(m²·h), BW flux of 90 L/(m²·h), BW duration of 30 s, pure water duration of 3 min, as well as oily feed at oil concentration of 10 mg/L and SDS concentration of 0.48 g/L through SM_1 membranes..... 149

Figure 76: Filtration curves for EXP 10 and EXP 14 with BW flux 90 and 230 L/(m²·h), respectively. Both experiments were performed at filtration flux of 140 L/(m²·h), filtration cycle duration 30 min, BW duration of 90 s, pure water duration of 3 min, as well as oily feed at oil concentration of 10 mg/L and SDS concentration of 0.48 g/L through SM_1 membranes..... 150

Figure 77: Filtration curves for EXP 11 and EXP 03 with BW duration of 90 and 30 s, respectively. Both experiments were performed at filtration flux of 60 L/(m²·h), filtration cycle duration of 60 min, BW flux of 90 L/(m²·h), pure water duration of 3 min, as well as oily feed at oil concentration of 10 mg/L and SDS concentration of 0.48 g/L through SM_1 membranes..... 151

Figure 78: Filtration curves for EXP 03 and EXP 19 with pure water duration of 3 and 7 min, respectively. Both experiments were performed at filtration flux 60 L/(m²·h), filtration cycle duration of 60 min, BW flux of 90 L/(m²·h), BW duration of 30 s, as well as oily feed at oil concentration of 10 mg/L and SDS concentration of 0.48 g/L through SM_1 membranes..... 152

Figure 79: Results of adsorption kinetic experiments of ABG-H, HMA-B and ORG-K PACs, presented as UV_{254} concentration in the permeate (C) related to the feed concentration(C_0) over time 153

Figure 80: UV_{254} elimination in percentage against the direct dosed concentrations of three PACs, ABG-H, HMA-B and ORG-K to the emulsified oil of 25 mg/L as TOC, one trial each..... 154

Figure 81: UV_{254} adsorption isotherms for the three different PAC, (a) ABG-H, (b) HMA-B and (c) ORG-K, four trials each 155

Figure 82: UV_{254} elimination in percentage against the direct dosed concentrations of ABG-H PAC to emulsified oil of 25 mg/L as TOC that is prefiltered through filter of 0.45 µm and not pre-filtered, one trial each 156

Figure 83: Relative concentrations of oil as DOC and UV_{254} in the supernatant of the coagulation/flocculation experiments (C) related to the feed concentration(C_0) for (a) $FeCl_3$ as iron-based coagulant and (b) $Al_2Cl(OH)_5$ as aluminum-based coagulant. Presented as average of two trials with the min. and max. error bars..... 157

Figure 84: Normalized permeability curve of the dead-end filtration experiments on standalone S100, combination of coagulation-S100, PAC-S100 and coagulation-PAC-S100 for emulsified oils of 25 mg/L as TOC at constant pressure of 1 bar..... 159

Figure 85: Normalized permeability curve of the dead-end filtration experiments on standalone UP 150, combination of coagulation- UP 150, PAC- UP 150 and coagulation-PAC- UP 150 membranes for emulsified oils of 25 mg/L as TOC at constant pressure of 1 bar 161

Figure 86: Normalized permeability curve for reference experiment for filtering surfactant-free emulsified oil of 10 mg/L as TOC at constant pressure of 0.4 bar through SM_1 membranes. BW for one minute at 1 bar. Two trials.. 163

Figure 87: Normalized permeability curve for filtering surfactant-free emulsified oil of 10 mg/L as TOC at constant pressure of 0.4 bar with a combination of coagulation – PAC – SM_1 with ABG-H PAC at dosage of 10 mg/L, Nüscofloc FE coagulant at dosage of 1 mg/L 163

Figure 88: Normalized permeability curve for filtering surfactant-free emulsified oil of 10 mg/L as TOC at constant pressure of 0.4 bar with a combination of PAC-SM_1 with 10 mg/L (a) ABG-H, (b) HMA-B and (c) ORG-K PAC 164

Figure 90: Normalized permeability curves for filtering surfactant-free emulsified oil of 10 mg/L as TOC at constant pressure of 0.4 bar with hybrid operation of coagulation – PAC – SM_1 experiments with ABG-H PAC at dosage of 10 mg/L, Nüscofloc FE coagulant at dosage of 1 mg/L 165

Figure 91: Elimination performance represented as percentage retention of UV_{254} for standalone S100, PAC-S100, coagulation-S100 and PAC-coagulation-S100 166

Figure 91: Normalized permeability of filtering emulsified oil with10 mg/L, 25 mg/L and 50 mg/L at CFV of 2.5 m/s compared with Normalized permeability of filtering emulsified oil with 50 mg/L at CVF of 0.75 m/s 167

Figure 92: Specific energy consumption of crossflow experiments with emulsified oils at concentration of 10, 25 and 50 mg_{TOC}/L at CFV of 2.5 m/s. Calculated for η_F = 0.8 (solid-colored) and 0.6 (hatched) 168

Figure 93: Normalized permeability of filtering surfactant-modified emulsified oils (a) at oil concentration of 10 mg/L with SDS concentrations of 0.12, 0.48 and 1.2 g/L and (b) at oil concentrations of 10, 25 and 50 mg/L with SDS concentration of 0.48 mg/L 169

Figure 94: Specific energy consumption of surfactant-enhanced dead-end UF experiments with surfactant-enhanced emulsified oils at a concentration of 10 mg/L with SDS concentration of 0.12, 0.48 and 1.2 g/L and an oil concentration of 25 and 50 mg/L with SDS concentration of 0.48 g/L. Calculated for η_F = 0.8 (solid-colored) and 0.6 (hatched) 170

Figure 95: Permeability of filtering surfactant-free emulsified oils at oil concentration of 10 mg/L through LM_2 membranes as standalone UF at constant flux of 100 L/(m²·h) 175

Figure 96: Permeability of filtering surfactant-modified emulsified oils at oil concentration of 10 mg/L and SDS concentration of 0.48 g/L through LM module as standalone UF at constant flux of 100 L/(m²·h) 176

Figure 97: Permeability of filtering surfactant-free emulsified oils at oil concentration of 10 mg/L through LM_2 modules as standalone UF or hybrid coagulant-UF. Nüscofloc FE was dosed as 1 mg/L. Both experiments werde done at constant flux of 100 L/(m²·h) 177

Figure 98: Permeability of filtering surfactant-free emulsified oils at oil concentration of 10 mg/L through LM_2 module as hybrid coagulant-UF. Nüscofloc FE was dosed as 1 mg/L, flux was set constant to 100 L/(m²·h) 178

Figure 99: Permeability of filtering surfactant-free emulsified oils at oil concentration of 10 mg/L through LM module as hybrid coagulation-UF at constant flux of 100 L/(m²·h) for three cycles followed by two CIP steps with NaOCl at chlorine concentration of 200 mg/L and SDS at concentration of 1.2 g/L. Two trials 179

8.3 List of Tables

Table 1: The tasks of the W-UFO project, the associated with the W-UFO I, II and III⁺ sub-projects and the respective work package 17

Table 2: A detailed list for planned and conducted experiments in all WPs during W-UFO III⁺ 21

Table 3: TOG Limits for offshore operations in different regions [83, 85, 89, 90, 92] .. 31

Table 4: CFP values of certain products 38

Table 5: Specifications for flat sheet membranes employed in this project 42

Table 6: Specifications for capillary membrane modules employed in this project 42

Table 7: Detailed listing of the parameter values for the design of experiments. The experimental conditions were set using nonlinear 2-factorial design of experiment (DOE) for five parameters: i.e., filtration flux, filtration duration, backwash flux and pure water filtration duration as well as the respective recovery for each combination. 58

Table 8: Emulsification parameters for the preparation of HPH-based emulsified oils $E_{1,B}$, $E_{1,M}$, and $E_{1,S}$ along with oil droplet size distributions 66

Table 9. Oil droplet size distributions for RE_2 (as reported [60], reproduced ($E_{2,P}$) and upgraded ($E_{2,U}$) emulsified oils 67

Table 10: TOC, UV_{254} absorbance, turbidity, conductivity, and pH for US-based emulsified oils. (±) represents standard error 69

Table 11: Technical comparison of HPH-based and US-based methods 73

Table 12: Conductivity and zeta potential of oily feeds prepared of E_1 emulsified oils with no salt, 0.5 M NaCl, 0.5 M $CaCl_2$, mix of 0.5 M NaCl and $CaCl_2$, 1 M NaCl and artificial sea water salts (ASW) 81

Table 13: Composition of polycyclic aromatic hydrocarbon (PAH) in crude oil, measured using GC-FID, according to the EPA 16 PAH list; < 3 means that the value was below the limit of determination 84

Table 14: The excitation and emission wavelength values for the main 16 compounds of PAHs 89

Table 15: Results of emulsified oil filtration experiments using UP150 at constant flux, incl. number of trials (N), average standard deviation of normalized permeability for each measurement point, and average pure water permeability and its respective standard deviation 99

Table 16: Oil droplet size distributions for the stock oil-in-water emulsion as well as surfactant-free and surfactant-modified emulsified oils 109

Table 17: Characteristics for surfactant-free and surfactant-modified emulsion oil employed in this study 110

Table 18: CMC measurement of SDS_{VWR} and SDS_{TS} together with two other reference SDS samples with purity of 95% and >99% 141

Table 19: A list of experiments completed in accordance with the statistical experimental plan with central composite design and the associated filtration flux, filtration cycle duration, backwash flux, backwash duration, and pure water filtration including experiments done on playground, number of successful cycle and total fouling 147

Table 20: Detailed operation conditions and the respective parameters included for E_s calculations in UF dead-end and crossflow modes. 170

Table 21: Price for 1 kg of SDS from three marketplaces for suppliers of industrial level 171

Table 22: Electricity price, the respective value for $\Delta Cost_{EN}$ considering an energy consumption of 0.778 kWh/m³ and the ΔCost considering an average SDS cost of 0,264 €/m³ for Germany. Saudi Arabia, Egypt and Sweden..... 172